Reliable Communication in Non-Gaussian Environments: Receiver Design and Analytical Aspects

by

Jeebak Mitra

B.E (Elec & Comm.), Birla Institute of Technology, 2002.
M.A.Sc (Elec & Comp.), University of British Columbia, 2005.

A THESIS SUBMITTED IN PARTIAL FULFILLMENT OF

THE REQUIREMENTS FOR THE DEGREE OF

DOCTOR OF PHILOSPHY

in

THE FACULTY OF GRADUATE STUDIES

(Electrical and Computer Engineering)

THE UNIVERSITY OF BRITISH COLUMBIA

(Vancouver)

May 2010

Abstract

With the plethora of devices that operate in current communication networks, there is a non-zero probability that radio frequency signals from disparate sources may interfere with each other and therefore one has to contend with *unwanted* signals that corrupt the desired signal. The unwanted part, collectively referred to as *noise*, may be attributed to a number of factors ranging from device irregularities to varied ambient phenomena. Traditionally by applying the central limit theorem, noise in communication systems has been characterized by a Gaussian distribution. However, it has been recognized time and again, that in plenty of cases this is an abstraction of the real characteristics of the noise since for a variety of reasons the central limit theorem may not hold true for the observed noise. Such noise is generally referred to as being non-Gaussian. The general belief about non-Gaussian noise is that it deteriorates signal fidelity, resulting in unreliable communication. However, the loss in reliability is due to the fact that almost all communication systems are designed to well handle Gaussian noise and hence suffers loss when this assumption is not true.

We characterize the performance of coded and uncoded communication systems in non-Gaussian noise. More specifically we consider *robust* decoding techniques when the noise is impulsive and is correlated. We incorporate the effect of non-ideal interleaving on system performance when the noise has memory and provide several design recommendations for such environments. We also propose techniques to acquire information on the statistics of the noise when it can be modeled as a Markovian-Gaussian process and analyse the performance of such estimators. These techniques are then applied to contemporary technologies such as cognitive transmission and impulse radio ultra wideband transmission, as a proof of concept, and to quantify the benefits that exist in accurately characterizing the interference in such systems. Furthermore, we use spatial diversity in mitigating the effects of non-Gaussian noise through a distributed multi-antenna approach. Better known as cooperative diversity, this approach is shown to require careful design when the facilitating nodes are affected by strong interference and we provide novel algorithms for the same.

Table of Contents

List of Tables

List of Figures

List of Abbreviations

APP	A Posteriori Probability
AWGN	Additive White Gaussian Noise
AF	Amplify and Forward
BCJR	Bahl-Cocke-Jelinek-Raviv
BPSK	Binary Phase Shift Keying
BPPM	Binary Pulse Position Modulation
BER	Bit Error Rate
BICM	Bit Interleaved Coded Modulation
CSI	Channel State Information
CR	Cognitive Radio
DF	Decode and Forward
EM	Expectation Maximization
EDSD	Euclidean Distance Soft Decision
EMD	Erasure Marking Decoder
EXIT	Extrinsic Information Transfer
GGD	Generalized Gaussian Detector
HPF	Huber Penalty Function
ILD	Interleaving Depth
IR	Impulse Radio

IT	Interference Temperature
JSS	Joint Sensing and Suppression
KSMLD	Known State Maximum Likelihood Detector
LLR	Log Likelihood Ratio
MAP	Maximum A Posteriori
ML	Maximum Likelihood
MNAD	Mean Absolute Deviation
MDAD	Median Absolute Deviaion
MSMLD	Memoryless Maximum Likelihood Detector
MUI	Multi-User Interference
PDF	Probability Density Function
PLC	Powerline Communications
RF	Radio Frequency
PSK	Phase Shift Keying
SISO	Soft Input Soft Output
SNR	Signal to Noise Ratio
SIR	Signal to Interference Ratio
SINR	Signal to Interference plus Noise ratio
TTD	Two Term Detector
TH	Time Hopping
UWB	Ultra Wideband

Acknowledgements

I would like to take this opportunity to convey my gratitude to my advisor, Dr. Lutz Lampe, for his able guidance throughout the course of this work. I have learnt a lot from him and consider it a privilege to have worked with him. His constant encouragement and support helped me in overcoming the challenges I faced while pursuing my doctoral work. I would also like to thank Prof. Robert Schober and Prof. Vikram Krishnamurthy for being on my doctoral committee and Prof. Cyril Leung and Prof. Vincent Wong for serving on my examination committee.

I have also been fortunate to have worked with very supportive colleagues in the Communication Theory Group, at UBC - Chris, Zahra, Anna, Anand, Alireza and all others deserve my deepest gratitude for creating a friendly and stimulating environment. To all my friends all over the world, I owe you for always being there for me.

Last but not the least, I would like to thank my family for being very patient and for believing in me during all these years. Without their love and support I would have not been the person I am.

CHAPTER 1

Introduction and Overview

The ability to communicate either through wireline or wireless transmission is regarded as one of the biggest inventions of mankind and is definitely a testament to the ways in which technology contributes to a higher quality of life. With greater possibilities come greater expectations and today's consumers expect to be *connected* anywhere, anytime and be able to use applications that demand huge bandwidths. Communications devices, both wireless and wireline, have made significant inroads into various segments of society, commercial and otherwise and are deemed indispensable for the success of any enterprise. However, this has also put the onus on service providers and innovators alike to develop communication strategies and devices that can meet or surpass an ever-increasing demand in data rates. One of the biggest factor that prevents the reliable data transfer at high speeds in environments with multiple trans-

mitters and receivers is the effect that undesired signals may have on the transmitted signal. In communication channels all undesired signals may be collectively referred to as noise. Both multiplicative and additive noise play a detrimental role in the error free reception of an electromagnetic signal in various transmission environments. In order to efficiently detect the desired signal from the noisy received signal one needs to be aware of the statistical characteristics of the noise. For example, in case of additive noise knowing the distribution of the noise allows us to perform maximum likelihood decoding to deduce the original signal. Multiplicative noise, more popularly known as fading, arises due to various phenomena such as shadowing and multipath propagation resulting from multiple reflections, diffractions and scattering. Fading is well investigated for both single and multichannel reception and measures for combating the effects of fading are well documented in the literature (see [2]). The traditional approach to modeling additive noise in a communication system has been to represent it as a white Gaussian process. Such a model works sufficiently well when one considers the so-called *background* noise only that is assumed to be always present and is primarily attributed to thermal noise of the device itself or other electromagnetic phenomena that raises the noise floor during the entire duration of signal transmission. The popularity of the Gaussian distribution is primarily on account of the central limit theorem (CLT) in addition to several desirable analytical properties of the Gaussian distributions that lead to tractable linear equations. However, real world communication systems operate in the vicinity of a finite number of electromagnetic sources where the applicability of CLT may be questionable. Moreover, in various wireless and wireline communication systems transmission is affected not only by the omnipresent thermal noise which is faithfully modeled as an additive white Gaussian noise (AWGN) process, but also by impulsive noise which has a non-Gaussian behavior. For example, measurements and analysis reported in [3–8] have shown that the ambient noise experienced in wireless, wireline, and power line communication (PLC) systems and interference from co-channel and ultra-wideband (UWB) interferers exhibit a decidedly non-Gaussian behaviour. Sources of non-Gaussian noise include both natural phenomena such as atmospheric noise as well as man-made noise due to, for example,

neon lights, vehicular noise, microwave ovens and the like. Furthermore, often the very nature of the communication environment may lead to a possibility that the collective interference due to other users operating in the vicinity of a desired user is impulsive for example multiuser interference (MUI) in impulse radio (IR) Ultra Wideband (UWB) transmission or switching noise in powerline communication (PLC) channels. There is thus a compelling need to address the issue of degradation of communication systems by impulsive non-Gaussian noise.

A natural question that arises is that what does non-Gaussian noise do that makes the received signal more unreliable than for Gaussian noise. For now, we provide an intuitive explanation and resort to elaborate mathematical descriptions in the next section. Gaussian noise implies that the probability of relatively high magnitude noise in the system is extremely low (the probability of occurrence decays exponentially with squared magnitude). This is however, not true for certain noise environments where for the same average power, high amplitude noise may occur sporadically with a much higher probability than accounted for by a Gaussian distribution. In such cases therefore a signal may be highly distorted due to the high value noise and the overall high magnitude for the received signal seldom indicates a signal received with greater reliability.

1.1 Non-Gaussian Noise

Gaussian distribution has had phenomenal success in describing the behaviour of noise in various systems for over centuries due to its mathematically appealing properties such as form preservation under linear transformations, entropy maximization and minimization of Fisher information to name a few [9]. Mathematically, the Gaussian distribution may be expressed as

$$f(x) = \frac{1}{\sqrt{2\pi\sigma^2}} \exp\left(\frac{-x^2}{2\sigma^2}\right) \tag{1.1}$$

In spite of its immense popularity, estimators derived with a Gaussian assumption are non-robust[1]. In particular when a least squares like estimator that is derived from a Gaussian assumption is applied to a sequence of observations that may have outliers, the performance of the estimator degrades severely. The presence of outliers is what makes a distribution non-Gaussian and when a severe interference causes the same phenomena in communication systems, it is referred to as non-Gaussian noise. In this thesis, the qualifier non-Gaussian is used for any additive noise that cannot be described faithfully by the Gaussian distribution.

We next provide a brief description of various approaches to describing non-Gaussian noise in communication systems that have been employed for several communication environments. We would like to point out that we do not make an effort to be exhaustive in our description, however, the reader should get a fair idea of the popular models that have been proposed so far.

1.1.1 Mathematical Descriptions of Non-Gaussian Noise

In order to characterize the performance of communication systems one requires a mathematical model that, although an abstraction, would well describe the behaviour of the noise process. Several models have been developed by researchers that are motivated either by the statistical description of the overall process or the actual underlying physical phenomena that gives rise to the non-Gaussian nature of the noise. Throughout this thesis we focus only on univariate non-Gaussian distributions.

Middleton's Noise Models

Middleton's efforts [11–13] in characterizing the non-Gaussian behaviour of various electromagnetic phenomena that are experienced in communication environments is till date one of the most prominent (please see [13] for a contemporary discussion and the relation of Middleton's models to other non-Gaussian distributions). More specifically, Middleton proposed a canonical model of impulsive noise categorizing the

[1]Robustness in the statistical sense, implies the stability of systems when deviations from assumed model may occur [10].

noise distributions as Class A, B and C [13]. The classification is based on the temporal coherence of the noise process whereby for Class A noise the duration of the impulse noise (T_{impulse}) is greater than the inverse of the receiver bandwidth (f_{Rx}), i.e.,

$$T_{\text{impulse}} \gg \frac{1}{f_{\text{Rx}}} \tag{1.2}$$

The opposite is true for Class B noise, and Class C is a mixture of the Class A and Class B noise. Effectively, therefore, Class A noise is referred to as *narrowband* interference and Class B as *broadband* interference. Mathematically, the noise distribution is an infinite sum of weighted Gaussians depicted as follows

$$f(x) = \sum_{m=0}^{\infty} \underbrace{\frac{\exp(-A)A^m}{m!}}_{\text{weighting factor}} \exp\left(\frac{-x^2}{2\sigma_m^2}\right) \Big/ \sqrt{2\pi\sigma_m^2}. \tag{1.3}$$

The parameter A is referred to as the impulsive index and is the parameter that governs the frequency of occurrence of the impulses. A lower value of A ($\rightarrow 0$) indicates structured interference while a high value of A ($\rightarrow \infty$) makes the noise more Gaussian. The variances σ_m^2 are related to the physical parameters of the noise and are given by

$$\sigma_m^2 = \frac{(m/A) + \Gamma}{1 + \Gamma} \tag{1.4}$$

where Γ is the ratio of power of the Gaussian component to the impulsive component and thus is a measure of the strength of the impulsive noise. The appeal of this model derives from its good fit to various noise and interference measurements. Interestingly, it has been observed in several studies, foremost of them being [14], that usually the first $M(\leq 3)$ coefficients are sufficient to provide excellent approximations to the actual noise processes and thus the infinite sum in Eqn. (1.3) can be conveniently truncated to a finite value without loss in estimation quality.

Gaussian Mixture Noise

Gaussian mixture noise (GMN) is a versatile family of noise distributions and can often provide a very accurate description of noise in practical communication systems. It is very well suited to transmission environments where the variance of noise may vary

from symbol to symbol. Mathematically it is expressed as

$$f(x) = \sum_{i=1}^{M} w_i \mathcal{N}(\mu_i, \sigma_i^2), \tag{1.5}$$

where the sum of weights w_i equals 1 and $\mathcal{N}(\mu_i, \sigma_i)$ denotes a Gaussian distribution with mean μ_i and variance σ_i^2. As opposed to the Middleton model, the number of terms in a Gaussian mixture noise model is always finite and will ideally depend on the disparate sources of interference in the system. However, for modelling purposes often times M need not be any greater than 3 for most communication systems. In fact when the number of terms in the above model is restricted to two, one obtains the widely popular ϵ-contamination model, where the background noise with nominal variance σ_w^2 is prevalent $(1-\epsilon)$ fraction of the time and a high variance, $\kappa\sigma_w^2,\ \kappa \gg 1$ Gaussian noise dominates for rest of ϵ fraction of time. The overall distributions is thus

$$f(x) = (1-\epsilon)\mathcal{N}(\mu, \sigma_w^2) + \epsilon\mathcal{N}(\mu, \kappa\sigma_w^2). \tag{1.6}$$

Such a two-term noise model is often used to represent or approximate non-Gaussian impulse noise, e.g. [15–20].

Symmetric α-Stable Noise

The α-stable distribution is a family of distributions that can model various impulsive noise phenomenon and also Gaussian noise as a special case. However, it was not widely used up until the last decade primarily due to the lack of a closed form expression for the probability density function (pdf) and also because, other than the Gaussian case, these distributions have an infinite variance. Recently, however, it has been employed in several works [21–23] by applying the generalized central limit theorem that states that the limiting distribution of a sum of i.i.d random variables is an α-stable distribution. A univariate symmetrical α-stable (SαS) distribution is best described by its characteristic equation

$$\psi(t) = \exp(-\gamma|t|^{\alpha}) \tag{1.7}$$

where the parameter γ is referred to as the dispersion of the distribution and $0 < \alpha \leq 2$ is the characteristic exponent that defines the tail of the distribution function. For

example, $\alpha = 2$ gives us a Gaussian distribution and is the only value of α for which a closed form expression of the pdf exists. SαS modeling of the interference distribution has been shown to be suitable when the interferers are distributed according to a Poisson distribution [23].

Other than the models mentioned above, there are several univariate distributions that have been employed to describe non-Gaussian behaviour, such as Laplace, Cauchy and the Lévy distributions. These distributions can be classified under the general category of *heavy tailed* distributions. We refrain from providing detailed description of them as they have not been extensively used in this thesis[2].

1.2 Is Impulsive Noise Bad ?

It is well known that impulse noise is in general detrimental to communication system performance. It is described by a non-Gaussian distribution. However, we would like to comment on the fact that it is not the non-Gaussianity of the impulse noise per se that causes the degradation. In fact, from an information theoretic perspective, for an additive noise channel with output of the form

$$Y = X + N \tag{1.8}$$

where X is the channel input and N denotes the additive noise, the worst case noise (amongst all power-constrained noise distributions) is Gaussian noise[3] [24, 25]. It is perhaps a little counter-intuitive then that non-Gaussian noise is regarded as more damaging. The explanation lies in the design of most communication system and the assumptions made thereof. Most (if not all) communication system use a Euclidean-distance based decoder, which is optimal for a background noise that is Gaussian. However, such a decision metric will clearly be ill-suited for heavy tailed noise distributions where large magnitude of received symbols is more likely due to ambient noise than a favorable channel condition. The increasingly complex transmission environments in

[2]We will use some of the univariate distributions in Chapter 4 for which a brief description is provided in the chapter itself.

[3]This follows primarily from Burg's maximum entropy theorem for covariance constrained process (see [24, Chapter 11] for a proof).

which next generation devices are expected to coexist with other heterogeneous radio frequency (RF) devices, the Gaussian assumption may not apply.

1.3 Memory in Noise

An important aspect of impairments that is often neglected in design of communication systems is the memory in the noise. Memory may be present in both multiplicative noise, i.e., fading and in additive noise for example in partial response channels. The primary reason for neglecting noise memory in traditional communication system analysis is the assumption of the noise being AWGN. Also where the noise has a certain correlation, the use of an ideal interleaver is assumed that spreads the symbols before transmission with a corresponding de-interleaver being employed at the receiver that restores the original order of symbols. Such an interleaver spreads out consecutive symbols far enough for the effect of memory to be nullified and an analysis with an independent identically distributed (i.i.d) assumption is valid. However, as we see later in Chapters 2-5, memory may not always be neglected, as interleavers are seldom ideal and typically their lengths are limited by the acceptable delay in the channel. Also, if the structured behaviour of an impulsive interference signal is known, it is in fact a more favorable environment to transmit in, than one with white noise of similar average power, as potentially one may put all the transmitter energy in the regions where noise is absent and transmit nothing when impulsive interference is present. In absence of the interference we then have infinite transmission capacity while it is zero when it is present. However, this is only a theoretical abstraction as some background noise will always be present and practical communication channels will never be absolutely devoid of all noise. We will use this as the underlying basis for all work in this thesis and approach design problems with the assumption that both background Gaussian noise and *additional* impulsive interference may corrupt the transmitted signal. We will account for noise memory primarily by using a Markovian approach. While the details of such modeling will be provided in the respective chapters, we would like to mention that Markov modeling of memory is an immensely popular approach and often provides fundamental insights into the role that correlations play in asserting system

performance. A simple Markov model that has been has historically popular is the Gilbert-Elliot model [26–28] where the channel is assumed to be in two states, namely, good and bad, with fixed transition probabilities between the states. Transmission is assumed to occur without error in a good state while a bad state invariably leads to an error. While this is only an abstraction and deals with binary outputs only, we are interested in systems with non-binary outputs and will provide a related model in Chapter 2.

In the following sections, we will briefly review certain specific transmission environments that have been considered in this thesis. These transmission environments relate to contemporary techniques in communication that are being considered as viable approaches to increase system capacity in future communication system. The description provided below should provide the reader with adequate background in understanding the content of the remaining chapters of the thesis. The relation of the specific problems that we seek to address in each of the following areas will be made clear in the introductory material of each of the chapters.

1.4 Hierarchical Spectrum Sharing

Historically, frequency bandwidth has been considered a scarce resource. In recent years, the dramatic surge in demand for bandwidth has led to innovators and governments re-evaluating the ways in which communication bandwidth is regulated in order to accommodate more users. In almost all parts of the world non-military frequency bands are allocated to operators for exclusive use, thus leading to the nomenclature of *fixed* or *licensed* spectral allocation. This implies that it is illegal to transmit in a frequency band if it is not owned by the transmitting entity. This is set to change as a radical new approach to spectrum sharing is gaining ground with both academics and wireless operators. This new approach is called *dynamic spectral access* (DSA) and one of the most favored approaches to DSA advocates creating hierarchies amongst users in terms of their rights to transmit. More specifically, *primary* users of a band will have the right to transmit at will and all other users will need to stop transmitting when

the primary user of the band is active. On the other hand, the pool of *secondary* users get to transmit when the band is idle. Such prioritized access to frequency bands is made possible by what is termed, rather intuitively, cognitive radio. Secondary users should be able to sense and learn their RF environment and ensure that they will not interfere with ongoing primary transmissions, if they were to transmit. While conceptually simple, actual implementation of a coexisting hierarchical network calls for strong and efficient interference management techniques [29]. In fact, the rules for spectral access only provide guidelines for interference avoidance which in itself is not adequate to ensure that mutual interference between primary and secondary networks do not occur. This can be primarily attributed to the lack of perfect power control in heterogeneous networks and the multipath nature of wireless transmissions. While empty spectral regions are referred to as white spaces in contrast to occupied spectrum being referred to as black, it has been found that there are is also abundant spectral space that is termed *gray*. Gray spaces refer to those spectral bands where the signals are too weak to be decodable and yet can cause considerable degradation in transmitted signals [29]. Stochastic models developed to characterize interference due to spurious transmissions in a cognitive environment have shown that such distributions can often be heavy-tailed [30]. So far however, little has been said about the ability of receivers to employ adequate signal processing to retrieve signals that are interfered. By applying intelligent processing at receivers one can very well ensure that successful transmissions occur in gray spaces and in some cases also in black spaces, i.e., in the presence of high levels of interference in the band. This facilitates a fair share of transmission opportunities for the so called secondary users. The viability of such transmission schemes is important from a commercial perspective as well. Since secondary users will also be charged a fee for using the band, albeit much lesser than a primary user, we need to ensure that secondary users get adequate opportunities to transmit to make it worth their money. For obvious reasons, stringent control of interference is required to protect a primary user but at the same time if those measures could be relaxed by using better interference mitigation techniques it would hugely benefit the total throughput of the system, which is the ultimate objective. We provide further elaboration on the

associated issues in Chapter 3.

1.5 Impulse Radio Ultra Wideband (IR-UWB)

Ultra-wideband (UWB) technology affords highly appealing features such as low-power transmission, high multipath resolution, and the unlicensed use of the frequency range from 3.1 GHz to 10.6 GHz (in USA for example). We will briefly introduce here the IR-UWB technology that has recently been hailed as a promising candidate for low power transmission of data over short distances. IR-UWB finds use in a range of applications from networking of heterogeneous devices in a home/office environment to sensor networks [31] for data aggregation and control. Essentially, impulse radio (IR) implies that transmission of data occurs through pulses of very short duration (of the order of nanoseconds) or *impulses* [32]. Naturally, if an RF signal has a very short duration it has a relatively wide spread in frequency and hence the qualifier *ultra wideband* is apt. IR avoids the need for frequency up-conversion, i.e., it is a carrier-less transmission technology. While at the outset this attribute may suggest that low cost transceivers are conceivable, the uniqueness of IR technology brings along several design challenges. For example, conventional design for coherent IR transmission requires very fast analog-to-digital converters and hence the current impetus has mostly been on low data rate IR-UWB technologies. Furthermore, the spread of energy over a bandwidth of several GHz implies limited radiated power is available for RF front-end functionalities such as signal acquisition. Reception may be further marred by the operation of several narrowband interferers in the frequency bands of operation of the IR.

IR by itself has several attributes that make it particularly attractive as a transmission technology primary amongst them being its high multipath resolution abilities. The short duration of the impulse makes possible a resolution accuracy of the order of nanoseconds implying that the effect of multipath fading may be handled very efficiently at the receiver and this has positive implications on the accuracy of positioning and tracking applications. The low duty cycle of the pulse, i.e., $T_p \ll T_s$, where T_p is the pulse duration and T_s is the baud rate/symbol duration of the transmission system, im-

plies that time-hopping may readily be used to accommodate multiple users. However, initial research [32, 33] failed to account for characteristics of the MUI that manifests when only few UWB devices are operational. Recent research that has accounted for the nature of the interference in IR-UWB [34] has found Gaussian distribution to be inadequate in describing the behaviour of the MUI and thus performance results obtained through such an assumption will lead to aberrant results. This calls for receiver designs that take into account the true statistical characteristics of the MUI and will be the focus of Chapter 4.

1.6 Diversity through Cooperation

Diversity techniques have been known to increase the overall quality of transmission in fading communication channels since the 1950s. They improve the link signal to noise ratio (SNR) by taking advantage of the multipath characteristics of the fading channels whereby multiple copies of the same signal are received through different paths between a source and destination. However, one of the requirements in taking advantage of such techniques is the ability to use multiple antennas at the terminals. Since user terminals may be limited in their ability to host multiple antennas due to device form factors, the idea of cooperation amongst terminals to extend the benefits of diversity to such systems has gained popularity in the recent past [35, 36]. The basic idea is to use intermediate nodes, known as *relays*, between a given source and destination terminal to retransmit the signal to the destination such that an independent copy of the signal is received over the relay-destination link. Ideally, the relays would be chosen such as to increase the signal power at the destination with no increase in the noise power (as they are uncorrelated), effectively increasing the link SNR. Performance analysis through a cooperative approach, as mentioned above, has therefore gained a lot of attention and several protocols have also been proposed that differ in, for example, scheduling of transmission, processing at the relays and also selection of relays. Due to the multiple entities involved in the scheme, a high level of coordination may be required to ensure that the predicted performance benefits are realized in practice. Nonetheless, the possibility of substantial performance gains through cooperative techniques has led

to several task groups within IEEE 802 standards committee to consider its inclusion as a part of the specification for future wireless systems.

1.7 Contributions of the Thesis

The unifying theme of this thesis is decoding and analysis in the presence of noise and interference that has an overall non-Gaussian distribution. It has been our endeavour to relate the proposed techniques to contemporary communication technologies by considering specific transmission attributes of these technologies. We make the following contributions

- *Decoding in Non-Gaussian Noise with Memory*: We first study the performance of a generic convolutionally coded system in an impulsive non-Gaussian environment and propose several decoding approaches that are suitable for implementation using a Viterbi decoder at the receiver. Moreover, temporal correlation in noise is considered by modeling it as a first-order Markov chain. The effect of such correlation with non-ideal channel interleaving is explicitly accounted for. Incorporating the interleaving depth (ILD) as a design parameter, analytical and semi-analytical expressions are derived to evaluate the cutoff rates and error rates associated with the decoding metrics. These expressions are shown to be an excellent match to results obtained from system level simulation and thus are very useful for characterizing system performance with explicit consideration of correlation effects. Finally, using the analytical developments of the chapter, we characterize the performance of narrow-band powerline channel as an example of a real-life transmission medium where a Markov-Gaussian noise model has been shown to faithfully describe the associated noise.

- *Joint Sensing and Suppression for Cognitive Transmission*: A joint sensing and suppression algorithm is developed to facilitate the active mitigation of interference at a primary user to protect it from spurious transmission such that secondary transmitters are provided with greater opportunities to transmit. The algorithm works in a non-data aided fashion and thus does not lead to band-

width inefficiencies. A significant improvement in error performance is achieved by applying the proposed algorithms and it is shown that estimation of noise state is highly beneficial when apriori information of its statistical properties is unavailable.

- *Multiuser Interference Mitigation in UWB Systems*: Our contribution to mitigation of MUI for IR-UWB systems is three-fold. First, novel receivers that are very well suited to a multi-user IR-UWB environment are proposed and are shown to perform substantially better or at par with previously proposed solutions. Secondly, semi-analytical techniques to characterize the performance of the proposed receiver designs are derived by taking the attributes of IR-UWB transmission into account. More specifically, we derive three expressions, which invoke different assumptions about the MUI that corrects previously derived results. Finally, since several of the proposed receivers are based on parametric detectors, the feasibility of rendering these detectors non-parametric by selection of an optimum parameter value is investigated.

- *Cooperation through Selection in Presence of Interference*: We characterize the performance of relay selection schemes when there is interference in the source-relay link. Two algorithms, namely NBR-ONE and NBR-WFT that warrant different levels of overheads are proposed for a Markovian interference environment. In particular NBR-WFT takes advantage of the memory in the interference to reduce the overheads substantially. An analytical treatment of the proposed algorithms is also provided to determine the outage probability and average BER. These analytical expressions are subsequently used to characterize the effects of the various associated parameters.

1.8 Organization of the Thesis

The rest of this thesis is organized as follows. In Chapter 2, we consider a convolutionally coded system where the ambient noise is impulsive and has memory that is modeled as first order Markov chain. Several new metrics are proposed for efficient

decoding in a transmission environment with impulsive noise, that lends *robustness* to the receiver. An analytical treatment of the system then follows that has the unique feature of incorporating the effect of non-ideal interleaving on system performance.

Chapter 3 considers interference mitigation through suppression for a cognitive radio environment that works in tandem with energy detection based sensing. We provide an elaborate description of a novel algorithm that can estimate noise state and power assuming availability of varying levels of information about the noise distribution. The algorithm involves an iterative refinement in the estimates of the noise and information bits through application of expectation-maximization principles. The quality of estimation is evaluated for several interference scenarios and is benchmarked against standard decoding approaches. The implications of memory on the estimation process is also studied from a mutual information transfer perspective.

Chapter 4 focuses on multi-user interference mitigation in IR-UWB systems wherein the distribution of the MUI is impulsive owing to the short duty cycle and random time hopping characteristic of the transmitted pulse. The need for robust detection in such environments is motivated and the applicability of detectors that account for the impulsive nature of the MUI is illustrated. This is followed by development of analytical approaches to BER evaluation in such environments that aid in the optimization of parameters of the proposed detectors.

In Chapter 5 we consider relay selection for cooperative transmission in the presence of interference. We show that when not accounted for, the state of the relay with respect to interference can render the conventional selection algorithms fairly ineffective and better solutions are called for. We propose algorithms that use order statistics of participating relays to provide substantially improved performance even in the presence of strong interference. Since, modifications to the original algorithm entails overheads, we quantify the same and suggest techniques to reduce it to acceptable levels. We also characterize the performance of the proposed algorithms through analytical techniques accounting for the multi-terminal nature of the system.

Finally Chapter 6, provides a brief summary of the thesis and the major outcomes of the work done. We also suggest ways to extend and build upon the work presented in this thesis.

CHAPTER 2

Transmission over non-Gaussian Channels with Memory

As mentioned in the previous chapter, the aggregate interference at the receiver for various practical communication channels can often deviate markedly from the classical AWGN assumption due to a multitude of reasons. Likewise, the assumption of a memoryless noise process is not valid for many transmission scenarios, cf. e.g., [7,37,38] (and references therein) for PLC, UWB, and wireless transmission under partial-time jamming, when delay constraints prevent the use of practically infinite-depth (ideal) interleaving. While a deviation from Gaussianity and the presence of memory in the noise process is beneficial in terms of an increase in channel capacity, systems based on conventional matched-filter receivers and decoding that assumes memoryless disturbance,

experience a considerable performance degradation in environments with non-Gaussian noise with memory. Although there exists a considerable body of literature on coding and decoding over non-Gaussian channels, non-Gaussian noise channels with memory in particular have received very little attention. The reasons for this may be traced to the facts that several of the previous works have (i) limited themselves to independent and identically distributed (i.i.d.), i.e., perfectly interleaved noise [16, 18, 39, 40], (ii) assumed perfect knowledge of the noise statistics at the receiver [39–41], or (iii) considered a specific (optimal or suboptimal) decoding metric [39–42], to either simplify the receiver design or to keep the analysis mathematically tractable.

In this Chapter, we study coded transmission for bursty impulse noise channels. More specifically, we model the impulsive noise using the two-term Gaussian mixture introduced in the Chapter 1 as a first-order noise distribution to model the overall non-Gaussian impairment. Furthermore, the memory in the non-Gaussian noise process is modelled by a two-state Markov chain to describe the sequence of noise variances. We thus apply a Markovian-Gaussian channel whose underlying state process is the same as in the Gilbert-Elliot channe,l which has been widely used to model burst noise channels, e.g. in [38] for jamming, in [37] for UWB interference, and in [41] for bursty noise in PLC. To put things into perspective we would like to point out that different from [26–28, 42, 43], that also consider a Gilbert-Elliot type channel, we consider non-binary channel outputs.

Thus the two aspects that we seek to address here are impulsiveness and memory. Considering a convolutionally coded system that uses a standard Viterbi decoder at the receiver, we first propose and compare several decoding metrics that are well suited to coded transmission over Markovian-Gaussian channels without assuming perfect knowledge of noise state or statistics. Moreover, by deviating from the approach of neglecting noise memory, we extend the work in the aforementioned papers by explicitly incorporating the effect of finite interleaving on overall system performance. The metrics presented include two novel metrics, which are appealing in that they require minimal knowledge about the noise statistics. While we do not attempt to modify the sequence-

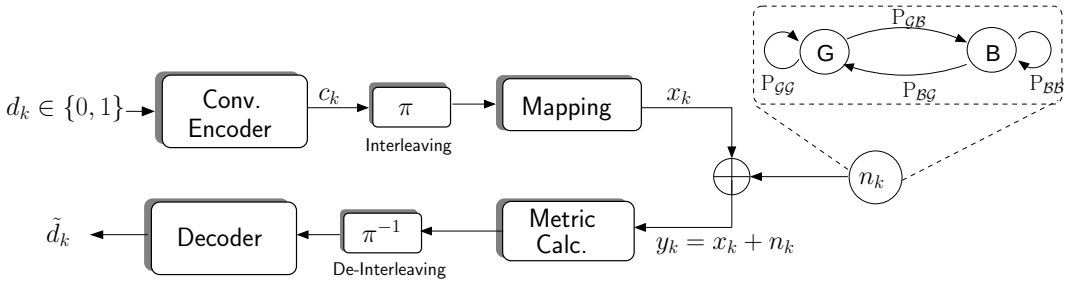

Figure 2.1 — System Model for the overall transmission and reception modules. The *robust* metrics are implemented by the metric calculation module and then the adequately penalized metrics are used by the decoder to produce bit decisions.

detection Viterbi decoder to exploit channel memory, our analysis also includes metrics based on noise-state information, which in practice would necessitate the use of a state estimator, cf. e.g. [26, 38, 44].

Chapter Organization: The remainder of this chapter is organized as follows. Section 2.1 introduces the transceiver structure and the noise model. In Section 2.2 the decoding metrics suitable to cope with non-Gaussian noise are presented. Section 2.3 is devoted to the theoretical performance analysis when applying the considered decoding metrics. Numerical and simulations results for the 2-state Markov-Gaussian noise are presented and discussed in Section 2.4, following which we consider the application of the methods developed in Section 2.3 to a multi-state Markov noise as applied to communication over a powerline channel in Section 2.5. Finally, some conclusions are offered in Section 2.6.

The following notation is used. $\Pr\{\cdot\}$ and $\mathcal{E}\{\cdot\}$ denote the probability of an event and statistical expectation, respectively. $\Re\{\cdot\}$ and $\Im\{\cdot\}$ are the real and imaginary part of a complex number. $Q(x) = 1/\sqrt{2\pi}\int_x^\infty \mathrm{e}^{-t^2/2}\mathrm{d}t$ is the Gaussian Q-function.

2.1 System Model

We consider the use of convolutional coding at the transmitter and Viterbi decoding at the receiver, which is still the most popular configuration in wireless communications. Figure 2.1 shows the structure and components of the overall coded transmission

system. In the following, we provide a brief description of transmitter and receiver operations and the noise model.

2.1.1 Transmitter

Information bits $d_k \in \{0,1\}$ ($k \in \mathbb{Z}$ is the discrete-time index) are emitted by a source with uniform probability and encoded by a binary rate-k_c/n_c convolutional encoder to produce coded bits c_k. The coded bits are interleaved and then mapped to binary phase-shift keying (BPSK) symbols by the mapper to generate transmit symbols $x_k \in \{-1,1\}$. A regular block interleaver with I rows and I_c columns is assumed, such that the encoder and the interleaver outputs (see Figure 2.1) are related via

$$c^{\pi}_{(jI+i)} = c_{(iI_c+j)} \quad 0 \leq i < I \ , 0 \leq j < I_c \ . \tag{2.1}$$

2.1.2 Channel and Receiver

The channel is assumed to be non-frequency selective and non-fading, i.e., we consider narrowband transmission with stationary or slowly mobile devices (e.g. [16, 19, 38]). [1] The equivalent discrete-time representation of the received symbol after filtering and sampling is given by

$$r_k = x_k + n_k \ , \tag{2.2}$$

where n_k are samples of the noise process, a detailed description of which is provided in the following section. The received samples r_k are subsequently used to compute decision metrics that are de-interleaved and passed to the Viterbi decoder. The decoding is discussed in detail in Section 2.2.

2.1.3 Markov Modulated Non-Binary Noise

We consider the noise term n_k to be the additive superposition of two terms, w_k and $b_k i_k$, where w_k and i_k are zero-mean Gaussian distributed and b_k is a $\{0/1\}$-random

[1] While low mobility is a faithful model for many communication applications, the assumption of a flat channel is also made for analytical tractability, as in e.g. [19]. The extension to frequency-selective fading would need to consider equalizer structures such as those in [45] together with coding/decoding, which is beyond the scope of this work.

variable. The motivation for such a model stems from the fact that while w_k represents the AWGN, $w_k + i_k$ describes the AWGN plus interference either from other users or from ambient phenomena. The former *state* is referred to as the good ($s_k = \mathcal{G} \Leftrightarrow b_k = 0$) state, and the latter as the bad ($s_k = \mathcal{B} \Leftrightarrow b_k = 1$) state. Conditioning on the noise state we can express the noise probability density function (pdf) by

$$p_s(n) = \exp\left(-|n|^2/(2\sigma_s^2)\right) / \left|\sqrt{2\pi}\sigma_s\right|^d , \tag{2.3}$$

where $d = 1$ for real-valued baseband transmission and $d = 2$ for complex-valued baseband transmission, and $s \in \mathcal{S} \triangleq \{\mathcal{G}, \mathcal{B}\}$. The noise variances are given by $\sigma_{\mathcal{G}}^2 = \sigma_w^2$ and $\sigma_{\mathcal{B}}^2 = \sigma_w^2 + \sigma_i^2$, and σ_w^2 and σ_i^2 are the variances of w_k and i_k per *real* dimension. For future reference we define the parameter $\kappa \triangleq \sigma_{\mathcal{B}}^2/\sigma_{\mathcal{G}}^2 = 1 + \sigma_i^2/\sigma_w^2$, which is indicative of the strength of the interference component compared to the thermal noise. Denoting the probability of being in the bad and good state by $\mathrm{P}_{\mathcal{B}} \triangleq \Pr\{s_k = \mathcal{B}\}$ and $\mathrm{P}_{\mathcal{G}} \triangleq \Pr\{s_k = \mathcal{G}\} = 1 - \mathrm{P}_{\mathcal{B}}$, the noise pdf is given by

$$p(n) = \mathrm{P}_{\mathcal{G}} p_{\mathcal{G}}(n) + \mathrm{P}_{\mathcal{B}} p_{\mathcal{B}}(n) . \tag{2.4}$$

This two-term noise model has been used in e.g. [15–20] and it is also a good approximation of Middleton's Class-A noise model [11, 40, 46]. The parallel treatment of real- and complex-valued baseband transmission in this chapter is (i) practically relevant as BPSK (or BPSK-type) transmission is also often used for carrier-based systems and (ii) allows us to compare the differences with the case of AWGN.

In the literature often ideal interleaving and thus independent noise samples are assumed, whereby (2.4) fully characterizes the noise model. However, the independence assumption may be invalid for typical finite-size interleavers. We therefore employ a first-order two-state Markov model to describe the sequence of noise states s_k. The Markov chain is assumed to be irreducible, aperiodic, and stationary with transition matrix

$$\mathcal{T} = \begin{bmatrix} \Pr\{s_k = \mathcal{G} | s_{k-1} = \mathcal{G}\} & \Pr\{s_k = \mathcal{B} | s_{k-1} = \mathcal{G}\} \\ \Pr\{s_k = \mathcal{G} | s_{k-1} = \mathcal{B}\} & \Pr\{s_k = \mathcal{B} | s_{k-1} = \mathcal{B}\} \end{bmatrix} \triangleq \begin{bmatrix} \mathrm{P}_{\mathcal{GG}} & \mathrm{P}_{\mathcal{GB}} \\ \mathrm{P}_{\mathcal{BG}} & \mathrm{P}_{\mathcal{BB}} \end{bmatrix} . \tag{2.5}$$

Since $\mathcal{T}$ is row-stochastic, two parameters, e.g., $\mathrm{P}_{\mathcal{GG}}$ and $\mathrm{P}_{\mathcal{BB}}$ fully describe the state

process. Furthermore, we have for the stationary distribution $\mathrm{P}_{\mathcal{G}} = (1 - \mathrm{P}_{\mathcal{BB}})/(2 - \mathrm{P}_{\mathcal{GG}} - \mathrm{P}_{\mathcal{BB}})$.

2.2 Decoding in Non-Gaussian Noise

We consider conventional Viterbi decoding [47] in the log-likelihood domain performing add-compare-select (ACS) operations and thus the path metric is the sum of branch (bit) metrics. Since the Euclidean-distance metric is not optimal anymore, in the following we present a number of different bit-metric formulations which are apt for decoding in non-Gaussian noise. As mentioned earlier, we do not attempt to modify the widely implemented ACS Viterbi decoder architecture, but only the computation of bit metrics. Hence, we do not pursue the explicit use of the memory of the noise process for noise state estimation. However, our framework allows us to include bit metrics assuming knowledge of the instantaneous noise state, which enables a more comprehensive comparison and provides performance limits.

2.2.1 Euclidean Distance Soft Decision Decoder (EDSD)

We start with the classical Euclidean-distance metric for the trial symbol $\tilde{x}_k$ at time k given the received sample r_k, which reads

$$\lambda(\tilde{x}_k | r_k) = -|r_k - \tilde{x}_k|^2 \tag{2.6}$$

and is employed by a Viterbi decoder designed for AWGN at the receiver. This metric formulation is oblivious to the presence of impulse noise and will mainly serve to benchmark the performance of other decoding metrics that are described in the following.

2.2.2 Known State Maximum Likelihood Decoder (KSMLD)

At the other end of the performance-complexity spectrum is the decoder that has perfect knowledge of the instantaneous noise state s_k and the pdf parameters, i.e., the pdf given by Eq. (2.3) is applied. The performance of such an idealized setting could be approached with a decision-feedback-aided state estimator [26] or an expectation-

maximization (EM) algorithm as described in [38][2]. The KSMLD branch metric is given by

$$\lambda(\tilde{x}_k|r_k, s_k, \sigma^2_{s_k}) = -|r_k - \tilde{x}_k|^2/(2\sigma^2_{s_k}) \ . \tag{2.7}$$

2.2.3 Memoryless Maximum Likelihood Decoder (MSMLD)

When the receiver is only aware of an impulsive component in the noise but is oblivious to any correlations in the noise and thus only considers the first-order statistics, the decoder uses the log-likelihood function

$$\lambda(\tilde{x}_k|r_k, \boldsymbol{\theta}) = \log(p(r_k - \tilde{x}_k)) \tag{2.8}$$

as branch metric, where $p(n)$ is given by Eq. (2.4). As can be seen from (2.8), the MSMLD requires knowledge of the noise parameters $\boldsymbol{\theta} = [\mathrm{P}_{\mathcal{G}}, \sigma^2_{\mathcal{G}}, \sigma^2_{\mathcal{B}}]$. Such a decoder has often been considered for i.i.d. non-Gaussian noise, cf. e.g. [16, 39, 40]. A useful simplification of this metric is obtained from the "max-log" approximation

$$\lambda(\tilde{x}_k|r_k, \boldsymbol{\theta}) = \max_{s\in\mathcal{S}} \{\log\left[\mathrm{P}_{\mathcal{S}} p_s(r_k - \tilde{x}_k)\right]\} \ , \tag{2.9}$$

which will be considered in the following.

2.2.4 Erasure Marking Decoder (EMD)

A simpler and thus perhaps more practical alternative to combat impulse noise is Viterbi decoding with erasure marking [44, 48]. Erasure marking could be performed before decoding or by the joint erasure marking and decoding technique developed in [44]. As an approximation of these types of decoders, we consider an ideal erasure decoder whose decoding metric is given by

$$\lambda(\tilde{x}_k|r_k, s_k) = \begin{cases} -|r_k - \tilde{x}_k|^2 \ , & \text{if } s_k = \mathcal{G}, \\ 0 & \text{if } s_k = \mathcal{B}. \end{cases} \tag{2.10}$$

As we see later, although simple, such an approach leads to an error floor for the considered transceiver.

[2]We will consider the design of such an estimator in Chapter 3 where varying levels of information about the channel state will be assumed at the

2.2.5 Huber Penalty Function Decoder (HPFD)

We now proceed with two novel bit metrics for Viterbi decoding in non-Gaussian noise. The first metric is adopted from the robust multiuser-detector design in [18] and applies Huber's penalty function (cf. [18, Eq. (33)]):

$$\lambda(\tilde{x}_k|r_k,\sigma_n^2,\xi) = \begin{cases} \dfrac{-|r_k-\tilde{x}_k|^2}{2\sigma_n^2}, & \text{if } |r_k-\tilde{x}_k| \le \xi\sigma_n^2, \\ \dfrac{\xi^2\sigma_n^2}{2} - \xi|r_k-\tilde{x}_k|, & \text{if } |r_k-\tilde{x}_k| > \xi\sigma_n^2, \end{cases} \tag{2.11}$$

where $\sigma_n^2 \triangleq \mathrm{P}_{\mathcal{G}}\sigma_{\mathcal{G}}^2 + \mathrm{P}_{\mathcal{B}}\sigma_{\mathcal{B}}^2$ is the average noise variance and ξ is the metric parameter.

2.2.6 α-Penalty Function Decoder (α-PFD)

The second new metric is based on the so-called α-detector devised in [49], again for multiuser detection. The corresponding branch metric reads

$$\lambda(\tilde{x}_k|r_k,\alpha) = \frac{1}{2\alpha}\mathrm{e}^{-\alpha|r_k-\tilde{x}_k|^2}\ , \quad \alpha > 0\ . \tag{2.12}$$

We note that the α-PFD metric tends to the Euclidean-distance metric for $\alpha \to 0$ [49, Eq. (9)].

The α-PFD has the unique advantage of the bit metrics being determined by adjusting just a single parameter, α. Similarly, the HPFD does not require knowledge of the mixture noise parameters, but only of the average noise variance σ_n^2, and ξ needs to be adjusted. Hence, these two metrics are particularly attractive alternatives to the more extreme cases of (i) not exploiting the non-Gaussian noise behavior at all (EDSD) and (ii) relying on the knowledge of the first-order statistic (MSMLD) or even the noise state (KSMLD, EMD).

2.3 Theoretical Analysis

In this section, we derive expressions for the bit-error rate (BER) and cutoff rate achievable with the decoding metrics introduced above, based on which we are able to compare their suitability for decoding in non-Gaussian noise. Our analysis draws significant practical relevance from the fact that we explicitly take the effect of finite

interleaving into account. To this end, we first specify the effective noise process including interleaving in Section 2.3.1. Then, the general approach to the analytical evaluation is presented in Section 2.3.2, while the specific expressions for the different decoding metrics are derived in Section 2.3.3.

2.3.1 Analysis for Markovian Noise and Finite Interleaving

We consider a block interleaver with dimensions $I \times I_c$ (see Section 2.1.1), which is typically dependent on the maximal transmission delay acceptable for the communication system. We make the usual assumption that I_c is much larger than the decoder constraint length measured in terms of number of code symbols. Therefore, it suffices to consider the number of rows I, also referred to as the interleaver depth, and we can conveniently incorporate the interleaver-deinterleaver operation into the noise process by replacing the state transition matrix $\mathcal{T}$ from (2.5) with the I-step transition matrix

$$\begin{aligned}\mathcal{T}^I &\triangleq \begin{bmatrix} \mathrm{P}_{I,\mathcal{GG}} & \mathrm{P}_{I,\mathcal{GB}} \\ \mathrm{P}_{I,\mathcal{BG}} & \mathrm{P}_{I,\mathcal{BB}} \end{bmatrix}. \\ &= \begin{bmatrix} \mathrm{P}_{\mathcal{G}} & \mathrm{P}_{\mathcal{B}} \\ \mathrm{P}_{\mathcal{G}} & \mathrm{P}_{\mathcal{B}} \end{bmatrix} + \mu^I \begin{bmatrix} \mathrm{P}_{\mathcal{B}} & -\mathrm{P}_{\mathcal{B}} \\ -\mathrm{P}_{\mathcal{G}} & \mathrm{P}_{\mathcal{G}} \end{bmatrix}, \end{aligned} \tag{2.13}$$

where

$$\mu = (1 - \mathrm{P}_{\mathcal{BG}} - \mathrm{P}_{\mathcal{GB}}) = (1 - \mathrm{P}_{\mathcal{BG}}/\mathrm{P}_{\mathcal{G}}), \quad (|\mu| < 1) \tag{2.14}$$

is the second eigenvalue of $\mathcal{T}$. Clearly, μ determines the performance as function of I, and it has been referred to as channel memory in [26]. Furthermore, μ^I can be approximated by

$$\mu^I \approx 1 - (\mathrm{P}_{\mathcal{BG}} I/\mathrm{P}_{\mathcal{G}}) \triangleq 1 - I/(\bar{\mathcal{D}}_{\mathcal{B}}\mathrm{P}_{\mathcal{G}}) \tag{2.15}$$

if $\mathrm{P}_{\mathcal{BG}}/\mathrm{P}_{\mathcal{G}} \ll 1$, where $\bar{\mathcal{D}}_{\mathcal{B}} = 1/\mathrm{P}_{\mathcal{BG}}$ is the average time spent in the bad state (average burst length). Hence, for given stationary probabilities, a first order approximation would be to choose the interleaver depth proportional to $\bar{\mathcal{D}}_{\mathcal{B}}$ to sufficiently disperse error bursts. We will consider the applicability of this design guideline in Section 2.4.

2.3.2 Performance Measures

As widely accepted performance yardsticks for convolutionally coded transmission we consider (i) the BER for given codes and (ii) the computational cutoff rate for ensembles of codes [47].

Bit-error Rate (BER)

Since we have a linear coding and modulation scheme and an output symmetric channel, it suffices to consider the all-zero word as the transmitted code word. As commonly done for convolutional coded systems [47, Section 4.4], we invoke the union bound to approximate the BER. There are two significant differences here with respect to the case of memoryless noise. First, the pairwise error probability is not only a function of the Hamming weight d of the error event, but also of the number of bad, $n_{\mathcal{B}}$, and good, $n_{\mathcal{G}} = (d - n_{\mathcal{B}})$, noise states occurring during the event. Secondly, the probability of an error event $\boldsymbol{e} = [e_1, e_2, \ldots]$ with Hamming weight $d_{\mathrm{H}}(\boldsymbol{e})$ depends on the error positions $\boldsymbol{p}(\boldsymbol{e}) = [p_1, \ldots, p_{d_{\mathrm{H}}(\boldsymbol{e})}]$, where $e_{p_i} = 1$, through the probability of noise-state sequences $\Pr\{\boldsymbol{s}|\boldsymbol{d}(\boldsymbol{e})\}$. This leads us to the union bound on the BER as

$$P_b \leq (1/k_c) \sum_{d \geq d_{\mathrm{free}}} \sum_{n_{\mathcal{B}}=0}^{d} \mathrm{PEP}(d, n_{\mathcal{B}}) \Upsilon(d, n_{\mathcal{B}}) \;, \tag{2.16}$$

where d_{free} denotes the free distance of the code, $\mathrm{PEP}(d, n_{\mathcal{B}})$ is the pairwise error probability (PEP) between the all-zero word and a code word with Hamming weight d given $n_{\mathcal{B}}$ bad and $(d - n_{\mathcal{B}})$ good noise states, respectively, and

$$\Upsilon(d, n_{\mathcal{B}}) = \sum_{\{\boldsymbol{e} \in \mathcal{V} | d_{\mathrm{H}}(\boldsymbol{e}) = d\}} W(\boldsymbol{e}) \sum_{\boldsymbol{s} \in \mathcal{S}^d_{n_{\mathcal{B}}}} \Pr\{\boldsymbol{s}|\boldsymbol{d}(\boldsymbol{e})\} \;. \tag{2.17}$$

In (2.17), $\mathcal{V}$ denotes the set of first event error vectors, $W(\boldsymbol{e})$ denotes the input weight for the error event $\boldsymbol{e}$ and $\mathcal{S}^d_{n_{\mathcal{B}}}$ is the set of noise-state vectors of length d with $n_{\mathcal{B}}$ bad states. The probability of the state sequence $\boldsymbol{s}$ is given by

$$\Pr\{\boldsymbol{s}|\boldsymbol{p}(\boldsymbol{e})\} = \Pr\{s_{p_1}\} \prod_{i=2}^{d_{\mathrm{H}}(\boldsymbol{e})} \mathrm{P}_{s_{p_{i-1}} s_{p_i}}^{((p_i - p_{i-1})I)} \;, \tag{2.18}$$

in which $\mathrm{P}_{s_{p_{i-1}} s_{p_i}}^{((p_i-p_{i-1})I)}$ are the transition probabilities according to the state transition matrix $\boldsymbol{T}^{(p_i-p_{i-1})I}$. In the evaluation of $\Upsilon(d, n_{\mathcal{B}})$ we take advantage of the generating series approach developed in [43] for finite state channels. The method of [43] however, requires adaptation for our case as [43] uses a binary-output channel model. More specifically, we decompose $\boldsymbol{T}^I$ into $\boldsymbol{P}(0) + \boldsymbol{P}(1) = \boldsymbol{T}^I$, where the first column of $\boldsymbol{P}(0)$ and the second column of $\boldsymbol{P}(1)$ are zero, which corresponds to the analogous definitions in [43, Eqs. (2), (3)]. We then have that $\Upsilon(d, n_{\mathcal{B}})$ is the coefficient of $y^d \omega^{n_{\mathcal{B}}}$ in the power series $\frac{\partial \mathcal{T}(\omega,x,y)}{\partial x}\big|_{x=1}$, where $\mathcal{T}(\omega, x, y)$ is referred to as the generating series for the probability of error patterns and expressed in [43, Eq. (18)] with explicit dependence on $\boldsymbol{P}(0)$ and $\boldsymbol{P}(1)$.

A commonly used BER approximation is obtained when only the dominant error events in the union bound, i.e., the error events whose Hamming weight d_{H} does not exceed an upper limit $d_{\mathrm{H,max}}$, are considered. The computation of the corresponding truncated series $\mathcal{T}(n_{\mathcal{B}}, x, d)$ can be done as described in [43, Section III.A]. Furthermore, since

$$\Upsilon(d, n_{\mathcal{B}}) \overset{I\to\infty}{=} \binom{d}{n_{\mathcal{B}}} P_{\mathcal{B}}^{n_{\mathcal{B}}} P_{\mathcal{G}}^{(d-n_{\mathcal{B}})} \sum_{\{\boldsymbol{e}\in\mathcal{V} | d_{\mathrm{H}}(\boldsymbol{e})=d\}} W(\boldsymbol{e}) \triangleq \binom{d}{n_{\mathcal{B}}} P_{\mathcal{B}}^{n_{\mathcal{B}}} P_{\mathcal{G}}^{(d-n_{\mathcal{B}})} W(d) \,, \tag{2.19}$$

we only need the regular distance spectrum $W(d)$ of the code for the case of ideal interleaving.

The PEP in (2.16) can be written as $\mathrm{PEP}(d, n_{\mathcal{B}}) = \Pr\{\Delta(d, n_{\mathcal{B}}) < 0\}$, where

$$\Delta(d, n_{\mathcal{B}}) \triangleq \sum_{i=1}^{n_{\mathcal{B}}} \delta_{i|\mathcal{B}} + \sum_{i=n_{\mathcal{B}}+1}^{d} \delta_{i|\mathcal{G}} \,, \quad \delta_{i|s} \triangleq [\lambda(\tilde{x}_i = +1) - \lambda(\tilde{x}_i = -1) | s_i = s] \,, \tag{2.20}$$

and $\lambda(\tilde{x}_i)$ are the bit-metrics presented in Section 2.2. In case of EDSD, KSMLD, and EMD metrics, (2.20) and thus the PEP can be obtained in closed-form, as will be shown in Section 2.3.3. For the other decoding metrics, it is advantageous to proceed in the Laplace-domain. Introducing the Laplace transform $\Phi_\delta(\zeta|s) \triangleq \mathcal{E}\{\mathrm{e}^{-\zeta\delta_{i|s}}\}$, and noting that conditioned on the noise state the metric differences are statistically independent, the PEP can be evaluated through the inverse Laplace transform

$$\mathrm{PEP}(d, n_{\mathcal{B}}) = \frac{1}{2\pi\mathrm{j}} \int_{\chi-\mathrm{j}\infty}^{\chi+\mathrm{j}\infty} [\Phi_\delta(\zeta|\mathcal{G})]^{(d-n_{\mathcal{B}})} [\Phi_\delta(\zeta|\mathcal{B})]^{n_{\mathcal{B}}} \frac{d\zeta}{\zeta} \,, \tag{2.21}$$

where $\chi > 0$ lies in the region of convergence of the integral. This integral lends itself to efficient numerical integration using Gauss-Chebyshev quadratures with N nodes [50, p. 889], [51, Eq. (10)] as follows

$$\mathrm{PEP}(d, n_{\mathcal{B}}) = \frac{1}{N} \sum_{i=1}^{N/2} \left(\Re\{\Phi(\chi + \mathrm{j}\chi\tau_i)\} + \tau_i \Im\{\Phi(\chi + \mathrm{j}\chi\tau_i)\} \right) , \tag{2.22}$$

where $\Phi(\zeta) \triangleq [\Phi_\delta(\zeta|\mathcal{G})]^{d-n_{\mathcal{B}}} [\Phi_\delta(\zeta|\mathcal{B})]^{n_{\mathcal{B}}}$ and $\tau_i \triangleq \tan((2i-1)\pi/(2N))$. The expressions for the Laplace transforms $\Phi_\delta(\zeta|s)$ are presented in Section 2.3.3. They also play a key role in computation of the cutoff rate, as explained in the next section.

Cutoff Rate

Since except for the KSMLD and MSMLD metrics that assume respectively the instantaneous and statistical knowledge about the noise process, the decision metrics considered in this work are non-ML, we employ the notion of generalized cutoff rate as an information-theoretic performance measure. The generalized cutoff rate has widely been used in the context of fading channels, e.g. [52, 53] with mismatched decoding. To this end, denoting the transmitted and received signal vectors of length L by $\boldsymbol{x} = [x_1, \ldots, x_L]$ and $\boldsymbol{r} = [r_1, \ldots, r_L]$, and introducing the decoding path metric for $\boldsymbol{x}$ given $\boldsymbol{r}$ by $\Lambda(\boldsymbol{x}|\boldsymbol{r})$, we upper bound the PEP between $\boldsymbol{x}$ and an alternative vector $\tilde{\boldsymbol{x}}$, for a given noise state sequence $\boldsymbol{s} = [s_1, \ldots, s_L]$, using the Chernoff bound

$$\mathrm{PEP}(\boldsymbol{x} \to \tilde{\boldsymbol{x}}|\boldsymbol{s}) \leq \min_{\rho \geq 0} \mathcal{E}_{\boldsymbol{r}|\boldsymbol{x},\boldsymbol{s}} \left\{ \exp\left[-\rho(\Lambda(\boldsymbol{x}|\boldsymbol{r}) - \Lambda(\tilde{\boldsymbol{x}}|\boldsymbol{r})) \right] \right\} . \tag{2.23}$$

While the Chernoff factor ρ could be optimized for each $\boldsymbol{s}$, the simpler (and looser) upper bound

$$\mathrm{PEP}(\boldsymbol{x} \to \tilde{\boldsymbol{x}}) \leq \min_{\rho \geq 0} \mathcal{E}_{\boldsymbol{s}} \left\{ \mathcal{E}_{\boldsymbol{r}|\boldsymbol{x},\boldsymbol{s}} \left\{ \exp\left[-\rho(\Lambda(\boldsymbol{x}|\boldsymbol{r}) - \Lambda(\tilde{\boldsymbol{x}}|\boldsymbol{r})) \right] \right\} \right\} \triangleq \min_{\rho \geq 0} C(\tilde{\boldsymbol{x}}, \boldsymbol{x}, \rho) \tag{2.24}$$

for the average PEP is obtained when choosing an optimized ρ independent of $\boldsymbol{s}$ (cf. [54] for a similar approach to obtain an upper bound for block fading channels based on random coding arguments). Employing (2.24) allows us to express the generalized cutoff rate as

$$R_0 = \lim_{L \to \infty} \max_{\rho \geq 0} -\frac{1}{L} \log_2 \left[\mathcal{E}_{\boldsymbol{x},\tilde{\boldsymbol{x}}} \left\{ C(\tilde{\boldsymbol{x}}, \boldsymbol{x}, \rho) \right\} \right] , \tag{2.25}$$

where R_0 is in bits/symbol. Exploiting the fact that additive metrics are used, i.e.,

$$\Lambda(\tilde{\boldsymbol{x}}|\boldsymbol{r}) = \sum_{k=1}^{L} \lambda(\tilde{x}_k|r_k) \ , \tag{2.26}$$

and that the transmitted symbols are chosen independently and uniformly distributed, the expression in (2.25) can be simplified to

$$R_0 = \lim_{L\to\infty} \max_{\rho\in\mathcal{R}} -\frac{1}{L}\log_2 \left[\sum_{s_0\in\{\mathcal{G},\mathcal{B}\}} \Pr\{s_0\} \sum_{\boldsymbol{s}\in\mathcal{S}^L} \prod_{k=1}^{L} \frac{1}{2}\Pr\{s_k|s_{k-1}\} \left(\Phi_\delta(\rho|s_k)+1\right) \right] \ , \tag{2.27}$$

where we use the stationary distribution for the initial state s_0, and ρ lies in the intersection $\mathcal{R}$ of the convergence regions of the Laplace transforms. With some thought [55, p. 184] and by defining

$$\boldsymbol{\Phi}(\rho) \triangleq \frac{1}{2}\begin{bmatrix} \Phi_\delta(\rho|\mathcal{G})+1 & 0 \\ 0 & \Phi_\delta(\rho|\mathcal{B})+1 \end{bmatrix}, \quad \boldsymbol{s}_0 \triangleq \begin{bmatrix} P_\mathcal{G} \\ P_\mathcal{B} \end{bmatrix}, \quad \mathbf{1} \triangleq \begin{bmatrix} 1 \\ 1 \end{bmatrix},$$

R_0 can be compactly written as

$$R_0 = \lim_{L\to\infty} \max_{\rho\in\mathcal{R}} -\frac{1}{L}\log_2 \left(\boldsymbol{s}_0^T (\boldsymbol{T}^I \boldsymbol{\Phi}(\rho))^L \mathbf{1}\right) . \tag{2.28}$$

Lemma 2.3.1 *Let $e_{\max}(\rho)$ denote the largest eigenvalue of the irreducible matrix $\mathcal{A} = \boldsymbol{T}^I\boldsymbol{\Phi}(\rho)$ and let ϱ denote the ratio of the largest and smallest component of the positive right eigenvector corresponding to $e_{\max}(\rho)$], then for any $\boldsymbol{\Phi}(\rho)$ and s_o we have [55, p. 184].*

$$\frac{[e_{\max}(\rho)]^L}{\varrho} \le \boldsymbol{s}_0^T \mathcal{A}^L \mathbf{1} \le [e_{\max}(\rho)]^L \varrho, \tag{2.29}$$

Using Lemma 2.3.1 we obtain the final expression as

$$R_0 = -\log_2 \left[\min_{\rho\in\mathcal{R}} e_{\max}(\rho) \right] \ . \tag{2.30}$$

From an optimization standpoint, it is convenient to express R_0 in terms of $e^2_{\max}(\rho)$, i.e., $R_0 = -\frac{1}{2}\log_2\left[\min_{\rho\in\mathcal{R}} e^2_{\max}(\rho)\right]$. Since $e^2_{\max}(\rho)$ is the largest eigenvalue of the symmetric matrix $\boldsymbol{A} \triangleq \boldsymbol{T}^I\boldsymbol{\Phi}^2(\rho)(\boldsymbol{T}^I)^T$, it is a convex function of the elements a_{ij}, $i,j = 1,2$, of $\boldsymbol{A}$ [56, Example 3.10]. Furthermore, since

$$e^2_{\max}(\rho) = \frac{1}{2}\left[a_{11}+a_{22}+\sqrt{4a_{12}a_{21}+(a_{11}-a_{22})^2}\right] \ , \tag{2.31}$$

and $a_{ij} > 0$, $i, j = 1, 2$, it is easy to show that $e^2_{\max}(\rho)$ is also monotonically increasing in a_{ij}. Hence, from the convexity of the Laplace transform and consulting the composition rules [56, p. 86], we conclude that $e^2_{\max}(\rho)$ is a convex function of ρ, which greatly facilitates the minimization problem (2.30). Furthermore, note that in case of ideal interleaving ($I \to \infty$),

$$e_{\max}(\rho) = \frac{1}{2}\left[\mathrm{P}_{\mathcal{G}}(\Phi_\delta(\rho|\mathcal{G}) + 1) + \mathrm{P}_{\mathcal{B}}(\Phi_\delta(\rho|\mathcal{B}) + 1)\right] \triangleq \frac{1}{2}\left[\Phi_\delta(\rho) + 1\right] \ , \tag{2.32}$$

and the familiar expression

$$R_0 = 1 - \log_2\left[1 + \min_{\rho \in \mathcal{R}} \Phi_\delta(\rho)\right] \tag{2.33}$$

is recovered.

2.3.3 Expressions for Different Metrics

We now present the expressions required to evaluate the PEP and cutoff rate for the different metrics introduced in Section 2.2.

EDSD

Substitution of (2.6) into (2.20) yields that $\Delta(d, n_{\mathcal{B}})$ is Gaussian distributed, and the PEP can be expressed as

$$\mathrm{PEP}(d, n_{\mathcal{B}}) = Q\left(\frac{d}{\sqrt{n_B\sigma^2_{\mathcal{B}} + (d - n_{\mathcal{B}})\sigma^2_{\mathcal{G}}}}\right) \ . \tag{2.34}$$

Likewise, the Laplace transform can also be expressed in closed form as

$$\Phi_\delta(\zeta|s) = \exp\left(\frac{2}{\sigma^2_{\mathcal{G}}}\zeta\left[\frac{\sigma^2_s}{\sigma^2_{\mathcal{G}}}\zeta - 1\right]\right) \ . \tag{2.35}$$

KSMLD

Also in the case of the KSMLD, $\Delta(d, n_{\mathcal{B}})$ is Gaussian distributed. The PEP and Laplace transform are obtained as

$$\mathrm{PEP}(d, n_{\mathcal{B}}) = Q\left(\sqrt{n_B\sigma^{-2}_{\mathcal{B}} + (d - n_{\mathcal{B}})\sigma^{-2}_{\mathcal{G}}}\right) \tag{2.36}$$

and

$$\Phi_\delta(\zeta|s) = \exp\left(2\sigma_s^{-2}\zeta(\zeta - 1)\right) \ , \tag{2.37}$$

respectively. Since the Chernoff factor $\rho = 1/2$ uniformly minimizes the eigenvalue $e_{\max}(\rho)$ for this case, the cutoff rate R_0 in (2.30) is obtained in closed form.

It is interesting to observe that the ratio of the arguments of the Q-functions in (2.36) and (2.34) is the ratio of the arithmetic and the harmonic mean of the variances σ_s^2. Hence the KSMLD is strictly superior to the EDSD in terms of BER unless $\sigma_{\mathcal{G}}^2 = \sigma_{\mathcal{B}}^2$.

EMD

The expressions for the EMD immediately follow from those for the KSMLD by letting $\sigma_{\mathcal{B}}^2 \to \infty$. We note that for asymptotically large signal-to-noise ratio (SNR) the average PEP is given by

$$\sum_{n_{\mathcal{B}}=0}^{d} \mathrm{PEP}(d, n_{\mathcal{B}}) \Upsilon(d, n_{\mathcal{B}}) \overset{\sigma_{\mathcal{G}}^2 \to 0}{\longrightarrow} \frac{1}{2} \Upsilon(d, d) \tag{2.38}$$

which implies that the BER curve will floor out with increasing SNR when decoding with this metric. The Laplace transform transform is obtained as

$$\Phi_\delta(\zeta|s) = \begin{cases} \exp\left(2\sigma_s^{-2}\zeta(\zeta-1)\right), & \text{if } s = \mathcal{G} \\ 1, & \text{if } s = \mathcal{B} \end{cases} \tag{2.39}$$

Again, $\rho = 1/2$ uniformly minimizes the maximum eigenvalue and a closed-form expression for R_0 results from (2.30). Furthermore, for asymptotically large SNR we find that $e_{\max}(\rho) \overset{\sigma_{\mathcal{G}} \to 0}{\to} 1 + \mathrm{P}_{I,\mathcal{BB}}$ and thus

$$R_0 = 1 - \log_2(1 + \mathrm{P}_{I,\mathcal{BB}}) \,, \tag{2.40}$$

which is strictly smaller than 1.

MSMLD

For the max-log MSMLD metric we need to evaluate the PEP based on (2.21) and thus are interested in the Laplace transforms $\Phi_\delta(\zeta|s)$ also for computation of BER. These are given by

$$\Phi_\delta(\zeta|s) = \int_n \left(\max_{s \in \mathcal{S}} \left[p_s(n + dE) \right] / \max_{s \in \mathcal{S}} \left[p_s(n) \right] \right)^{\zeta} p_s(n) \, \mathrm{d}n \,. \tag{2.41}$$

However, when the max-log approximation is employed the MSMLD metric simplifies to the following form

$$\delta \;=\; \max(f_1(n+d_{\mathrm{E}}),\; f_2(n+d_{\mathrm{E}})) - \max(f_1(n_k),\; f_2(n_k)) \tag{2.42}$$

with

$$\begin{cases} f_1(x) = -\frac{|x|^2}{2\sigma_{\mathcal{G}}^2} + \log(\underbrace{P_{\mathcal{G}}/\sqrt{2\pi\sigma_{\mathcal{G}}^2}}_{\Omega_{\mathcal{G}}}) \\ f_2(x) = -\frac{|x|^2}{2\sigma_{\mathcal{B}}^2} + \log(\underbrace{P_{\mathcal{B}}/\sqrt{2\pi\sigma_{\mathcal{B}}^2}}_{\Omega_{\mathcal{B}}}) \end{cases}$$

The max operation implies that depending on the value of n one of the components in the max operation dominates and consequently the integral in Eqn.(2.41) can be written as the sum of four integrals, where the integrand is a Gaussian pdf and the domains of integration are given by $\{n : |n|^2 > \mathcal{R} \wedge |n+2|^2 > \mathcal{R}\}$, $\{n : |n|^2 > \mathcal{R} \wedge |n+2|^2 < \mathcal{R}\}$, $\{n : |n|^2 < \mathcal{R} \wedge |n+2|^2 > \mathcal{R}\}$, $\{n : |n|^2 < \mathcal{R} \wedge |n+2|^2 < \mathcal{R}\}$ and

$$\mathcal{R} = \frac{2\sigma_{\mathcal{G}}^2}{1-\sigma_{\mathcal{G}}^2/\sigma_{\mathcal{B}}^2} \log\left(\frac{\mathrm{P}_{\mathcal{G}}/\mathrm{P}_{\mathcal{B}}}{\sigma_{\mathcal{G}}^2/\sigma_{\mathcal{B}}^2}\right) \tag{2.43}$$

is the threshold at which the two terms of the Gaussian mixture pdf attain the same value and effectively determines the region of dominance of each of the terms in Eqn. (2.42). Based on the value of $\mathcal{R}$ closed form expressions can be obtained for $\phi_\delta^S(s),\; S \in \{\mathcal{G},\; B\}$ by dividing the region of integration into smaller segments and computing

$$\begin{aligned} \Phi_\delta^S(s) \;&= \sum_{\text{segments}} \int_a^b \exp\left(-s\left[\frac{|n+d_{\mathrm{E}}|^2}{2\sigma_1^2} + \frac{|n|^2}{2\sigma_2^2} + \log(\Omega_{\mathcal{G}}\Omega_{\mathcal{B}})\right]\right)\left(\frac{\exp(-|n|^2/2\sigma_S^2)}{\sqrt{2\pi\sigma_S^2}}\right) dn, \\ &= \Bigg[\sum_{\text{segments}} \frac{\Omega_{\mathcal{G}}^{-s}\Omega_{\mathcal{B}}^{-s}\sqrt{\sigma_1^2\sigma_2^2(\sigma_1^2(\sigma_2^2+\sigma^2 s)-\sigma^2\sigma_2^2 s)}}{2(s\sigma_2^2\sigma^2 - \sigma_1^2(\sigma_2^2+s\sigma^2))} \exp\left(\frac{d_{\mathrm{E}}^2 s(s\sigma^2+\sigma_2^2)}{2(\sigma_1^2(\sigma_2^2+s\sigma^2)-s\sigma^2\sigma_2^2)}\right) \\ &\qquad \times \mathrm{erf}\left(\frac{\sigma_2^2(s\sigma^2(n+d_{\mathrm{E}})-n\sigma_1^2) - sn\sigma^2\sigma_1^2}{\sqrt{2\sigma^2\sigma_1^2\sigma_2^2(\sigma_1^2)}}\right)\Bigg]_b^a \end{aligned} \tag{2.44}$$

where $\sigma_1^2, \sigma_2^2, \sigma_S^2 \in \{\sigma_{\mathcal{B}}^2, \sigma_{\mathcal{G}}^2\}$

A closed-form solution as sum of Gaussian Q-functions results in the real-valued channel case (please see Appendix A for relevant expressions), while using the alternative rep-

resentation of the Q-function [2] simple one-dimensional integrals need to be computed for complex-valued channels.

HPFD

For the HPFD also, we need to evaluate (2.21) to obtain the PEP. Similar to the case of MSMLD, we can express the Laplace transforms $\Phi_\delta(\zeta|s)$ in closed form as sums of Q-functions for real-valued baseband transmission. In the complex-valued case we need to resort to numerical integration. Defining the unit-step function as $u(x) = 1$ iff $x \geq 0$, and, for convenience, the variables

$$\begin{aligned}
\tau_{k,\ell} &\triangleq \tan\left(\frac{(2k-1)\pi}{2N}\right) + \mathrm{j}\tan\left(\frac{(2\ell-1)\pi}{2N}\right), \\
\omega_{k,\ell} &\triangleq \cos\left(\frac{(2k-1)\pi}{2N}\right)\cos\left(\frac{(2\ell-1)\pi}{2N}\right), \\
a_{k,\ell} &\triangleq \xi\sigma_n^2 - |\tau_{k,\ell}|, \;\; b_{k,\ell} \triangleq \xi^2\sigma_n^2/2 - \xi|\tau_{k,\ell}|, \\
c_{k,\ell} &\triangleq \xi\sigma_n^2 - |\tau_{k,\ell}+2| \text{ and } d_{k,\ell} \triangleq \xi^2\sigma_n^2/2 - \xi|\tau_{k,\ell}+2|,
\end{aligned} \tag{2.45}$$

we can well approximate the $\Phi_\delta(\zeta|s)$ using Gauss-Chebyshev quadratures [50, p. 889]

$$\Phi_\delta(\zeta|s) \approx \frac{\pi^2}{N^2}\sum_{k=1}^{N}\sum_{\ell=1}^{N} \mathrm{e}^{-\zeta\left[-\frac{|\tau_{k,\ell}|^2}{2\sigma_n^2}u(a_{k,\ell})+b_{k,\ell}u(-a_{k,\ell})+\frac{|\tau_{k,\ell}+2|^2}{2\sigma_n^2}u(c_{k,\ell})-d_{k,\ell}u(-c_{k,\ell})\right]}\frac{p_s(\tau_{k,\ell})}{\omega_{k,\ell}^2}, \tag{2.46}$$

which we found to converge well for $N = 100$ nodes.

α-PFD

Due to the form of the metric for the α-PFD (2.12) there is no closed-form expression for the PEP or the Laplace transform $\Phi_\delta(\zeta|s)$. The latter can efficiently be approximated by

$$\Phi_\delta(\zeta|s) \approx \frac{\pi^2}{N^2}\sum_{k=1}^{N}\sum_{\ell=1}^{N}\exp\left(-\frac{\zeta}{2\alpha}\left[\mathrm{e}^{-\alpha|\tau_{k,\ell}|^2} - \mathrm{e}^{-\alpha|\tau_{k,\ell}+2|^2}\right]\right)\frac{p_s(\tau_{k,\ell})}{\omega_{k,\ell}^2} \tag{2.47}$$

in the complex-valued baseband channel case, while a single summation is sufficient for real-valued channels. The PEP then follows from (2.21).

2.4 Numerical Results and Discussion

In this section, we put the analytical and semi-analytical expressions obtained in the previous section to use to (a) gauge the different metrics for their effectiveness in alleviating non-Gaussian noise when used in Viterbi decoding, (b) optimize the single parameter of the HPFD-metric and the α-PFD metric, (c) study the interplay of channel memory and interleaving and their effect on performance, and (d) substantiate the benefit of using both quadrature components in complex-valued channels.

2.4.1 Cutoff Rate

In order to clearly separate the effects of decoding metrics and interleaving, we first present cutoff rate results assuming ideal interleaving and thereafter proceed to discuss the performance degradation incurred due to non-ideal interleaving, i.e., finite I, using a rate loss criteria defined later.

Figure 2.2 presents the R_0 results, as a function of SNR ($1/\sigma_w^2$), for decoding with the different metrics for both real- and complex-valued baseband transmission. The exemplarily considered channel noise parameters are $\kappa = 100$ and $\mathrm{P}_{\mathcal{B}} = 0.1$, which represents a channel with a strong and frequent impulse noise component. The parameters for the HPFD and α-PFD metrics are $\xi = 0.1/\sigma_n$ and $\alpha = 0.5$, respectively (see below for the optimization of these parameters).

Ideal Interleaving ($I \to \infty$)

We note that for the cases where the noise-state is assumed known, i.e., KSMLD and EMD, no additional information can be drawn from the quadrature component of the received signal, and thus the R_0 curves for real and complex baseband transmission are identical. Furthermore, since the EDSD treats in-phase and quadrature components independently, it is not able to exploit the statistical dependencies between the two signal components (see Eqn. 2.3)), and hence only one R_0 curve is observed for the EDSD in Figure 2.2. In contrast to this, the MSMLD, HPFD, and α-PFD utilize these dependencies and achieve notably higher rates in the complex-valued channel scenario.

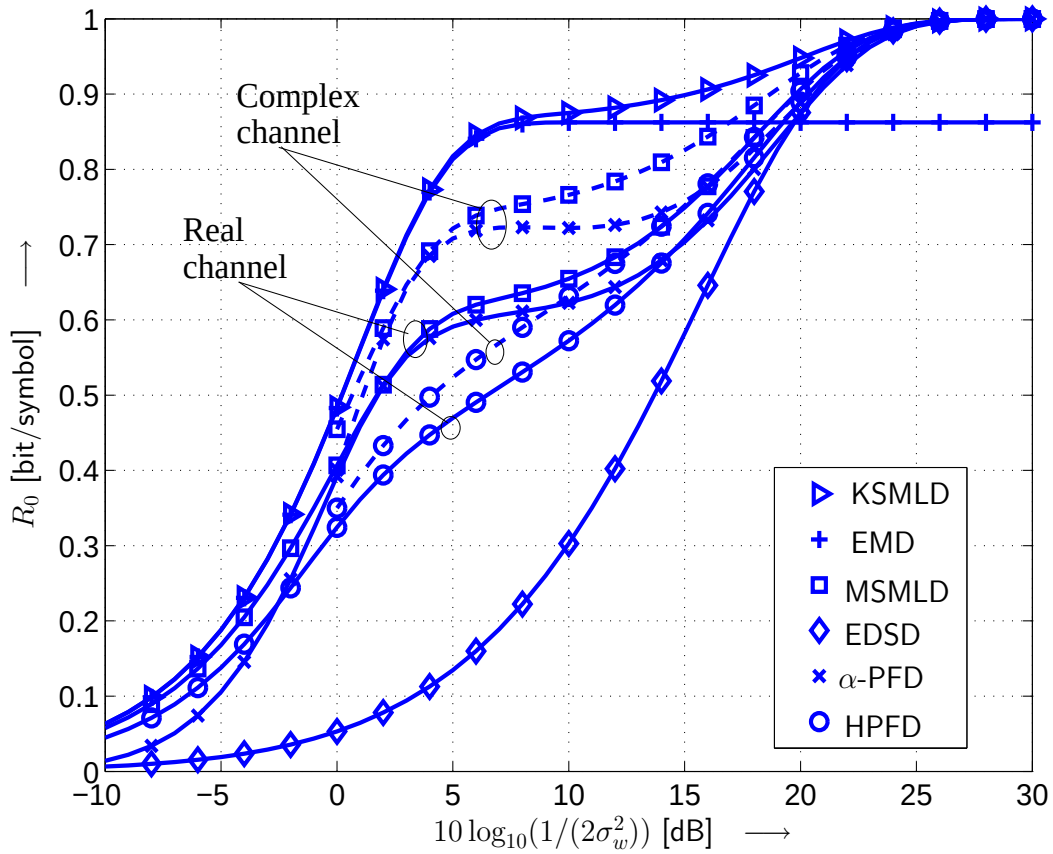

Figure 2.2 — Cutoff rate for decoding with different metrics (proposed in Section 2.2) for ideal infinite interleaving. Noise parameters: $\kappa = 100$, $\mathrm{P}_{\mathcal{B}} = 0.1$. HPF metric with $\xi\sigma_n = 0.1$, αPF metric with $\alpha = 0.5$. Solid lines: Baseband transmission. Dashed lines: Passband Transmission.

While the cutoff-rate curve for the EMD saturates at $R_0 = 1 - \log_2(1 + \mathrm{P}_{\mathcal{B}}) = 0.86$ bits/(channel use) [cf. (2.13) with $I \to \infty$ and (2.40)], the cutoff rate for the KSMLD steadily approaches 1 with increasing SNR, by extracting information from noisy (bad state) received samples as well. In fact, the R_0 curve consists of two parts, which, as can be inferred from the representation for $e_{\max}(\rho)$ in (2.32), correspond to the good and bad noise states. This two-part characteristic of the R_0 curves also manifests for the other decoding metrics with the exception of the conventional Euclidean-distance metric, which is evidently ill-suited for the non-Gaussian noise.

In terms of absolute performance the KSMLD can be considered as an idealized benchmark. Clearly, the acquisition of instantaneous state information requires additional

bandwidth and computational resources. For example, the EM algorithm proposed in [38] consists of two forward-backward algorithms and pilot symbols are needed for its initialization. It is interesting to observe that, until its saturation point, the EMD performs almost as good as the KSMLD, which suggests that decoding of bad-state received signals can be omitted with negligible performance loss. We note that the EMD considered here also relies on instantaneous noise-state information. Amongst the decoders that do not require state estimation, the MSMLD is the optimal choice. However, the α-PFD, which has the distinct advantage of requiring the selection of only a single parameter, approaches the MSMLD performance closely. Furthermore, the gains achieved with the α-PFD and HPFD over the conventional Euclidean-distance based decoder are significant for all but almost uncoded transmission for the noise scenario considered in Figure 2.2.

Effect of Non-ideal Interleaving

We now turn to the case of finite interleaving depth I. We chose the exemplary state transition parameters $\mathrm{P}_{\mathcal{GB}} = 0.003$ and $\mathrm{P}_{\mathcal{BG}} = 0.025$, such that the average burst length is $\bar{\mathcal{D}}_{\mathcal{B}} = 40$ symbols and the stationary probabilities are $\mathrm{P}_{\mathcal{G}} = 0.9$ and $\mathrm{P}_{\mathcal{B}} = 0.1$ as in the previous section. Again, $\kappa = 100$ is chosen. As an indicator of the effect of finite interleaving we define the relative rate loss

$$\mathcal{L} \triangleq \frac{R_0(\infty) - R_0(I)}{R_0(\infty)}\,, \tag{2.48}$$

where $R_0(I)$ denotes the cutoff rate for given interleaver depth I. The rate loss $\mathcal{L}$ is plotted in Figure 2.3 as a function of the SNR for the decoding metrics which do not rely on knowledge of the instantaneous channel state. As discussed in Section 2.3.1 (cf. Eqn. (2.15)), we consider different interleaver depths parameterized by $\bar{\mathcal{D}}_{\mathcal{B}}$, namely $I = [0, \bar{\mathcal{D}}_{\mathcal{B}}/2, 2\bar{\mathcal{D}}_{\mathcal{B}}]$.

From Figure 2.3 we observe significant losses in the absence of interleaving ($I = 0$), which are mitigated with increasing I and virtually disappear for $I = 2\bar{\mathcal{D}}_{\mathcal{B}}$. Since $0.9 \lesssim \mathrm{P}_{\mathcal{G}} < 1$ for typical mixture noise scenarios, we conclude that configuring the interleaver depth according to double the average burst length is sufficient for most

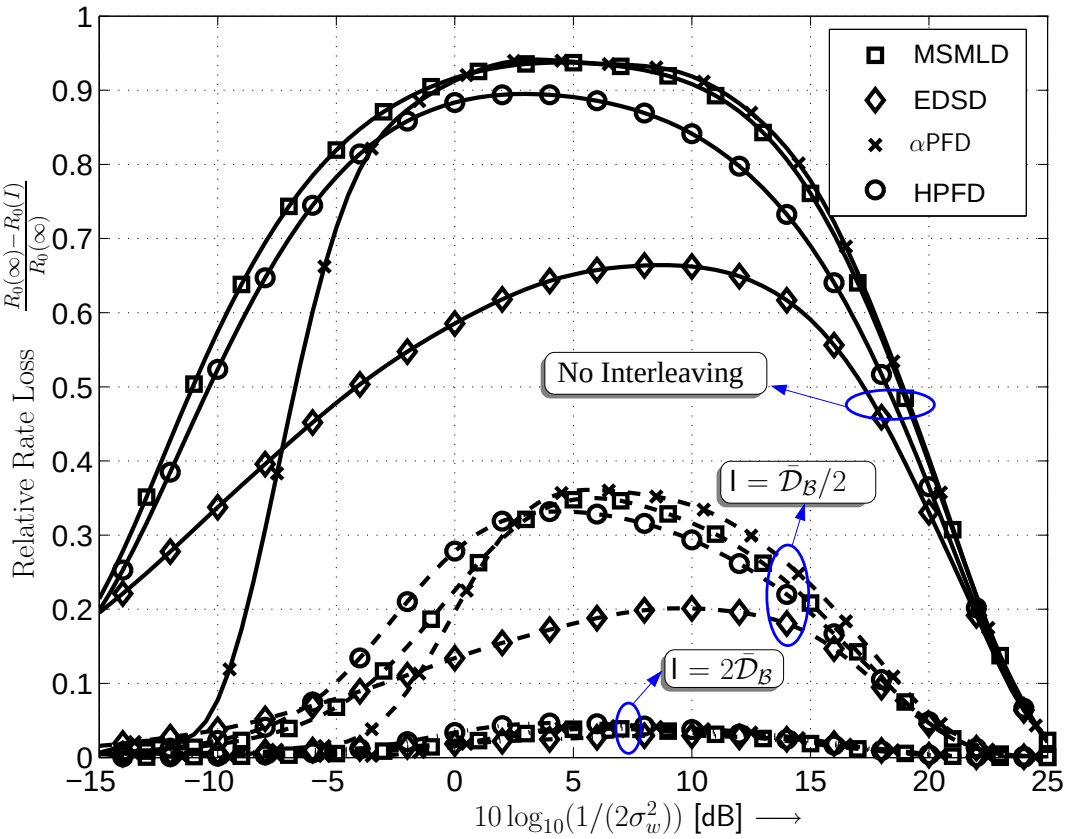

Figure 2.3 — Loss in cutoff rate (R_0) in the case of non-ideal interleaving with Markovian-Gaussian noise compared to memoryless noise through various levels of interleaving. Noise parameters $\kappa = 100$, $\mathrm{P}_{\mathcal{B}} = 0.1$, mean occupation time of bad state $\bar{\mathcal{D}}_{\mathcal{B}} = 40$ symbols.

practical purposes. Note that our results are not a contradiction to the paradigm that memory increases capacity [26], since (i) the considered decoders do not attempt to make use of the channel memory and (ii) it is known that cutoff rate deteriorates with increasing channel memory even if the channel state is known [57].

2.4.2 Parameter Optimization based on Cutoff Rate

While the uni-parameter definition of the proposed α-PF metric makes it particularly attractive, a better understanding of the metric is obtained by obtaining the optimal values for the parameter α for the various noise scenarios. In particular, we consider the SNR required to achieve a cutoff rate $R_0 = 0.5$ bits/symbol, i.e., transmission with code

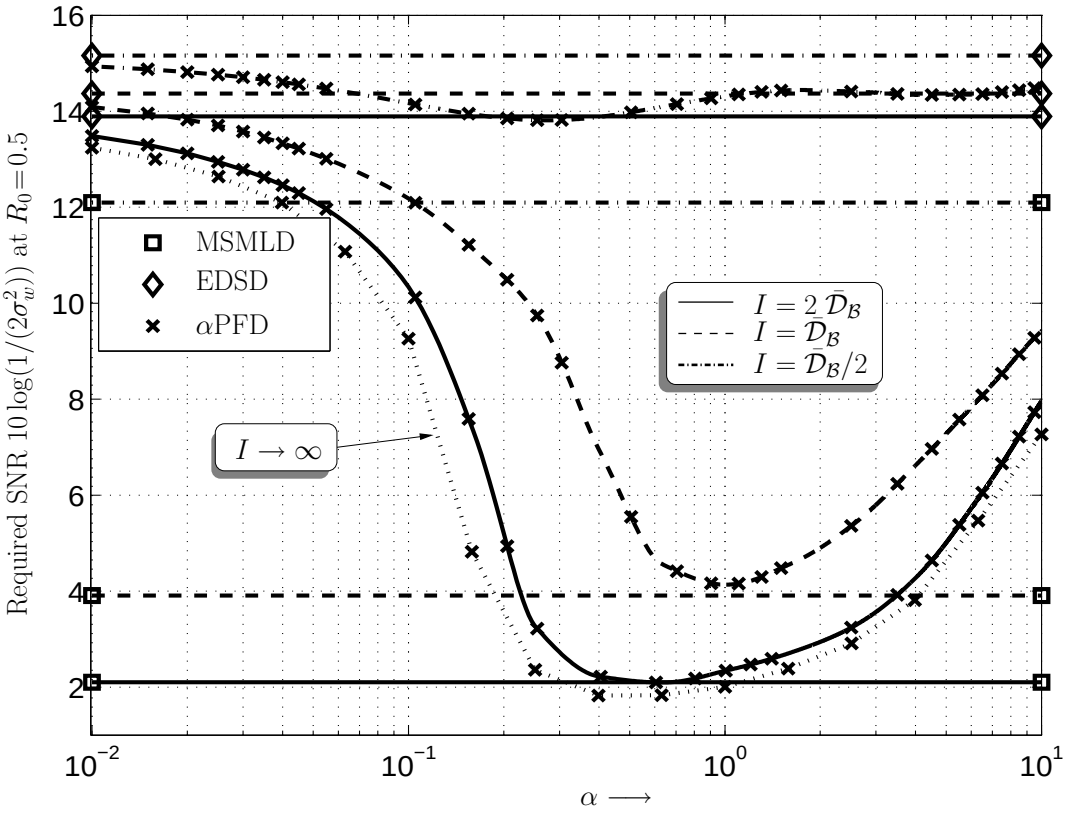

Figure 2.4 — Optimization of α for the αPFD based on required SNR for a desired cutoff rate of $\mathcal{R}_0 = 0.5$ bits/symbol. The corresponding values for MSMLD and EDSD are also shown for comparison. Noise parameters: $\kappa = 100$, $\bar{\mathcal{D}}_{\mathcal{B}} = 40$, $\mathrm{P}_{\mathcal{B}} = 0.1$. The optimal value with $I = 2\bar{\mathcal{D}}_{\mathcal{B}}$ matches very well with that of of the infinite interleaving.

rate 1/2, as function of α as the optimization criteria. To this end, Figure 2.4 depicts the variation with increasing values of α for baseband transmission with $\mathrm{P}_{\mathcal{B}} = 0.1$, $\kappa = 100$, and multiple interleaver depths. As reference, curves for MSMLD and EDSD are also plotted. We observe that $\alpha \in [0.5, 2]$ provides close-to-optimal performance for different interleaver depths. Furthermore, at $I = 2\bar{\mathcal{D}}_{\mathcal{B}}$ the performance for the memoryless channel is well approached, which corroborates our previous conclusions from Fig. 2.3. We note that the α-PFD converges to the EDSD for $\alpha \to 0$, cf. [49, Eq. (9)]. This also indicates that for decreasing $\mathrm{P}_{\mathcal{B}}$ the optimum value of α will decrease. However, the results for $\mathrm{P}_{\mathcal{B}} = 0.01$ (not shown here) reveal that $\alpha \in [0.5, 2]$ is a good choice for this case also.

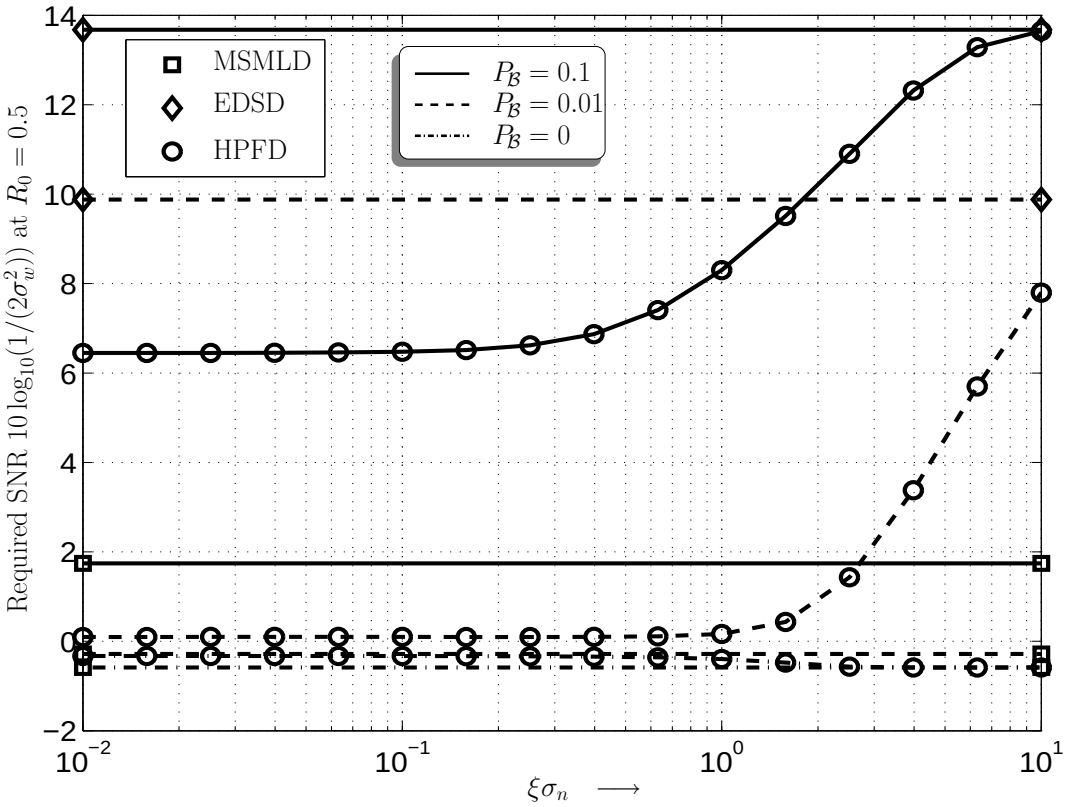

Figure 2.5 — Optimization of ξ for the HPFD for different interleaving depths based on required SNR for a desired cutoff rate of $\mathcal{R}_0 = 0.5$ bits/symbol. Relatively flat performance in the region of optimality indicates that its less sensitive to variations in ξ. Performance is worse than MSMLD but large gains exists with respect to EDSD.

The HPFD is also attractive in terms of the effort required for noise parameter estimation. The optimization of the parameter ξ can be inferred from Figure 2.5, which shows the required SNR (as in Figure 2.4) as function of $\xi\sigma_n$. This time we assume $I \to \infty$ and plot results for $\mathrm{P}_{\mathcal{B}} \in \{0.1, 0.01, 0\}$. We observe that relatively small values of $\xi\sigma_n$ are advantageous in impulse noise channels, whereas larger values achieve a slightly better performance in the Gaussian noise case We note that the HPFD approaches the EDSD for large values of ξ (see (2.11)). Similarly flat optima (as in Fig 2.5) were found for finite interleaver depth (not shown here). Using, e.g., $\xi = 0.1/\sigma_n$ appears to be a good compromise for all scenarios.

2.4.3 Bit-error Rate

We now present BER results obtained from the analytic expressions derived in Section 2.3 and simulations, whereby, the relative non-Gaussian interference suppression capabilities of the different metrics are asserted. As a relevant example, we consider the maximum free-distance, rate-1/2, memory-4 convolutional code with generator polynomials $(23)_8$ and $(35)_8$, for which $d_{\text{free}} = 7$. We apply a truncated union bound with $d_{\text{H,max}} = 21$ for the ideal interleaving case and $d_{\text{H,max}} = d_{\text{free}}$ for the case of finite interleaving, which requires $\Upsilon(d, n_{\mathcal{B}})$ to be generated. Hence the presented analytical BER curves are approximations, rather than a bound. The noise parameters are $\mathrm{P}_{\mathcal{B}} = 0.1$ and $\kappa = 100$.

Ideal Interleaving

Figure 2.6 shows the BER versus SNR from the union bound (2.16) (lines) and from simulations (markers) for the convolutional coded system and memoryless noise process (i.e., $I \to \infty$). For the sake of clarity, complex-baseband channel results are only included for MSMLD. As in Figure 2.2, the parameters for the HPF and α-PF metrics are $\xi = 0.1/\sigma_n$ and $\alpha = 0.5$, respectively.

We observe that the union bound approximation matches the simulated BER curves very well and is fairly tight in the region of interest, which emphasizes the relevance of the PEP expressions derived in Section 2.3. With regards to error-rate performance, it can be seen that the α-PFD stands out by closely following the MSMLD performance for a constant value of α. Both α-PFD and HPFD clearly outperform the conventional EDSD over a wide range of BERs. Furthermore, exploiting the information in the quadrature component of the received signal, if available, provides order of magnitude improvements in BER. This is decidedly different from the case of AWGN. The significant performance gains achievable by noise-state estimation are evident from the BER curves for KSMLD and EMD. The EMD though is the only detector which suffers an error floor at about $\frac{1}{2}W(d_{\text{free}})\mathrm{P}_{\mathcal{B}}^{d_{\text{free}}} = 2 \cdot 10^{-7}$ (see Eq. (2.38)).

We note that the BER curves for the more robust detectors in Figure 2.6 consist

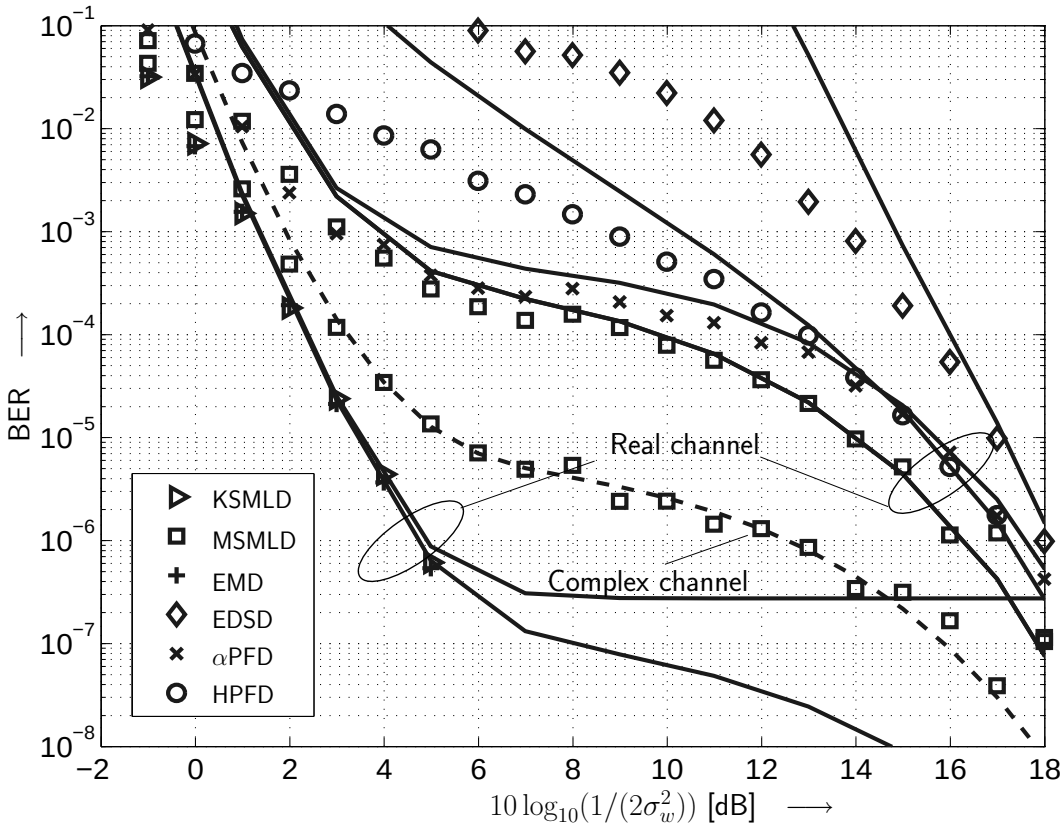

Figure 2.6 — BER performance of the various metrics proposed in Section 2.2 with ideal infinite interleaving and for noise parameters $\kappa = 100$ and $\mathrm{P}_{\mathcal{B}} = 0.1$. Lines: Analytical results. Markers: Simulation.

of two segments, most discernible for the KSMLD, which is reminiscent of error-rate curves for Turbo codes. This behaviour is made more explicit in Figure 2.7, where we plot the analytical BER approximation for $d = d_{\text{free}}$ (solid lines) together with $\mathrm{PEP}(d_{\text{free}}, n_{\mathcal{B}})\Upsilon(d_{\text{free}}, n_{\mathcal{B}})$ with $n_{\mathcal{B}} = 1$ and $n_{\mathcal{B}} = d_{\text{free}}$ (dashed lines) for the EDSD, KSMLD, and α-PFD. Clearly, for sufficiently high SNR the BER is eventually determined by the maximal PEPs for which $n_{\mathcal{B}} = d_{\text{free}}$. However, the EDSD suffers from contribution of impulsive noise sequences with $n_{\mathcal{B}} < d_{\text{free}}$ at relatively low SNR, e.g., with $n_{\mathcal{B}} = 1$ as shown in Figure 2.7, since the increase of the corresponding PEPs outweighs the lower effective multiplicity $\Upsilon(d_{\text{free}}, n_{\mathcal{B}})$ with increasing $n_{\mathcal{B}}$. The ideal KSMLD successfully suppresses those error events and thus BER drops quickly with increasing SNR to the level of the minimum distance event ($n_{\mathcal{B}} = d_{\text{free}}$), i.e., a waterfall

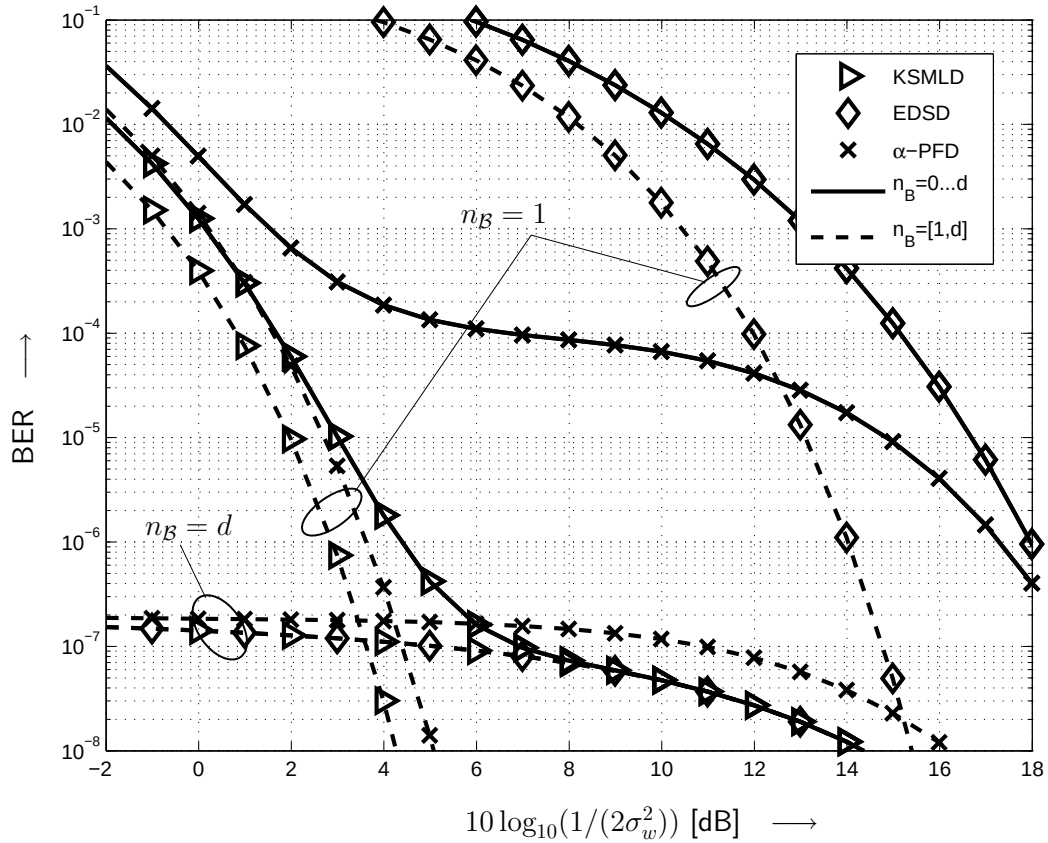

Figure 2.7 — Analytical BER results for different metrics proposed in Section 2.2 using ideal infinite interleaving with noise parameters $\kappa = 100$ and $\mathrm{P}_{\mathcal{B}} = 0.1$. Only events with $d = d_{\text{free}}$ are considered. Solid lines show (2.16) for $d = d_{\text{free}}$ and $n_{\mathcal{B}} = [0 \dots d]$. Dashed lines show (2.16) for $d = d_{\text{free}}$ and $n_{\mathcal{B}} = 1$ and $n_{\mathcal{B}} = d$, respectively.

region occurs[3]. The proposed α-PFD approximates this behaviour, as can be seen for the case of $n_{\mathcal{B}} = 1$, which results in the significant gains over the EDSD for a certain SNR range.

Non-Ideal Interleaving

We consider Markovian-Gaussian noise with the same parameters as in Section 2.4.1 and interleaving with a short block interleaver of $I = \bar{\mathcal{D}}_{\mathcal{B}}/2 = 20$ and $I_c = 50$ (cf.

[3]Note that there is an overlap in the BER curves when considering $n_{\mathcal{B}} = d_{\text{free}}$ and $n_{\mathcal{B}} = \{0 \dots d_{\text{free}}\}$ in the post-waterfall region for the KSMLD, substantiating our claim of $\mathrm{PEP}(d_{\text{free}}, d_{\text{free}})\Upsilon(d_{\text{free}}, d_{\text{free}})$ being the dominant error term.

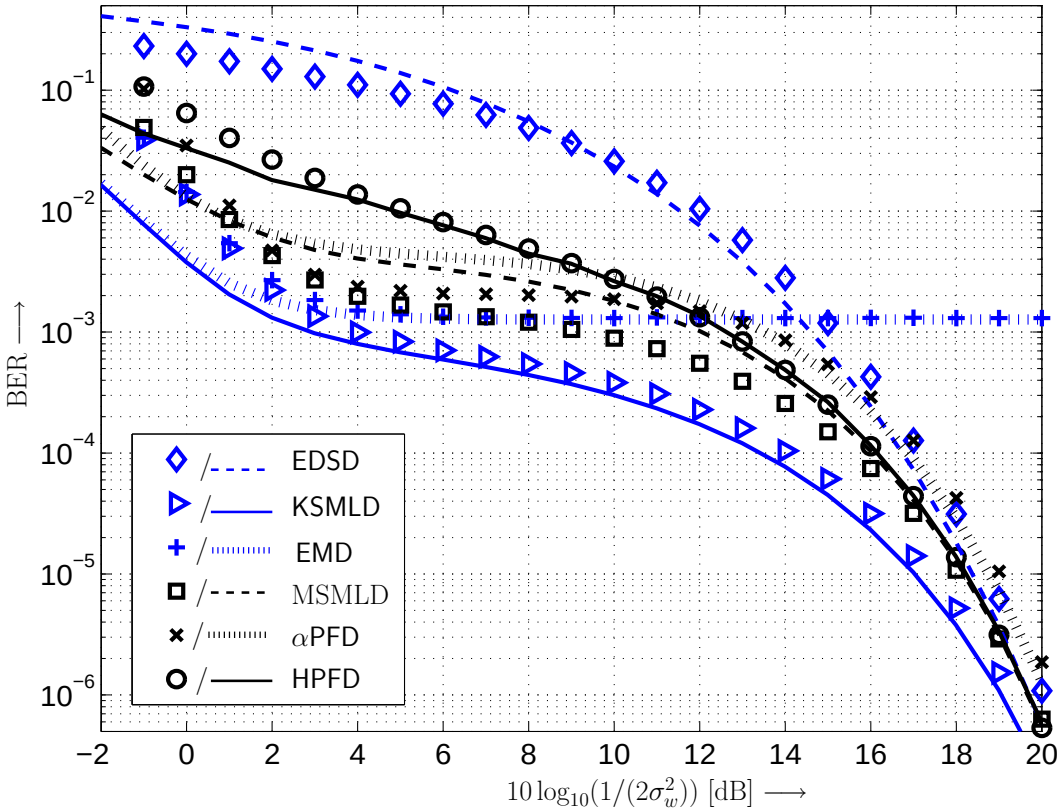

Figure 2.8 — BER performance of the various metrics proposed in Section 2.2 in the presence Markovian-Gaussian noise and a finite block interleaver of with depth $I = 20$. Lines: Analytical results. Markers: Simulations.

Section 2.3.1). Figure 2.8 shows the analytical (lines) and simulated BER (markers) results for the different detectors. For the sake of readability of the figure, only results for real-valued baseband transmission are shown. It can be seen that the BER expressions well approximate the simulation results for all the receivers. Furthermore, we observe that, different from ideal interleaving, the BER curves in Figure 2.8 tend to bunch up in the low BER region. This is a consequence of the larger multiplicative factors $\Upsilon(d, n_{\mathcal{B}})$ for $n_{\mathcal{B}} > 0$ compared to the ideally interleaved case. This also results in a rapid convergence of the BER curves for all detectors with increasing SNR. This fact is further highlighted in Figure 2.9, which shows the asymptotic BER approximation $\mathrm{PEP}(d_{\mathrm{free}}, d_{\mathrm{free}})\Upsilon(d_{\mathrm{free}}, d_{\mathrm{free}})$ (lines), i.e., only minimum distance error events, for the EDSD, MSMLD, and KSMLD, together with the corresponding simulation results.

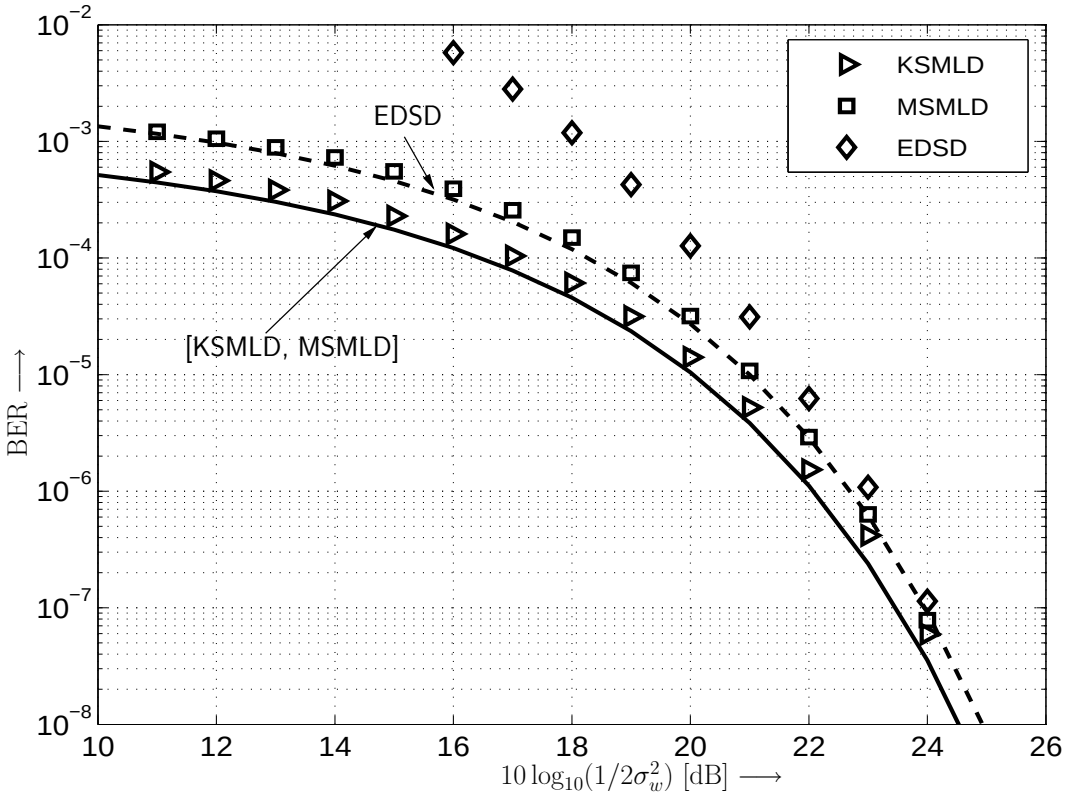

Figure 2.9 — Asymptotic BER results for different metrics proposed in Section 2.2 in the presence Markovian-Gaussian noise and a finite block interleaver of with depth $I = 20$. Lines show BER $\approx \mathrm{PEP}(d_{\mathrm{free}}, d_{\mathrm{free}})\Upsilon(d_{\mathrm{free}}, d_{\mathrm{free}})$. Markers: Simulation results.

Since this error event is seen to dominate performance for even moderately high SNRs, we conclude that insufficient interleaving limits the benefits of robust detection over EDSD to relatively high BERs. The necessary interleaver depth can quickly be determined by means of the analytical BER expressions derived in Section 2.3. To this end, Figure 2.10 presents the BER approximations for different effective interleaver depths, specified by the ratio $I/\bar{\mathcal{D}}_{\mathcal{B}}$. We consider the conventional EDSD and ideal KSMLD as benchmarks and recommend the α-PFD as an improved practical solution. We observe that $I/\bar{\mathcal{D}}_{\mathcal{B}} = 2$ leads to a BER performance close to that for ideal interleaving, which is consistent with the cutoff-rate results in Figure 2.3. We also note that the absolute value of $\bar{\mathcal{D}}_{\mathcal{B}}$ has negligible influence on performance, as can be seen from the curves for $I/\bar{\mathcal{D}}_{\mathcal{B}}$ with $\bar{\mathcal{D}}_{\mathcal{B}} = 40$ (solid line) and $\bar{\mathcal{D}}_{\mathcal{B}} = 20$ (dashed line). This can be expected

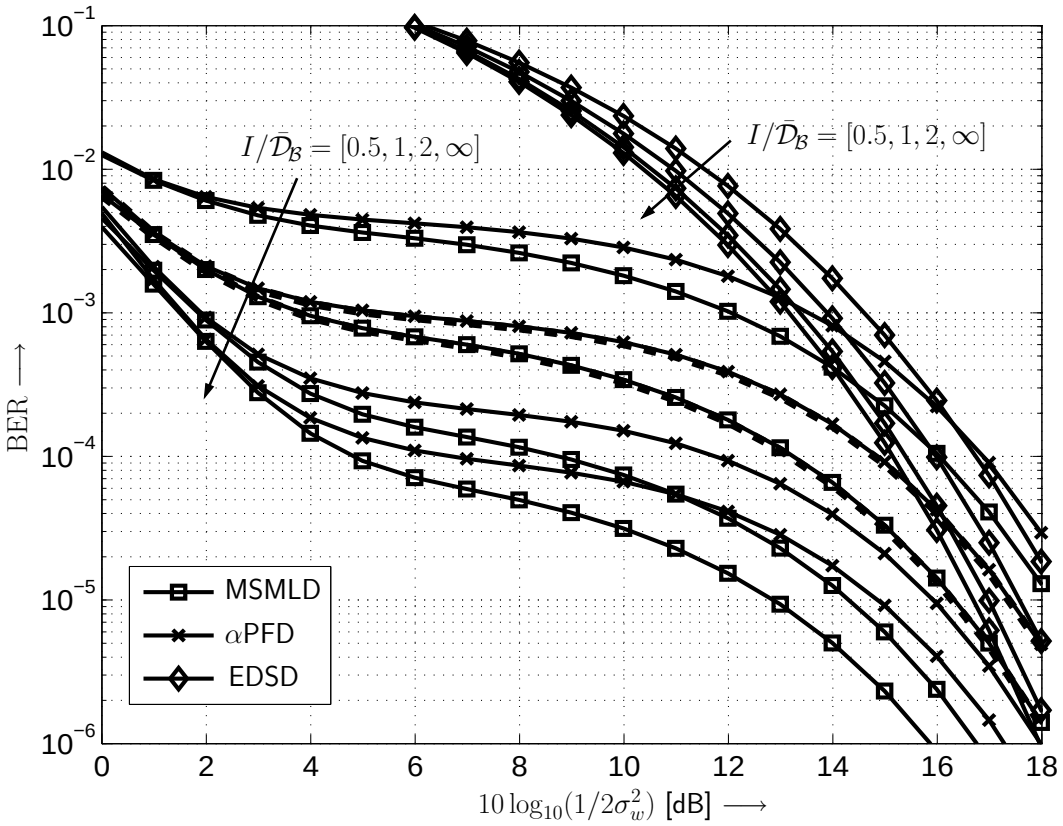

Figure 2.10 — BER performance for different metrics proposed in Section 2.2 in the presence Markovian-Gaussian noise and a finite block interleaver with depths $I = \bar{\mathcal{D}}_{\mathcal{B}} \times [0.5, 1, 2, \infty]$. Solid lines: $\bar{\mathcal{D}}_{\mathcal{B}} = 40$. Dashed lines (only for $I = \bar{\mathcal{D}}_{\mathcal{B}}$): $\bar{\mathcal{D}}_{\mathcal{B}} = 20$.

from the approximation in (2.15). Finally, we remark that the results in Figure 2.10 emphasize the importance of interleaving in order to realize performance gains with improved decoding metrics over the conventional EDSD.

In the next section, we apply the analytical techniques derived so far to coded communication over a narrowband powerline channel as a practically relevant example of a transmission medium that suffers from Markov modulated Gaussian noise.

2.5 Example Application: Powerline Channel

Transmission of data over powerlines has been known to be particularly challenging due to the numerous electromagnetic phenomena that may degrade the quality of the

transmitted signal at an intended receiver [58]. In fact, various measurement campaigns [1, 59, 60], has shown PLC to be impaired by high amplitude noise of bursty nature. Incidentally, the choice of the electric power distribution line as a candidate for ubiquitous data connectivity is motivated by the fact that it is the network with the most extensive coverage and hence is a medium that can provide access to even the remotest locations. Since the infrastructural investment for a powerline network is already in place for any geographical region which has an electrical power transfer line passing through it, the PLC comes to mind as the most promising solution to the last mile connectivity problem in many traditionally underdeveloped areas. Another reason for a lot of researchers being interested in transmitting data over PLCs is that several state-owned and power generation companies have a growing mandate of implementing smart (power) grids that are able to use more data than can be currently transmitted using the control channel of grid for intelligent utilization and distribution of power. However, since initially the potential for data communication over powerline channels was not identified, communicating data reliably over the PLC is susceptible to numerous impediments that if not accounted for may have pronounced detrimental effects on the transmitted data rendering it irrecoverable at the destination. As has been verified by several researchers, the primary reason for the PLC being regarded as a horrible channel [58] to transmit data is that the noise on a PLC channel cannot be described by a Gaussian distribution, as can be done to faithfully describe the statistical characteristics of the additive noise in other (conventional) communication systems. Such a limitation arises from the inability of a uni-variate Gaussian distribution in modeling the *impulsive* nature of the additive impairments on a PLC. In particular, impulsive noise on powerline channels may be time-varying periodic synchronous to the mains frequency, periodic but asynchronous to the mains frequency and asynchronous noise caused by, for example, random switching transients (cf. [1, 58, 61]).

2.5.1 Background and Related Work

Most research work that has considered performance evaluation for powerline channels models the non-Gaussian behaviour of the additive noise as an independent identically

distributed (i.i.d) by employing either a Class A model [11] or the ϵ-contamination model [16] (cf. Section 1.1.1). However, due to the characteristics of the powerline channels and the periodicity of the interfering signals from disparate sources associated with the PLC it is more than likely that the impulsive interference occurs in bursts. Recently, as a first step towards decoder design for PLCs where noise memory is decidedly non-negligible [41] considered a two-state Markov process to model the memory of the associated noise. In a powerline context, however, partitioned Markov chains (PMCs), have been shown to provide a better statistical characterization of the noise process [1]. PMCs were initially used by Fritchman [62] to describe the statistical dependence of errors in binary bursty channels. By comparison with experimental measurements, [1] showed that PMCs are excellent means to realistically model the additive noise in PLC as it allows one to account for the bursty nature of impulses. PMCs have been successfully used to characterize memory in communication channels in, for example, [62–64]. However, performance analysis of transmission schemes for PLC based on a PMC model has received limited attention. To the best of our knowledge an effort on these lines was made only in [65] where the performance results were presented for Turbo codes using Monte Carlo simulations.

In the following, we characterize the performance of transmission schemes using a realistic model for a narrowband PLC channel based on partitioned Markov chains as proposed in [1]. We obtain performance limits in the presence of the additive Markov modulated noise process by adapting the analytical techniques obtained in Section 2.3 to PMC. Rigorous methods are then developed to evaluate the expressions are for the cutoff rate and bit error rate of a convolutionally coded system. Furthermore, we consider the applicability of some of the robust metrics introduced in Section 2.2 to decoding in a PLC environment. Their respective capabilities are then highlighted by numerical evaluation of the R_0 and BER expressions applicable to each metric. The multi-state nature of the MCs considered require a computationally intensive evaluation. We propose a novel approach for faster evaluation of the theoretical BER expressions that is based on a state reduction of the multi-state MC. As before, interleaving is also investigated as one of the design parameters of the system and its effect

is quantified in the results obtained.

2.5.2 PLC Additive Noise Model

Since we consider the same system model as in Figure 2.1, we urge the reader to refer to the same for a description. A frequency-flat channel is considered in order to focus more on the detrimental additive impairments in PLC environments. Thus the results and discussion are better suited to narrowband PLC systems where the bandwidth can be of the order of MHz. The noise model characterized by a PMC has several interesting features that are different from the two-state model that we had adopted so far. The received symbol can still be written in the following simple form (this is same as in Section 2.1 and has been reproduced here only for convenience)

$$r_k = x_k + n_k \ , \ \text{with } n_k = w_k + i_k \ , \tag{2.49}$$

where n_k is the total noise comprised of the additive white Gaussian noise (AWGN) component w_k with variance σ_w^2 and the impulsive component i_k. The characteristics of the powerline channel entail that more than two states would be required to adequately model the occurrence of the impulsive noise over a PLC. i_k has typically been observed to be bursty with varying impulse widths and hence Markov chains have been found to be an effective way to model the dependence and the inter-arrival times (IATs) amongst bursts [1, 41, 62, 63]. Although a two-state Gilbert-Elliot (GE) model [41] provides higher mathematical tractability and ease of analysis, here we follow a multi-state Markov model as proposed in [1] because of its strong agreement with actual powerline channels. The need for a multi-state model arises since the distribution of IATs and widths of the impulsive phenomenon have been found to be better described as a superposition of exponential distributions. Therefore, an extension of the GE model to a partitioned Markov chain with variable number of states, each modeling a certain inter-arrival time and belonging to one of the two partitions seems a plausible choice. We describe next the implications of such a model for the asynchronous impulsive noise.

Partitioned Markov Chains

Since the particular details of modeling memory using discrete Markov chains has been extensively explained elsewhere, (cf. e.g. [66]) we will very briefly present here the basics of PMCs and the flexibility they afford in modeling the impulsive phenomena that impairs transmission in a PLC environment. More generally, we represent the noise state at instant k as s_k and it is postulated that $s_k \in \mathcal{S}$ where $\mathcal{S}$ now denotes the state space of the Markov chain and has a cardinality $K{=}|\mathcal{S}|$, i.e., we consider a K-state Markov chain. Out of the K states, ν states are considered to belong exclusively to a set $\mathcal{G}$ and the rest of the $\mu{=}(K-\nu)$ states belong to set $\mathcal{B}$, therefore, $\mathcal{G}$ and $\mathcal{B}$ are disjoint sets. In the context of PLC, the sets $\mathcal{G}$ (good) and $\mathcal{B}$ (bad) denote respectively the absence and presence of impulsive noise. When $s_k{\in}\mathcal{G}$ the noise variance is $\sigma^2_{\mathcal{G}}{=}\sigma^2_w$ and $s_k{\in}\mathcal{B}$ implies a variance of $\sigma^2_{\mathcal{B}_i}{=}\kappa_i\sigma^2_w$ where $i{\in}\{1,2,\ldots,\mu_i\}$ and $\kappa_i \gg 1$ is indicative of the strength of the impulse with respect to the background noise. A flow graph description of the above is shown in Figure 2.11 where $K=5$ and $\nu=3$. Figure 2.11 shows the representation of the PMC using both the original Fritchman model [62] and the model used in [1] that introduces latent transition states U and V between the sets $\mathcal{G}$ and $\mathcal{B}$ for ease of representation. While the Fritchman representation uses a probability transition matrix $\mathbf{T}$ where the $(i,j)^{\text{th}}$ entry $\mathbf{T}_{i,j}$, is given by $p(s_k{=}j|s_{k-1}{=}i)$ which is the probability of state s_k given s_{k-1}, the state-augmented approach of [1] allows us to obtain independent transition matrices $\mathbf{G}$ and $\mathbf{B}$ for the respective sets $\mathcal{G}$ and $\mathcal{B}$ such that

$$\mathbf{G}{=}\begin{bmatrix} g_{1,1} & 0 & 0 & g_{1,U} \\ 0 & g_{2,2} & 0 & g_{2,U} \\ 0 & 0 & g_{3,3} & g_{3,U} \\ g_{V,1} & g_{V,2} & g_{V,3} & 0 \end{bmatrix},\ \mathbf{B}{=}\begin{bmatrix} b_{1,1} & 0 & b_{1,V} \\ 0 & b_{2,2} & b_{2,V} \\ b_{U,1} & b_{U,2} & 0 \end{bmatrix}, \tag{2.50}$$

when $|\mathcal{G}|=3$ and $|\mathcal{B}|=2$ and $g_{i,j}$ and $b_{i,j}$ are the respective state transition probabilities. The transition between the models is rather seamless and in fact [62] employs a modified Markov Chain (refer Fig. 3 in [62]) which forms the basis of state augmentation. $\mathbf{T}$, $\mathbf{G}$ and $\mathbf{B}$ are all row-stochastic matrices. The transition probability matrix along with the initial state probability distribution $\boldsymbol{\pi}_0 = \{\pi_0(1)\ldots\pi_0(K)\}$ specifies the Markov chain completely. Moreover, it is assumed that if both $s_k, s_{k-1} \in \mathcal{G}$ or $\mathcal{B}$, then

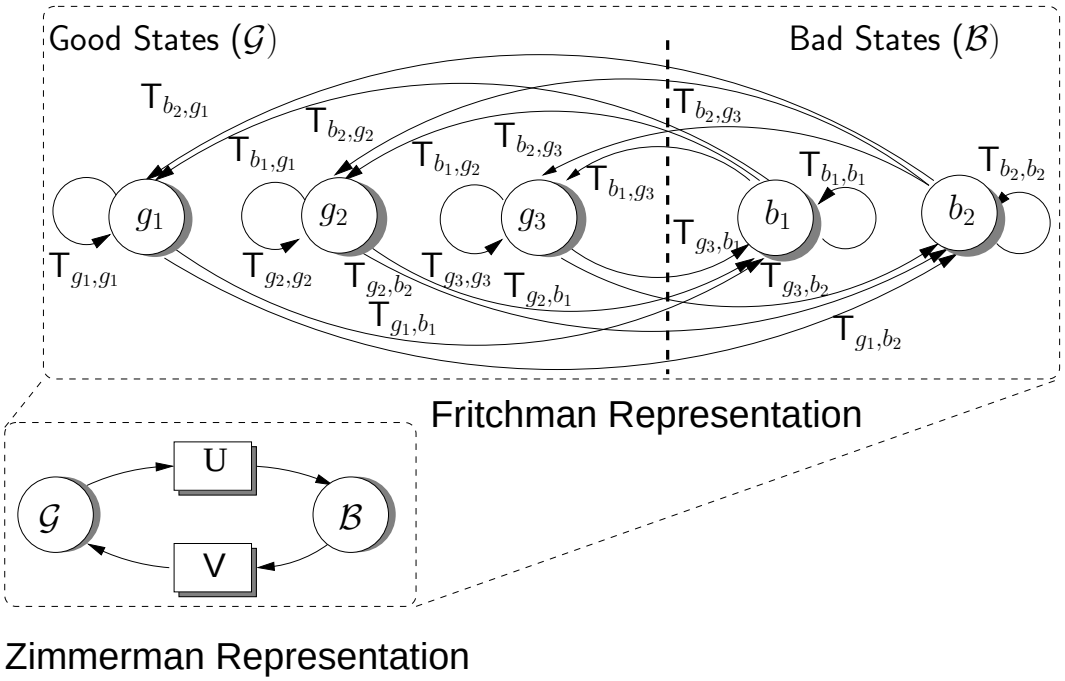

Figure 2.11 — Modeling asynchronous powerline channels using a partitioned Markov Chain with $\mathcal{G}$ denoting a collection of AWGN noise states while $\mathcal{B}$ states denote the presence of impulsive noise.

it implies that $s_k{=}s_{k-1}$ otherwise $p(s_k|s_{k-1}) \neq 0$ iff $s_{k-1} \in \chi,\ s_k \in \bar{\chi},\ \chi \in \{\mathcal{G}, \mathcal{B}\}$ i.e., inter-state transitions within $\mathcal{G}$ or $\mathcal{B}$ are prohibited (see Fig. 2.11).

2.5.3 Decoding

At the receiver decoding proceeds in a manner similar to that described in Section 2.1 and Section 2.2 for 2-state Markovian noise. We evaluate the EDSD, KSMLD, MSMLD and the α-PFD as these represent different design strategies that may be pursued in multi-state noise environments. Based on the received signal samples, metrics are computed to determine the transmitted signals based on a maximum likelihood (ML) criterion using a Viterbi decoder as before. We remark that a KSMLD-like detector may be practically infeasible for a PLC channel even if estimation were to performed, due to the large number of states involved. The MSMLD metric on the other hand represents an idealized memoryless detector with the milder requirement of the impulsive noise process with different IATs and the respective variances without the need for estimating

any temporal correlation. The MSMLD metric is therefore a weighted average of the respective state metrics and is given by

$$m(\tilde{x}_k|r_k) = \sum_{i=1}^{K} \pi_i \frac{1}{\sqrt{2\pi\sigma_{s_i}^2}} \exp\left\{\frac{|r_k - \tilde{x}_k|^2}{2\sigma_{s_i}^2}\right\}, \tag{2.51}$$

where π_i is the stationary probability of being in state $s_i \in \mathcal{S}$.

The α-PFD does not require any changes to be applied to the PLC channel, however prior offline optimization of the parameter α will definitely improve performance. For simulative results, we will use a fixed value of α, however an optimization exercise on the lines of Section 2.4.2 should be straightforward.

2.5.4 Error Performance Analysis

The use of a Markovian structure to characterize the powerline channel allows one to consider it as a finite state channel whereby it is completely described by the conditional probability measure $P(y_k, s_k|x_k, s_{k-1})$ [67]. In what follows, we use this fact to obtain analytical expressions for the cutoff rate and BER of the PLC channel. Much of the development presented here relies heavily on the derivations in Section 2.3 and hence for the sake of brevity, details of the derivation will be omitted and the interested reader can always revisit Section 2.3 for the same. Considering data transmission in blocks of length N, the transmitted and received signal vectors are denoted as $\boldsymbol{x} = [x_1, \ldots, x_N]$ and $\boldsymbol{r} = [r_1, \ldots, r_N]$ respectively, with a cumulative decoding metric $\Lambda(\boldsymbol{x}|\boldsymbol{r})$.

We again choose to obtain (union) bounds on the BER due to infeasibility of computation of an exact error rate expression, which for a rate$-k/n$ convolutional code is given by

$$P_b \leq (1/k) \sum_{d_{\mathrm{H}}=d_{\min}}^{\infty} W(\boldsymbol{e}) \sum_{\boldsymbol{s}\in\mathcal{S}^{Le}} \mathrm{PEP}(\boldsymbol{e}|\boldsymbol{s_e})\Pr(\boldsymbol{s_e}) \,, \tag{2.52}$$

where $W(\boldsymbol{e})$ is the input weight of the error vector $\boldsymbol{e}$ of length $L_{\boldsymbol{e}}$ and $\boldsymbol{s_e}$ is the sequence of noise states corresponding to $\boldsymbol{e}$. $d_{\mathrm{H}}(\boldsymbol{e})$ denotes the Hamming weight of $\boldsymbol{e}$ and $d_{\min}$ is the minimum Hamming distance between two valid codewords. $\mathrm{PEP}(\boldsymbol{e}|\boldsymbol{s_e})$ is the pairwise error probability (PEP) between the correct vector $\boldsymbol{x}$ and the alternative

vector $\tilde{\boldsymbol{x}}$ that results in the error vector $\boldsymbol{e}$. Computation of PEP($\boldsymbol{e}|\boldsymbol{s_e}$) will depend on the metric considered (refer Section 2.2) and the respective approaches for each of the considered metrics are detailed in Section 2.3. For the KSMLD, we use the closed form expressions developed earlier. The second summation averages over all possible noise state vectors $\boldsymbol{s_e}$ of length $L_{\boldsymbol{e}}$. The key consideration for computation of BER is therefore finding $\Pr(\boldsymbol{s_e})$. We denote the m^{th} possible sequence of states (out of K^{L_e} possible sequences) for a path of length $L_{\boldsymbol{e}}$, as ℓ_m. Depending on the value of K, the averaging could be over a prohibitively large number of sequences and would require considerable computational effort in evaluating $\Pr(s_{\boldsymbol{e}})$, which is wasteful.

State Reduction for multi-state Markov Chains

Interestingly, in spite of $K(>2)$ noise states most noise models can well incorporate different impulse strengths with a maximum of 2 or 3 different variances. Therefore, a significant reduction in computational effort can be obtained by defining *observation sequences* (OS). An OS is the sequence of noise variances (rather than noise states) in a transmitted block of data. For the purposes of BER computation it suffices to average over OSs since it is the variance of the noise that determines the probability of error at each epoch. For example, although it is possible that at time t the noise process is at any of the ν good states, the variance is σ_w^2 regardless of which particular good state it is in. We denote an OS of length $L_{\boldsymbol{e}}$ as $\boldsymbol{o}=[o_1 \dots o_{L_e}]$ where $o_i \in \{\sigma_1^2, \dots, \sigma_\nabla^2\}$, ∇ being the total number of variances of the multi-modal noise process and hence $\boldsymbol{o} \in \nabla^N$. Consequently, there is a significant reduction in the number of sequences to be considered from K^{L_e} to $\nabla^{L_e}, (\nabla \leq 3)$.

Computation of Probability of Observation Sequences: Reducing the state space of the MC from K to ∇, poses the task of incorporating the the respective subset states of $\mathcal{G}$ and $\mathcal{B}$. We devise here an algorithm that allows the computation of probability of OSs from the original transition probability matrix $\mathbf{T}$. For the ℓ_m^{th} OS, let the probability of being in a state $s_i \in \mathcal{S}$ at time t, given the observation sequence up to time t, be denoted by $\beta^{\ell_m}(t, s_i)$. The following forward algorithm is used to recursively

compute $\beta^{\ell_m}(t, s_i)$

$$\beta^{\ell_m}(t, s_i) = \sum_{s_j \in \mathcal{S}} \beta^{\ell_m}(t-1, s_j)\mathbf{T}^{m_d}(s_j, s_i)\Pr(o_t|s_i) \tag{2.53}$$

where $s_i, s_j \in \mathcal{S}$, m_d is the the distance between consecutive bits in error for a given $\boldsymbol{e}$ and $\mathbf{T}^m$ denotes the m^{th} power of $\mathbf{T}$. $\Pr(o_t|s_i)$ is an indicator function such that $\Pr(o_t|s_i) = 1$ when both o_t and s_i belong to the same partition, i.e., $\mathcal{G}$ or $\mathcal{B}$. Finally, the probability of an OS is computed as

$$\Pr(\boldsymbol{o}|\boldsymbol{e}) = \max_{s_i} \beta^{\ell_m}(L_{\boldsymbol{e}}, s_i) \tag{2.54}$$

2.5.5 Cutoff Rate with Multi-State Markov Modulated Noise

As in Section 2.3.2 we resort to the *generalized* cutoff rate here as well with the added consideration of the multiple states of the PMC. To keep the derivations tractable we obtain average PEP expressions independent of $\boldsymbol{s}$ and recalling the cutoff rate expressions from Section 2.3.2 we have

$$R_0 = \lim_{N\to\infty} \max_{\lambda \in \mathcal{R}} -\frac{1}{N} \log_2 \Bigg[\sum_{s_0 \in \mathcal{S}} p(s_0) \sum_{\boldsymbol{s} \in \mathcal{S}^N} \prod_{k=1}^{N} p(s_k|s_{k-1}) \left(\frac{\Phi_\delta(\lambda|s_k) + 1}{2} \right) \Bigg], \tag{2.55}$$

where $\Phi_\delta(\lambda|s_k)$ is the Laplace transform of the metric difference $\delta = m(-1|r_k) - m(+1|r_k)$ and $\mathcal{S}$ denotes the K-fold state space of the noise process. We find it convenient to use the Fritchman representation here with the overall transition probability matrix $\mathbf{T}$ defined in Section 2.5.2. Substituting

$$\mathbf{\Phi}(\lambda) \doteq \begin{pmatrix} \Phi_\delta(\lambda|g_1)+1 & 0 & \dots & \dots & 0 \\ 0 & \Phi_\delta(\lambda|g_2)+1 & 0 & \dots & \vdots \\ 0 & \ddots & \ddots & \ddots & 0 \\ \vdots & \ddots & \Phi_\delta(\lambda|g_{|\mathcal{G}|})+1 & \ddots & \vdots \\ \vdots & \ddots & 0 & \Phi_\delta(\lambda|b_1)+1 & \vdots \\ \vdots & \ddots & \ddots & \ddots & 0 \\ 0 & \dots & \dots & 0 & \Phi_\delta(\lambda|b_{|\mathcal{B}|})+1 \end{pmatrix} \tag{2.56}$$

Table 2.1 — Transition probability matrices of the good (**G**) and bad (**B**) states from [1].

$$\mathbf{G} = \begin{pmatrix} 0.999978 & 0 & 0 & 0 & 0 & 0.000022 \\ 0 & 0.817342 & 0 & 0 & 0 & 0.182658 \\ 0 & 0 & 0.999213 & 0 & 0 & 0.000787 \\ 0 & 0 & 0 & 0.990030 & 0 & 0.009970 \\ 0 & 0 & 0 & 0 & 0.720266 & 0.279734 \\ 0.443289 & 0.046604 & 0.090819 & 0.113522 & 0.305765 & 0 \end{pmatrix}$$

$$\mathbf{B} = \begin{pmatrix} 0.884490 & 0 & 0.115510 \\ 0 & 0.399129 & 0.600871 \\ 0.078748 & 0.921252 & 0 \end{pmatrix}$$

in Eqn. (2.55) leads to the same compact form of Eqn. (2.28). Furthermore, invoking the Perron-Frobenius theorem again, allows as to represent the cutoff rate in the convenient form of Eqn. (2.30) with $\mathbf{\Phi}$ now defined as Eqn. (2.56). The expressions for $\Phi_\delta(\lambda|s_k)$ for each of the metrics are straightforwardly computed from the results for a 2-state Markov Chain presented in Section 2.3.

2.5.6 Numerical Results and Discussion

In this section we present the results of numerical evaluation of the expressions in Section 2.3 in order to gain a better understanding of the behaviour of the noise process and infer design considerations for PLC. Following [1], we have $\nu = 5$ and $\mu = 2$. The matrices **G** and **B** were computed in [1] based on experimental measurements of IATs and are depicted in Table 2.1 for reference. While a single variance $\sigma^2_{\mathcal{G}}$ is applicable to all states in $\mathcal{G}$, two different variances ($\sigma^2_{\mathcal{B}_i} = \kappa_i \sigma^2_{\mathcal{G}}, i = 1, 2$) with $\kappa_1 = 10^4$ and $\kappa_2 = 10^2$ were identified for the observed impulses in the measurements of [1]. The cutoff rate results apply to an ensemble of codes of a certain rate and are independent of the specifics of the code. The BER results, however, are for a memory $M = 4$, rate-1/2 convolutional code with generator polynomials $(23, 35)_8$ and thus are applicable for designs that require low computational effort and delay, as opposed to using iterative

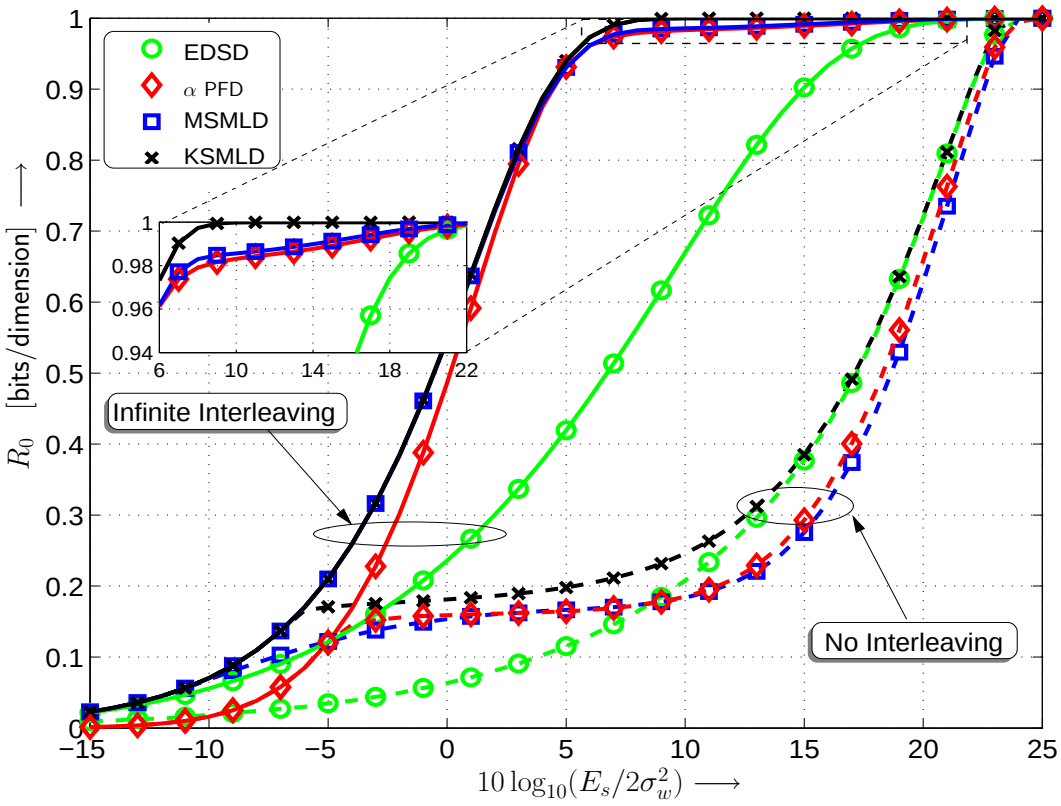

Figure 2.12 — Cutoff rate for transmission over a PLC modeled as partitioned Markov Chain with same variances $\sigma^2_{\mathcal{B}2}$ for all the bad states.

decoding techniques [65, 68].

We note that for the α-PFD the choice of the parameter α plays an important role here as well. When the noise is more Gaussian a value of α closer to 0.1 is preferred whereas $\alpha \geq 1.0$ is favorable when the noise is highly impulsive [49].

Cutoff Rate Evaluation

Using the expressions from Section 2.5.5, we evaluate R_0 for the different decoding metrics first with the same variance ($\sigma^2_{\mathcal{B}_2}$) for all bad states in Figure 2.12 and then different variances ($\sigma^2_{\mathcal{B}_1}$, $\sigma^2_{\mathcal{B}_2}$) in Figure 2.14. In order to highlight the effect of memory of the noise process on overall performance, we present results for (a) no interleaving (dashed lines, R_0^{mem}) and (b) infinite interleaving (solid lines, R_0^{inf}).

As is evident from Figure 2.12 the performance with interleaving is markedly better for all metrics, however, different metrics stand to have different gains from the interleaving process. All decoders other than the EDSD are seen to ramp up quickly to the maximum, $R_0^{\text{inf}} = 1$ for SNR > 0 dB, with gains of up to of 0.8 bits/dimension for R_0^{inf} over the respective R_0^{mem} at about 5dB. EDSD is however rather deficient in terms of coping with the impulsive noise and requires SNRs as high as 20 dB to achieve the same performance levels. It should also be noted that R_0^{mem} for all metrics has very similar behaviour for moderate to high SNRs. While R_0^{mem} for MSMLD is seen to be the worst of all detectors, the improvements with infinite interleaving lead to an overlap of the corresponding R_0^{inf} curve of MSMLD with that of KSMLD (which is the best possible). In fact, only minor losses in the MSMLD cutoff rate (with respect to KSMLD) are seen to occur at high R_0^{inf} values as shown in the zoomed in version in the inset block of Figure 2.12. Furthermore, it is highly encouraging to note that the relatively blind α-PFD again performs very close to the MSMLD and KSMLD curves that have partial and perfect SI respectively.

Unlike the EDSD, the KSMLD, MSMLD and the α-PFD make a conscious effort to mitigate the degrading effects of the impulse noise and hence we see a two-part behaviour of their respective R_0^{mem} curves with a threshold SNR point. Beyond this SNR point, the limits on error-free communication are set by the impulsive noise rather than the background Gaussian noise. Interestingly, this is also the point where the R_0^{inf} and R_0^{mem} curves part ways for the aforementioned detectors. This is intuitive as the AWGN is i.i.d and hence in the regions of SNR where it dominates, in effect, the received signal is impaired by a memoryless process. However, beyond this threshold point the impulsive process dominates and hence the memory in the noise process plays a role. This is further substantiated in Figure 2.13 where the variation in R_0^{mem} for KSMLD with respect to κ is shown. As expected, a higher κ implies a higher required SNR for a given R_0. The curves are seen to be identical till a threshold SNR of about -5

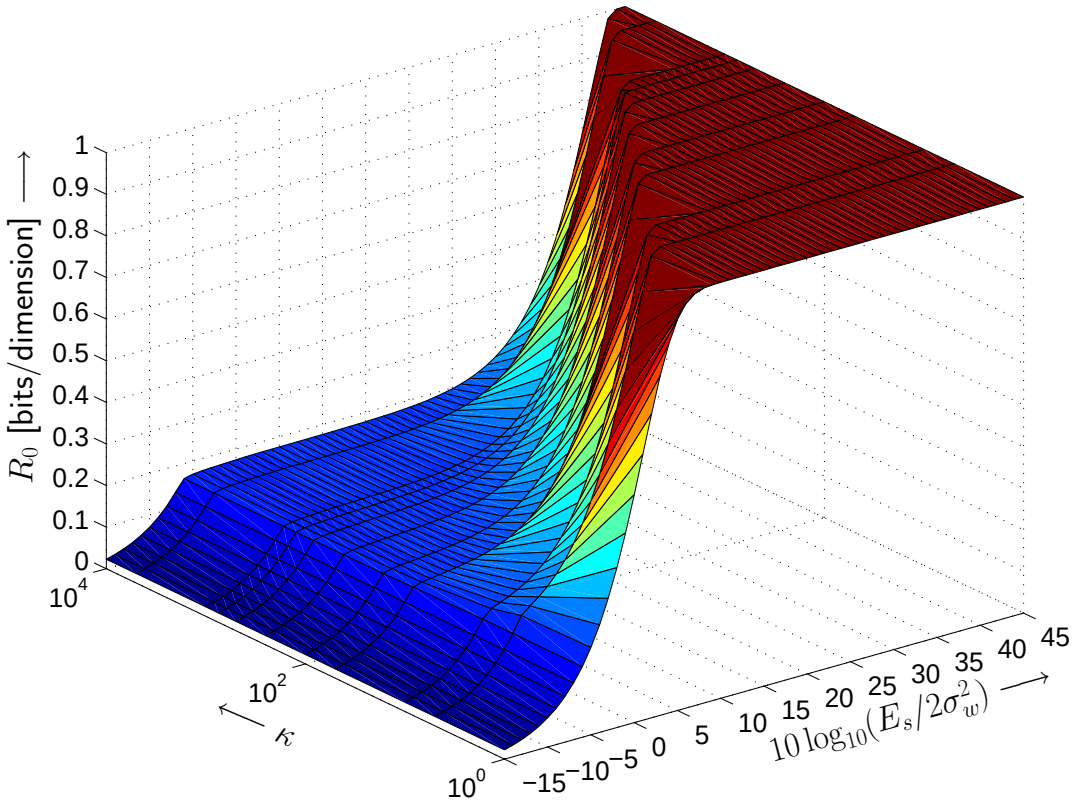

Figure 2.13 — Cutoff rate of KSMLD with varying κ when no interleaving is used. A distinct two-part behaviour is exhibited due to noise memory with $10\log(E_s/N_0) = -5$dB being the threshold point.

dB, regardless of the value of κ and beyond this point a higher κ pushes the R_0 curve further to the right.

Figure 2.14 provides even more interesting insights when the impulses have two different variances. In this case the R_0^{mem} curves are seen to exhibit a 3-part behaviour depending on which of the noise variances dominate. For obvious reasons, a much higher SNR is required for the detectors to reach $R_0^{\text{mem}} = 1$ bit/dimension, however, surprisingly with sufficient interleaving the R_0^{inf} curves are exactly the same as when the impulses have same variance ($\sigma^2_{\mathcal{B}_2}$). Unlike the previous case, the R_0^{mem} is noticeably better for KSMLD than other detectors. The EDSD fails to perform well even when requisite interleaving is present and requires prohibitively high SNRs for error free transmission even for moderate code rates.

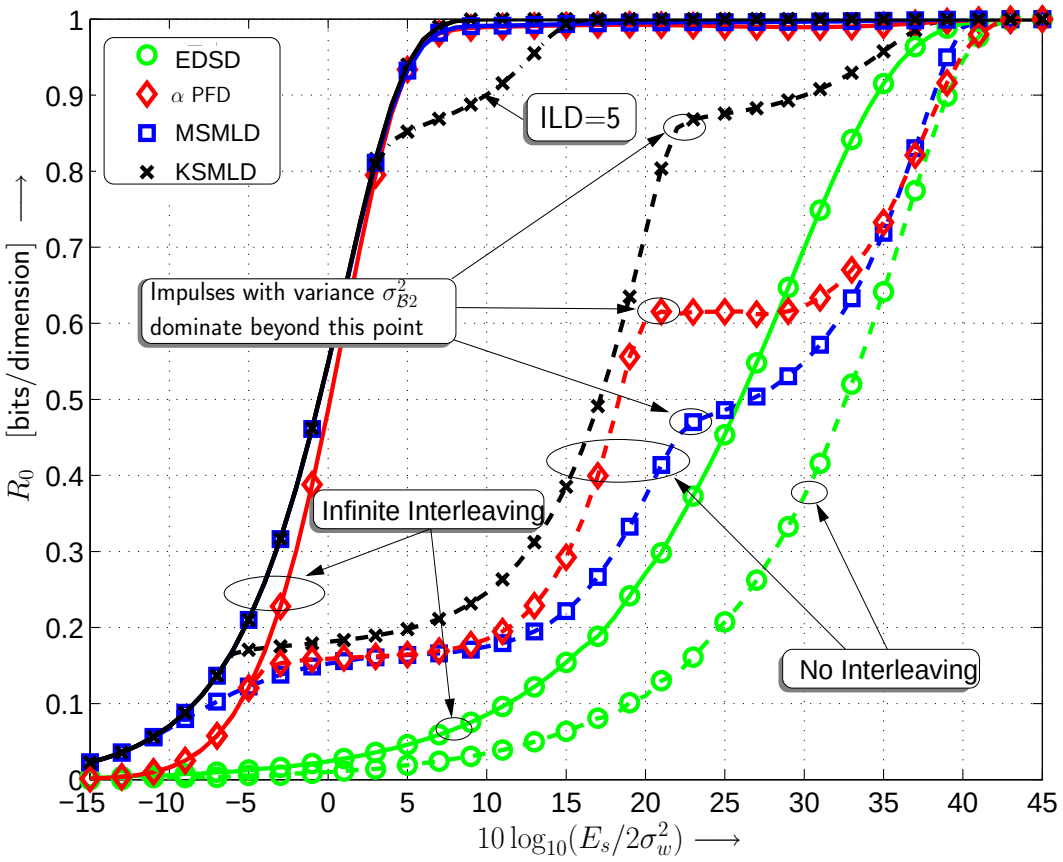

Figure 2.14 — Cutoff rate for transmission over a PLC with 2 bad states with variances $\sigma^2_{\mathcal{B}1}$ and $\sigma^2_{\mathcal{B}}$. A 3-part behavior of the non-interleaved curves shows the distinct regions of dominance of $\sigma^2_{\mathcal{G}}$, $\kappa_1\sigma^2_G$ and $\kappa_2\sigma^2_{\mathcal{G}}$.

Comments on Interleaving Depth (ILD): While the above results clearly show that there are huge performance gains when the noise process can be rendered memoryless, practical interleavers are limited by the acceptable delay at the receiver and hence we will have a finite ILD. However, the ILD needs to be only large enough to closely mimic infinite interleaving. The average burst duration ($\bar{\mathcal{D}}_{\mathcal{B}}$), i.e. the average time spent in the bad state once the noise process enters a bad state/partition [69], is the key parameter that determines the requisite ILD. Since $b_{i,j}=0$ if $i\neq j$ we put forth the notion of state-based $\bar{\mathcal{D}}_{\mathcal{B}}$ leading to the parameters $\bar{\mathcal{D}}_{\mathcal{B}_1}$ and $\bar{\mathcal{D}}_{\mathcal{B}_2}$ corresponding to the two bad states in the current PMC model, where

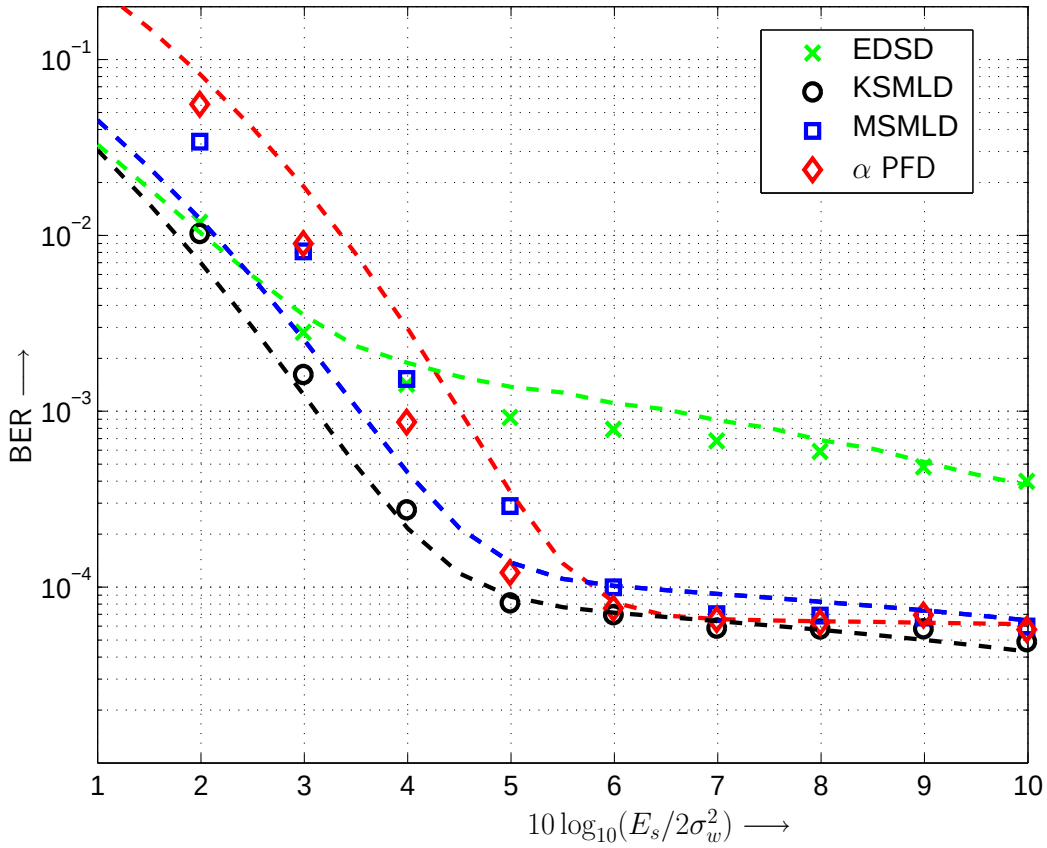

Figure 2.15 — BER performance over a PLC channel with a rate-1/2 convolutional code with no interleaving. Finite memory in noise process leads to an error floor. Lines: Analytical results. Markers: Simulation results.

$$\bar{\mathcal{D}}_{\mathcal{B}_i} = \frac{\Pr\left(s_0 \in \mathcal{G}, s_k \in \mathcal{B}_i, s_{\bar{\mathcal{D}}_{\mathcal{B}_i}+1} \in \mathcal{G}\right)}{\Pr\left(s_k \in \mathcal{G}, s_{k+1} \in \mathcal{B}_i\right)} = b_{i,i}^{-1}\,, \tag{2.57}$$

with $k = \{1, 2 \ldots \bar{\mathcal{D}}_{\mathcal{B}_i}\}$. Therefore, $\bar{\mathcal{D}}_{\mathcal{B}_1} = 8.66$ and $\bar{\mathcal{D}}_{\mathcal{B}2} = 1.67$ (refer Table 2.1). We further note that the design guideline of ILD $= 2\bar{\mathcal{D}}_{\mathcal{B}}$ when $0 \leq \sum_{i\in\mathcal{B}} \pi_i \leq 0.1$ for the noise to *appear* memoryless at the receiver regardless of κ, is further highlighted in Figure 2.14. We plot in Figure 2.14 the R_0-curve for KSMLD with ILD$=5$. Although sufficient to mitigate the effect of impulses corresponding to noise state $\mathcal{B}_2$, this level of interleaving fails to completely eliminate the correlation of impulses from $\mathcal{B}_1$.

BER performance

We next present the results for the numerical evaluation of BER expressions obtained in Section 2.3 and verify their level of accuracy by comparing with Monte Carlo simulations. We again use only $\sigma_{\mathcal{B}2}$ We first consider the results for non-interleaved transmission in Figure 2.15. The bursty impulsive noise severely limits performance and an error floor sets in at BER $= 10^{-4}$ even when the noise states are known. The dashed lines represent the BER obtained analytically through union bounding techniques and can be seen to provide a noticeably good match with the simulation results in the high SNR regions, however, discrepancies do exist in the high BER region, which nonetheless is not the region of interest. Similar to the R_0 curves the α-PFD is seen to compare favorably with both KSMLD and MSMLD. The EDSD floors out at a much higher level compared to the other decoders and thus is clearly not the decoder of choice.

Next, a 80×25 (ILD $= 80$) block interleaver is employed to mitigate the memory effects and at the same time keep the delay at moderate levels. The corresponding BER results are shown in Figure 2.16. Although, admittedly the convolutional code considered is rather weak, the decoders are still able to achieve sufficiently low BERs $\rightarrow 10^{-8}$ and the capabilities of the α-PFD are further visible with a performance within 0.3 dB of the KSMLD. Furthermore, BER performance of the naive EDSD deviates significantly from the rest of the decoders with an increase in SNR. This can be attributed to the fact that at moderate to high SNRs most errors are due to impulsive noise and the EDSD is ill-equipped to handle the same.

2.6 Summary and Conclusions

In this chapter, we studied convolutionally coded transmission for communication environments where the overall noise process exhibits an impulsive behaviour and hence is non-Gaussian. Furthermore, the noise is temporally correlated and the correlation is modeled using a first-order Markov chain. We have considered and proposed several

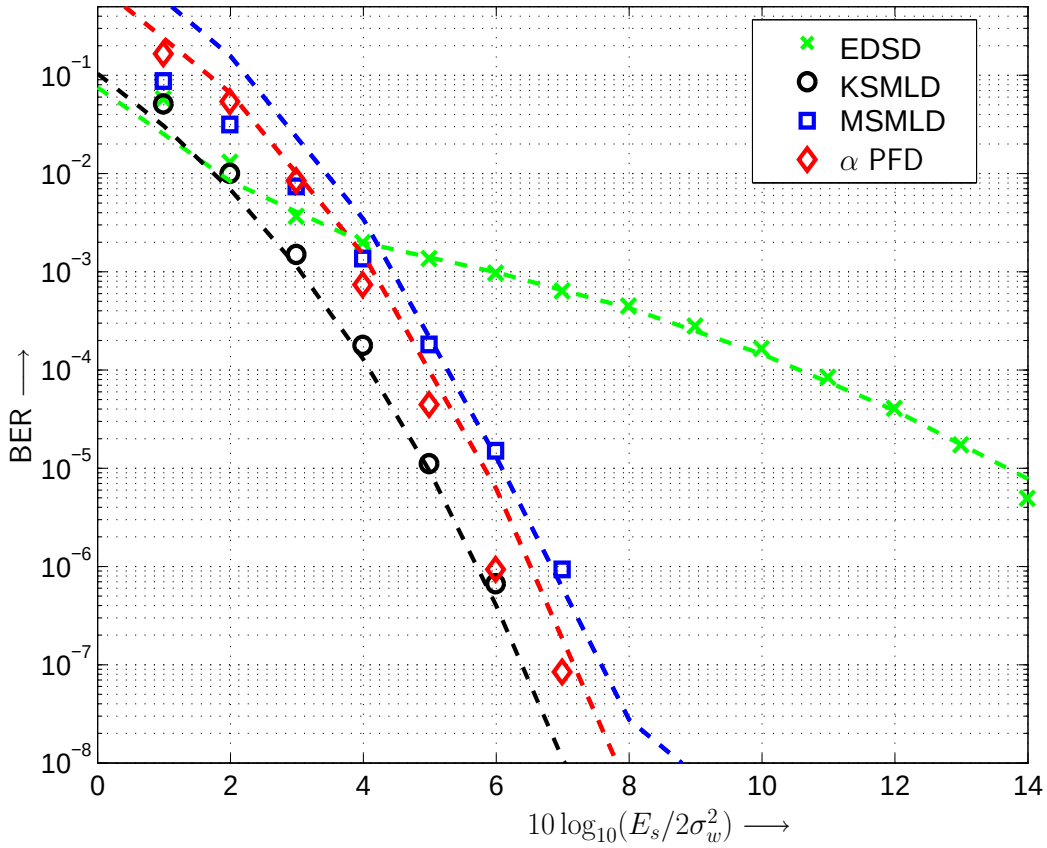

Figure 2.16 — BER of different decoding metrics on a PLC channel modelled as PMC with a 80×25 block interleaver. Lines: Analytical results. Markers: Simulation results.

decoding metrics for the resulting Markov-Gaussian environment than are better suited to decoding in such environments than conventional Euclidean distance metric, which is optimal in Gaussian noise. We further account for non-ideal channel interleaving in communication systems which has traditionally been used as an effective means of mitigating memory in channel impairments. Incorporating the interleaving depth (ILD) as a design parameter, we have derived analytical and semi-analytical expressions for the evaluation of the cutoff rates and BERs associated with the decoding metrics. These expressions are applicable to the prediction of decoding performance with finite-depth interleaving, which as a special case includes the memoryless channel as well. Numerical evidence has been presented that confirms the usefulness of the analytical results, shows

the efficacy of robust decoding metrics, and also highlights the differences to the case of transmission over AWGN channels. Finally, we considered narrow-band transmission over a powerline channel as an example of a real-life transmission medium where a Markov-Gaussian noise model has been shown to faithfully describe the associated noise.

CHAPTER 3

Hierarchical Spectral Access: Coexistence through Improved Cognition

In this chapter, abandoning the assumption of knowledge of interference parameters for the perfect receiver, we consider the estimation of the interference at the receiver when it has the same correlation structure as introduced in Chapter 2 and evaluate the applicability of receiver structures based on such estimation to cognitive radio (CR). The idea of estimation of interference parameters when such information is unavailable fits quite naturally to the framework of CR and we would like to take advantage of that to design interference-tolerant receivers. As mentioned in Chapter 1, CR is a communication paradigm that is set to play an increasingly important role in future

generations of wireless systems. It is considered to be the enabling technology for dynamic spectral access (DSA), a relatively new frequency allocation regime, which has become increasingly popular over the last decade. Ever since the idea of spectral allocation came about, frequency bands have been regulated through *licensed* use and this has led to radio frequency spectrum being increasingly scarce due to unprecedented demands. Hence it was natural to question how well the allocated spectrum was being used. The findings of the Spectrum Policy Task Force [70], although a surprise to many, established that depending on the population density of a geographical region most spectral bands tend to be vastly underutilized [71]. This makes a strong case for more efficient use of the available spectrum through DSA [72, 73]. DSA advocates a much more flexible approach to spectral allocation and several mechanisms have been proposed to achieve the same. Most DSA approaches can be classified into one of the following three [73,74]: 1) a *dynamic exclusive* model which is only a minor variation of the existing license allocation method where license holders may lease unused spectrum to other users, 2) an *open sharing* model which abolishes licensing altogether and allows for open access to all spectrum and 3) a *hierarchical model* where users are categorized as **primary** and **secondary**, with primary users having non-exclusive prioritized rights for a given frequency band. As the first model doesn't quite open up the spectrum as flexibly as one would hope and the second method may cause severe interference issues, the hierarchical model has garnered a lot of interest and support as the preferred DSA technique. More specifically the classification as primary and secondary users implies that (unlicensed) secondary users may operate in spectral regions that are unused, when it can be ensured that the (licensed) primary users of that band do not face *harmful* interference due to transmission by secondary users. While this idea has opened up a huge window of opportunity for the beyond 3G wireless scenario, namely the realm of *cognitive radio*, the technical challenges that need to be overcome in order to ensure an amiable coexistence of primary and secondary users are formidable [75,76]. In particular, as pointed out in [74], it leads to interference models with increasing

complexity as it is governed by the access policies in place. Furthermore, the amount of interference will also depend on the degrees of freedom in the network namely spatial, temporal and/or frequency. The most interesting case and possibly the one that will be most frequently encountered in congested networks is one where primary and secondary users are in good proximity and thus the possibility of spatial non-interference may be ruled out. In this chapter we consider the rather practical case where partial temporal and/or frequency overlap between the transmissions of primary and secondary users is inevitable and propose receiver designs that are viable in such environments. To put the problem in perspective and to provide the reader with some relevant background and motivation, we briefly discuss in the next section the unique characteristics and expected capability of a cognitive transmission environment.

3.1 Overview of CR

The first and foremost task in order for secondary[1] users to be able to make use of the unutilized spectrum is to sense the band of interest and to ensure that it is not being used by a primary user. In CR terminology this is referred to as Radio Scene Analysis (RSA) [75]. Using the information gathered through RSA, a conventional cognitive user follows the following dictum: initiate transmission iff the band is sensed to be free [75]. Depending on whether the secondary user is multi-band or not it will either hop to a different frequency band and repeat the RSA operation or it will continue to sense the same band till it is free, before it eventually transmits. Thus the basic premise of cognitive radio is to be able to sense the surrounding RF environment and then react accordingly. Interference being the single most important limiting factor that prevents a secondary user from using available spectrum, it is imperative to define as to what can categorically stated to be *harmful* interference for a primary user. Of the two techniques that have been proposed to achieve the same, one uses

[1]Throughout the paper the terms *secondary* and *cognitive* have been used interchangeably to denote the unlicensed users of the frequency band.

a spectral mask in so-called *underlay* networks where the secondary users transmit at power levels that are undetectable over the primary user's band of operation. UWB receivers considered in Chapter 4 fall in this category. The second approach is known as the *overlay* approach where concurrent transmission are allowed using smart interference avoidance techniques at nominal power levels. Towards this end, the two metrics that are typically used to sense the level of interference [77] in the band of interest are the signal-to-(interference + noise) ratio (SINR), which entails a data-aided (pilot symbols) or blind estimation of both the wanted and unwanted signal powers and a relatively newly coined metric known as *interference temperature* (IT) [70, 75] which can be rather easily measured at the receiver by collecting the RF power in given frequency band when no useful information is being received. The latter metric allows CR to deviate from the traditional view of imposing transmit power limits and puts forth a receiver-centric perspective in determining the feasibility of transmission for a secondary user. More specifically, based on an acceptable IT upper limit, the proponents of the IT based approach argue that simultaneous transmission by secondary users may very well be permitted as long as as the noise floor at a licensed user can be maintained below the IT limit [70, 75, 77, 78]. Therefore, a higher utilization of the spectrum can potentially be achieved. While this is a passive approach and can be more aptly labeled as interference *tolerance*, a more effective way would be to actively mitigate the *unknown* interference at the primary user, thus allowing for a much higher cap on the instantaneous interference temperature. The latter will be the focus of the work presented here and offers multiple advantages including higher throughput and reduction of the so-called *region of interference* for the primary user [30]. The idea is to take a more active stand to opportunistic spectral access by creating more *opportunities* for unlicensed users to transmit data through improved protection for the primary users of a given frequency band. This in effect increases the sum capacity of the system [79], however, our approach does not go as far as recently advocated information theoretic techniques [80] that assume the availability of the codebook of the interference signals

in a non-causal fashion and calls for substantial coordination amongst the various users.

We note that sensing a cognitive user's RF environment to detect a transmission from a primary user when it is active, is a fairly challenging problem and the current state-of-the-art cannot guarantee detection of a primary signal transmission in all situations [76, 81, 82]. Hence, in a CR environment, we can expect additional interference at the primary receiver apart from the Gaussian thermal noise $\mathcal{N}(0, \sigma_{\mathcal{G}}^2)$, that is typically considered to impair the received signal in conventional communication systems. The same holds true for secondary receivers since although a secondary transmitter would sense its RF environment before transmitting, the corresponding receiver may be susceptible to co-channel interference from other secondary users in its vicinity unless an elaborate centralized access scheme is deployed [83]. Furthermore, secondary traffic is expected to be intermittent, which combined with the technical specifications of next generation wireless systems, e.g., frequency hopping in a multi-band orthogonal frequency division multiplexing (MB-OFDM) system, will lead to the interference in a frequency band of interest to be more structured than can be described using a Gaussian distribution alone [30, 75, 84]. As was seen in Chapter 2, such non-Gaussian behaviour leads to considerable performance degradation with matched filtering techniques at the receiver [10].

We use a probabilistic approach, similar to that used in Chapter 2, to model the correlated interference plus noise at the primary receiver, leading to parameterization of the unknown interference. In particular, again a Markovian assumption for the temporal behaviour of the interference is made, however, different from the problem considered in Chapter 2, we now focus more on how a receiver may obtain such information efficiently, i.e., with minimal increases in overhead.

Chapter Outline: We introduce the considered system model in Section 3.2 which is similar to that of Chapter 2 with additional modules for estimation, followed by a detailed description of the interference environment for cognitive radio. Section 3.3 then

describes the estimation algorithms for interference and forms the primary contribution of this chapter. The proposed algorithms are evaluated in Section 3.4 through Monte Carlo simulations and we conclude the chapter with some remarks in Section 3.5.

3.2 System Model

In this section, we introduce the transmission system and provide details of the model used for the interference caused by simultaneous transmissions or other spurious signals in the RF neighborhood of the desired primary receiver. Figure 3.1 presents a block diagram of the essential transmitter and receiver units and the channel model. Usually all primary receivers are equipped with the requisite circuitry to sense the radio environment, which has heretofore been used only for channel estimation. We propose the use of the primary user's sensing abilities also during reception of user data along with an additional comparator block at the RF front-end of the primary receiver which acts as a decision device. This is somewhat akin to RSA, which has been associated only with the cognitive user in CR systems [75]. The end goal of such a sensing exercise at the primary user would, however, be different from that at a secondary. In our proposed communication framework, the functional use of the primary's sensing abilities would be to determine if a received symbol was impaired by interference. We postpone a discussion on the details of the interference estimation through sensing until Section 3.3 and for now focus of the rest of the receiver blocks in Figure 3.1. The primary user's message is composed of information bits $d_k \in \{0, 1\}$, emitted by a source with uniform probability that are subsequently encoded by an encoder to produce coded bits c_k. We note that encoding is crucial for a primary user to be able to mitigate interference from CRs. As can be seen in Figure 3.1, an interleaver is used to reduce the effects of contiguous bits being in error and the interleaved symbols are then mapped to binary phase shift keyed (BPSK) symbols by the mapper to generate transmit symbols $x_k \in \{-1, 1\}$. When discussing performance results in Section 3.4 we

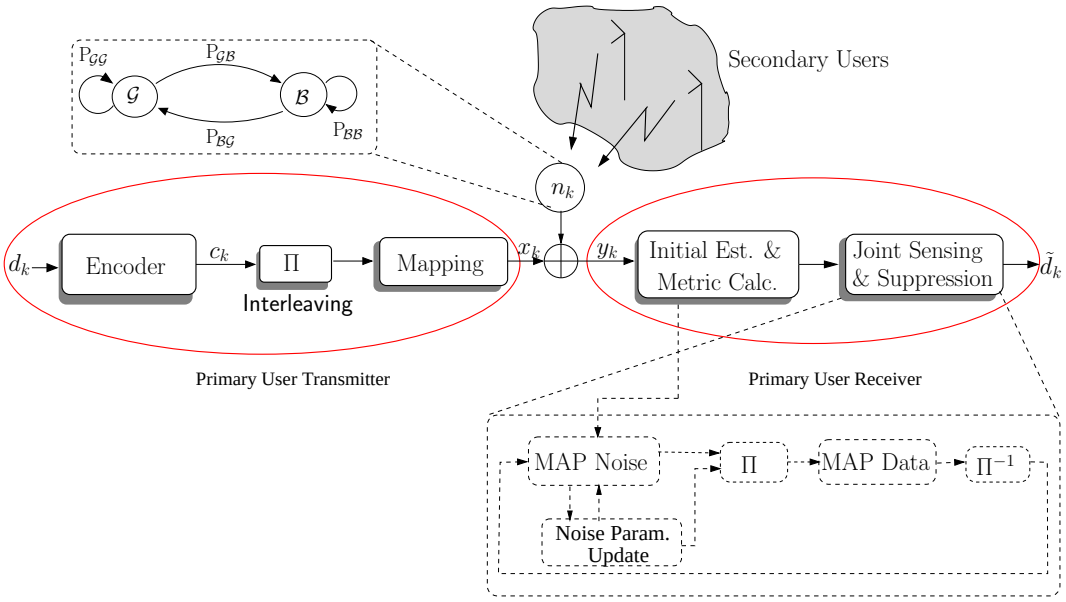

Figure 3.1 — System model for the overall transmission and reception modules. The joint sensing and suppression block forms the core of the receiver where the MAP Noise modules uses the inherent memory of the non-interleaved received sequence to estimate the noise states while data detection is carried out on the interleaved symbols by MAP Data.

will consider interleavers with both finite and infinite interleaving depth (ILD). The transmitted BPSK symbols (x_k) are received after being affected by thermal noise and interference, hereafter collectively referred to as *noise*, and the equivalent discrete-time representation of the received symbol after filtering and Nyquist rate sampling is given by

$$y_k = \sqrt{E_s}x_k + n_k; \quad n_k = \begin{cases} w_k, & \text{no interference} \\ w_k + i_k, & \text{with interference} \end{cases} \tag{3.1}$$

where E_s is the energy of the received symbol and coherent detection is assumed. We assume that the primary-user channel remains static for a number of codeword transmissions and thus the effect of possible fading is included in E_s. w_k represents self-generated thermal noise at the primary receiver and i_k denotes the aggregate interference, a mathematical description of which is provided in the following. In Figure 3.1,

the joint sensing and suppression (JSS) block is of primary interest as it implements the algorithms to determine if a received symbol is impaired by interference or not and accordingly applies a weighting factor to the decision metric for the corresponding symbol. The JSS block is based on an iterative exchange of soft information [85] between two blocks (MAP Noise and MAP Data in Figure 3.1) using an instance of the forward-backward (FB) [86] algorithm, one each for noise and data estimation. In Section 3.3 we will see that the weight factor is in effect the instantaneous signal-to-noise power ratio (SNR) for the corresponding received symbol and hence the JSS also plays the role of a symbol-by-symbol SNR estimator. It should be noted that the JSS is fundamentally different from SNR estimators for additive white Gaussian noise (AWGN) channels [87] since the noise distribution is non-homogeneous in our case.

3.2.1 Interference Model

We adopt a spatially Poisson distribution of the interferers which has frequently been used to model the geographical distribution of interferers in both cognitive [30, 88] and non-cognitive [84, 89] communication systems. Such a distribution implies that the number of interferers in a region $\mathcal{R}$ is directly proportional to the area of the region $\mathcal{A}_{\mathcal{R}}$. Furthermore, the probability distribution function (pdf) of interference with such a model, when $\mathcal{A}_{\mathcal{R}}$ is a circular region around the primary user (refer Figure 3.2), indicates that the distribution function is primarily governed by a few dominant interferers close to the receiver and thus has much heavier tails than a Gaussian [30]. This RF neighborhood of the primary user will be referred to as the *region of interference*, which in Figure 3.2 is the the disc of radius r_p with the primary user, P_u, in the center[2]. Alternatively, the region of interference may also be defined as the minimum physical perimeter around the primary user that is regarded as the *no-talk zone* for a secondary user in order to meet the corresponding interference temperature constraints.

[2]Note that a circular depiction of the region of interference in Figure 3.2 is based on the assumption of an omnnidirectional antenna of the primary user. In general, due to physical phenomenon such as shadowing and short term fading the actual region of interference will be an arbitrary polygon.

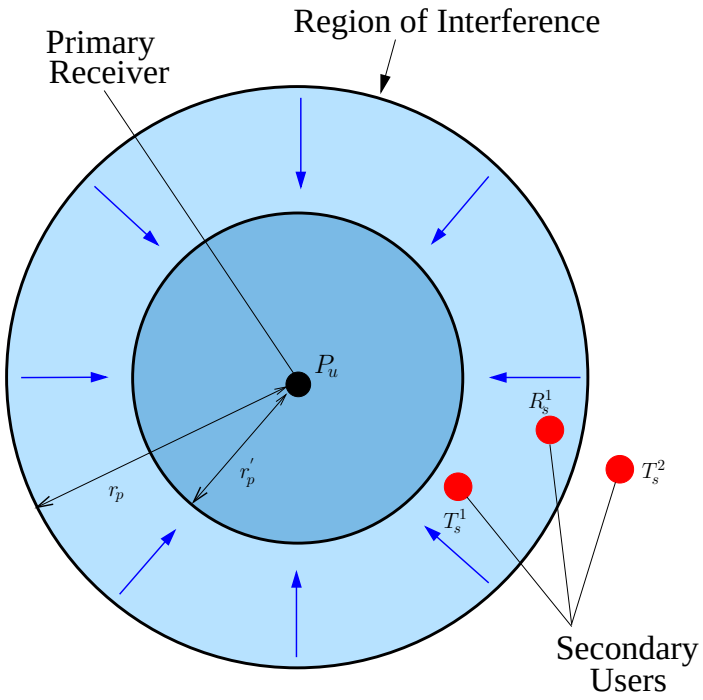

Figure 3.2 — Typical interference scenario for a cognitive transmission environment with multiple secondary users that are expected to transmit only when there is no harmful interference to the primary user, P_u. Circle with radius r_p denotes the region of interference for P_u where transmission by cognitive users may result in harmful interference to it. Reduction of r_p to $r_p^{'}$ permits users such as T_s^1 and R_s^1 to communicate.

The mandate of cognitive radios [30, 75], dictates that transmission from say secondary transmitter T_s^1 to a secondary receiver R_s^1, as depicted in Figure 3.2, concurrently and in the same band as primary user P_u may only be allowed if T_s^1 is outside P_u's region of interference. Our objective here is to reduce the region of interference for a given primary user from a circle of radius r_p to say $r_p^{'}$, $r_p^{'} < r_p$ (see Figure 3.2) by making the receivers more tolerant to the evidently non-Gaussian interference, thereby raising the cap on IT.

The above communication scenario dictates that the received signal at P_u is impaired by a superposition of signals from all potential interferers in a given time slot. As already mentioned earlier, we stipulate that the non-Gaussian distribution of such interference at the primary receiver can be well modeled using a two-term Gaussian

mixture distribution. Furthermore, we assume that the temporal correlation of the interference, which can be attributed to both secondary traffic patterns and channel access techniques of the unlicensed users that give rise to non-overlapping dwell times in time and/or frequency, is modeled using a first order Markov Chain, whose states are characterized by zero-mean conditionally Gaussian random variables with variances $\sigma_{\mathcal{G}}^2$ and $\sigma_{\mathcal{B}}^2$. The idea is to be able to model two different channel conditions one of which is when no other user (primary or secondary) is using the channel and thus transmitted packets are affected only by the self-generated additive white Gaussian noise (AWGN) of the receiver. Since this state is favorable for transmissions it is referred to as the good ($\mathcal{G}$) state. The component i_k in Eqn. (3.1) models the cumulative interference with signal power that is several times greater than can be modeled using the AWGN term w_k, warranting the need for a higher variance term for the so called bad ($\mathcal{B}$) state. Following the notation of Chapter 2, we denote by $s_k \in \{\mathcal{G}, \mathcal{B}\}$, the *state* of the noise process at the k^{th} instant and by definition then s_k is conditionally independent of the rest of the noise samples given s_{k-1}. The conditional distribution in a state $\mathcal{S} \in \{\mathcal{G}, \mathcal{B}\}$ is given by

$$p_{\mathcal{S}}(n_k) = p(n_k | s_k = \mathcal{S}) = \frac{1}{\pi \sigma_{\mathcal{S}}^2} \exp\left(-\frac{|n_k|^2}{\sigma_{\mathcal{S}}^2}\right), \tag{3.2}$$

The variances $\sigma_{\mathcal{G}}^2$ and $\sigma_{\mathcal{B}}^2$ are used respectively to define the signal to thermal noise ratio, SNR $= 10\log(E_s/\sigma_{\mathcal{G}}^2)$ and signal to interference ratio, SIR $= 10\log(E_s/\sigma_{\mathcal{B}}^2)$ of the overall system. The region of interference may thus be interpreted to be the region where the primary receiver can meet target performance criteria, e.g. bit error rate (BER), within a certain lower limit on the SIR. In Eqn. (3.2), the evolution of n_k is governed by the transition probabilities $P_{\mathcal{S}\mathcal{S}'}$ from state $\mathcal{S}$ to state $\mathcal{S}'$, $\mathcal{S}, \mathcal{S}' \in \{\mathcal{G}, \mathcal{B}\}$. Since we have two states we will have four sets of transitions that are governed by the respective transition probabilities depicted in the flow graph of Figure 3.1. We assume that the Markov chain is irreducible and aperiodic and hence is completely specified by the transition probabilities $P_{\mathcal{G}\mathcal{B}}$ and $P_{\mathcal{B}\mathcal{G}}$ which in turn depend on the average duration

in the states $\mathcal{G}$ and $\mathcal{B}$ respectively. We will specifically be focussing on the case where $P_{\mathcal{BG}} \gg P_{\mathcal{GB}}$ implying that the interference is intermittent.

3.3 Joint Sensing and Suppression (JSS)

We present here the JSS approach that uses energy detection (ED) based sensing at the receiver in conjunction with an expectation maximization (EM)-like [90] interference estimation that is shown to increase the tolerance of the intended receiver to spurious interference. Sensing at the primary user is carried out to determine the correct weighting factor applicable to the decoding metric of a received symbol, which is very different from the objective of spectrum sensing at the secondary where it allows a secondary to gauge a transmission opportunity. RF sensing in itself relates to the classical binary hypothesis testing problem where the *null hypothesis* ($\mathcal{H}_0$) represents the $\mathcal{G}$ state and $\mathcal{B}$ is the *alternate hypothesis* ($\mathcal{H}_1$) [76, 91]. The utility of the JSS stems from more than just its hypothesis testing abilities, in fact it is more about what we do with the information gleaned from the hypothesis testing exercise. In order to get a thorough understanding of the estimation process we assume varying levels of information being available at the receiver about the interference process.

In estimating the vector of transmitted symbols $\boldsymbol{x} = [x_1, \ldots, x_N]$, N being the block-length, from the vector of received symbols $\boldsymbol{y} = [y_1, \ldots, y_N]$, we are faced with the lack of knowledge of the interference parameters $\boldsymbol{\theta} = \{\sigma^2_{\mathcal{G}}, \sigma^2_{\mathcal{B}}, P_{\mathcal{BG}}, P_{\mathcal{GB}}, P(s_1 = \mathcal{G})\}$. We formulate the maximum likelihood estimation of $\boldsymbol{x}$ and $\boldsymbol{s}$ on the lines of [92], where for a similar setting with interference by jamming, $\boldsymbol{\theta}$ is augmented by an auxiliary variable $\boldsymbol{P} = [P(x_1 = -1), \ldots, P(x_N = -1)]$, the probability of $\boldsymbol{x}$ on which the decisions on $\boldsymbol{x}$ are eventually based, as

$$\begin{aligned} \hat{\boldsymbol{\theta}} &= \underset{\boldsymbol{\theta}}{\text{argmax}}\{p(\boldsymbol{y}, \boldsymbol{x}, \boldsymbol{s}|\boldsymbol{\theta})\} \\ &= \underset{\boldsymbol{\theta}}{\text{argmax}}\{p(\boldsymbol{y}|\boldsymbol{\theta}, \boldsymbol{x}, \boldsymbol{s})p(\boldsymbol{x}|\boldsymbol{\theta})p(\boldsymbol{s}|\boldsymbol{\theta})\}\ , \end{aligned} \tag{3.3}$$

where $\boldsymbol{x}$ and $\boldsymbol{s} = [s_1, \ldots, s_N]$ are the variables of interest that we wish to determine by applying the EM-approach [90]. As illustrated in Figure 3.1 and also well outlined in [92], an EM approach naturally develops into an iterative estimation and decoding procedure for $\boldsymbol{s}$ (MAP Noise) and $\boldsymbol{x}$ (MAP Data), with the MAP Noise module augmented with a noise-parameter update. In the following we describe the modules for noise state estimation that builds on the Markovianity of the ambient noise and the MAP based estimator for the transmitted bits which uses the code memory of the channel code.

3.3.1 Interference State Estimation

The MAP algorithm for the noise state estimation uses the the received symbols $\boldsymbol{y}$ together with the current parameter estimate $\boldsymbol{\theta}^{(n)}$ after n iterations. Denoting the probability of transition from state $s_{k-1} \rightarrow s_k$ at the $(n+1)^{\text{th}}$ iteration, by Ψ we have [86]

$$\Psi^{(n+1)}(s_k, s_{k-1}) = p^{(n)}(s_k|s_{k-1}) \sum_{\tilde{x}_k \in \{\pm 1\}} p^{(n)}(y_k|s_k, \tilde{x}_k) p^{(n)}(\tilde{x}_k) \,, \tag{3.4}$$

where $p^{(n)}(\tilde{x}_k)$ and $p^{(n)}(s_k|s_{k-1})$ are given by $\boldsymbol{\theta}^{(n)}$. All other relevant quantities of the MAP algorithm such as the forward metrics $P(s_k|s_{k-1}, \boldsymbol{y}_1^k)$ and the backward metrics $P(s_k|s_{k+1}, \boldsymbol{y}_{k+1}^N)$ for the FB algorithm can be computed using $\Psi(s_k, s_{k-1})$ to finally obtain the a-posteriori probabilities (APPs) $p_{s_k}^{(n+1)}(\mathcal{S})$ of the noise states [86, 92]. The stationary transition probabilities of the Markov chain $P_{\mathcal{S}_k \mathcal{S}_{k-1}}$ can be determined from the joint probabilities of the noise states. For example, $P_{\mathcal{BG}}$ is computed as

$$P_{\mathcal{BG}}^{(n+1)} = \sum_{k=1}^{N} \nu_k(\mathcal{B}, \mathcal{G}) \Big/ \sum_{k=1}^{N} \big[\nu_k(\mathcal{G}, \mathcal{G}) + \nu_k(\mathcal{B}, \mathcal{G})\big] \tag{3.5}$$

where $\nu_k(A, B) = \Psi^{(n+1)}(A, B)$, $[A, B] \in \{\mathcal{G}, \mathcal{B}\}^2$.

Derivation of variance update equations: The maximization step of the EM algorithm also yields the expression for the update of the variances of the noise process [92]. In particular, setting the derivative of $\mathcal{E}\{\log(p(\boldsymbol{y}|\boldsymbol{\theta},\boldsymbol{s},\boldsymbol{x})|\boldsymbol{y},\boldsymbol{\theta}^{(n)})\}$ with respect to the variance of a given noise state to zero, we obtain the following new estimate

$$\frac{\partial}{\partial\sigma_{\mathcal{S}}^2}\Bigg\{-\sum_{k=1}^{N}\Bigg\{\sum_{\mathcal{S}\in\{\mathcal{G},\mathcal{B}\}}\Bigg[p_{s_k}(\mathcal{S}|\boldsymbol{y},\boldsymbol{\theta}')\log(2\pi\sigma_{\mathcal{S}}^2)+\left(\frac{p_{s_k}(\mathcal{S}|\boldsymbol{y},\theta')}{2\sigma_{\mathcal{S}}^2}\right)\sum_{\tilde{x}_k\in\{-1,+1\}}p(\tilde{x}_k|\boldsymbol{y},\boldsymbol{\theta}')|y_k-E_s\tilde{x}_k|^2\Bigg]\Bigg\}\Bigg\}=0 \tag{3.6}$$

where we have made use of the fact that the noise states are independent of the transmitted bits. Eqn. (3.6) can be differentiated with respect to each of the variances $\sigma_{\mathcal{G}}^2$ and $\sigma_{\mathcal{B}}^2$ to obtain the respective update equations. We provide below the final update equation for a given state $\mathcal{S}$. For ease of exposition we denote $p(A|y,\boldsymbol{\theta}')$ as $p(A)$. Therefore differentiating and equating to 0 gives us

$$\sum_{k=1}^{N}\frac{p_{s_k}^{(n)}(\mathcal{S})}{2(\sigma_{\mathcal{S}}^2)^2}\left\{\sum_{\tilde{x}_k\in\{-1,+1\}}p(\tilde{x}_k|\boldsymbol{y},\boldsymbol{\theta}')|y_k-E_s\tilde{x}_k|^2\right\}=\sum_{k=1}^{N}\frac{p_{s_k}^{(n)}(\mathcal{S})}{\sigma_{\mathcal{S}}^2}$$

$$\sum_{k=1}^{N}\frac{p_{s_k}^{(n)}(\mathcal{S})}{2(\sigma_{\mathcal{S}}^2)^2}\left[p(\tilde{x}_k=1)\left(|y_k-E_s|^2\right)+p(\tilde{x}_k=-1)\left(|y_k+E_s|^2\right)\right]=\sum_{k=1}^{N}\frac{p_{s_k}^{(n)}(\mathcal{S})}{\sigma_{\mathcal{S}}^2}$$

$$\sigma_{\mathcal{S}}^2=\left(\frac{\sum_{k=1}^{N}\left\{p_{s_k}^{(n)}(\mathcal{S})\left[p(\tilde{x}_k=1)\left(|y_k-E_s|^2\right)+p(\tilde{x}_k=-1)\left(|y_k+E_s|^2\right)\right]\right\}}{2\sum_{k=1}^{N}p_{s_k}^{(n)}(\mathcal{S})}\right).$$

Thereby, for the $(n+1)^{\text{th}}$ iteration we have

$$(\tilde{\sigma}_{\mathcal{S}}^2)^{(n+1)}=\left(\sum_{k=1}^{N}p_{s_k}^{(n)}(\mathcal{S})\left[(|y_k|^2+E_s+2\Re\{y_k^*\})\Delta^{(n)}(x_k)\right]\right)\Big/2\sum_{k=1}^{N}p_{s_k}^{(n)}(\mathcal{S})\,, \tag{3.8}$$

where $\Delta^{(n)}(x_k)=p^{(n)}(\tilde{x}_k=-1)-p^{(n)}(\tilde{x}_k=+1)$. The updated values of the variances and noise state APPs as obtained above are used by MAP Data as described below.

3.3.2 MAP Decoding for the Code

An FB decoder similar in spirit to the one described above for the noise states is employed to determine the APPs of the information and the coded bits, where the states of the trellis are the states of finite state machine (FSM) that describes the code[3]. The received symbols and noise state APPs are de-interleaved and fed to the block denoted as MAP Data in Figure 3.1. The branch transition probability $\Gamma(z_{k-1}, z_k)$, where z_k is the state of the FSM at the k^{th} instant, is computed using the following channel metric

$$\lambda(\tilde{x}_k) = \sum_{\mathcal{S}\in\{\mathcal{G},\mathcal{B}\}} p(y_k|x_k, \mathcal{S}) p_{s_k}^{(n+1)}(\mathcal{S}) p^{(n)}(\tilde{x}_k) \ , \tag{3.9}$$

where $p_{s_k}^{(n+1)}(\mathcal{S})$ is obtained from MAP Noise. Note that in Eqn. (3.9), $p(y_k|x_k, \mathcal{S})p_{s_k}^{(n+1)}(\mathcal{S})$ is the implicit weighting that was mentioned in Section 3.2 as the Euclidean distance between y_k and $\tilde{x}_k$ is weighed by $p_{s_k}^{(n+1)}(\mathcal{S})$, the probability of being in state $\mathcal{S}$ in the $(n+1)^{\text{th}}$ iteration and, the corresponding variance estimate $(\hat{\sigma}_{\mathcal{S}}^2)^{(n+1)}$. The metrics $\lambda(\tilde{x}_k)$ can be used to recursively compute the forward and backward metrics required to obtain the APPs $p^{(n+1)}(\tilde{x}_k)$, which are used in the next iteration of MAP Noise as components of $\boldsymbol{\theta}^{(n+1)}$.

3.3.3 Initial Estimation for Noise Variances

The successive refinement of the APPs of the noise states and the transmitted symbols through an exchange of soft information improves the performance of the JSS over iterations. For each iteration at the receiver, MAP Noise runs first so that MAP Data has a sufficiently good estimate of the state and the corresponding weighting factor. However, for the first iteration of MAP Noise, no information on $\boldsymbol{\theta}$ is available. Simulative evidence shows that while the initialization of the unknown Markovian probabilities

[3]Here we use a convolutional code and thus a trellis based approach is favorable, however, codes that are decoded by a factor graph, e.g., low density parity check (LDPC) codes are equally applicable.

to 0.5 does not affect the estimation process much (which is in agreement with the findings in [92]), the knowledge of the noise state variances is critical to successful decoding of the transmitted symbols. To this end, we next present semi-blind and blind techniques to obtain initial estimates for the noise variances that help bootstrap the iterative estimation algorithm described above. The approaches presented below make use of a comparator (refer Section 3.2) that acts as a decision device following the RF sensing at the receiver. In particular *outliers* are identified in the received symbol block in order to distinguish between desired and undesired RF signals. These methods are applicable to small blocklengths and are bandwidth efficient at the same time as no pilot symbols are used.

Semi-Blind Estimation

For semi-blind estimation, we assume that $\sigma_{\mathcal{G}}^2$ is known at the receiver, however, no further knowledge regarding either the frequency or strength of the interfering signals is available. The rationale is that thermal noise is primarily attributed to device irregularities and hence can be measured off-line. The key sources of uncertainty in sensing the interference environment, therefore, are the other opportunistic (cognitive) transmitters in the region of interference of the desired user [30, 93]. Denoting the power of the k^{th} received symbol y_k as ψ_k, the semi-blind algorithm declares y_k as an outlier if $\psi_k > \mathscr{T}_{\text{semi}}$ where $\mathscr{T}_{\text{semi}} = 5\sigma_{\mathcal{G}}^2$. An initial estimate for $\sigma_{\mathcal{B}}^2$ is obtained as

$$\hat{\sigma}_{\mathcal{B}}^2 = \sum_{y_k \in \mathcal{O}} \eta_k \left(\frac{|y_k + \sqrt{E_s}|^2 + |y_k - \sqrt{E_s}|^2}{2} \right) \tag{3.10}$$

where $\mathcal{O} = \{y_k : \psi_k > \mathscr{T}_{\text{semi}}, 1 \leq k \leq N\}$ and $\eta_k = \psi_k \big/ \sum_{k \in \mathcal{O}} \psi_k$. Using a weighting factor η_k instead of equal weighting with say $1/|\mathcal{O}|$ ensures that an estimate $\hat{\sigma}_B^2$ is not overly skewed due to the presence of one or more strong interferers in a few time slots.

Blind Estimation

We now consider the case where the receiver has absolutely no knowledge of the noise parameters and all the information needs to be obtained from the received data. Such a communication environment may very well occur when there are multiple cognitive nodes at a distance from the primary user that appear as weak Gaussian interference, in effect raising the noise floor beyond the device thermal noise, over a duration that is longer than that of the typical frame of the primary user and thus leading to an ambiguity regarding the value of $\sigma_{\mathcal{G}}^2$ as well. As is obvious, this is a far more challenging task than the semi-blind approach described above. We propose two techniques here that use tools from the domain of *robust statistics* [94] in arriving at initial estimates for $\sigma_{\mathcal{G}}^2$ and $\sigma_{\mathcal{B}}^2$. In particular we use two different measures of statistical dispersion [95], namely the mean absolute deviation ($\mathcal{M}_e$) and the median absolute deviation ($\mathcal{M}_d$). In the following, we define $\mathcal{M}_e$ and $\mathcal{M}_d$ and discuss the relative advantages of each. It should be noted that simply computing the conditional expectation of the variance is not feasible here due to the fact that the overall distribution is a mixture of univariate Gaussians and thus the expectation would be prone to errors due to outliers for each component Gaussian distribution.

- *Mean Absolute Deviation* (MNAD): The mean absolute deviation, $\mathcal{M}_e$ for a sample set $\mathcal{X} = \{X_1, \ldots, X_N\}$ of a random variable X, is defined as

$$\mathcal{M}_e(\mathcal{X}) = \sum_{i=1}^{N} |X_i - \text{mean}(\mathcal{X})|/N \tag{3.11}$$

  Since the computation of $\mathcal{M}_e$ involves only summation and averages, the overall complexity of the estimation algorithm (and effectively of the receiver) increases only incrementally. Initial estimates are then obtained by setting $\mathscr{T}_{\text{blind}} = \mathcal{M}_e$ as the threshold to declare outliers. One caveat that needs to be noted here is that although inordinately simple to compute, the $\mathcal{M}_e$ requires double averaging and hence the quality of estimate using $\mathcal{M}_e$ is susceptible to the variations in $P_{\mathcal{B}}$ (for

same SIR levels) and therefore also on sample size. We next present an improved approach that is more robust to such variations.

- *Median Absolute Deviation* (MDAD): The median absolute deviation is considered to be a robust parameter in the presence of statistically deviant observations [95] and the motivation partly stems from MDAD being similar to rank-based non-parametric tests, for example the Wilcoxon detector [91, pp. 117-118], that are typically considered to be robust statistical tests. We use the median of the received block of symbols to compute a threshold ($\mathcal{M}_d$) that is robust to the Markov chain probabilities governing the evolution of the noise process. The MDAD is computed as

$$\mathcal{M}_d(\mathcal{X}) = \sum_{i=1}^{N} |X_i - \text{median}(\mathcal{X})| \tag{3.12}$$

  The threshold $\mathscr{T}_{\text{blind}} = \mathcal{M}_d$ is applied to identify outliers in this case. While the MDAD is in general more robust than the MNAD, it should be noted that there is an additional complexity of computing the median of the received samples. We employ a truncated selection sort algorithm (k^{th} smallest out of N) to compute the median, thus the order of complexity is $O(N^2/2)$ rather than $O(N^2)$ that is typical of selection sort algorithms.

For both MNAD and MDAD the estimation proceeds similar to the semi-blind case and Eqn. (3.10) is again employed to obtain $\hat{\sigma}^2_{\mathcal{B}}$ from the set $\mathcal{O}$, where the elements of $\mathcal{O}$ are now obtained using $\mathscr{T}_{\text{blind}}$, as computed in Eqns. (3.11) and (3.12). Furthermore, an initial estimate for $\sigma^2_{\mathcal{G}}$ is also obtained using $y_k \in \bar{\mathcal{O}}$ in Eqn. (3.10). However, for the computation of the $\sigma^2_{\mathcal{G}}$ equal weighting factors, $\eta_k = |\bar{\mathcal{O}}|^{-1}$ are used, which effectively renders the estimate to be the conditional mean of $\bar{\mathcal{O}}$. Statistically, this is prudent since under the assumption that $\bar{\mathcal{O}}$ contains only non-interfered samples, the mean is the best unbiased estimator for univariate noise [91]. It is obvious that the unique advantage of the blind methods is that prior information regarding the parameters of

the noise process is not a pre-requisite for the estimation the statistics of the interfering signals.

3.4 Simulation Results and Discussion

We now present the results of the performance evaluation of the proposed semi-blind and blind estimation approaches through Monte Carlo simulations. The channel code is the same that was used in Chapter 2. When considering non-ideal interleaving we use interleaving depth that are integer multiples of $\bar{\mathcal{D}}_{\mathcal{B}}$. For the simulative results we will have $\bar{\mathcal{D}}_{\mathcal{B}} = 40$ symbols for all results presented unless specified differently. All other relevant parameters of the noise process can be determined from $P_{\mathcal{B}}$ and $\bar{\mathcal{D}}_{\mathcal{B}}$ [26, 96]. In order to put its performance into context, we consider two other receivers from Chapter 2, namely the KSMLD and the EDSD (please refer to Section 2.2 for a description).

We use BER as a target performance criteria and set BER $= 10^{-4}$ to be the maximum allowable error rate at a primary receiver when secondary users are active. The factors that affect the BER at a given SNR are the probability of interference $P_{\mathcal{B}}$ and the SIR levels at the primary receiver. The underlying assumption with an interference temperature based cognitive transmission environment is that secondary users be allowed to transmit as long as $\sigma_{\mathcal{G}}^2 + \sigma_{\mathcal{B}}^2$ is less than a certain IT threshold, however, since the interference occurs with a probability $P_{\mathcal{B}}$ it plays a defining role in determining what threshold levels are allowed. To highlight this we consider two different interference environments. The first has a fixed SIR over all SNR ranges and we refer to this as Case I. Additionally, we have $P_{\mathcal{B}} = [0.1, 0.01]$, representing two different rates of occurrence for interfering signals in Case I. Case II comprises of the interference model considered in Chapter 2 where $\kappa = \sigma_{\mathcal{B}}^2/\sigma_{\mathcal{G}}^2$ is held constant and thus the effective SIR varies over the SNR range. We remark that Case I is a more practically relevant case as the interference signal strength is usually uncorrelated to background noise, however, results for

Interference Case	Parameters	
	$P_{\mathcal{B}}$	SIR
I-A	0.1	-4 dB
I-B	0.01	-8 dB
II	0.1	$\kappa\sigma_{\mathcal{G}}^2$ ($\kappa = 100$)

Table 3.1 — Simulation Parameters for the various interference scenarios considers. Case I focusses on a fixed SIR value while Case II uses the popular interference model with $\sigma_{\mathcal{B}}^2 = \kappa\sigma_{\mathcal{G}}^2$.

Case II are included for the sake of completeness as it is an immensely popular model for describing non-Gaussian noise. Given a BER upper limit of 10^{-4}, it was found that the minimum allowable SIR for the conventional detector (EDSD) with $P_{\mathcal{B}}=0.1$ is -4 dB and with $P_{\mathcal{B}}=0.01$ is SIR is -8 dB, when no measures for interference mitigation are adopted. The SIRs corresponding to the two interference scenarios will be referred to as *sustainable* SIRs for the respective $P_{\mathcal{B}}$s. For evaluative purposes, in the following we denote the parameterizations with $[P_{\mathcal{B}}=0.1, \text{SIR}=-4$ dB] and $[P_{\mathcal{B}}=0.01, \text{SIR}=-8$ dB as] Case I-A and Case I-B respectively. Both the interference environments are summarized in Table 3.1.

3.4.1 Convergence of the Algorithms: Estimation Error

A classical performance metric for any statistical estimation technique is the error in estimating the quantities of interests. For our case the two relevant quantities are (a) the variance of the noise at each epoch and (b) the noise state itself.

Variance Estimation: We quantify the variance estimation error for the blind and semi-blind estimation techniques in terms of the mean estimation error (MEE), $\xi_{\mathcal{S}} = \mathrm{E}\big[|\sigma_{\mathcal{S}}^2 - \tilde{\sigma}_{\mathcal{S}}^2|\big]$ and the normalized mean estimation error $\xi_{\mathcal{S}}^{\text{norm}} = \xi_{\mathcal{S}}/\sigma_{\mathcal{S}}^2$ which is indicative of the order of magnitude error in the estimation process. Figure 3.3(a) and 3.3(b) depict respectively $\xi_{\mathcal{B}}$ and $\xi_{\mathcal{B}}^{\text{norm}}$ for the initial estimates obtained by applying Eqn. (3.10). We present results for both Case I-A (solid lines) and Case I-B (dashed lines) in order to highlight the effect of $P_{\mathcal{B}}$ and the strength of the interfering signals on the respective

performances of MDAD and MNAD. Asymptotically, we observe that a lower $P_{\mathcal{B}}$ will lead to larger errors in estimation of $\sigma^2_{\mathcal{B}}$ as the sample size for $\mathcal{O}$ is smaller. We will see that the opposite holds true for the estimation of $\sigma^2_{\mathcal{G}}$ as the corresponding sample size is larger with lower $P_{\mathcal{B}}$. Also, we note that due to the way the threshold is defined for the semi-blind algorithm, its error curves exhibit an inflexion that is a consequence of its explicit dependence on $\sigma^2_{\mathcal{G}}$, whereas the curves for blind methods are monotonic. Furthermore, it is encouraging to note that for SNRs of interest, $\xi^{\text{norm}}_{\mathcal{B}} \leq 1$ for almost all detectors, i.e. the error is less than order of magnitude. The results of Figure 3.3 also indicate that regardless of the interference scenario, asymptotically, both the blind methods perform similarly implying similar bootstrap values for $\sigma^2_{\mathcal{B}}$ at these SNR values. Since the estimation algorithm begins uninformed with respect to Markovianity of the overall noise, we expect that the key performance differentiator at high SNRs will be the estimation of $\sigma^2_{\mathcal{G}}$, which we discuss next.

In Figure 3.4 we provide the corresponding estimation error results for $\sigma^2_{\mathcal{G}}$ when blind estimation is employed. Different from the results for $\sigma^2_{\mathcal{B}}$, we observe that while $\xi_{\mathcal{G}}$ values are fairly nominal, the values for $\xi^{\text{norm}}_{\mathcal{G}}$ reveal that in general $\hat{\sigma}^2_{\mathcal{G}}$ is several times higher than $\sigma^2_{\mathcal{G}}$ for moderate to high values of SNR. This can intuitively be explained by taking a closer look at the role of E_s in the expression for initial estimate in Eqn. (3.10). It is apparent that E_s, regardless of the transmitted symbol, will have a key contribution in determining $\hat{\sigma}^2_{\mathcal{S}}$. While this is not an issue for low to moderate SNRs, it puts a limit on the accuracy of the estimation of $\sigma^2_{\mathcal{G}}$ at high SNRs as $\sigma^2_{\mathcal{G}}$ is several orders lower than E_s, for example at $\text{SNR} = 12$ dB it is ~ 16 times lower than E_s. This explains the higher $\xi^{\text{norm}}_{\mathcal{G}}$ for higher SNRs and the corresponding flatness in $\xi_{\mathcal{G}}$. Interestingly, we see far more variations in the slope of the MEE curves for $\sigma^2_{\mathcal{G}}$ than for $\sigma^2_{\mathcal{B}}$. We attribute this behaviour of $\xi_{\mathcal{G}}$ to the existence of *regions of ambiguity* in determining the membership of a received symbol in $\mathcal{O}$. For SNR ranges where $E_s + \sigma^2_{\mathcal{G}}$ is comparable to $\sigma^2_{\mathcal{B}}$, the ability of the decision device to discern if the energy contained in the received

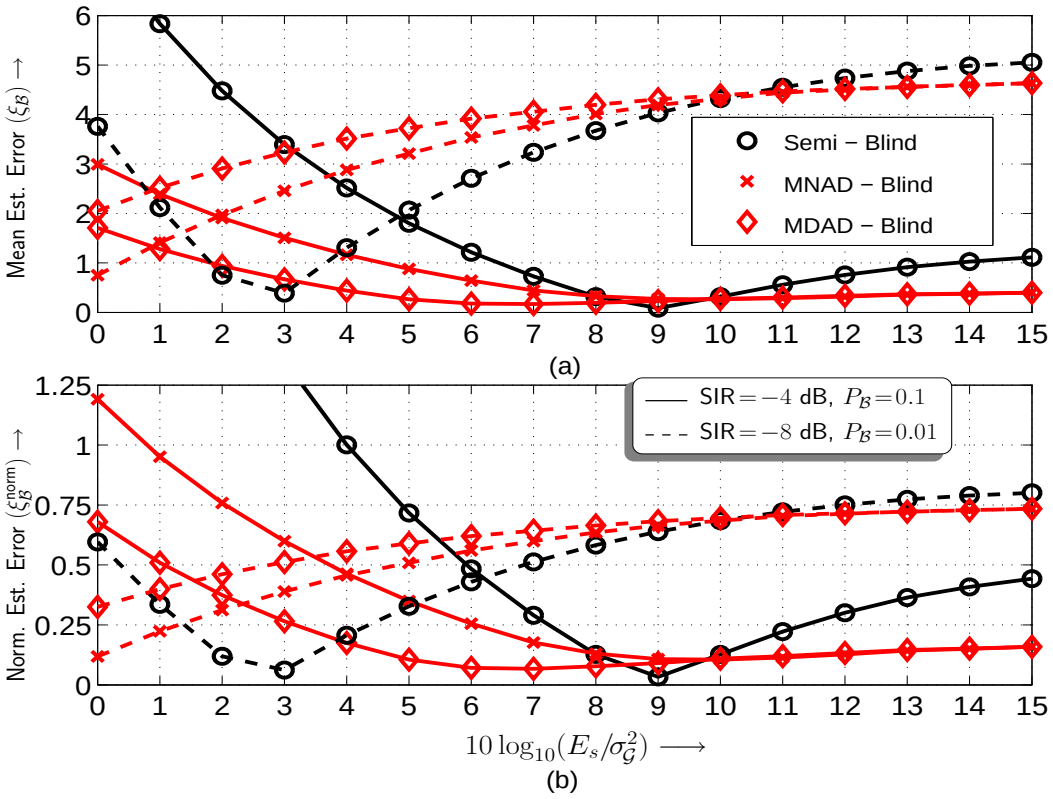

Figure 3.3 — Estimation error for the noise variance in bad state employing semi-blind and blind JSS approaches. (a) MEE and (b) Normalized MEE for $P_{\mathcal{B}} = 0.1, \text{SIR} = -4$ dB (dashed lines) and $P_{\mathcal{B}} = 0.01, \text{SIR} = -8$ dB (solid lines). Estimation errors can be seen to be limited to within an order of magnitude for SNR values of interest.

symbol is attributed primarily to the transmitted signal, the white Gaussian noise or to the interference signal is impaired and may result in erroneous classification of a received symbol. These ambiguities manifests themselves to a much lesser extent in the estimation of $\sigma_{\mathcal{B}}^2$ as $\sigma_{\mathcal{B}}^2/\sigma_{\mathcal{G}}^2 \gg 1$ for most reasonable values of channel SNR, implying that, contrary to $\hat{\sigma}_{\mathcal{G}}^2$, added contribution from E_s or $\sigma_{\mathcal{G}}^2$ causes only minor changes in the value of $\hat{\sigma}_{\mathcal{B}}^2$. We further note that in terms of impact on BER, the need to make this distinction is less critical at very low SNRs where $\sigma_{\mathcal{G}}^2$ itself is high and consequently so are the receiver error rates. Moreover, it is easy to see that such distinctions are relatively easier to make for low SIRs and high SNRs. We present results in Section 3.4.4 that further elaborate the impact of regions of ambiguity on BER.

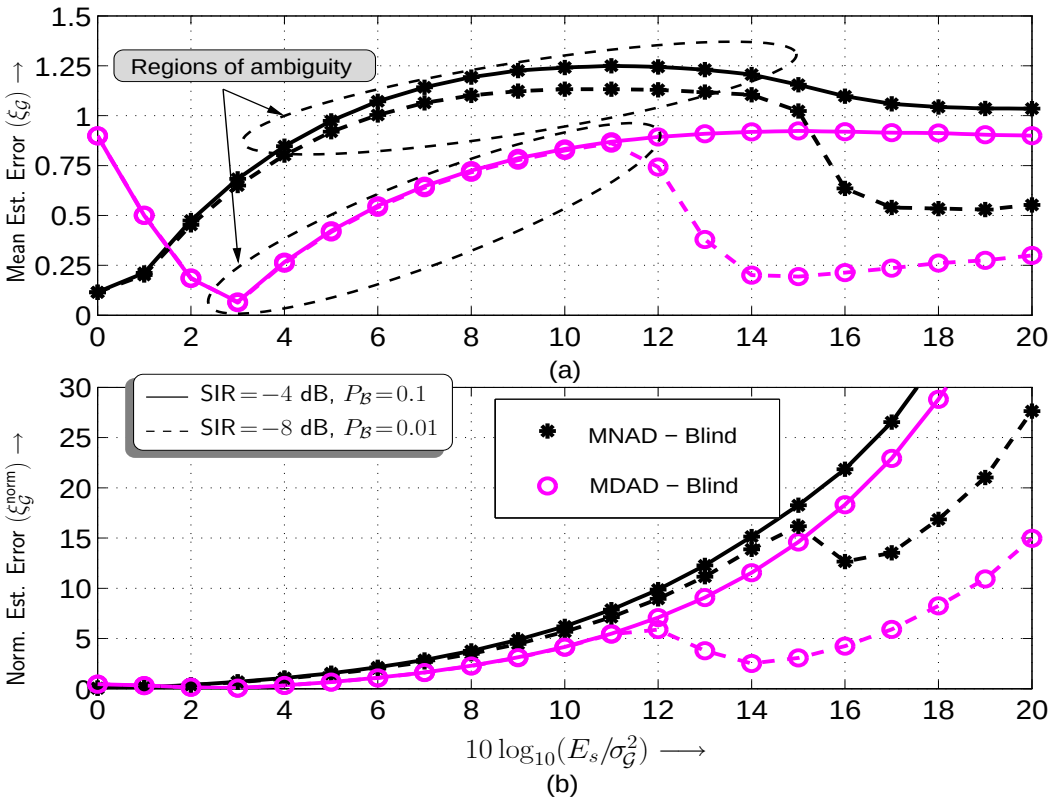

Figure 3.4 — Estimation error for the noise variance in good state, $\sigma_{\mathcal{G}}^2$ when blind estimation techniques from Section 3.3.3 are employed. (a) MEE and (b) Normalized MEE with $P_{\mathcal{B}} = [0.1, 0.01]$ and SIR $= [-4\text{dB}, -8\text{dB}]$ respectively . The absolute error in estimation is fairly small compared to $\sigma_{\mathcal{B}}^2$ although normalized MEE may be several times higher.

Results for Case II are presented in Figure 3.5. Note that the absolute values decrease with increasing SNR in this case for both $\sigma_{\mathcal{G}}^2$ and $\sigma_{\mathcal{B}}^2$ as they are directly proportional. The estimators exhibit a higher level of consistency in performance as classification with a threshold that varies with $\sigma_{\mathcal{G}}^2$ yields better results owing to a similar variation in $\sigma_{\mathcal{B}}^2$. Moreover, we observer that the normalized MEEs are less that 1 over a wide range of SNR and the relative flatness of the $\xi_{\mathcal{S}}^{\text{norm}}$ curves reinforces the consistency in estimation. While this represents an easier case for estimation, its utility might be limited due to reasons mentioned earlier.

Noise State Estimation: We now focus on the refinement in estimation of $\boldsymbol{s}$ over iterations by considering the probability of false estimation of states, (P_{FE}) for Cases

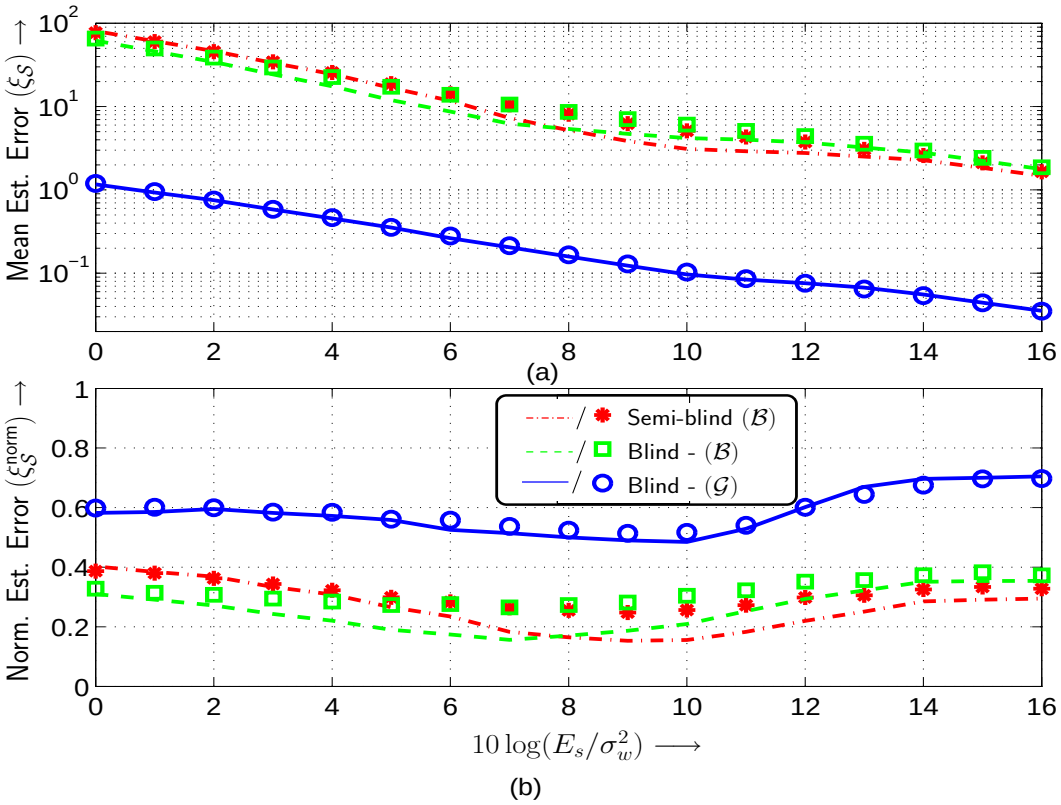

Figure 3.5 — (a) Mean estimation error and (b) Normalized mean estimation error for interference scenario of Case II using semi-blind and MNAD - blind estimation techniques. Lines: Infinite interleaver. Markers: Block interleaver with ILD = $2\bar{\mathcal{D}}_{\mathcal{B}}$.

I and II. Typically the probability of false alarm (P_{FA}) i.e., the probability of deciding that an interferer is present when there is none (asserting $\mathcal{H}_1$ is true instead of $\mathcal{H}_0$) and the probability of missed detection (P_{MD}) ($\mathcal{H}_0$ when $\mathcal{H}_1$ is true) are used to determine the efficiency of a statistical hypothesis test [91]. P_{FE} subsumes both these criteria by considering the case when $\mathcal{H}_T$ is inferred and $\mathcal{H}_{\bar{T}}$, $T \in \{0, 1\}$, is true, i.e. $P_{\text{FE}} = P_{\text{FA}} + P_{\text{MD}}$. Table 3.2 presents P_{FE} for semi-blind and blind JSS approaches in percentage form for up to 10 iterations at SNR = 8 dB. Semi-blind estimation can be seen to be highly effective as the number of wrongly estimated states is reduced to less than 1.0% for both cases with a maximum of 10 iterations. Also, in both interference scenarios, the rate of decay of P_{FE} with iterations is much faster for semi-blind JSS than the blind methods. We also observe that P_{FE} is in general several times lower for SIR $= -8$ dB

Iters.	Semi-blind		MDAD -Blind		MNAD-blind	
	Case I-A	Case I-B	Case I-A	Case I-B	Case I-A	Case I-B
2	14.2850	14.1126	9.9698	0.9187	12.6256	0.9011
4	7.0016	4.4046	9.9639	0.8676	12.3718	0.8535
6	3.6192	1.4834	9.6562	0.7348	10.1035	0.7248
8	1.4725	0.5832	8.9799	0.6898	9.9466	0.6283
10	0.6027	0.2514	8.1472	0.6304	9.8853	0.6177

Table 3.2 — Percentage (%) of falsely estimated states (P_{FE}) using the semi-blind and blind estimation algorithms at SNR $E_s/\sigma_{\mathcal{G}}^2 = 8$ dB for Case I-A ($P_{\mathcal{B}}=0.1, \mathrm{SIR} = -4\mathrm{dB}$) and Case I-B ($P_{\mathcal{B}}=0.01, \mathrm{SIR} = -8\mathrm{dB}$).

No. of	Semi-blind		Blind	
Iter	Inf. Ilv.	ILD $= 2\mathcal{D}_{\mathcal{B}}$	Inf. Ilv.	ILD $= 2\mathcal{D}_{\mathcal{B}}$
1	4.6078	4.8200	8.6273	10.5857
2	2.3158	2.3592	2.0629	2.0430
3	0.5258	0.5267	0.4831	0.5443
4	0.1774	0.1894	0.4060	0.4127
5	0.1772	0.1783	0.4084	0.4104

Table 3.3 — Percentage (%) of false hits using the semi-blind and MNAD - blind estimation algorithms for Case II at SNR ($10\log(E_s/\sigma_{\mathcal{G}}^2)$) = 10 dB

than for SIR$=-4$ dB corroborating our earlier assertion that lower SIR aids in reducing ambiguity in outlier rejection. The order of error observed for the blind techniques after the first iteration is comparable to frequency of occurrence of the impulsive signal, i.e. $P_{\mathcal{B}}$, which is seen to diminish gradually over iterations.

Similarly, Table 3.3 presents the results for Case II where we now make comparisons with the case of infinite interleaving. We observe that the initial estimates for $\sigma_{\mathcal{B}}^2$ for semi-blind estimation lead to less than 5% wrongly estimated states, regardless of the ILD and this figure is further reduced to less than 0.2% with 5 iterations. Arguably, the state estimation is far more accurate in this case. Nonetheless, the improvement in estimation for the blind method is rather sluggish across the board, which suggests that far greater iterations than the semi-blind method will be required for substantial improvements in the BER. Guided by this inference, we next delve into the possible BER enhancements achievable through the proposed methods.

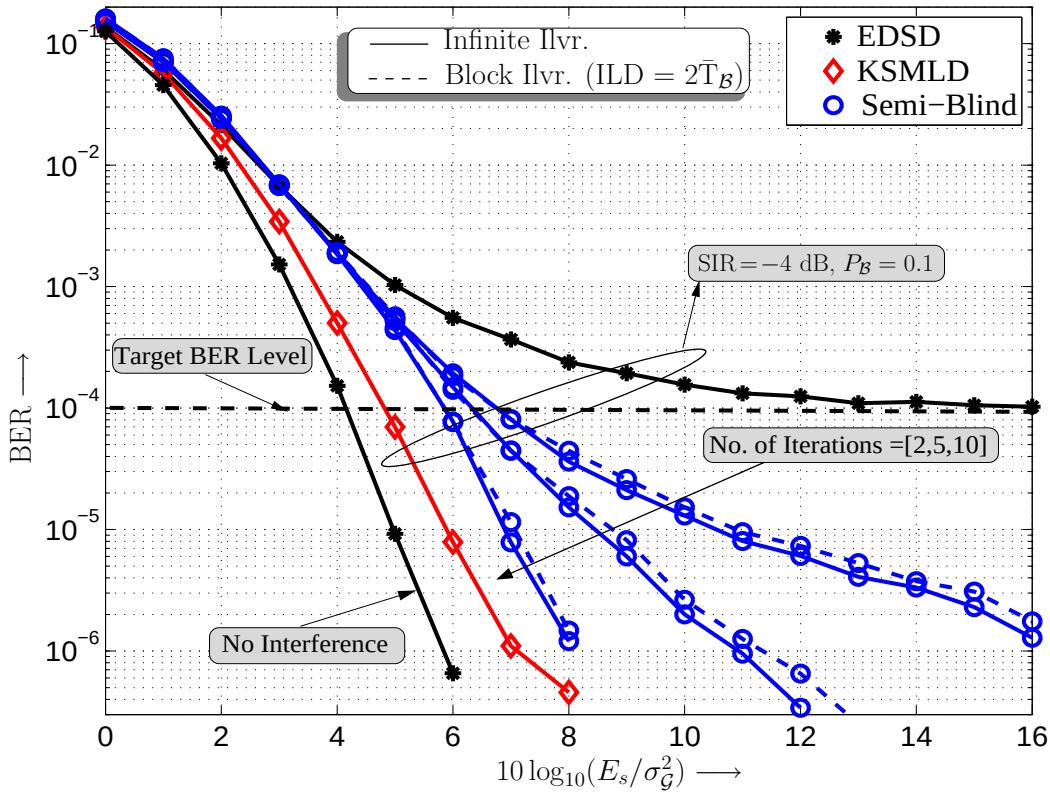

Figure 3.6 — Bit Error rates for semi-blind JSS with $P_{\mathcal{B}} = 0.1$ and SIR $(10\log(E_s/\sigma^2_B))$ = -4 dB. Performance with 10 iterations closely approaches that of KSMLD while GND floors at relatively higher BERs needing a boost of about 10 dB in its operating SNR to meet the target BER levels.

3.4.2 Bit-error Rate

Bit error rate represents possibly the most tangible payoff in the current framework as it is a measure of the allowable increase in IT threshold while meeting reliability constraints, e.g. packet loss and maximum number of retransmissions. In this section, we present the BER results when employing JSS as described in Section 3.3.1 and the results are benchmarked with KSMLD and EDSD. Towards this end, Figure 3.6 presents the performance curves for semi-blind JSS with 2, 5, and 10 iterations when $P_{\mathcal{B}} = 0.1$ and SIR $= -4$ dB. We show results for both infinite and finite interleaving with ILD $= 2\bar{\mathcal{D}}_{\mathcal{B}}$ to emphasize that practical interleavers that are designed to meet maximum delay requirements are equally applicable. Comparing the EDSD performance curves

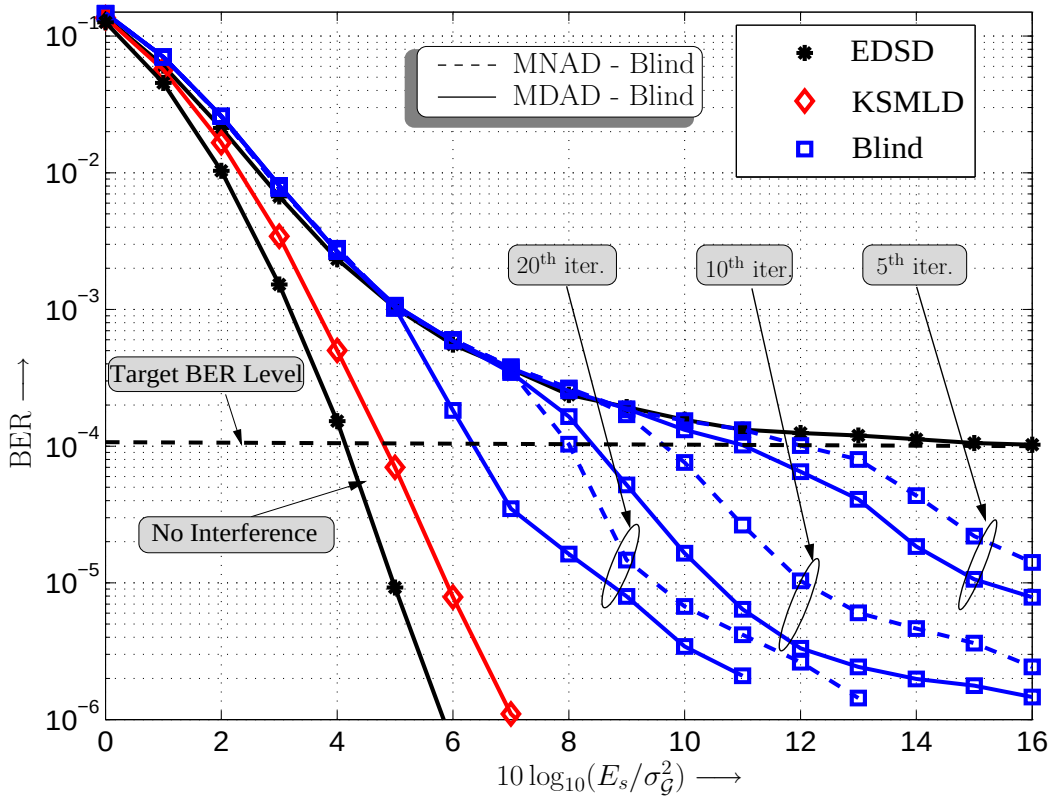

Figure 3.7 — Performance comparison of the MNAD and MDAD blind JSS methods with $P_{\mathcal{B}} = 0.1$ and SIR $(10\log(E_s/\sigma_B^2)) =$ -4 dB. Substantial gains in operating SNR are observed after 10 iterations which are, however, distinctively lesser than the semi-blind method. Using twice the number of iterations as the semi-blind approach is seen to achieve similar performance gains.

for AWGN only (no interference) and with interference as in Case I-A, we conclude that an increase of $\sim$10 dB in the operating SNR is required to meet our target BER level. Our primary motivation in estimating the noise state and variance stems from the fact that perfect knowledge of these parameters (KSMLD curve) allows reduction of the required increment in the operating SNR to about 1 dB, which is a huge improvement over the EDSD. To this end, it is encouraging to observe that semi-blind JSS can recover much of the damage done by the interfering signals and although not ideal, it does offer reductions of about 7 dB in the operating SNR after only 2 iterations. Moreover, the error floor witnessed for the EDSD is pushed lower by orders of magnitude through more iterations of the algorithm, whereby performance after 10 iterations is seen to

closely approach that of the KSMLD. In addition, the BER performance curves with finite ILD is seen to be only slightly worse than those with infinite interleaving implying minor degradations due to non-ideal interleaving. The improvements observed through the application of the semi-blind JSS algorithm serves as a classic example of a case where JSS can bring in enormous gains. In particular, depending on the applicable path loss model [97], and assuming that SNR boosts of up to 10 dB (as in Figure 3.6) can be accommodated by the primary transmission system, we can significantly reduce the region of interference of the primary user (refer Figure 3.2). This in effect, implies that far more cognitive users may be allowed to be active as they are no longer in the no-talk zone of the primary receiver.

In Figure 3.7 we compare the performance of the blind approaches presented in Section 3.3.3 with the conventional approaches applying infinite interleaving for the interference scenario of Case I-A. We see that for both MNAD and MDAD blind estimation, the gains for up to 10 iterations are relatively less compared to the semi-blind technique. In general, MDAD-blind performs better than MNAD-blind for the considered $P_{\mathcal{B}}$ and SIR values. The gain in terms of required SNR reduction after 10 iterations is limited to $\sim$ 4 dB and $\sim$ 6 dB for MNAD-blind and MDAD-blind respectively. Nonetheless, these gains are large enough to allow for a reduced link budgets and/or reduced regions of interference for the primary receiver. Figure 3.7 also shows that if the primary receiver has the requisite processing power and is not limited by delay constraints, 20 iterations of the blind JSS algorithms can improve the performances further by $\sim$2 dB for both MNAD and MDAD. Admittedly, the blind approaches are less effective than the semi-blind approach in terms of lowering the error floor of the system but they are an order of magnitude or more lower than the EDSD. Although, not shown here due to space constraints, similar performance patterns were observed for Case I-B with MDAD performing visibly better than the MNAD approach.

In Figure 3.8 we present performance results after 5 iterations with case II parameters,

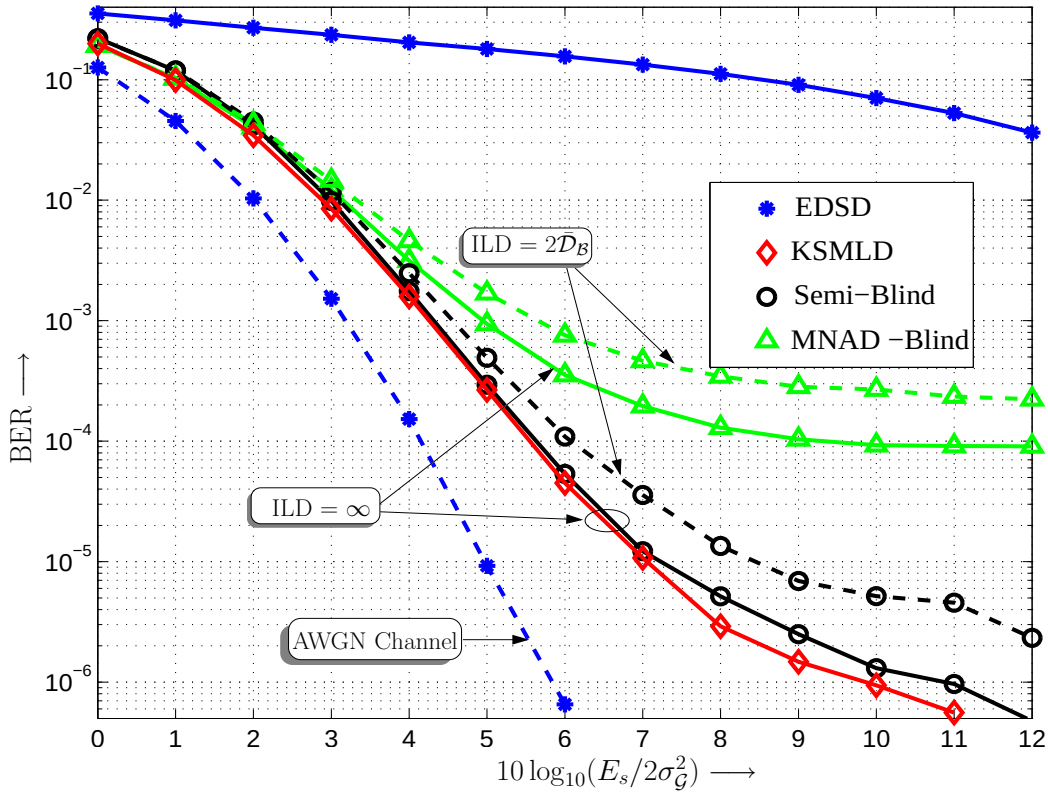

Figure 3.8 — Performance comparison of the JSS methods with various decoding approaches. Blind decoding is seen to have a higher error floor than the semi-blind technique but fares much better than the EDSD.

again consider the role of ILD as a design parameter. The lesser number of iterations reflect the relatively less challenging interference conditions for case II. The performance curve for semi-blind estimation is seen to practically overlap that of KSMLD indicating that further iterations would only be wasting valuable power. We omit results for MDAD-blind for clarity of the figure and only results for MNAD-blind are shown. MNAD-blind suffers a much lower penalty compared to the semi-blind and KSMLD curves in attaining the target BER levels. Interleaving depth is seen to play a definite role in overall estimation. Also, for all the results obtained here one should bear in mind that the code used here is rather weak and far stronger error-correcting codes can be used to lower the error rate.

We next discuss the interplay of memory and estimation accuracy and the effect of

memory on overall system performance.

3.4.3 Analytical Aspects: Effect of Memory

It is conceivable that the accuracy of the estimation is directly dependent on the memory of the noise process. In this section we make an attempt at characterizing the possible effects that the amount of memory may have on the quality of estimation by obtaining simulative BERs and also through mutual information transfer from the input of the MAP Noise to its output. To separate the effects of ambiguity of classification mentioned in Section 3.4.1 we consider estimation only for the semi-blind approach.

The concatenation of MAP Noise and MAP Data modules in JSS allows us to analyze it as an iterative estimation engine and thus renders the use of extrinsic information transfer (EXIT) particularly appealing[4] [98]. In particular, to gain insight into possible gains from information exchange between the MAP Noise and MAP Data, we are interested in two special cases: (a) MAP Data provides MAP Noise with a priori information $I_A = 1$ bit/symbol about coded bits c_j and the noise statistics $\boldsymbol{\theta}$ are known, and (b) MAP Noise operates without input from MAP Data, i.e., $I_A = 0$ bit/symbol and $\boldsymbol{\theta}$ is initialized as described in Section 3.3. The latter case corresponds to the first decoding iteration, while the former approximates the situation after successful convergence of iterative decoding. The extrinsic information I_E about the coded bits c_j obtained at the output of MAP Noise for the two cases are shown for different values of signal-to-noise ratio (SNR) $1/\sigma_{\mathcal{G}}^2 = [0, 5, 10]$ dB in Table 3.4. The noise parameters are $\kappa = 100$, $P_{\mathcal{B}} = 0.1$, i.e., we use Case II. Furthermore, the memory is characterized using the parameter μ introduced in Section 2.3 and set it as $\mu = 0.99$ for obtaining the mutual information transfer values in Table 3.4. It can be easily seen that there exists

[4]Iterative decoding principles dictate that for consistent improvement of performance over iterations each module be fed with information which is *new* information for the component module. However, from the update equations of MAP Noise (cf. Section 3.3) it is evident that this is not entirely the case for JSS as (a) MAP Data and MAP Noise estimate probabilities of two different random variables and (b) the respective bit and state probabilities follow different distributions.

Initial cond. / SNR	I_E	
	$I_A=0$, Est. $\boldsymbol{\theta}$	$I_A=1$, Known $\boldsymbol{\theta}$
0 dB	0.330809	0.370982
2.0 dB	0.455022	0.510404
4.0 dB	0.585955	0.659112
6.0 dB	0.695332	0.787057
8.0 dB	0.759633	0.866546
10.0 dB	0.787042	0.897536

Table 3.4 — Extrinsic mutual information between the output of the MAP Noise and the coded bits for (a) known $\boldsymbol{\theta}$ and perfect a priori information ($I_A = 1$) and (b) estimated $\boldsymbol{\theta}$ (except $\sigma_{\mathcal{G}}^2$) and $I_A = 0$.

an obvious and widening (with SNR) gap in I_E at the output, between the worst and the best cases. Hence, we conclude that for the case of initially unknown parameters of the noise process, iterations between MAP Noise and MAP decoder improve BER performance. This is decidedly different from [41, Figure 8], where, for known $\boldsymbol{\theta}$, I_E is shown to be practically independent of I_A. We can use the mutual information measures I_A and I_E to obtain an estimate of the BER after MAP decoding as

$$P_b = Q\left(\sqrt{\frac{J^{-1}(I_A) + J^{-1}(I_E)}{2}}\right) , \tag{3.13}$$

where the invertible function $J(\cdot)$ is defined in [98, Eq. (15)] and a Gaussian approximation (GA) (cf. [98]) for log-likelihood ratio (LLR) bit-metrics is invoked. We found this approximation to be a good match for the first decoding iteration. However, it is apparent that GA is not valid for later iterations by noting that the distribution of the LLRs at the output of MAP Noise approaches a mixture Gaussian distribution with better estimates of the noise states.

We show the effect of memory on BER performance of the semi-blind algorithm in Figure 3.9 where MSMLD (refer Chapter 2) represents a receiver that neglects the inherent memory of the interference but has complete knowledge of the distribution of the noise. We choose the values of μ as 0.5 and 0.99 to reflect moderate and high levels of correlation respectively. While memory barely has any effect after first iteration, it is

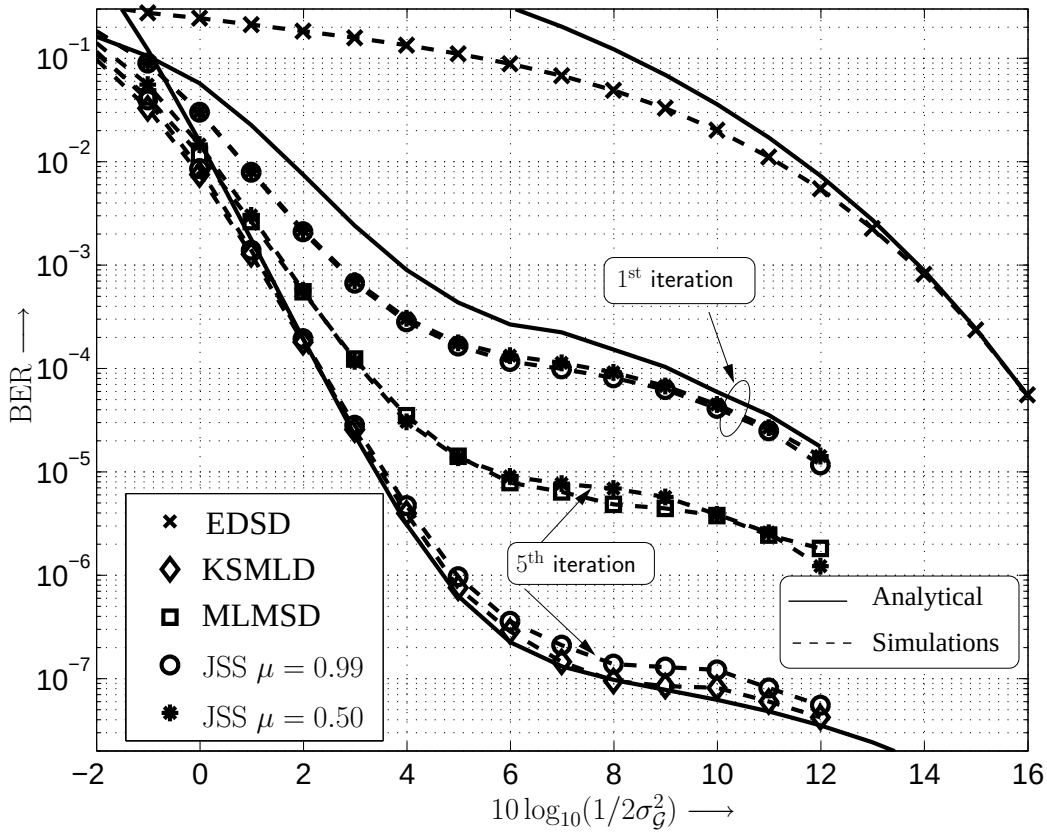

Figure 3.9 — BER results for a rate-1/2 convolutionally coded system over a two-state Markovian impulsive interference channel.

seen to greatly facilitate estimation by the end of the 5th iteration. The analytical curves for KSMLD and EDSD were obtained by following the procedure outline in Section 2.3. We present below PEP expressions of KSMLD and EDSD where the state dependency of Eqns. (2.34) and (2.36) is eliminated by application of elementary combinatorics

$$\mathrm{PEP}(\boldsymbol{e}) = \begin{cases} \displaystyle\sum_{i=0}^{d} \gamma Q\left(d/\sqrt{(d-i)\sigma_{\mathcal{G}}^2 + i\sigma_{\mathcal{B}}^2}\right), & \text{EDSD} \\ \displaystyle\sum_{i=0}^{d} \gamma Q\left(\sqrt{(d-i)/\sigma_{\mathcal{G}}^2 + i/\sigma_{\mathcal{B}}^2}\right), & \text{KSMLD} \end{cases} \tag{3.14}$$

where $\gamma = \binom{d}{i} P_{\mathcal{G}}^{d-i} P_{\mathcal{B}}^{d}$ and $Q(\cdot)$ is the Gaussian Q-function. Application of union

bounding techniques yields the analytical curves depicted in Figure 3.9. Since MSMLD disregards the memory of the noise, the value of μ is irrelevant to its performance. Consequently from Figure 3.9 we observe that although simple, MSMLD stands to perform fairly poorly in highly correlated noise environments.

3.4.4 Benefits of JSS in a Cognitive Environment

In this section, we briefly discuss the benefits of the JSS algorithm in a multiuser cognitive environment that pertain to both primary and secondary users. We remark that the overall benefits of trying to sense the channel before and/or during transmissions should outweigh the effort that one expends at estimating the channel conditions. With this goal in mind we aim to quantify the achievable gains of JSS below.

Increased Interference Tolerance

The BER results for the proposed receiver structures in Figure 3.6 and Figure 3.7 suggest that there are distinctive gains associated with the interference state and variance estimation as proposed in this chapter. Therefore, it is of interest to discern as to what maximum levels of interference can be tolerated at the receiver, i.e., how large can $\sigma_{\mathcal{B}}^2$ allowed to be such that nominal increases in the link budget can help meet our target BER requirements. To this end, we present in Figure 3.10 the BERs of various detectors (except MNAD-blind) as a function of decreasing SIR with the probability of interference held constant at $P_{\mathcal{B}} = 0.1$. For the EDSD and the MDAD-Blind detectors we present results for SNR $= [5, 6, 7, 8]$ dB that depicting the achievability of the target BER at these SNRs. For semi-blind JSS and KSMLD, results are presented only for SNR $= [6, 7]$ dB and these values are seen to be sufficient to attain BER values lower than 10^{-4} over the entire range of SIR values considered. There are several insightful observations that can be made here that help appreciate the capabilities of the proposed algorithms. Firstly, we see that the conventional EDSD is ill-equipped to handle interference levels beyond SIR $= -4$ dB with nominal increases in the SNR. In fact in

Figure 3.7 it was observed that even at substantially high SNRs the EDSD runs into an error floor in presence of interference. On the contrary, for JSS based receivers we see that effective mitigation of fairly high levels of SIR is possible by increasing the operating SNR by only a few dBs over the required SNR valued for an AWGN only channel (refer Figure 3.7). However, for low values of SIR, we do see the region of ambiguity to be in play where discriminating between primary signal and interfering signals solely on the criteria of received energy is challenging. Also, semi-blind JSS is seen to closely mimic the performance of the KSMLD beyond a certain threshold SNR. Overall, Figure 3.10 is indicative of the fact that effective interference mitigation can allow the primary receiver to maintain its quality of service (QoS) levels while accommodating several unlicensed users.

Advantages to Secondary User

Use of a JSS based receiver implies that a secondary user is not restricted to *white spaces* in the spectrum, i.e., transmitting only when a frequency band is devoid of any primary transmission. Depending on the tolerance levels of the primary user, a secondary user may also transmit in the so-called gray or black spaces [74, 75] with improved protection to the primary user.

While most of the discussion in this chapter has centered around the primary user, JSS can also be applied at the secondary receiver to provide greater protection against other cognitive users (say T_s^2 in Figure 3.2) that will play the role of a co-channel interferer. In real world transceivers, filters are never ideal and noise is neither Gaussian nor white [76], thus one can hardly guarantee complete immunity from impulsive interference to secondary users when they are allowed to transmit. Implementing a JSS based receiver is easier at CR transceiver since it has in-built sensing abilities by definition. Moreover, JSS can also reduce link budgets for secondary users and consequently the perceived IT levels at the primary user, which is our primary goal.

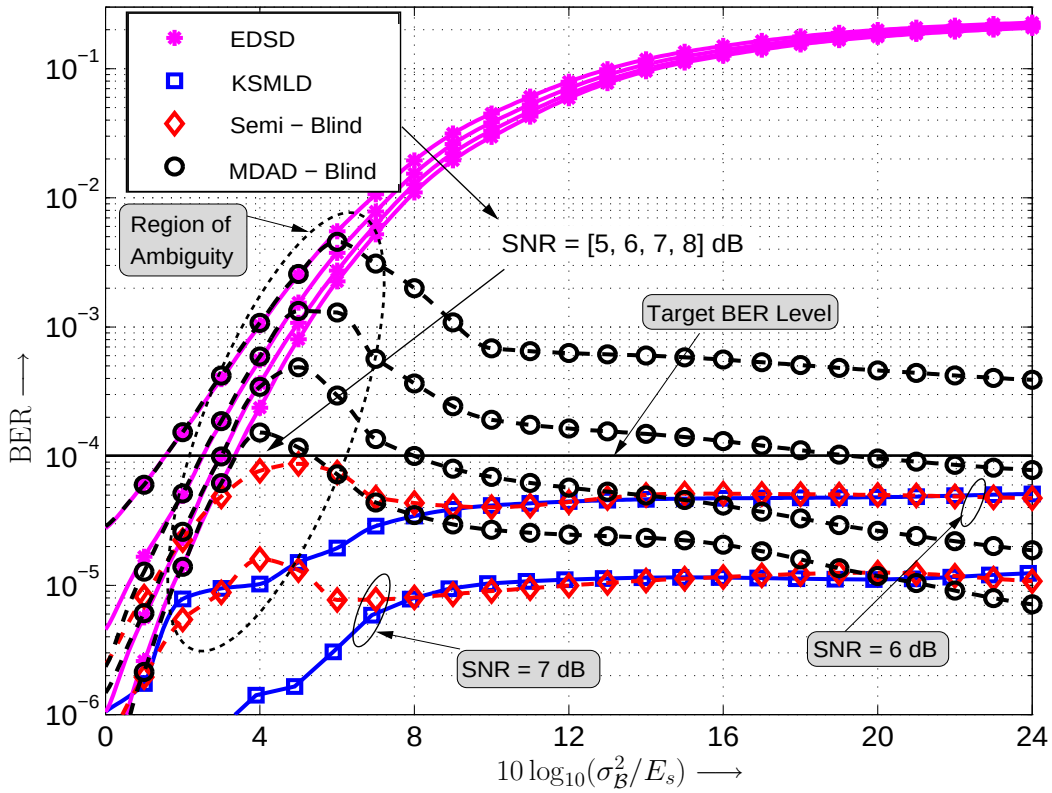

Figure 3.10 — Interference tolerance of the various detectors depicted in terms of achievable BER with decreasing SIR when $P_{\mathcal{B}}$ is held constant at 0.1 and target BER $= 10^{-4}$. Beyond a certain region of ambiguity, which is SNR dependent, target BER levels are seen to be easily achieved with 10 iterations of the JSS algorithms and only minor increases in the link budgets of the primary user.

3.5 Concluding Remarks

In this chapter, we provide a design paradigm for throughput enhancement in a cognitive radio environment where a receiver-centric approach to interference mitigation is advocated, allowing for a reduction in the region of interference of the primary user. The non-Gaussian nature of the interference is exploited in a way that permits the receivers to have a much higher instantaneous IT threshold than permitted by conventional receiver structures. In particular, a joint sensing and suppression algorithm is presented that allows a primary user to communicate with a low probability of error

even when there are potentially harmful interfering signals. Novel semi-blind and blind approaches to estimation of the interference process are presented when the temporal correlation in interference is modeled by a first order Markovian process. Both approaches are shown to offer significant enhancements in interference mitigation with the semi-blind method exhibiting only minor degradations with respect to an hypothesized ideal receiver that has perfect knowledge of the instantaneous noise state and variance. The algorithms are evaluated in terms of their estimation error and interference mitigation abilities. The benefits derived are in the form of a potentially higher spectrum utilization and increased protection from ambient interfering signals.

CHAPTER 4

Mitigation of Multiuser Interference in IR-UWB Systems

We now consider a specific transmission technology, namely IR-UWB, which by virtue of its inherent characteristics gives rise to a transmission environment where the effect of transmission by multiple users at a desired receiver is impulsive. IR-UWB technology [33] is a promising solution for short range communication when energy-efficient and inexpensive transceiver implementations are desirable while *moderate* data rates are sufficient. IR-UWB comprises of the transmission of very short pulses with durations of the order of 1 ns. To enable multiple access, i.e., simultaneous transmission by multiple users, time hopping (TH) is applied to IR-UWB pulses to avoid catas-

trophic collisions [33]. Recently, investigations have been performed to characterize the performance of TH IR-UWB systems in multiuser environments employing both pulse position modulation (PPM) and phase shift keying (PSK), e.g. [34, 99–104]. While initial work on analyzing IR-UWB systems in presence of multiple users employed a Gaussian distribution to characterize the statistical properties of the multiuser interference and hence the matched filter (MF) was considered as the optimum receiver [99], more recent work, cf. e.g. [34,100–104], has established that unless the number of users is substantially large, the Gaussian assumption (for MUI) leads to a significant underestimation of the achievable bit-error rates (BERs). It should be noted that since UWB signalling is being explored typically for short-range communication, the case of large number of users is of less interest as for most cases there will only be a few users in that range of a UWB receiver that interfere with the desired signal. The statistics of the multiuser interference (MUI) for TH IR-UWB and low to moderate number of users is better characterized as being non-Gaussian due to the impulsive nature of the MUI [105, 106]. Hence the MF receiver is no longer optimum and *robust* receivers that are more suited to an impulsive environment are required.

In this chapter, we design receivers for TH IR-UWB systems in the presence of MUI. This being an active area of work within the UWB research community over the past several years [107–113], various detection approaches have been proposed to mitigate the effect of MUI on the TH IR-UWB received signal. A relatively simple but rather limited approach is the soft-limiting detector proposed in [107, 108] which uses a soft threshold to limit the effect of the MUI signal. Also, recent work by other authors has applied known concepts from detection in non-Gaussian noise. In particular, Fiorina [109] presents a receiver structure based on the generalized Gaussian distribution, Cellini, Erseghe and Doná [110–112] and Flury and Le Boudec [113] have considered detectors modeling interference as Gaussian mixtures while Kim *et al.* [114] apply the Cauchy density for receiver design. The latter detectors can be stated to be in-

spired chiefly from the classical literature on signal detection in non-Gaussian noise, especially [10, Ch. 3] which suggests various heavy tail univariate probability density functions (pdfs). These include the generalized Gaussian, generalized Cauchy, and (Gaussian) mixture noise to model non-Gaussian interference. While the Gaussian mixture model was presented in Chapter 1, we introduce the generalized Gaussian and the generalized Cauchy distributions later in this chapter.

We will focus on receiver structures conforming to the need for robustness to MUI for TH IR-UWB transmission systems and propose novel receiver designs that are compared to representative designs in the literature. The comparison is facilitated by extensive analytical techniques that are derived to allow for a thorough performance evaluation of these receivers. In particular, we propose a new receiver structure that derives directly from the distribution of the MUI when applying an interference model that was developed in [34] by accounting for the specific attributes of TH IR-UWB systems. We make use of the distribution of the MUI to derive a simple, intuitive and yet highly effective detector that we refer to as the *two-term detector*. Furthermore, we apply the *α-penalty function detector*, introduced in Chapter 2, to the MUI mitigation problem for IR-UWB and present it as an elegant uni-parametric solution to containing the ill-effects of MUI. We remark that previous approaches that were mentioned above have also focussed on *one* particular parametric noise model and parameter estimation using e.g. an iterative expectation maximization approach [110, 113]. On the other hand, our work focuses a lot more on developing analytical techniques for the previously proposed detectors as well as the ones proposed in this Chapter and a comprehensive comparison of their relative abilities employing these techniques. In this context, we will investigate the sensitivity of the *parametric* detectors with respect to parameter adjustment. The rationale being that a predefined parameter adjustment would result in essentially non-parametric detectors, which are preferable for implementation. The parameter optimization and performance evaluation is particularly facilitated by the

semi-analytical expressions for the BER of TH IR-UWB employing the different detectors. Also different from the mentioned literatures, we consider both binary PPM (BPPM) and binary PSK (BPSK) modulation in a unified framework. For the introduction of the different robust detectors as well as for this performance analysis, we will assume a free-space propagation model. Such an approach is commonly applied in the literature concerned with MUI in TH IR-UWB systems, cf. e.g. [34, 99–104], as it allows separation of the effects caused by MUI and multipath transmission, where the latter are closely linked to the chosen RAKE-receiver structure, cf. [115]. We will then incorporate the robust detectors into a RAKE structure and evaluate the performance for multipath transmission by means of simulations.

Chapter Outline: The remainder of this chapter is organized as follows. The system model considered for TH-IR UWB transmission and a model for MUI are introduced in Sections 4.1 and 4.2 respectively. Several detectors are then presented in Section 4.3 that will later be shown to be robust to MUI. Expressions for performance evaluation are derived in Section 4.4, and the extension of robust detection for multipath channels is given in Section 4.5. A discussion of the performance results and comparisons follows in Section 4.6 and some concluding remarks are provided in Section 4.7.

4.1 System Model

In this section, we introduce the system model for TH IR-UWB transmission with N_u asynchronous users employing BPPM or BPSK modulation. The description and notation follows closely those used in previous works, e.g. [99, 103]. Following the approach in [34] (see also [105, 106]), we also present a suitable model for MUI in TH IR-UWB transmission.

As mentioned earlier, we consider free-space propagation for the sake of a lucid derivation as well as analytical tractability of the proposed robust detectors. Such an approach is common and was chosen in various related literatures on MUI in TH IR-UWB

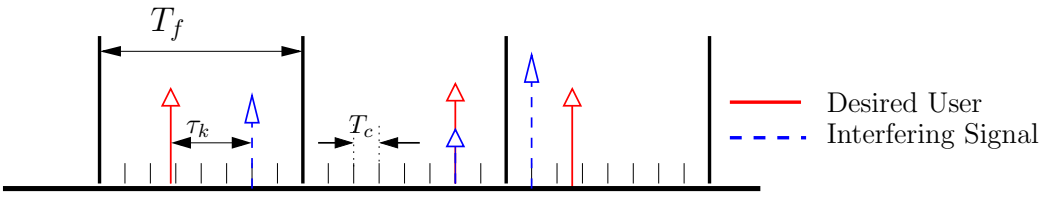

Figure 4.1 — Typical time Hopped IR UWB transmission interspersed with the arrival of interfering IR pulses from other users.

systems, cf. e.g. [34, 99–104, 106]. The extension to the frequency-selective UWB channels will be presented in Section 4.5.

4.1.1 Transmitted Signal

The transmitted signal of the k^{th} user is given as

$$s^k_{\text{BPPM}}(t) = \sqrt{\frac{E_b}{N_s}} \sum_{j=-\infty}^{\infty} p\left(t - jT_f - c^k_j T_c - b^k_{\lfloor j/N_s \rfloor}\delta\right) \tag{4.1}$$

for BPPM modulation and

$$s^k_{\text{BPSK}}(t) = \sqrt{\frac{E_b}{N_s}} \sum_{j=-\infty}^{\infty} d^k_{\lfloor j/N_s \rfloor} p\left(t - jT_f - c^k_j T_c\right) \tag{4.2}$$

for BPSK modulation. In (4.1) and (4.2) $p(t)$ denotes the transmitted pulse with autocorrelation function $R_p(t) \triangleq \int_{-\infty}^{\infty} p(\tau + t)p(\tau)\,\mathrm{d}\tau$ normalized such that $R_p(0) = 1$. The other parameters are defined as follows (cf. [99, 101, 103]). E_b and N_s denote the transmitted energy per information bit and the number of frames transmitted per information bit, respectively. T_f and T_c are the frame and chip duration, respectively, where $N_h T_c < T_f$ and N_h is the number of hops. One pulse is transmitted per frame and hence, the data rate is defined as $R_b \triangleq 1/(N_s T_f)$. c^k_j represents the TH code for the j^{th} bit of the k^{th} user and takes integral values in the range $[0, N_h - 1]$. $b^k_i \in \{0, 1\}$ is the i^{th} information bit of the k^{th} user, and $d^k_i \triangleq 1 - 2b^k_i$. Finally, δ denotes the PPM delay. An illustration of the transmitted frame is provided in Fig. 4.1 where we also show an interfering signal and how it may superimpose on the desired signal to

corrupt it. The parameter τ_k captures the asynchronicity of the users and its statistical properties will be explained shortly.

We digress briefly to make a few comments regarding the choice of the pulse $p(t)$ employed for IR-UWB transmissions. The shape of $p(t)$ bears significance as it determines the spectral characteristics of the transmitted signals which need to meet stringent spectral mask constraints for UWB to be a viable underlay technology. One of the most popular choices for UWB transmission is the Gaussian monocycle [116], which is the second derivative of the Gaussian pulse and is given by

$$p(t) = \left[1 - 4\pi \left(\frac{t}{\tau_p}\right)^2\right] \exp\left[-2\pi \left(\frac{t}{\tau_p}\right)\right] \tag{4.3}$$

with an autocorrelation function given by

$$R_p(t) = \left[1 - 4\pi \left(\frac{t}{\tau_p}\right) + \frac{4\pi^2}{3}\left(\frac{t}{\tau_p}\right)^4\right] \exp\left[-\pi \left(\frac{t}{\tau_p}\right)^2\right] \tag{4.4}$$

where τ_p is a time constant used to normalize the pulse. We will use this Gaussian monocycle to obtain numerical results in Section 4.6, with all other UWB transmission parameters being as summarized in Table 4.1, cf. e.g. [99, 101, 103, 113]. Figure 4.2 shows a Gaussian monocycle with $\tau_p = 0.7$ ns.

4.1.2 Received Signal and Filtering

The received signal can be written as

$$r(t) = \sum_{k=1}^{N_u} A_k s_{\mathrm{X}}^k(t - \tau_k) + n(t) \ , \quad \mathrm{X} \in \{\mathrm{BPPM,BPSK}\} \ , \tag{4.5}$$

where A_k represents the amplitude of the received signal for the k^{th} user at the receiver. Without loss of generality, we consider user $k = 1$ as the user of interest and assume perfect synchronization, i.e., $\tau_1 = 0$, as well as $c_j^k = 0$. We further assume that the

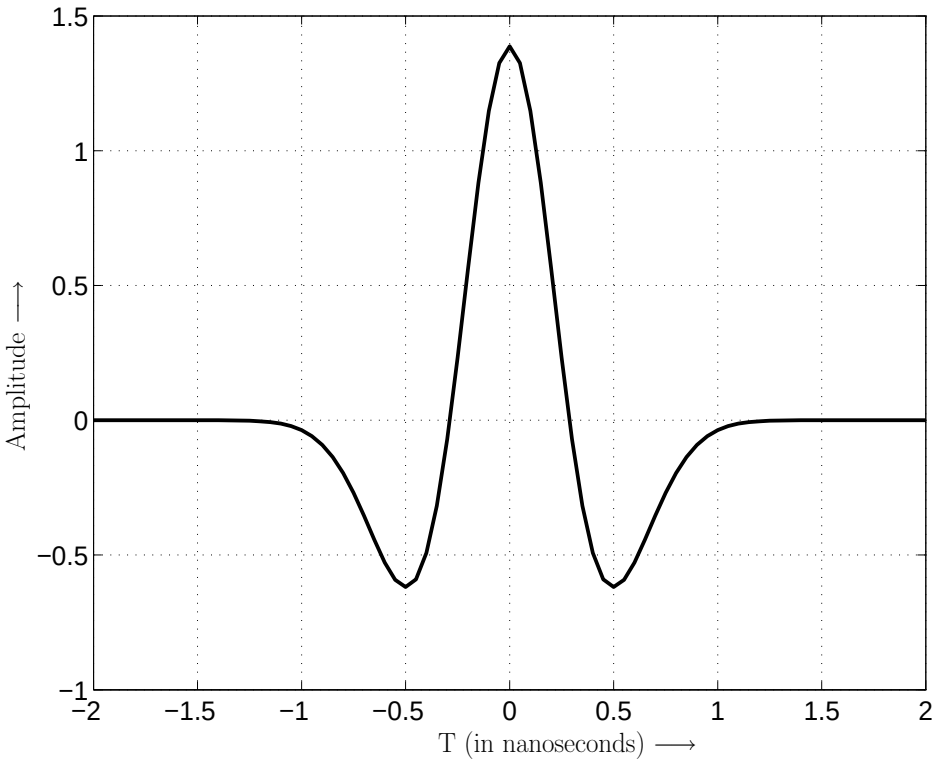

Figure 4.2 — Second derivative of a Gaussian monocycle with $\tau_p = 0.7$ ns.

delays τ_k, $k = 2, \ldots, N_u$, are uniformly distributed over one bit interval, where we choose $\tau_k \in (T_c, N_s T_f + T_c]$ for convenience. $n(t)$ is additive white Gaussian noise (AWGN) with two-sided power spectral density $N_0/2$.

At the receiver a matched filter is used to coherently demodulate the received signal. The correlator template matched to the first user is given by $v(t) = p(t) - p(t - \delta)$ for BPPM and $v(t) = p(t)$ for BPSK. The output of the correlator for the j^{th} frame, given by

$$r_j = \sqrt{\frac{N_s}{E_b}} \int_{jT_f}^{(j+1)T_f} r(t) v(t - jT_f)\, \mathrm{d}t \tag{4.6a}$$

$$\triangleq S_{\mathrm{X},j} + I_{\mathrm{X},j} + n_j\ , \quad \mathrm{X} \in \{\text{BPPM,BPSK}\}\ , \tag{4.6b}$$

is used to obtain the decision statistic. The desired signal components are $S_{\text{BPPM},j} =$

$d^1_{\lfloor j/N_s \rfloor} A_1(1 - R_p(\delta))$ and $S_{\mathrm{BPSK},j} = d^1_{\lfloor j/N_s \rfloor} A_1$ and n_j is a Gaussian random variable with variance given by

$$\sigma_n^2 = \begin{cases} \dfrac{[1 - R_p(\delta)]N_s N_0}{E_b} & \text{BPPM} \\ \dfrac{N_s N_0}{2E_b}, & \text{BPSK.} \end{cases} \tag{4.7}$$

Furthermore, the MUI terms $I_{\mathrm{X},j}$ can be expressed as

$$I_{\mathrm{BPPM},j} = \sum_{k=2}^{N_u} \sum_{i=-\infty}^{\infty} A_k [R_p(\gamma^k_{i,j} - b^k_{\lfloor i/N_s \rfloor}\delta) - R_p(\gamma^k_{i,j} - (b^k_{\lfloor i/N_s \rfloor} - 1)\delta)] \,, \tag{4.8}$$

$$I_{\mathrm{BPSK},j} = \sum_{k=2}^{N_u} \sum_{i=-\infty}^{\infty} A_k d^k_{\lfloor i/N_s \rfloor} R_p(\gamma^k_{i,j}) \,, \tag{4.9}$$

where $\gamma^k_{i,j} \triangleq (j-i)T_f - c^k_i T_c - \tau_k$. Denoting the width of $p(t)$ as T_p and making the usually valid assumptions that $T_p + \delta < T_c$ and $N_h T_c \leq T_f - T_c$, only one term of the sum over i in (4.8) and (4.9) can be nonzero for each k. To make this explicit let us write $\tau_k \triangleq l_k T_f - \alpha_k$, where $l_k = \lceil (\tau_k - T_c)/T_f \rceil$ and α_k is uniformly distributed in $[-T_c, T_f - T_c)$. Then we can rewrite the MUI terms as

$$I_{\mathrm{BPPM},j} = \sum_{k=2}^{N_u} A_k [R_p(\alpha_k - c^k_{j-l_k} T_c - b^k_{\lfloor (j-l_k)/N_s \rfloor}\delta) - R_p(\alpha_k - c^k_{j-l_k} T_c - (b^k_{\lfloor (j-l_k)/N_s \rfloor} - 1)\delta)] \,, \tag{4.10}$$

$$I_{\mathrm{BPSK},j} = \sum_{k=2}^{N_u} A_k d^k_{\lfloor (j-l_k)/N_s \rfloor} R_p(\alpha_k - c^k_{j-l_k} T_c) \,. \tag{4.11}$$

4.2 Interference Modeling

In modeling the interference from asynchronous users as depicted in Eqn. (4.10) and Eqn. (4.11), we adapt the approach for performance evaluation of the conventional detector from [34] (see also [105, 106]). In particular, we derive expressions for the

(marginal) pdfs of $I_{\mathrm{BPPM},j}$ and $I_{\mathrm{BPSK},j}$ taking into account their characteristics. These expressions will motivate the robust detectors and in particular the novel two-term detector presented in Section 4.3.

Let us denote the pdf of the MUI by $f_I(x)$, which is independent of j (the dependence on the modulation type will become apparent below). Since the signals from different users are independent, $f_I(x)$ can be expressed as ("$*$" denotes convolution)

$$f_I(x) = \underbrace{\frac{f_u(x/A_2)}{A_2} * \frac{f_u(x/A_3)}{A_3} \cdots * \frac{f_u(x/A_{N_u})}{A_{N_u}}}_{N_u-1} , \tag{4.12}$$

where $f_u(x)$ is the pdf of the interference signal resulting from user k normalized with respect to the gain A_k. Forouzan *et al.* suggested the following closed-form approximation for $f_u(x)$ [34, Eqn. (18)] :

$$f_u(x) = \beta_1 \delta_D(x) + \beta_2 (u(x + m_p) - u(x - m_p)) , \tag{4.13}$$

where $m_p \triangleq \int_{-\infty}^{\infty} p(t)v(t)dt$ is the maximal possible interference value, which is $m_p = 1 - R_p(\delta)$ for BPPM and $m_p = 1$ for BPSK, $\delta_D(x)$ is the Dirac delta function, and $u(x)$ is the unit step function. Furthermore, $\beta_1 = 1 - 2\beta_2 m_p$ and $\beta_2 = (3\sigma_a^2/2m_p^3)$, and σ_a^2 is the variance of the normalized interference process [34, 99]

$$\sigma_a^2 = \frac{1}{T_f} \int_{-\infty}^{\infty} \left[\int_{-\infty}^{\infty} v(t) p(t - s) \, \mathrm{d}t \right]^2 \mathrm{d}s . \tag{4.14}$$

Using the Gaussian approximation [34, Approx. (21)]

$$\sum_{\nu=0}^{\mu} \binom{\mu}{\nu} \left(\frac{x}{m_p} + \mu - 2\nu \right)^{\mu-1} u \left(\frac{x}{m_p} + \mu - 2\nu \right) \approx \frac{2^\mu (\mu - 1)! m_p}{\sqrt{2\pi\sigma_\mu^2}} \exp\left(-\frac{x^2}{2\sigma_\mu^2} \right) , \tag{4.15}$$

defining $q \triangleq 2m_p\beta_2 = 3\sigma_a^2/m_p^2$ and assuming, for the moment, perfect power control $A_k = A$ for all $k \in \{2, 3, \ldots, N_u\}$ as in [34], the pdf $f_I(x)$ (4.12) can be approximated

as

$$f_I(x) \approx (1-q)^{N_u-1}\delta_D(x) + \sum_{\mu=1}^{N_u-1} \binom{N_u-1}{\mu} (1-q)^{N_u-1-\mu} q^{\mu} \frac{\exp\left(-\frac{x^2}{2\sigma_\mu^2}\right)}{\sqrt{2\pi\sigma_\mu^2}} \ , \qquad (4.16)$$

where $\sigma_\mu^2 \triangleq (A^2 m_p^2 \mu^2)/3$. This means that the interference is modeled as Gaussian mixture noise plus a zero-interference term [the Dirac-delta term in (4.16)].

In the next section, when presenting the two-term detector, we will consider only the first two terms of the mixture density $f_I(x)$, which greatly facilitates the implementation. Thus only the parameters q and σ_1^2 are of interest. Abandoning the assumption of perfect power control, the variance σ_1^2 becomes

$$\sigma_1^2 = \frac{1}{N_u - 1} \left(\sum_{k=2}^{N_u} \frac{A_k^2 m_p^2}{3} \right) \ . \qquad (4.17)$$

4.3 Detection Strategies: Imparting *Robustness*

The approximation of the effective interference by the mixture model (4.16) suggests the application of detectors that are *robust* with respect to non-Gaussian noise. Such detectors have been considered, for example, for multiuser detection for DS-CDMA in [117, 118]. They share the common feature that the correlator output, i.e., r_j from (4.6b), is processed by a nonlinearity before the decision is made [10], implying that the TH IR-UWB decision variable attains the form

$$M_i = \sum_{j=0}^{N_s-1} \Delta(r_{iN_s+j}) \ , \qquad (4.18)$$

where the "metric difference" $\Delta(x)$ is a nonlinear function in x in general. If $M_i > 0$, then the bit-decision is $\hat{b}_i^1 = 0$ and if $M_i < 0$, then $\hat{b}_i^1 = 1$.

In the following, we present several *reasonable* candidates for this nonlinear function that try to account for the non-Gaussianity of the interference signal. These include the soft-limiting detector (SLD) from [107] and two detectors based on heavy-tail distributions [10, Ch. 3] first presented for TH IR-UWB in [109] and [114], respectively, and two novel detectors [119]. First, however, we briefly review the conventional detector for TH IR-UWB.

4.3.1 Conventional Detector (CD)

The conventional (single user) detector (CD) (a.k.a. correlator detector) employs [99]

$$\Delta(r_j) = r_j \ . \tag{4.19}$$

Considering (4.18) and (4.19) we note that when one or more of the N_s frames per bit are impaired by interference from other users, the potentially large absolute value of the corresponding statistic r_j will likely distort the decision metric M_i. Hence a nonlinearity is required such that the detrimental effects due to large distortions are mitigated.

4.3.2 Soft-Limiting Detector (SLD)

This observation has led Beaulieu and Hu to propose the SLD for TH IR-UWB with BPSK modulation [107]. The SLD applies a threshold $t_{\max}$ that limits the maximal contribution from each statistic r_j in (4.18). The modified metric can be written as

$$\Delta(r_j) = |r_j + t_{\max}| - |r_j - t_{\max}| \ , \tag{4.20}$$

where $t_{\max} = |S_{\mathrm{BPSK},j}|$ is chosen in [107]. Clearly, $\Delta(r_j)$ can also be applied to TH IR-UWB with BPPM, using $t_{\max} = |S_{\mathrm{BPPM},j}|$, and it is optimal if the interference-plus-noise variable is Laplacian distributed. Furthermore, the application of an adaptive

threshold was devised in [108], where the optimization of the threshold relies on BER simulations and thus the optimal value $t_{\max}$ depends on various TH IR-UWB system parameters as well as the signal-to-noise power ratio (SNR) and the signal-to-interference power ratio (SIR). Therefore, although setting the threshold for soft-limiting is non-parametric in itself, adapting the threshold for optimal performance makes this detector parametric. Moreover, since the improvements due to adaptation were observed mostly for relatively high BERs [107], we consider only the non-adaptive SLD later for performance comparisons.

4.3.3 Detectors Based on Heavy-Tail Distributions

As evidenced from the the distribution of interference, a Gaussian density function is clearly far from optimal in describing the interference processes. Intuitively, a plausible remedy derived from a Gaussian distribution seems to exist by using a generalized family of *Gaussian-like* distributions that provide a degree of freedom through a variable rate of exponential decay. These distributions are aptly categorized as heavy-tailed densities owing to the larger probability of extreme values allowed by them. In particular, two such heavy tailed densities have frequently been used to model non-Gaussian noise, and thus are potentially suited as basis for robust detectors for TH IR-UWB. These are the generalized Gaussian pdf and the Cauchy pdf [10, Ch. 3.2], [120].

Generalized Gaussian Detector (GGD): The generalized Gaussian pdf is given by

$$f_{\mathrm{GGD}}(x) = \frac{c_1(\beta)}{\sigma} \exp\left(-c_2(\beta) \left| \frac{x}{\sigma} \right|^{\frac{2}{1+\beta}} \right) , \tag{4.21}$$

where $\left(\frac{2}{1+\beta}\right)$ describes the rate of exponential decay and $c_1(\beta)$, $c_2(\beta)$ are functions of the parameter β but independent of x, and σ^2 denotes the variance. We provide the

relevant expressions below for the sake of completeness

$$c_1(\beta) = \frac{(\eta/2)\Gamma\left(3/\eta\right)}{\Gamma^{\frac{3}{2}}\left(1/\eta\right)}, \quad c_2(\beta) = \left[\frac{\Gamma\left(3/\eta\right)}{\Gamma\left(1/\eta\right)}\right]^{\frac{\eta}{2}} \tag{4.22}$$

where $\eta = 2/(1+\beta)$. The decision metric for the GGD (derived from Eqn. 4.21) is rendered in the following simple form by taking logarithms,

$$\Delta(r_j) = |r_j + S_{\mathrm{X},j}|^{\eta} - |r_j - S_{\mathrm{X},j}|^{\eta}\,, \tag{4.23}$$

X$\in$ {BPPM,BPSK}. This class of densities is interesting as it contains both the Gaussian , i.e. CD ($\beta = 0$), and Laplacian, i.e. SLD ($\beta = 1$), densities as special cases and the parameter β, also known as the shaping parameter [10], can be adapted according to impulsiveness of the process. Due to the symmetry of the distribution only even moments are non-zero. The general expression for the $(2n)^{\mathrm{th}}$ moment is given by

$$m_{2n} = \mathcal{E}[X^{(2n)}] = \left[\frac{\Gamma\left((2m+1)/\eta\right)}{\Gamma(1/\eta)}\right]\sigma^{2n} \tag{4.24}$$

In [109] such an approach is adopted and the shaping parameter is chosen such that the excess kurtosis matches that of the the MUI as measured using simulations.

Definition : *Kurtosis $\mathfrak{K}$ is a dimensionless quantity that is defined as the normalized fourth central moment of a distribution and measures the flatness of tails of a probability distribution. Mathematically it is computed as*

$$\mathfrak{K} = \frac{\mathcal{E}[X^4]}{(E[X^2])^2} \tag{4.25}$$

$\mathfrak{K} = 3$ for a Gaussian distribution and hence excess kurtosis is defined as $\mathfrak{E} = \mathfrak{K} - 3$.

Therefor the parameter β for the GGD may be estimated from the following relation

$$\mathfrak{E} = \left[\frac{\Gamma\left(\frac{5(1+\beta)}{2}\right)\Gamma\left(\frac{1+\beta}{2}\right)}{\left(\Gamma\left(\frac{3(1+\beta)}{2}\right)\right)^2} \right] - 3 \tag{4.26}$$

$\mathfrak{E} > 0$ indicates flatness of the distribution tails while $\mathfrak{E} > 0$ indicates peakiness of the distribution. The kurtosis of the MUI can be measured for e.g., by measuring the received signal when the desired user is silent. Following which β may be adaptively adjusted such as to satisfy Eqn. (4.21). However, we remark that the measurement of kurtosis in itself is *non*-robust [121].

Cauchy Detector (CaD):The Cauchy density is given by

$$f_{\mathrm{CaD}}(x) = \frac{\gamma}{\pi(\gamma^2 + x^2)} \tag{4.27}$$

with scale parameter γ. The corresponding Cauchy detector (CaD) for TH IR-UWB uses the decision metric

$$\Delta(r_j) = \log\left(\gamma^2 + (r + S_{\mathrm{X},j})^2\right) - \log\left(\gamma^2 + (r - S_{\mathrm{X},j})^2\right) \ , \tag{4.28}$$

$\mathrm{X} \in \{\mathrm{BPPM,BPSK}\}$. We remark that detection based on the Cauchy density function for an interfered IR-UWB environment has previously been considered in [114]. However, different from our work, the MUI was actually *generated* as a Cauchy distributed random variable which changes the motivation and intuition in employing the Cauchy-type penalty function. Also, the parameter γ was assumed perfectly known at the receiver which makes it a far less challenging design problem.

The proper choice of the parameters β for the GGD and γ for the CaD will be discussed in Section 4.6 using the semi-analytical BER expressions derived in Section 4.4. Next, we propose two new detectors.

4.3.4 Two-Term Detector (TTD)

This novel detector for TH IR-UWB is directly based on the mixture model for $f_I(x)$ in (4.16). The first step in deriving the TTD is to incorporate the effect of the AWGN at receiver into the mixture model, which consequently yields the pdf for noise and interference as

$$f_{I+n}(x) \triangleq f_I(x) * f_n(x) = \sum_{\mu=0}^{N_u-1} \frac{w_\mu \exp\left(-\frac{x^2}{2\xi_\mu^2}\right)}{\sqrt{2\pi\xi_\mu^2}}, \tag{4.29}$$

where $w_\mu \triangleq \binom{N_u-1}{\mu} q^\mu (1-q)^{N_u-1-\mu}$ and $\xi_\mu^2 \triangleq \sigma_\mu^2 + \sigma_n^2$ with $\sigma_0^2 = 0$. Clearly, $f_{I+n}(x)$ represents a Gaussian mixture noise model [10, Ch. 3.2.3]. The weights w_μ have a very intuitive interpretation in that they reflect the probability of experiencing interference plus noise with a variance ξ_μ^2, $\mu = 0, \ldots, N_u - 1$, [40].

Motivation for using only two terms: It has been observed that using typical parameters for IR-UWB systems, the value of q is limited to the order of 10^{-2} [99,106]. For example, $q = [0.002 \ldots 0.030]$ for the parameters shown in Table 4.1. Figure 4.3 presents the weights w_μ for $N_u = [4, 8, 16]$ using parameter values for free-space propagation case in Table 4.1. It can be seen from the figure that the weights have a rapidly decaying profile and that the first two terms are the dominant terms for $N_u \leq 16$, i.e., when MUI can be regarded highly impulsive. This observation and the fact that the full pdf $f_{I+n}(x)$ in (4.29) does not lend itself to low-complexity detection motivate the approximation of $f_{I+n}(x)$ by the two-term pdf

$$f_{\mathrm{TTD}}(x) = \rho \frac{\exp\left(-\frac{x^2}{2\sigma_n^2}\right)}{\sqrt{2\pi\sigma_n^2}} + (1-\rho)\frac{\exp\left(-\frac{x^2}{2(\sigma_1^2+\sigma_n^2)}\right)}{\sqrt{2\pi(\sigma_1^2+\sigma_n^2)}}\ , \tag{4.30}$$

where $\rho \triangleq (1-q)^{N_u-1}$. The optimum detector based on $f_{\mathrm{TTD}}(x)$ would compute the per-frame metrics

$$\tilde{\Delta}(r_j) = \log\left(f_{\mathrm{TTD}}(r_j - S_{\mathrm{X},j})\right) - \log\left(f_{\mathrm{TTD}}(r_j + S_{\mathrm{X},j})\right)\ , \tag{4.31}$$

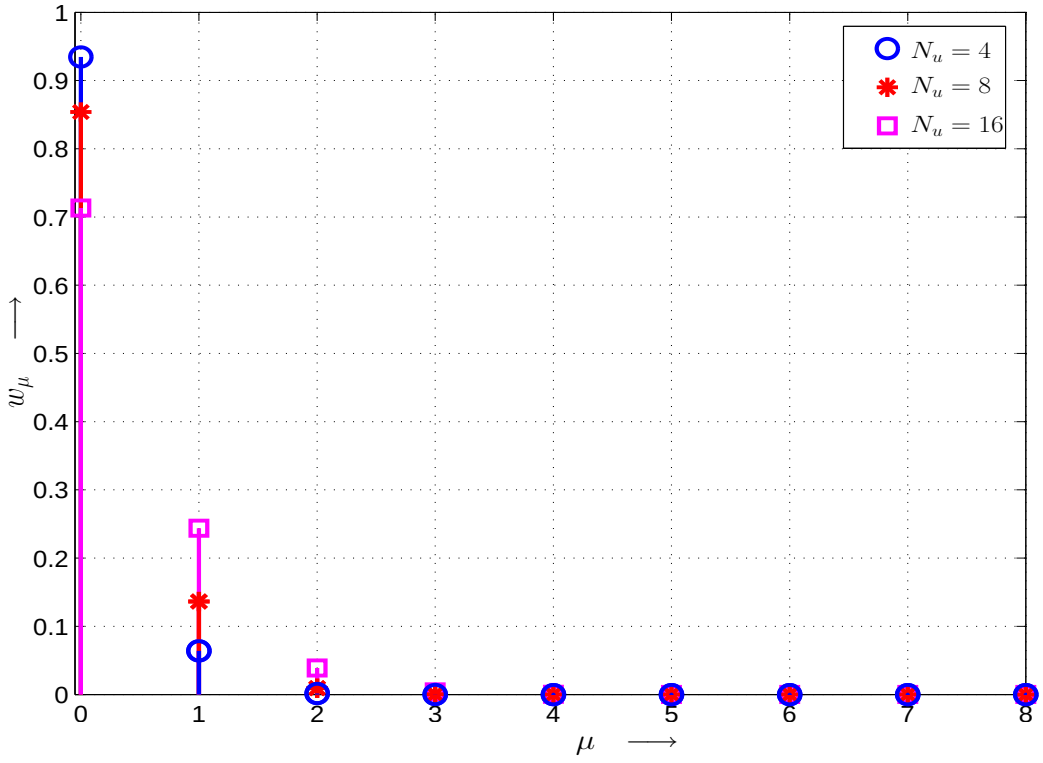

Figure 4.3 — Weights w_μ for different number of users (N_u). UWB transmission parameters for free-space propagation case from Table 4.1 and $N_s = 4$. A rapid decay of weight values can be observed.

X$\in$ {BPPM,BPSK}. This can be further simplified by applying the *max-log* approximation, which leads to the final two-term metric

$$\Delta(r_j) = \max\{t_1(r_j - S_{\mathrm{X},j}), t_2(r_j - S_{\mathrm{X},j})\} - \max\{t_1(r_j + S_{\mathrm{X},j}), t_2(r_j + S_{\mathrm{X},j})\}\ , \quad (4.32)$$

where

$$t_a(x) \triangleq \begin{cases} \log\left(\frac{\rho}{\sigma_n}\right) - \frac{x^2}{2\sigma_n^2} & ,\ \text{a=1.} \\ \log\left(\frac{1-\rho}{\sqrt{\sigma_1^2+\sigma_n^2}}\right) - \frac{x^2}{2(\sigma_1^2+\sigma_n^2)} & ,\ \text{a=2.} \end{cases} \quad (4.33)$$

This two-term detector (TTD) requires an estimate of ρ, which is the probability that r_j is not affected by MUI, and estimates of the variances σ_n^2 and $\sigma_1^2 + \sigma_n^2$ of noise and MUI plus noise. The overhead of estimating these parameters is minimal as they could

be obtained be obtained through a simple channel sensing operation when no desired signal is transmitted .

We note that related detectors based on Gaussian mixture models (GMM) have been developed in [110, 113]. The differences in our approach lie in the mathematical basis that is provided here for such a detector based on a derivation from (4.16) and (4.29) and the explicit *two-term* structure with max-log approximation in (4.32). The approaches in [110, 113] on the other hand try to approximate the overall pdf using a GMM from a heuristic perspective.

4.3.5 α-Penalty Function Detector (α-PFD)

The second novel detector for TH IR-UWB is based on the α-penalty function presented in Section 2.2 where it was noted that its exponential form allows for efficient rejection of outliers in a distribution. For IR-UWB receivers, the α-PFD computes the metric

$$\Delta(r_j) = \exp(-\alpha(r_j - S_{\mathrm{X},j})^2) - \exp(-\alpha(r_j + S_{\mathrm{X},j})^2), \tag{4.34}$$

X$\in$ {BPPM,BPSK}. Admittedly, the performance of TH IR-UWB employing the α-PFD will depend on the choice of α, therefore, an investigation of the optimal α is of interest here as well. We pursue such optimization of α based on the semi-analytical BER expressions derived in Section 4.4, in Section 4.6.

4.3.6 Illustration of the Nonlinearities

The nonlinear functions $\Delta(x)$ for the different robust detectors are shown in Figure 4.4, where $S_{\mathrm{X},j} = 1$ is assumed. The parameters are $\beta = [4,\ 0.5]$ for the GGD, $\gamma = [4,\ 0.3]$ for the CaD, and $\alpha = [1.5,\ 3.5]$ for the α-PFD, respectively. For TTD the parameters for the free-space propagation case in Table 4.1 with $N_s = 4$, SIR$=10$ dB, and $E_b/N_0 = [10, 15]$ dB are adopted. For clarity of illustration and readability of the figure the curves are normalized (which has no effect on the data decision) and $-\Delta(x)$ is shown

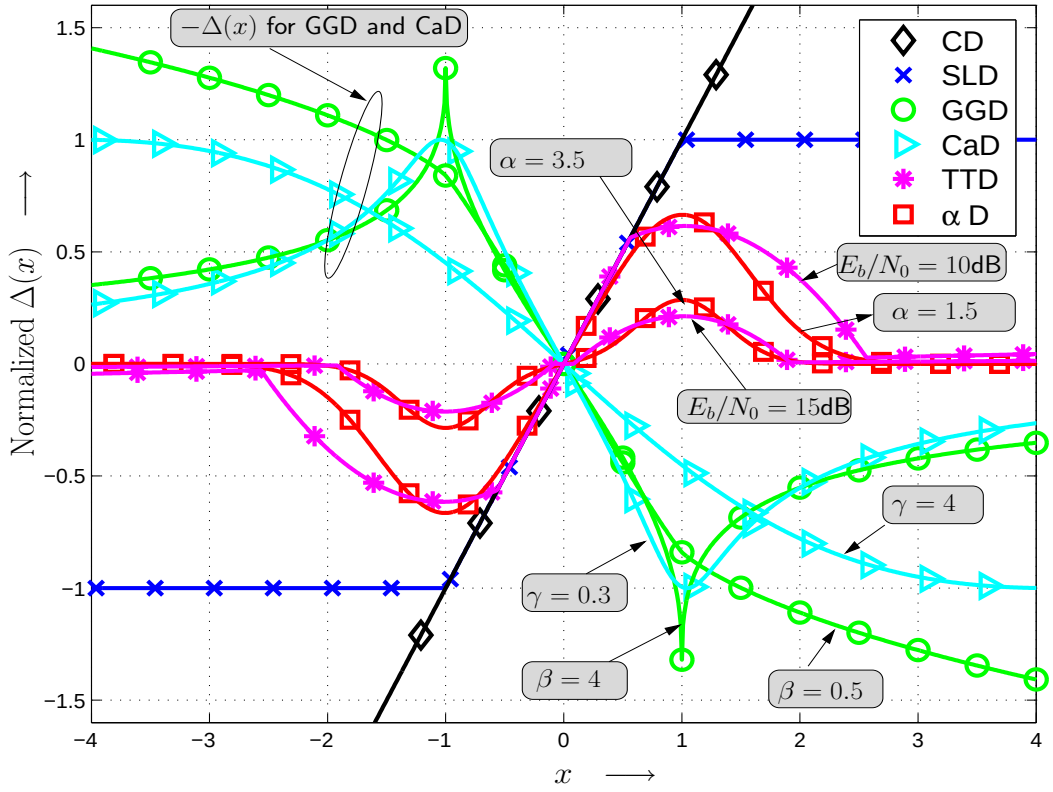

Figure 4.4 — Nonlinearities $\Delta(x)$ versus x for the different robust detectors from Section 4.3 assuming $S_{\mathrm{X},j} = 1$. Parameters: $\beta = 0.5$ and $\beta = 4$ for GGD, $\gamma = 0.3$ and $\gamma = 4$ for CaD, $\alpha = 1.5$ and $\alpha = 3.5$ for α-PFD. For TTD: Parameters for the free-space propagation case in Table 4.1 with $N_s = 4$, SIR = 10 dB, $E_b/N_0 = 10$ dB and $E_b/N_0 = 15$ dB.

for the GGD and CaD, respectively. It is interesting to observe that for $E_b/N_0 = 10$ dB and small absolute values of $|x|$, the TTD and the CD have the same slope of one, which then changes for large $|x|$ to a slope of $\sigma_n^2/(\sigma_1^2 + \sigma_n^2)$ for the TTD. This means that the TTD switches between the Gaussian-noise models with variances σ_n^2 and $(\sigma_1^2 + \sigma_n^2)$, respectively, depending on the magnitude of the input $|x|$. When the SNR increases, e.g. $E_b/N_0 = 15$ dB, the slope of the TTD nonlinearity becomes $\sigma_n^2/(\sigma_1^2 + \sigma_n^2)$ also around $x = 0$, i.e., received samples deviating considerably from ± 1 are assumed to be affected by MUI and thus attenuated. The SLD effectively truncates the contribution from large inputs to the overall decision variable. For $\beta > 1$ the nonlinearity for the

GGD has a cusp at ± 1 and falls off quickly towards large $|x|$, while it lies between those of the SLD and CD when $0 \leq \beta \leq 1$. Hence, better suppression of highly impulsive MUI is achieved for larger β. Similarly, the CaD is expected to be more robust to impulsive MUI for smaller values of the parameter γ. Finally, the nonlinearity of the α-PFD shows a close resemblance to that of the TTD and thus seems well suited for suppression of MUI in TH IR-UWB (see also [118, Fig. 1] for a plot of the penalty function).

4.4 Performance Analysis

In this section, we derive expressions that can be used to evaluate or approximate the achievable BER with the detectors we introduced in Section 4.3. We will consider the free-space propagation model from Section 4.1. An effort has been made to keep the derivations general enough so that they are applicable for nonlinear metrics $\Delta(r_j)$ that have not been included in the current treatise. Therefore the obtained expressions are very useful for performance comparison and parameter optimization. For convenience, we use the notation Δ_j instead of $\Delta(r_j)$ in the following.

4.4.1 Simplified Analysis I: Independent Interference per frame

The first expression for the BER is based on the assumption that the interference terms I_j in different frames are statistically independent, i.e., the MUI is independent and identically distributed (i.i.d.). We note that this assumption has been used in both [34] and [106] considering TH IR-UWB with conventional detection. Introducing the Laplace transform

$$\Phi_{\Delta_j}(s) \triangleq \mathcal{E}\left\{\mathrm{e}^{-s\Delta_j(x)}\right\} = \int_{-\infty}^{\infty} \mathrm{e}^{-s\Delta_j(x)} f_I(x)\,\mathrm{d}x \tag{4.35}$$

of the pdf $f_I(x)$, which is independent of j [see (4.12)], the error probability can be expressed as

$$P_e = \frac{1}{2\pi \mathrm{j}} \int_{c-\mathrm{j}\infty}^{c+\mathrm{j}\infty} \frac{1}{s} [\Phi_{\Delta_j}(s)]^{N_s} \, \mathrm{d}s \ , \tag{4.36}$$

where $c \in \mathcal{R}$ is in the region of convergence of this integral. Both integrals can be efficiently evaluated numerically using, e.g., Gauss-Chebyshev quadratures [122, Chapter 4.5] [51]:

$$P_e \approx \frac{1}{K} \sum_{i=1}^{K/2} \Re\{[\Phi_{\Delta_j}(c + \mathrm{j}c\nu_i)]^{N_s}\} + \nu_i \Im\{[\Phi_{\Delta_j}(c + \mathrm{j}c\nu_i)]^{N_s}\} \ , \tag{4.37}$$

$$\Phi_{\Delta_j}(s) \approx \frac{\pi}{K} \sum_{i=1}^{K} \left[\mathrm{e}^{-s\Delta_j(\nu_i)} f_{I+n}(\nu_i)\right] / \mu_i \ , \tag{4.38}$$

where $\Re\{\cdot\}$, $\Im\{\cdot\}$ denote real and imaginary part, respectively, $f_{I+n}(x) \triangleq f_I(x) * f_n(x)$, $\nu_i \triangleq \tan((2i-1)\pi/(2K))$, $\mu_i \triangleq \cos((2i-1)\pi/(2K))$, and the number of nodes K is typically chosen in the order of 400 to achieve sufficient accuracy. The pdf $f_I(x)$ can be modeled by substituting Eqn. (4.13) in Eqn. (4.12).

4.4.2 Correct Analysis: Correlated Interference over frames

The key assumption in the above simplified analysis is the independence of interference terms I_j. Generally, this assumption is not met, as will be illustrated with numerical examples in Section 4.6. A correct analysis needs to condition the independence of interference terms on the realization of relative delays, represented by the vectors $\boldsymbol{\alpha} \triangleq [\alpha_2 \, \alpha_3 \, \ldots \, \alpha_{N_u}]$ and $\boldsymbol{l} \triangleq [l_2 \, l_3 \, \ldots \, l_{N_u}]$ (recall that $\tau_k \triangleq l_k T_f - \alpha_k$), and data $\boldsymbol{b} \triangleq [b_0^2 \, b_1^2 \, b_0^3 \, b_1^3 \, \ldots \, b_0^{N_u} \, b_1^{N_u}]$ when considering detection of b_1^1. (Note that the two data symbols b_0^k and b_1^k can affect detection of b_1^1, see (4.10) and (4.11).) Denoting by $\Delta_{j|\boldsymbol{\alpha},\boldsymbol{l},\boldsymbol{b}}(x)$ the metric difference for the jth frame given $\boldsymbol{\alpha}$, $\boldsymbol{l}$, $\boldsymbol{b}$, the conditional error

probability can be written on the lines of Eqn. (4.36) be written as

$$P_{e|\boldsymbol{\alpha},\boldsymbol{l},\boldsymbol{b}} = \frac{1}{2\pi \mathrm{j}} \int_{c-\mathrm{j}\infty}^{c+\mathrm{j}\infty} \frac{1}{s} \prod_{j=0}^{N_s-1} \Phi_{\Delta_{j|\boldsymbol{\alpha},\boldsymbol{l},\boldsymbol{b}}}(s)\, \mathrm{d}s \ . \tag{4.39}$$

Numerical evaluation of (4.39) is done as shown in (4.37). Employing the usual assumption that the TH code is random, i.e., c_j^k are uniformly distributed in $\{0,\, 1,\, \ldots,\, N_h{-}1\}$, and that interference terms originating from different users are statistically independent, the pdf of interference plus noise is readily found as

$$f_{I+n|\boldsymbol{\alpha},\boldsymbol{l},\boldsymbol{b}}(x) = \frac{1}{N_h^{N_u-1}} \sum_{\boldsymbol{h}} \frac{1}{\sqrt{2\pi\sigma_n^2}} \exp\left(\frac{-\left[x - I_j(\boldsymbol{h})\right]^2}{(2\sigma_n^2)} \right) \ , \tag{4.40}$$

where $I_j(\boldsymbol{h})$ equals, respectively, $I_{\mathrm{BPPM},j}$ (4.8) and $I_{\mathrm{BPPM},j}$ (4.9) given $\boldsymbol{\alpha}$, $\boldsymbol{l}$, $\boldsymbol{b}$, and $\boldsymbol{h} \triangleq [h_2 \ldots h_{N_u}]$ with $h_k \in \{0, 1, \ldots N_h - 1\}$ and $c_i^k = h_k$. Substituting $f_{I+n|\boldsymbol{\alpha},\boldsymbol{l},\boldsymbol{b}}(x)$ from (4.40) into (4.38) yields the conditional Laplace transform $\Phi_{\Delta_{j|\boldsymbol{\alpha},\boldsymbol{l},\boldsymbol{b}}}(s)$. To find out the overall probability of error P_e we still need to average the conditional error probability $P_{e|\boldsymbol{\alpha},\boldsymbol{l},\boldsymbol{b}}$ over $\boldsymbol{\alpha}$, $\boldsymbol{l}$, $\boldsymbol{b}$, and $\boldsymbol{h}$ such that

$$P_e = (4T_f N_s)^{-(N_u-1)} \int_{\boldsymbol{\alpha}} \sum_{\boldsymbol{l}} \sum_{\boldsymbol{b}} P_{e|\boldsymbol{\alpha},\boldsymbol{l},\boldsymbol{b}}\, \mathrm{d}\boldsymbol{\alpha} \ , \tag{4.41}$$

where $\boldsymbol{\alpha} \in [-T_c, T_f - T_c)^{N_u-1}$, $\boldsymbol{l} \in \{1, 2, \ldots, N_s\}^{N_u-1}$, and $\boldsymbol{b} \in \{0, 1\}^{2(N_u-1)}$.

We note that $P_{e|\boldsymbol{\alpha},\boldsymbol{l},\boldsymbol{b}}$ is periodic along each coordinate α_k for an interval of length $N_h T_c$ with period $T_c/2$. In the remaining interval of length $T_f - N_h T_c$, interference does not occur and $P_{e|\boldsymbol{\alpha},\boldsymbol{l},\boldsymbol{b}}$ equals the error probability for the AWGN channel. Exploiting these facts can speed up the integration in Eqn. (4.41) considerably. Furthermore, for summation over $\boldsymbol{h}$ in (4.40) only those cases have to be explicitly considered for which $I_j(\boldsymbol{h})$ is non-zero. Nevertheless, the exponential increase of the summation terms limits the applicability of this correct analysis to relatively small values of N_u.

4.4.3 Simplified Analysis II

In order to reduce the computational burden in obtaining the theoretical limits presented above we now consider a second simplified analysis, which retains conditioning of the error rate on $\boldsymbol{\alpha}$ but abandons conditioning of the interference pdf on $\boldsymbol{l}$ and $\boldsymbol{b}$. The rationale being that data randomization, i.e., averaging interference with respect to $\boldsymbol{l}$ and $\boldsymbol{b}$, is actually possible by introducing a frame interleaver with a depth corresponding to N_s data bits at the transmitter and a corresponding deinterleaver at the receiver.

Considering interference terms conditioned on $\boldsymbol{\alpha}$ to be statistically independent for different frames as, we need to consider the pdf of interference plus noise averaged with respect to the data,

$$f_{I+n|\boldsymbol{\alpha}}(x) = \frac{1}{(2N_h)^{N_u-1}} \sum_{\boldsymbol{b}'} \sum_{\boldsymbol{h}} \frac{1}{\sqrt{2\pi\sigma_n^2}} \exp\left(\frac{-\left[x - I_j(\boldsymbol{h}, \boldsymbol{b}')\right]^2}{2\sigma_n^2} \right) , \tag{4.42}$$

where $\boldsymbol{b}' \triangleq [b^2 \ \ldots \ b^{N_u-1}]$ and $b^k \in \{0, 1\}$. Alternatively, for large values of N_u, we may evaluate the pdf as inverse Fourier transform, which for the case of BPSK can be written as

$$f_{I+n|\boldsymbol{\alpha}}(x) = \frac{1}{\pi} \int_0^\infty \cos(\omega x) \mathrm{e}^{-\omega^2\sigma_n^2/2} \prod_{k=2}^{N_u} \left[\frac{1}{N_h} \sum_{h=0}^{N_h-1} \cos(\omega A_k R_p(\alpha_k - h_k T_c)) \right] \mathrm{d}\omega \ . \tag{4.43}$$

In Eqn. (4.43) we used the fact that $f_{I+n|\boldsymbol{\alpha}}(x)$ is real-valued and the even symmetry of the integrand. Complexity for numerical evaluation of (4.43) is almost independent of N_u and numerical integration can be done applying Gaussian quadratures. Substituting $f_{I+n|\boldsymbol{\alpha}}(x)$ into (4.38) yields $\Phi_{\Delta_{j|\boldsymbol{\alpha}}}(s)$, and then $P_{e|\boldsymbol{\alpha}}$ is obtained from (4.37). When averaging $P_{e|\boldsymbol{\alpha}}$ with respect to $\boldsymbol{\alpha}$, again the periodicity of $P_{e|\boldsymbol{\alpha}}$ can be exploited for faster numerical convergence.

Remark: We note that the expressions derived above require numerical integration, whereby the complexity is dependent on the extent to which simplifications are invoked. Nonetheless, performance analysis of TH IR-UWB with conventional detection requires numerical integration as well and hence the computational burden is very much in the league of earlier investigations into IR-UWB performance, cf. [102–104].

4.5 Receiver Processing for Multipath Channel

We now move on to the case with greater practical relevance by extending the application of robust detection to the case of TH IR-UWB transmission over multipath channels. In conformance with related work in the area e.g. [105, 111, 113, 123] we assume that the frame duration T_f is long enough such that practically no inter-frame interference occurs. The multipath channel between user k and the receiver is characterized by the impulse response

$$g^k(t) = \sum_{l=0}^{L-1} w_l^k \delta_D(t - \tau_l^k) \ , \tag{4.44}$$

where L is the number of paths, and w_l^k and τ_l^k are the weight and delay for the l^{th} path of the k^{th} user, respectively. For the numerical results in Section 4.6 we will adopt the channel model developed for 802.15.4a [124] for the parameters L, w_l^k, and τ_l^k. As usual, the channel is assumed to be invariant during the transmission of at least one bit. Assuming that N_u users are active the received signal is given by

$$r(t) = \sum_{k=1}^{N_u} s^k(t) * g^k(t) + n(t) = \sum_{k=1}^{N_u} \sum_{l=0}^{L-1} w_l^k s^k(t - \tau_l^k) + n(t) \ . \tag{4.45}$$

A RAKE receiver structure with a certain number K of fingers is commonly applied, where after filtering with the correlator template $v(t)$ the fingers are assigned to those paths with the largest gains. Here we assume that the delays of this selective RAKE (SRAKE) differ by integer multiples of the chip duration T_c [115]. Denoting the channel

coefficients of the effective impulse response after filtering and sampling for the desired user by g_p, $0 \leq p < T_f/T_c$, the received samples for the jth frame are given by

$$r_{j,p} = g_p S_{\mathrm{X},j} + I_{j,p} + n_{j,p}, \qquad 0 \leq p < T_f/T_c \,, \mathrm{X} \in \{\mathrm{BPSK}, \mathrm{BPPM}\} \,, \tag{4.46}$$

where $I_{j,p}$ is the collective MUI and $n_{j,p}$ is a Gaussian random variable with the same statistics as n_j in (4.6b).

The SRAKE for robust detection combines K received samples per frame to yield the decision variable

$$M_i = \sum_{j=0}^{N_s-1} \sum_{p \in \mathcal{K}} \Delta(r_{iN_s+j,p}) \,, \tag{4.47}$$

where the set $\mathcal{K}$ contains the indices of the K RAKE fingers with the largest magnitudes g_p and, as is clear from (4.46), $g_p S_{\mathrm{X},j}$ replaces $S_{\mathrm{X},j}$ in the expressions for $\Delta(x)$ derived in Section 4.3 for the free-space propagation case. We note that the nonlinearity $\Delta(x)$ is applied to all RAKE finger outputs in (4.47). This is different from the robust receiver in [109], where for BPSK TH IR-UWB the received signal is filtered with $p(t) * g^1(t)$ and sampled with T_s before the nonlinearity is applied.

4.6 Results and Discussion

In this section we discuss the performances for the different robust detectors presented above as well as the selection of the parameters α, β, and γ for the α-PFD, the GGD, and the CaD, respectively. For the sake of clarity, as in Sections 4.1 to 4.4, we first consider the case of free-space UWB propagation, and thereafter results for multipath UWB channels are presented. We concentrate on multiuser interference from a relatively small number of interferers, namely one ($N_u = 2$) and three ($N_u = 4$) interferers, since these scenarios are practically relevant and best suited to study the non-Gaussian nature of MUI. Furthermore, we assume perfect channel estimation at the receiver. (The effects of imperfect channel estimation are discussed in [123], and joint chan-

Table 4.1 — Parameters of the TH IR-UWB system used for numerical results.

Parameter	Notation	Free-space propagation	Multipath channel
Pulse shape time constant	τ_p	0.2877 ns	0.7ns
Frame duration	T_f	20 ns	512 ns
BPPM delay	δ	0.1567 ns	0.1567ns
Chip duration	T_c	0.9 ns	2ns
Number of users	N_u	2, 4	2, 4
Number of chips per frame	N_h	20	128
Number of frames per bit	N_s	4, 8	4

nel and MUI statistics estimation in [105, 113].) The TH IR-UWB parameters are as specified in Table 4.1, cf. [99, 101, 103, 113].

4.6.1 Free-Space Propagation Channel

For the following we define the signal-to-interference ratio (SIR) as [103]

$$\mathrm{SIR} \triangleq \frac{A_1^2 N_s m_p^2}{\left(\sigma_a^2 \sum_{k=2}^{N_u} A_k^2\right)} \tag{4.48}$$

with σ_a^2 given in (4.14) and $m_p = 1 - R_p(\delta)$ for BPPM and $m_p = 1$ for BPSK. Since the BER performance results are qualitatively very similar for BPPM and BPSK, we restrict ourselves to showing results for BPSK in this section.

Detector Parameters

From an implementation point of view it would be desirable to adopt fixed values for the parameters of the GGD, CaD, and α-PFD, such that a "good" performance is achieved in a variety of interference scenarios. For this reason, we consider the effect of the parameters α, β, and γ on the performances of these detectors. Figure 4.5 shows the BER for the three detectors as function of (α, β, γ) for $N_u = 2$ (top) and $N_u = 4$ (bottom) users and SIR = 10 dB. The curves are parameterized by the SNR values

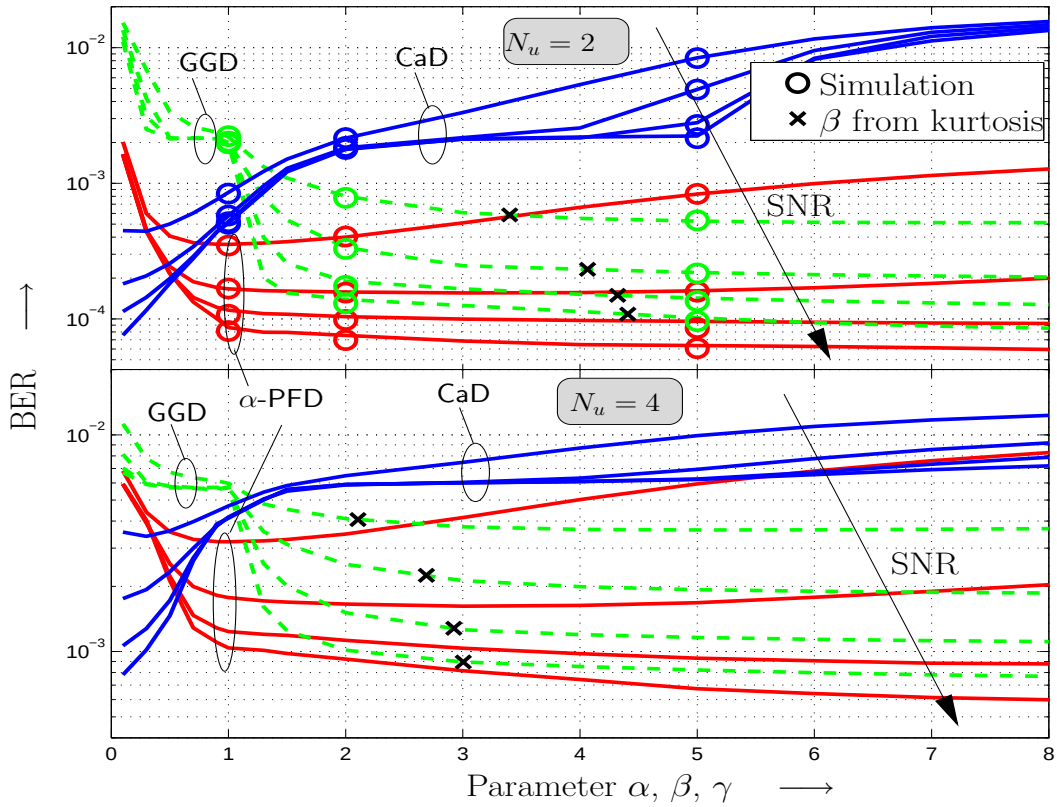

Figure 4.5 — BER vs. value for detector parameters α for α-PFD (4.34), β for GGD (4.21), and γ for CaD (4.28). BPSK and parameters for the free-space propagation case in Table 4.1 with $N_s = 4$. SIR = 10 dB, $E_b/N_0 = [10, 15, 20, 25]$ dB. "x" indicates the β-values according to the kurtosis of MUI and noise. Top: $N_u = 2$. Bottom: $N_u = 4$ (equal interference powers). Lines: Numerical results according to the analysis in Section 4.4.2. Circles: Simulation results.

$E_b/N_0 = [10, 15, 20, 25]$ dB. The numerical results (lines) are obtained by evaluation of (4.41), which is well confirmed by the excellent match of the numerical results with exemplary simulated results (circles) also included in Figure 4.5. Furthermore, the BER for TH IR-UWB without MUI, i.e., for an AWGN channel, is plotted as function of E_b/N_0 for different parameter values in Figure 4.6. Again, numerical results from evaluation of (4.41) are shown. It can be seen from Figure 4.5 that when MUI dominates, i.e., at high SNR, the BER performance improves with increasing α, β and decreasing γ, respectively. Not surprisingly, this agrees with the findings in Section 4.3.6 when

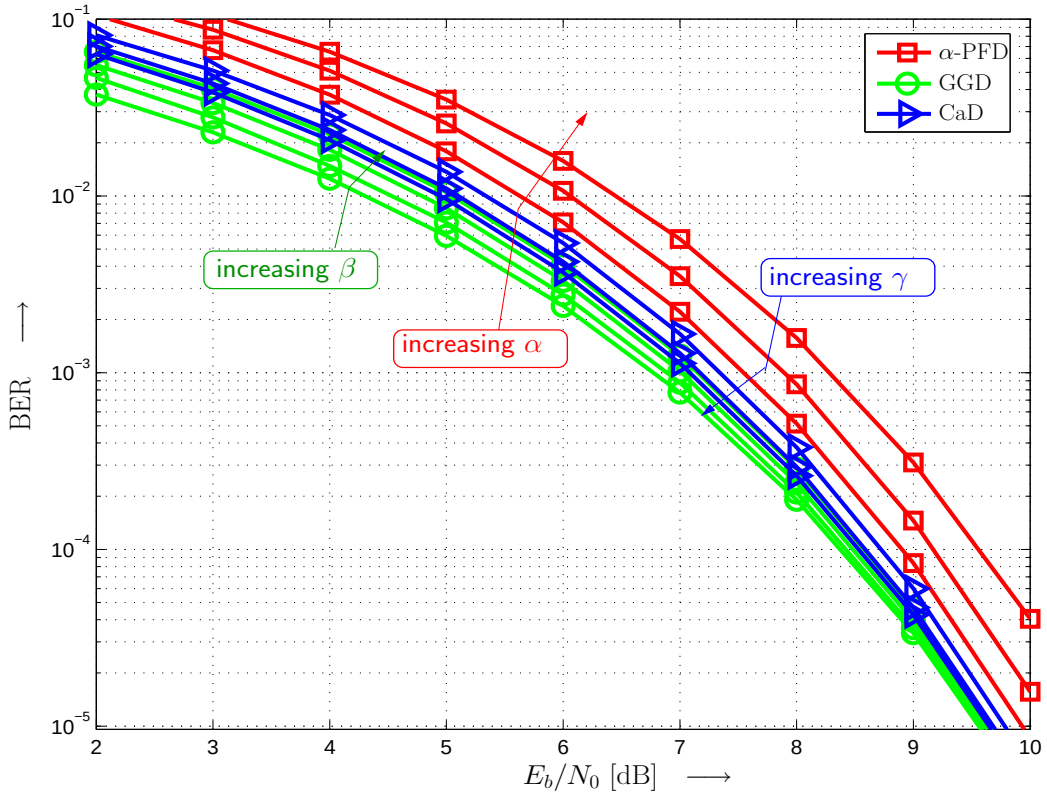

Figure 4.6 — BER vs. E_b/N_0 for TH IR-UWB with BPSK and AWGN, i.e., $N_u = 1$. α-PFD with $\alpha = [1, 2, 4]$, GGD with $\beta = [0, 1, 2, 4]$, CaD with $\gamma = [0.1, 0.3, 0.5]$. Numerical results.

considering the detector nonlinearities (see Figure 4.4). What is more interesting is that for both α-PFD and GGD the BER does not significantly vary as long as α and β are larger than a certain value, say $(\alpha, \beta) \geq 2$. Since, on the other hand, $\alpha \to 0$ and $\beta = 0$ are optimal for the case of AWGN, it is advisable to chose moderately large values for α and β. More specifically, the results in Figure 4.6 for the AWGN case indicate that the performance of the GGD degrades gracefully with larger β, while more significant degradations are observed for the α-PFD and large α. Hence, values of around $\beta = 4.0$ and $\alpha = 2.0$ seem a good compromise. Similarly, values of about $\gamma = 0.3$ achieve effective MUI suppression with the CaD (see Figure 4.5), while affording high performance also in the AWGN case (see Figure 4.6). We adopted these values for the simulation results presented below.

Figure 4.5 also shows the (β, BER)-pair when selecting β according to the kurtosis of MUI and noise (which can be determined analytically) as suggested in [109]. We observe that the corresponding BERs are close to optimum. However, adapting β, which entails the need for kurtosis estimation, does not provide advantages over using a constant $\beta = 4.0$ for the scenarios considered in Figures 4.5 and 4.6.

Finally, we note that the conclusions drawn above remain valid for other SIR values and interference with unequal powers, for which the results are qualitatively similar, but omitted for space limitations.

BER Comparison

Considering the same two- and four-user scenario as in Figure 4.5, the BER versus SNR are plotted for the different detectors in Figure 4.7. Numerical results from evaluation of (4.41) (lines) and additional simulation results (markers) are shown. The CD experiences an error floor at about 10^{-2}, which can be considerably lowered by the application of robust detection. More specifically, all robust detectors except the SLD show very similar performances with TTD consistently achieving the lowest BER for all SNR values. We note that the TTD requires adaption of three parameters [see (4.32)-(4.33)], which were adjusted as specified in Section 4.2, while the preset parameters as given above are applied for the GGD, CaD, and α-PFD. On the other hand, we found in that the performance of the TTD is rather insensitive to variations of the parameters from their nominal values. It is interesting to observe that the BER for the CD improves with increasing N_u, whereas it deteriorates for the robust detectors. The former can be attributed to the MUI becoming more "Gaussian-like" with increasing N_u, while the latter is due to an increased frequency of impulsive-noise events for larger N_u.

Different BER Approximations: Next we compare the different semi-analytically BER approximations from Section 4.4. To this end, Figure 4.8 shows the BER according

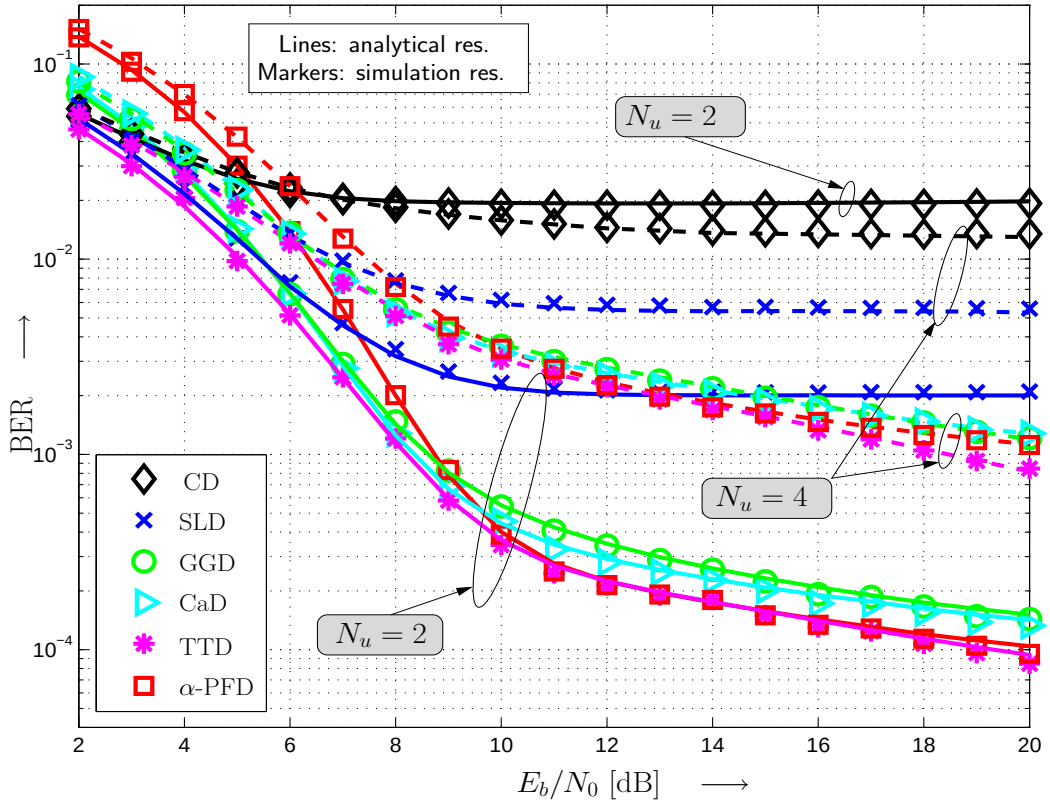

Figure 4.7 — BER vs. E_b/N_0 for different detectors. BPSK and parameters for the free-space propagation case in Table 4.1 with $N_s = 4$. $N_u = 2$ and $N_u = 4$ (equal interference powers) and SIR = 10 dB. Detector parameters: $\alpha = 2.0$, $\beta = 4.0$, $\gamma = 0.3$. Lines: Numerical results according to the analysis in Section 4.4.2. Markers: Simulation results.

to the expressions derived in Sections 4.4.1, 4.4.2, and 4.4.3, respectively, as function of E_b/N_0. $N_u = 2$ and $N_s = 8$ are chosen to emphasize the effects discussed in the following. For clarity, the BERs for only the CD, SLD, and TTD are plotted. Also included in Figure 4.8 are simulation results for TH IR-UWB, for TH IR-UWB with *frame interleaving*, and TH IR-UWB with i.i.d. MUI. We recall that the approximation in Section 4.4.1 (labeled "Approx. 1" in the figure) assumes i.i.d. MUI, the analysis from Section 4.4.2 (labeled "Correct") corresponds to the actual TH IR-UWB scheme, and the approximation in Section 4.4.3 (labeled "Approx. 2") assumes TH IR-UWB with frame interleaving. Clearly, the numerical results under the different assumptions are well matched by the corresponding simulation results. We observe that the BERs for

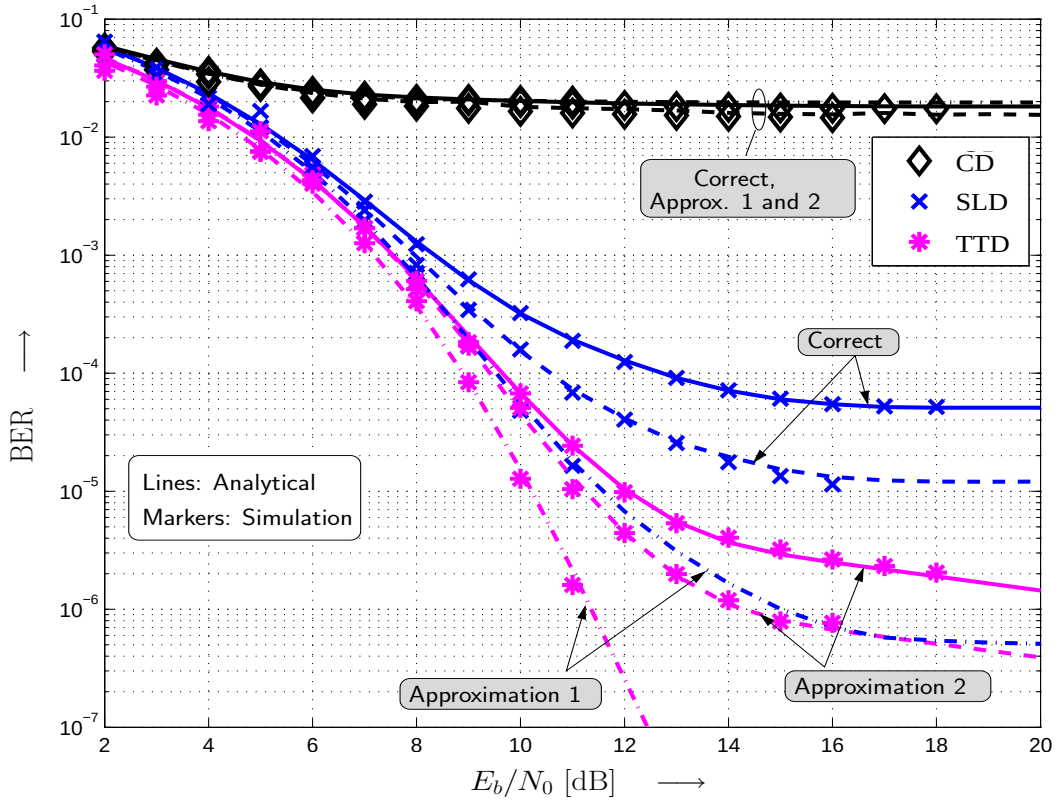

Figure 4.8 — BER vs. E_b/N_0 for different interference scenarios. BPSK and parameters for the free-space propagation case in Table 4.1 with $N_s = 8$. $N_u = 2$ and SIR = 10 dB. Lines: Numerical results according to the analysis in Sections 4.4.1 (Approx. 1), 4.4.2 (Correct), and 4.4.3 (Approx. 2). Markers: Simulation results (TH IR-UWB as described in Section 4.1.1, TH IR-UWB with frame interleaving, and TH IR-UWB with i.i.d. MUI, respectively).

the CD are almost identical in all three cases, which also explains why the assumption of i.i.d. MUI for the BER analysis made in [34,106] yields acceptable results. In the case of robust detection, however, the joint statistics of MUI affecting N_s frames representing one data bit need to be considered to faithfully predict the BER. It can be seen from Figure 4.8 that the BER notably decreases due to frame interleaving, and even more significantly in case of i.i.d. MUI. While the latter represents an artificial idealization, the application of frame interleaving is indeed possible and thus a means to ameliorate performance in the presence of MUI. We note that an interleaving depth corresponding to N_s data bits would be sufficient to achieve the same effect as infinite interleaving,

and thus the incurred interleaving delay appears feasible.

4.6.2 Multipath Channel

We now turn to the case of transmission over multipath channels. We adopt the standardized UWB channel model from [124] and exemplarily apply the channel model (CM) for line-of-sight residential environments (CM1 in [124]). To obtain representative results, we averaged the BER over 100 channel realizations for the desired user. To adjust a predefined SIR, we kept the same $N_u - 1$ realizations for the interferers. In particular, normalizing the energies of the interferer impulse responses and the energy of the effective impulse response after sampling for the desired user to one, we applied gains A_k and the relation (4.48) to fix an SIR of 10 dB for the following results. The number of RAKE fingers was set to $L = 16$, for which performance is reasonably close to the all-RAKE (ARAKE) receiver [115]. Furthermore, since the analysis from Section 4.4 is only applicable to free-space propagation, all results in this section are simulated BERs.

Detector Parameters

Figure 4.9 shows the BER for the the GGD, CaD, and α-PFD as function of their respective parameters for $N_u = 2$ and $N_u = 4$, where equal interference powers are assumed, and $E_b/N_0 = [10\,, 15\,, 20]$ dB. We observe similar dependencies of the BER performance on the parameter values as for the case of free-space propagation in Figure 4.5. The BER degradations for low-to-medium SNR and increasing β and α for the GGD and α-PFD, respectively, are somewhat more pronounced than for the free-space propagation case (note the different ranges of the x-axis), which can be attributed to the lower per-finger SNR before RAKE combining.

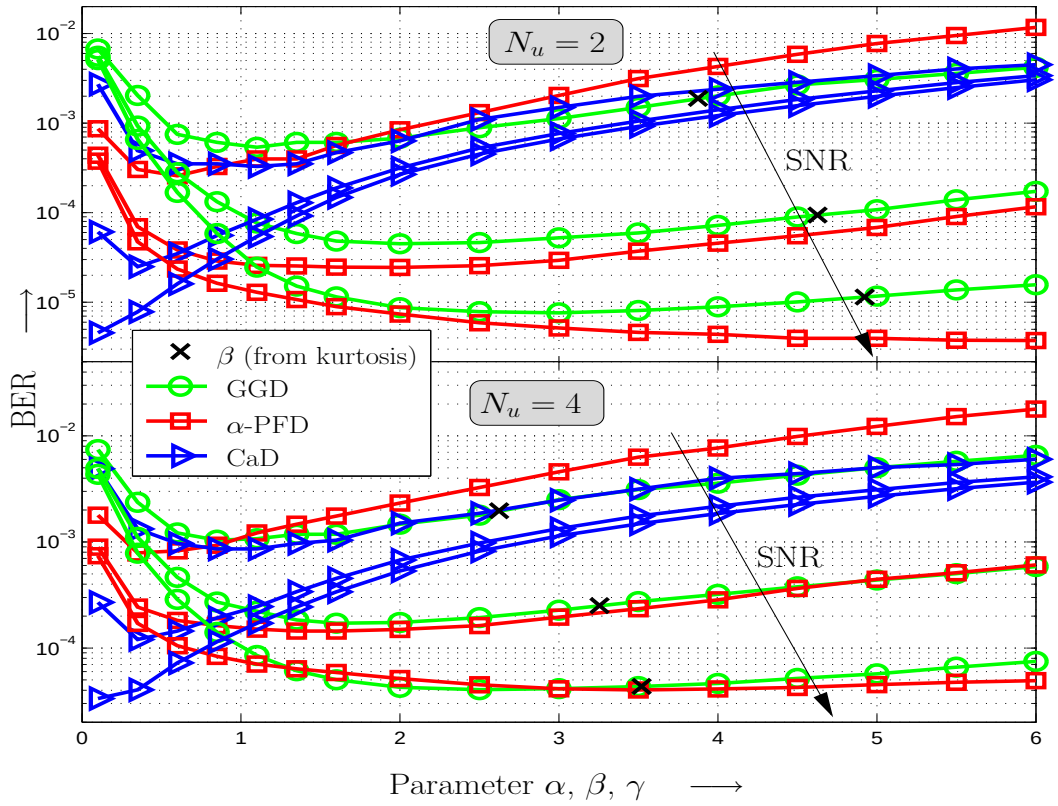

Figure 4.9 — BER vs. value for detector parameters α for α-PFD (4.34), β for GGD (4.21), and γ for CaD (4.28). BPSK and parameters for multipath-channel case in Table 4.1. SIR = 10 dB, $E_b/N_0 = [10, 15, 20]$ dB. "x" indicates the β-values according to the kurtosis of MUI and noise. Top: $N_u = 2$. Bottom: $N_u = 4$ (equal interference powers). Simulation results.

BER Comparison

The BER performance for the different detectors are compared in Figures 4.10 and 4.11 for the exemplary cases of BPSK and $N_u = 2$ users and BPPM and $N_u = 4$ users, respectively. For BPPM with $N_u = 4$ we assumed unequal interference power such that the powers of interferers two and three are 10 dB and 20 dB below that of interferer one, respectively. The parameters for the GGD, CaD, and α-PFD are $[\beta, \gamma, \alpha] = [4, 0.3, 2]$, i.e., the same as for the free-space propagation case. The parameters ρ and $\sigma_1^2 + \sigma_n^2$ for the TTD were estimated by measuring the frequency and variance of samples of aggregate interference and noise whose magnitude exceeded $5\sigma_n$. The BER for the

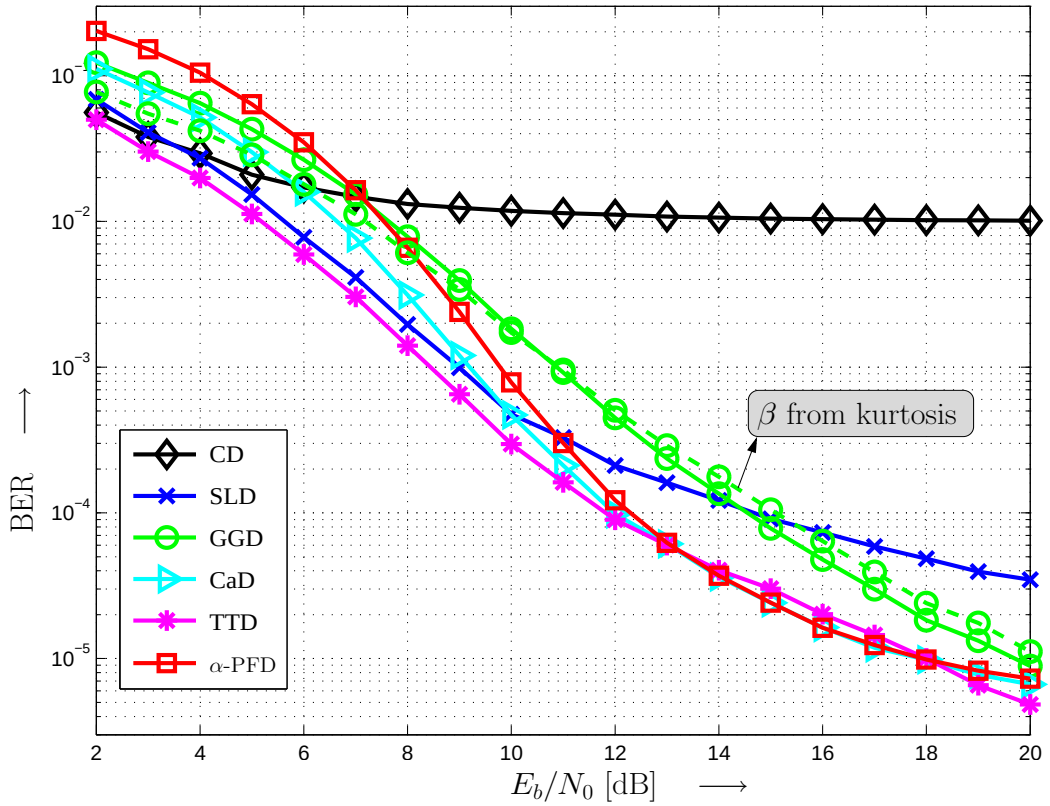

Figure 4.10 — BER vs. E_b/N_0 for different detectors. BPSK and parameters for multipath-channel case in Table 4.1. $N_u = 2$ and SIR = 10 dB. Detector parameters: $\alpha = 2.0$, $\beta = 4.0$, $\gamma = 0.3$. Simulation results.

GGD with adaptive β according to the kurtosis of the interference plus noise is also shown.

We observe that all robust detectors outperform the CD for BERs below 10^{-2}, which is the error floor for the CD in the considered cases. The TTD performs consistently well and always achieves the best performance. The performances for the CaD and α-PFD approach that of the TTD for medium SNRs, while the GGD becomes advantageous for high SNR. Of course, the particular shape of the BER curves for the parametric detectors can be tweaked by parameter modification, but employing fixed parameters for various scenarios is preferable for implementation. Furthermore, it can be seen that β-adaptation improves the performance of the GGD for low SNR only, i.e., relatively high BERs, which corroborates the usefulness of studying the performance as function

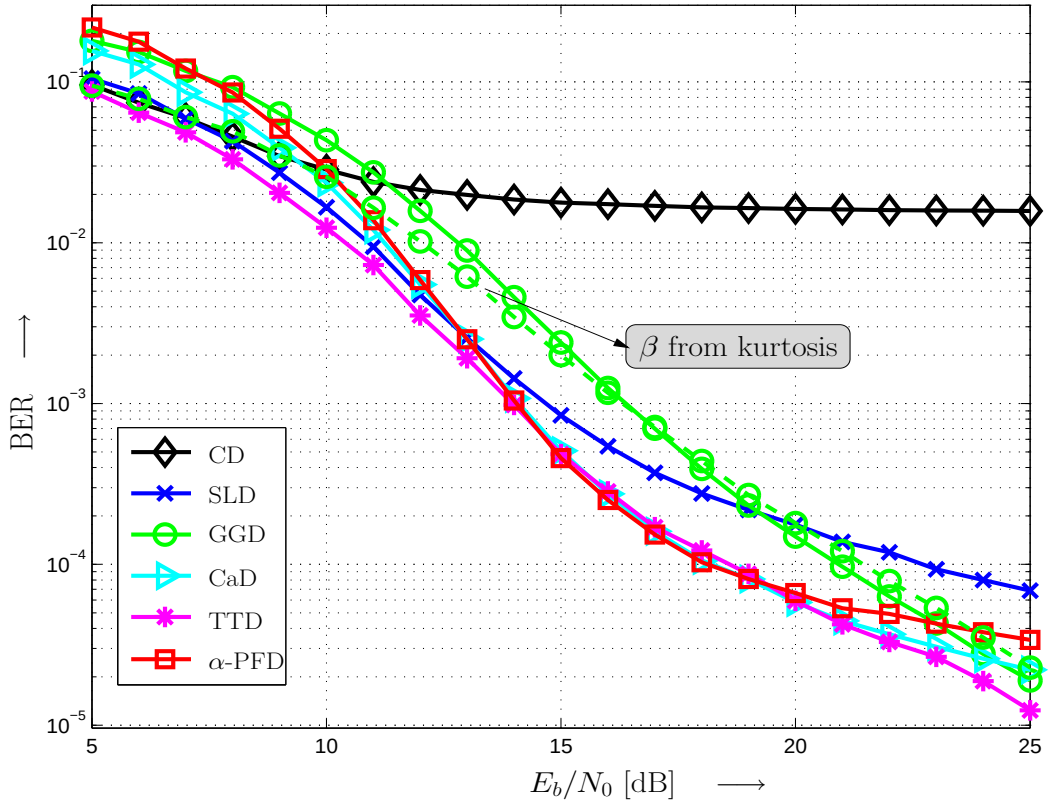

Figure 4.11 — BER vs. E_b/N_0 for different detectors. BPPM and parameters for multipath-channel case in Table 4.1. $N_u = 4$ and SIR = 10 dB. Unequal interference powers. Detector parameters: $\alpha = 2.0$, $\beta = 4.0$, $\gamma = 0.3$. Simulation results.

of the parameter value (Figures 4.5 and 4.6) leading to the choice of $\beta = 4$.

The main findings of this section can be summarized as follows. If the TTD parameters can be estimated, the TTD should be implemented for robust detection. The GGD, CaD, and α-PFD often well approach the performance of the TTD, and the single parameter of these detectors can be fixed for various interference and noise scenarios. While inferior in performance to the other robust detectors, the SLD affords significant gains over the CD and is perhaps the most simple to implement variant of all robust detectors.

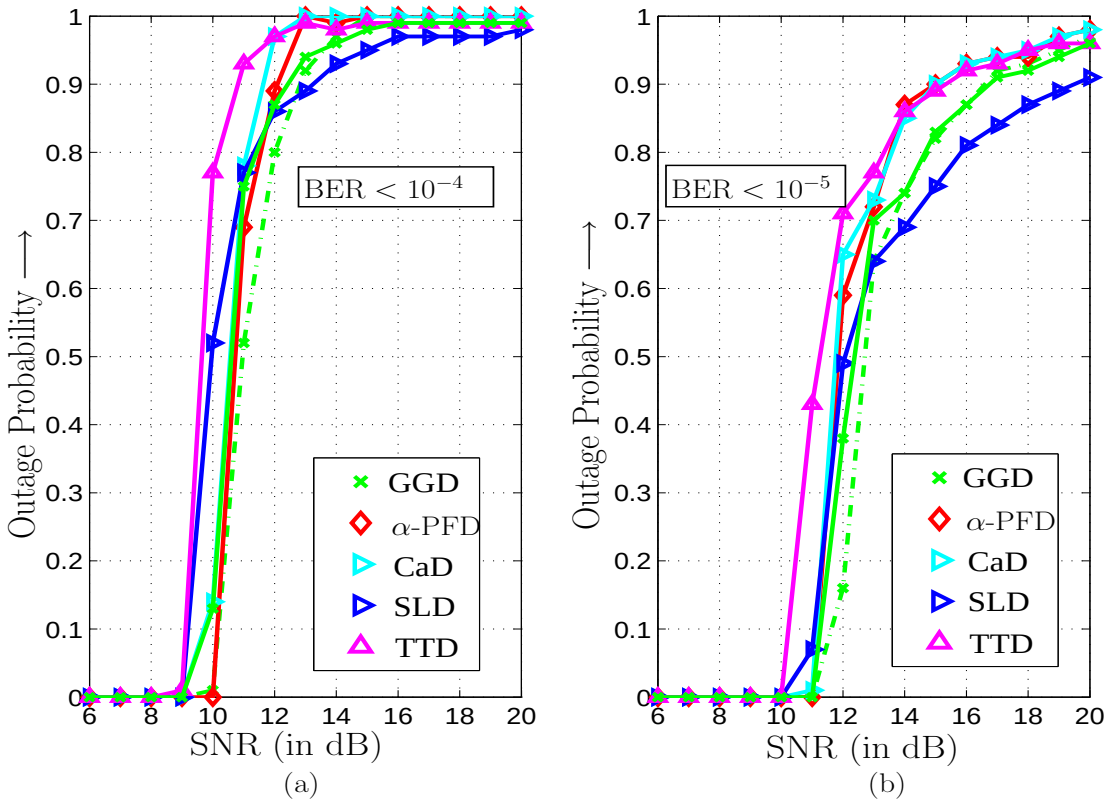

Figure 4.12 — P_{outage} for different robust detectors over a sample of 100 UWB channel realizations for the desired user. Plots are shown for P_{outage} with a threshold BER of (a) Threshold = 10^{-4} and (b)Threshold = 10^{-5}. Parameters: $\beta = 2.5$, $\alpha = 2.0$ and $\gamma = 0.3$

4.6.3 Comparison based on Outage Probability

In fading channels, an excellent parameter for gauging system performance is the outage probability of the considered link. To put the outage performance of the considered detectors in context, we set a target BER and plot the outage probability (P_{out}), i.e., the probability that the BER is less than the target BER in Figures. 4.12(a) and 4.12(b) over a sample of 100 randomly chosen user channel realizations with target BERs of 10^{-4} and 10^{-5} respectively. As can be seen all detectors except the SLD ensure a BER of atleast 10^{-4} at SNRs of 15 dB and higher. In Fig. 4.12(b) TTD, CaD and α-PFD can be seen to have BERs of less than 10^{-5} for $> 90\%$ of the cases for SNR > 15 dB. However, the relatively simple SLD is unable to ensure this at all and the GGD is able

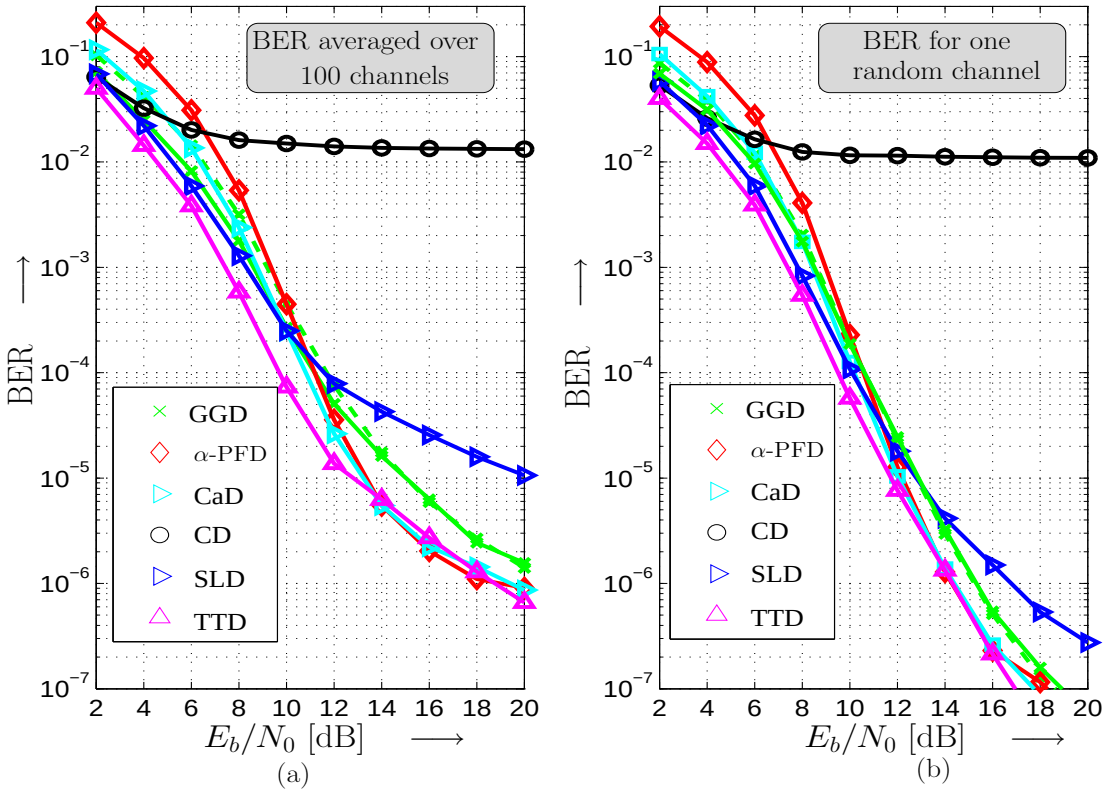

Figure 4.13 — BER vs. E_b/N_0 for different detectors for (a) 100 different channel realizations and (b) one realization of the UWB multipath-channel. $N_u = 2$ and SIR = 10 dB. Parameters: $\beta = 2.5$ (for fixed case), $\alpha = 2.0$ and $\gamma = 0.3$.

to do so only at very high SNRs. Hence this gives us an idea as to what detectors should we implement if the error rate requirements and SNR operating conditions are known *a priori*. GGD with a fixed value of β (dashed curve) is seen to lag slightly behind the the adaptive β (solid curve), based on measured MAI, only for lower values of SNR. As the impairment becomes more impulsive (with higher SNR), the α-PFD, CaD and TTD all perform similarly while at lower SNRs TTD is consistently the best, exhibiting agility with respect to level of interference.

4.6.4 A Note on the Ergodicity of the Results

Interestingly, through simulations, it was found that the usual approach of averaging performance over N UWB channel realizations ($N \geq 100$) exhibits vast variations in

the results depending on the set of channels selected. To highlight this point Figure 4.13 (b) shows the results for one randomly selected user channel. The observation is that depending on the channel, the relative performances of the detectors could vary significantly. For example, although it is evident from Figure 4.13 (a) that the TTD offers a 7dB advantage at BER of 10^{-5} on an average, for the channel in Figure 4.13 (b), this is reduced to about 1 dB. Thus even though the average case performance can be regarded as a good indicator of the detectors' capabilities, the actual error rates at given SNR will be subject to prevalent channel conditions.

4.7 Conclusions

In this chapter, we have investigated detection for TH IR-UWB transmission impaired by multiuser interference. In particular, we have considered five "robust" detectors, including the novel two-term detector (TTD) and α-detector (α-PFD), which are better suited than the conventional (matched filter) detector (CD) to cope with multiuser interference (MUI). To facilitate detector optimization and performance evaluation we have derived semi-analytical expressions for the bit-error rate (BER) with robust detection. From the evaluation of these expressions it has been found that the performances of the generalized Gaussian detector (GGD), the Cauchy detector (CaD), and the α-PFD are relatively insensitive to the value of the detection parameter as long as this parameter is chosen larger/smaller than a certain threshold. It has furthermore been shown that the assumption of i.i.d. MUI significantly distorts the BER estimation in the case of robust detection, while the performance of the CD is hardly affected. On the other hand, the BER for robust detection can be improved by the application of frame interleaving for TH IR-UWB. The performance comparison for the different robust detectors has shown that the TTD is advantageous in terms of BER performance, but that the GGD, CaD, and α-PFD with fixed parameters, which actually renders them non-parametric in operation, are attractive alternatives.

CHAPTER 5

Cooperative Communication in the Presence of Interference

Our work so far has focussed only on single antenna point-to-point communication. However, due to the ever-increasing demand for higher data rates the use of diversity techniques in either time, frequency or spatial domains has gained a lot of attention as it helps in reducing error rates significantly. Time diversity may typically be employed using error correcting codes combined with interleaving and we have studied, for example, convolutional codes in some detail in the preceding chapters. While the use of multiple antennas has been shown to provide multiple benefits such as increase in data rate that is proportional to the number of antennas employed [125] (spatial

multiplexing), increased reliability (spatial diversity), there exist physical limitations in using multiple antennas on devices with small form factors. This led to the idea of cooperation amongst different users gaining prominence to extend the benefits of spatial diversity to such user terminals. Over the past few years a lot of effort has been spent to quantify the performance gains achievable through cooperations as well as devising protocols that can translate the design goals from mathematical abstractions to real-world transceivers for such systems. In this chapter, we shift our focus on the use of such spatial diversity to enhance the link SNRs and consequently its error performance. Essentially, cooperative transmission extends the benefits of spatial diversity to communication devices that are unable to support multiple antennas [126] by using intermediate nodes, known as *relays*, between a source (S) and destination (D) pair, hereafter referred as an SD pair, that are idle and may thus be used for transmitting information for the SD pair. The concept has garnered a lot of interest after it was first introduced in [127] (see [35] for a code-division multiple-access (CDMA) based implementation), where it was shown that cooperation of users in general enhances the system throughput.

Interestingly, an important aspect that has been mostly ignored in deriving the potential benefits of cooperation amongst terminals is the effect of interfering signals from non-cooperating nodes. It can be argued that interference will in general diminish the performance gains that have been envisaged through cooperation. Moreover, since such interference signals will not be present at all times owing to intermittent transmissions of the respective sources, system designers will have to deal with an interfering environment where the interference strength will vary with time. Sources of interference may include co-channel and adjacent channel (due to spectral leaks) transmitters as well as ambient electromagnetic phenomena. In essence, the cooperation protocols and achievable rate results that were established heretofore will need to be re-examined when such interference is strong enough to impede reliable communication. Applying the central

limit theorem on interference signals with similar strengths we can categorize the interference as a Gaussian mixture model as has been previously done in Chapters 2 and 3. In this chapter, we focus on the applicability of the existing cooperative protocols to an interference limited environment and propose and analyse possible improvements to them in the face of strong interference. In order to make our treatise practically relevant we will investigate the effect of bursty interference that persists over a group of consecutive data symbols. As we will see later, memory in the interference will have important implications for cases where we are restricted to the use of only one relay amongst a set of available relays.

Chapter Outline: The rest of the chapter is organized as follows. We provide a brief description of the cooperative concept and discuss relevant literature in Section 5.1. Following which, Section 5.2 describes the associated protocols and system architecture along with a discussion of the interference model adopted in this chapter. Section 5.3 considers conventional cooperation using relays and the effect of interference on system performance which is followed by a discussion on relay selection aspects in interference environments in Section 5.4. We propose a novel relay selection algorithm that is well suited to relay selection in interference-limited environments in Section 5.5 and an improved version of it in Section 5.6 which also provides their respective analytical evaluation and a rigorous discussion on their applicability aspects. Finally, in Section 5.7 we look at attendant increase in overheads when using the novel algorithms proposed, ending the chapter with some relevant conclusions in Section 5.8.

5.1 Cooperative Diversity

The idea of cooperative communication is to use other nodes in the vicinity of the SD pair to transmit information from the source to the destination. In principle, cooperation is made possible due to the broadcast nature of wireless transmission[1].

[1]We assume that the source, relays and destination have at least one frequency band in common that is used for transmission. If the relay is unable to transmit/receive in the frequency bands of

The diversity benefits arise due to the possibly different channels that exist between the relays and the destination node. The cooperative concept may be applied to the uplink transmission of cellular communication, see for example [35], whereby a user at the cell edge may be assisted by nodes/users that are closer to the base station. Another scenario where cooperation may potentially benefit is sensor networks where the advantages can be in terms of increased lifetime of the sensor nodes by using reduced transmit power as well as improvement in overall connectivity of the sensor network.

From an operational standpoint, we will assume that inexpensive relays that lack full-duplex ability are used. This implies that the relays can only transmit or receive information in a given phase. Furthermore, information transmitted from S to D is considered to be not available non-causally to the relays. Therefore, when employing orthogonal resources, transmission will occur in two phases for transfer of data from S to D via relays. In the first phase, the source broadcasts its message to both relay(s) and destination and in the second phase the participating relays transmit the information obtained from the source in the first phase towards the destination after requisite processing. The key features attributed to a cooperative communication system are illustrated in Figure 5.1, where $R_\ell,\ \ell \in \{1, \ldots, L\}$, denotes the cooperating relays and $\gamma_{\mathrm{SR}_\ell}$, $\gamma_{\mathrm{R}_\ell\mathrm{D}}$ and γ_{SD} denote the instantaneous SNRs of the respective links. More details on the operational aspects are introduced later in the chapter.

Several protocols have been widely investigated for achieving performance gains through cooperative diversity [36] that differ in attributes such as scheduling of transmission, amount of processing at the relays and, information required at the various nodes amongst others. Depending on the processing at the relay the most popular protocols have been broadly categorized into two categories, first of which is the amplify-and-forward (AF) technique, where the relay simply multiplies the received signal with a scalar factor to maintain an aggregate power constraint. In the second approach, the

operation of the SD pair, cooperation will not be possible.

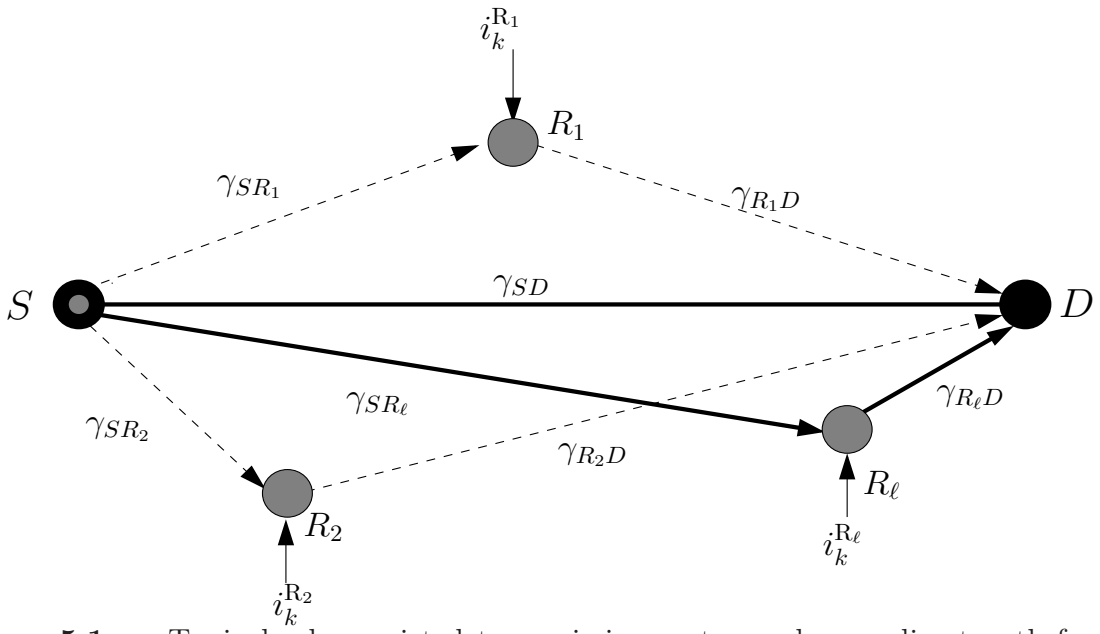

Figure 5.1 — Typical relay assisted transmission system, where a direct path from the source (S) to destination (D) node may or may not exist, and L relay nodes in the vicinity of the SD pair may potentially cooperate to provide a signal with a high receive SNR at the destination.

relays actually decode the symbols received from S and based on the results of decoding, may or may not transmit the information to D, and is aptly called the decode-and-forward (DF) approach. AF and DF each have their own advantages and depending on the resources available may or may not be well suited to a given communication environment. The primary appeal of the AF protocol lies in its simplicity of design and the rather minimal resources required at the relays for cooperation. However, since no decoding occurs at the relay, the destination needs to be provided with an estimate of both the SR channel and the RD channel. This can in general prove to be expensive as there is no way for the destination to directly determine the fading gains for the SR link from the received symbols. The relay either needs to convey this information in preamble packets or a two-level channel estimation may be required where the destination first estimates the RD link from pilot symbols between the relay and destination and uses this information to obtain estimates for the SR link. On the other hand, DF networks need the destination to know the channel for a single hop

only which is standard in several communication systems. The tradeoff, however, is the effort expended at individual relays to decode the symbols. A fair comparison will need to account for external parameters such as time variance of the channel, the quality of the $S-R-D$ link etc. In this work we will primarily consider AF relay channels and the role that interference plays in determining the gains possible through use of relays.

For a multi-relay environment, the initial focus of research in the area was on using all the relays that are able to cooperate. However, it is evident that employing multiple relays for a single transmission may incur a loss in bandwidth when one is restricted to using orthogonal transmissions. Assuming L relays, $L+1$ resource units are required which may be either time slots or frequency bands. Alternatively, one may choose to use only one of the several cooperating relays, which is referred as *opportunistic* communication (OC). Opportunistic relaying is of special interest as it has been shown to be capable of providing a diversity order equivalent to that of distributed space time codes [128, 129]. In opportunistic relaying, at a given time the best relay according to a certain criterion, usually the end-to-end channel SNR, is chosen and is used over the entire channel coherence time. Thus requiring only one extra time slot for a time division scheme for example. As a result, a lot of recent research effort has been towards devising efficient schemes for relay selection [129–132]. However, as we will see in Section 5.3, the conventional relay selection criterion requires considerable modification in the face of interference in the transmission environment. In fact this was recently recognized in [133], where selection strategies for AF relay networks have been proposed by factoring in the effect of interference from neighbouring clusters. As has been correctly pointed out in [133], expecting perfect power control amongst heterogeneous networks is too ideal a situation and would be rarely the case in practice. Nonetheless, the model and assumptions of [133] have certain shortcomings that we believe do not quite reflect the nuances of collaborative communication and we point them out in Section 5.2. Furthermore, related work in the area includes [134] where space-time

coded cooperative transmission affected by Class A impulsive noise was considered and union bounds on BER were obtained when using a conventional receiver. Also, Zhong et al. [135] consider the performance of a dual-hop relay channel when the destination is affected by Rayleigh faded interfering signals and derive expressions for outage probability and related performance parameters.

As can be inferred from the very few references mentioned above, relatively little effort has been put so far into investigating the effect of interference on the performance of relay-based systems. In this chapter, we aim at remedying that by explicitly considering the effect of interference on both the operation and performance of relay based AF cooperative communications.

5.2 System Model

In this section, we introduce the system model, describe the processing done at the relays and destination and introduce relevant system parameters. We consider a network where multiple users are present and a designated node, the source, wishes to transmit information to a destination node. A slotted transmission system is assumed where the transmission of a single symbol spans over two time slots. During the first time slot the source node broadcasts its message to the destination node (if a direct path exists) as well as the relay nodes[2] $R_\ell, \ell = 1, 2 \ldots, L$. The source transmits binary phase shift keyed (BPSK) symbols $x_k \in \{+1/-1\}$ that are then received at the relay and destination nodes after being affected by respective channel gains h_{ij}, where $i \in \{S, \mathcal{R}\}$, $j \in \{\mathcal{R}, D\}$ and $\mathcal{R}$ denotes the set of all participating relays. The received signal at the relay is degraded by the additive white Gaussian noise at each receiver. Assuming that receivers are of comparable quality, it is fair to assume the variance of the AWGN, σ_n^2, will be identical at all receivers. We refer to the case where the relays are affected only

[2]We assume that the source has already notified the destination of its intent to transmit through a *handshake* procedure. Details of such initial handshake may vary and possible options can be found in [129, Section II].

by AWGN as the good state ($\mathcal{G}$) and denote the variance in the good state as $\sigma_{\mathcal{G}}^2 = \sigma_n^2$.

In addition, each relay node may be affected intermittently by an interference term i_k (refer Figure 5.1), that is caused either by non-cooperating transmitters in the vicinity or other ambient phenomena. The variance σ_i^2 of i_k may be upto several orders of magnitude higher than σ_n^2 and the intermittent nature of i_k causes the overall noise at the relay nodes R_ℓ to be impulsive. The variance of noise in an interfered or bad ($\mathcal{B}$) state will be $\sigma_{\mathcal{B}}^2 = \sigma_i^2 + \sigma_n^2$. The distribution of the overall noise at the relays can therefore be modeled as

$$f(n) = \frac{P_{\mathcal{G}}}{\pi\sigma_{\mathcal{G}}^2} \exp\left(-\frac{|n|^2}{\sigma_{\mathcal{G}}^2}\right) + \frac{P_{\mathcal{B}}}{\pi\sigma_{\mathcal{B}}^2} \exp\left(-\frac{|n|^2}{\sigma_{\mathcal{B}}^2}\right) \tag{5.1}$$

where, as in previous chapters, $P_{\mathcal{G}}$ and $P_{\mathcal{B}}$ denote the probability of being in an uninterfered and interfered state respectively. By assumption, therefore, a harmful interfering signal is not always present. We believe that this in general, would be a more likely scenario than the one considered in [133,135], where in order to account for interference it is assumed that the interfering signals manifest during the entire duration of transmission. The latter assumption simplifies the analysis to a great extent and gives us an idea of the effect of interference. However, taking into account the non-permanent nature of interference is important as (a) estimates of system performance with permanent interference signals are rather conservative and prevents us from exploiting the full potential of the system, (b) emergent communication technologies such as cognitive radio (refer Chapter 3) thrive on the fact that transmission from various communication devices is intermittent and hence accounting for it will be beneficial in the long run from a system design perspective.

Memory in interference: It is conceivable that if an interference signal affects a relay at a certain time epoch then it is rather likely that it will continue to do so over more than one symbol period. The reasons for this could range from lack of synchronicity

amongst heterogeneous systems to the bursty nature of the interference signal itself. As in Chapter 2, we again use a 2-state Markov chain to model the interference at each participating relay. Thus the system is modeled by L Markov chains, one for each participating relay. In a given time slot the probability of a relay being interfered is dependent on the *state* of the relay in the previous time slot due to the Markovian assumption. The stationary probabilities of being in good or bad states are

$$P_{\mathcal{G}} = \frac{P_{\mathcal{BG}}}{P_{\mathcal{GB}} + P_{\mathcal{BG}}} \text{ and } P_{\mathcal{B}} = \frac{P_{\mathcal{GB}}}{P_{\mathcal{GB}} + P_{\mathcal{BG}}} \tag{5.2}$$

where $P_{\mathcal{XY}}$, $(\mathcal{XY}) \in \{\mathcal{G}, \mathcal{B}\}^2$ have the same definition as in Chapter 2.

5.2.1 Received Signal

We assume that the desired signal, the AWGN and the interference signal at the relay are mutually independent, which is a plausible assumption given that the respective signals are generated by independent sources. The received signal at the destination and the relays can be expressed as (k is the discrete time index)

$$y_k^{\mathrm{SD}} = h_{\mathrm{SD}}^k x_k + n_k^{\mathrm{SD}}, \qquad (S \to D) \tag{5.3a}$$

$$y_k^{\mathrm{SR}_\ell} = h_{\mathrm{SR}_\ell}^k x_k + n_k^{\mathrm{SR}_\ell} + i_k^{\mathrm{SR}_\ell}, \qquad (S \to R_\ell) \tag{5.3b}$$

$$y_k^{\mathrm{R}_\ell\mathrm{D}} = h_{\mathrm{R}_\ell\mathrm{D}}^k g(y_k^{\mathrm{SR}_\ell}) + n_k^{\mathrm{R}_\ell\mathrm{D}}, \qquad (R_\ell \to D) \tag{5.3c}$$

where h_{AB}, $[\mathrm{A} \in \{S, R_\ell\},\ \mathrm{B} \in \{R_\ell, D\}]$ denotes the fading coefficient for the link A→B, which is modelled as a zero mean complex Gaussian (ZMCG) random variable [136], i.e., the respective links experience Rayleigh fading. The individual channels between source, relay and destination are assumed to be independent of each other. We define the SNR of the various links shown in Figure 5.1 as follows,

$$\gamma_{\mathrm{SD}} = \frac{E_s |h_{\mathrm{SD}}|^2}{\sigma_n^2},\ \gamma_{\mathrm{SR}} = \frac{E_s |h_{\mathrm{SR}\ell}|^2}{\sigma_n^2},\ \text{ and } \gamma_{\mathrm{RD}} = \frac{E_s |h_{\mathrm{R}_\ell\mathrm{D}}|^2}{\sigma_n^2}, \tag{5.4}$$

where E_s is the transmitted symbol energy. Since the fading coefficients are Rayleigh distributed, γ_{SD}, γ_{SR} and γ_{RD} are exponentially distributed random variables [96] and thus $\bar{\gamma}_{\mathrm{SD}}$, $\bar{\gamma}_{\mathrm{SR}}$ and $\bar{\gamma}_{\mathrm{RD}}$ denote the average values of the corresponding variables. Furthermore, the channels are assumed to be quasi-static with a coherence time $T_{\mathbb{C}}$ that spans several symbols. The quasi-static assumption makes estimation of the channel feasible and we therefore consider coherent detection at the destination node (see [137] for methods to acquire such information). In (5.3), $g(z) = \mathcal{A}_\ell z$ when using AF transmission, whereby $\mathcal{A}_\ell$ is the amplification factor employed by the ℓ^{th} relay node. The i_k term in Eqn. (5.3b) indicates that there is interference only in the SR link.

Amplification factor

For AF systems, the relay nodes apply a certain amplification factor to the signal received over the SR link before forwarding it to the destination, while maintaining its own processing power constraints. The amplification is more of a normalization that is applied to the re-transmitted signal to ensure that the relay does not have to inject more power for the transmission of a given symbol[3]. Furthermore, the amplification factor $\mathcal{A}_\ell$ is dependent on the information gathered at the relay node about the transmission neighbourhood. For example, at the very least the relay needs to know the fading gains over the SR link and the AWGN power $\sigma_{\mathcal{G}}^2$, in order to scale the signal accordingly. While knowing $\sigma_{\mathcal{G}}^2$ and h_{SR} is in conformance with legacy communication systems, there will be an interference power component in the total power of the received signal at the relays that will be unknown. We assume that the relays make no efforts to determine or remove this additional component and consequently will end up transmitting an amplified version of the corrupted signal. A scaling factor proportional

[3]In power-constrained networks, $\mathcal{A}_\ell$ may be used for optimal power allocation such that the overall power consumption of the network is minimized. Often the knowledge of the channel gains at source may be required for the same. We assume that no information regarding the channels is available at the source or that it is in general unable to exploit such information.

to the instantaneous channel gain and the noise power in the $\mathcal{G}$ state,

$$\mathcal{A}_\ell = \sqrt{\frac{E_s}{E_s|h_{\mathrm{SR}}|^2 + \sigma_{\mathcal{G}}^2}}. \tag{5.5}$$

is applied to the relayed signal

5.2.2 Effective End-to-End SNR with Single Relay Cooperation

We now obtain an expression for the received SNR at the destination node for the signal received over the relay channel when the ℓ^{th} relay is selected. For AF relay channels, from (5.3) we have (ignoring the time index k for brevity)

$$y^{\mathrm{R}_\ell\mathrm{D}} = \mathcal{A}_\ell h_{\mathrm{R}_\ell\mathrm{D}} h_{\mathrm{SR}_\ell} x + \underbrace{\mathcal{A}_\ell h_{\mathrm{R}_\ell\mathrm{D}} n^{\mathrm{SR}_\ell} + n^{\mathrm{R}_\ell\mathrm{D}}}_{\tilde{n}_{\mathrm{RD}}}. \tag{5.6}$$

where $\tilde{n}_{\mathrm{RD}}$ is the effective noise for the signal received through a relay. Using $\kappa = \sigma_{\mathcal{B}}^2/\sigma_{\mathcal{G}}^2$ to denote the relative strength of the interference with respect to the background noise the end-to-end SNR of a relay link is given as

$$\gamma_{\mathrm{SR}_\ell\mathrm{D}} = \begin{cases} \dfrac{\mathcal{A}_\ell^2 E_s |h_{\mathrm{R}_\ell\mathrm{D}}|^2 |h_{\mathrm{SR}_\ell}|^2}{(\mathcal{A}_\ell^2 |h_{\mathrm{R}_\ell\mathrm{D}}|^2 + 1)\sigma_{\mathcal{G}}^2} & \text{in good state} \\ \dfrac{\mathcal{A}_\ell^2 E_s |h_{\mathrm{R}_\ell\mathrm{D}}|^2 |h_{\mathrm{SR}_\ell}|^2}{(\mathcal{A}_\ell^2 \kappa |h_{\mathrm{R}_\ell\mathrm{D}}|^2 + 1)\sigma_{\mathcal{G}}^2} & \text{in bad state} \end{cases} \tag{5.7}$$

On substituting the value of $\mathcal{A}_\ell$ and through simple mathematical manipulations the SNR is expressed in the following convenient form for no interference,

$$\gamma_{\mathrm{SR}_\ell\mathrm{D}}^{\mathcal{G}} = \frac{\gamma_{\mathrm{SR}_\ell}\gamma_{\mathrm{RD}_\ell}}{\gamma_{\mathrm{SR}_\ell} + \gamma_{\mathrm{RD}_\ell} + 1}, \tag{5.8}$$

and when the relay is interfered we have the SNR for the bad state as

$$\gamma^{\mathcal{G}}_{\mathrm{SR}_\ell \mathrm{D}} = \frac{\gamma_{\mathrm{SR}_\ell}\gamma_{\mathrm{RD}_\ell}}{\gamma_{\mathrm{SR}_\ell} + \kappa\gamma_{\mathrm{RD}_\ell} + 1}. \tag{5.9}$$

We will perform maximal ratio combining (MRC) of the signal received from the selected relay and that from the direct path based on a conventional combining approach, i.e., using the effective SNRs for the good state (Eqn. 5.8). The overall SNR at the destination node will then be a summation of the SNR of the selected relay and that of the direct path. Therefore, we have the combined signal, using the respective channel gains, as [2]

$$\begin{aligned} z_{\mathrm{MRC}} &= h^*_{\mathrm{SD}} y^{\mathrm{SD}} + \left(\frac{\mathcal{A} h^*_{\mathrm{R}_\ell \mathrm{D}} h^*_{\mathrm{SR}_\ell}}{\sqrt{(\mathcal{A}^2 |h_{\mathrm{R}_\ell \mathrm{D}}|^2 + 1)}} \right) y^{\mathrm{R}_\ell \mathrm{D}} \\ &= |h_{\mathrm{SD}}|^2 x + h^*_{\mathrm{SD}} n^{\mathrm{SD}} + |\Omega|^2 x + \Omega\, \tilde{n}^{\mathrm{R}_\ell \mathrm{D}} \end{aligned} \tag{5.10}$$

where $\Omega = \left(\frac{\mathcal{A} h^*_{\mathrm{SR}_\ell} h^*_{\mathrm{R}_\ell \mathrm{D}}}{\sqrt{\mathcal{A}^2 |h_{\mathrm{R}_\ell \mathrm{D}}|^2 + 1}} \right)$. The overall received SNR is thus

$$\gamma_{\mathrm{tot},\mathcal{G}} = \frac{(|h_{\mathrm{SD}}|^2 + |\Omega|^2)^2 E_s}{(|h_{\mathrm{SD}}|^2 + |\Omega|^2)\sigma^2_{\mathcal{G}}} = \gamma_{\mathrm{SD}} + \gamma^{\mathcal{G}}_{\mathrm{SR}_\ell \mathrm{D}} \tag{5.11}$$

For now we would like the reader to bear the above effective SNR in mind and wait till Section 5.5 for the expressions for the overall SNR for the novel algorithms that we propose, as it will depend on the criterion used for relay selection. Towards this end we present in the next section, a relay selection criterion based on the maximization of SNRs obtained above. Also note that the the MRC combining as done above assumes that the relays are in good state. Throughout our work the receiver at the destination will work with this assumption. MRC based on $\gamma^{\mathcal{G}}_{\mathrm{SRD}}$ does not ensure that correct weights are used when the relay is in bad state and hence is suboptimal when the selected relay is interfered.

5.3 Cooperation through Selection: Conventional Approach

When L relays cooperate, there are L paths from the source to destination other than a direct path, which is usually weaker than the relay links. Thus potentially the destination receives $L+1$ copies of the transmitted signal. In conventional cooperative systems employing coherent decoding, copies of the transmitted signal received over all these paths are combined at the receiver through MRC. However, the loss in bandwidth in combining signals from all L relays has led to the consideration of using only one relay which is deemed most suited according to a pre-selected criterion [131]. To increase transmission efficiency, the use of a distributed space-time coding has also been investigated by many [138–140]. However, distributed space time coding spanning L relays has been concluded to be challenging from an implementation perspective due to a variety of reasons including mobility of relays, synchronization amongst multiple nodes and the need for accurate CSI for all links involved [131]. On the other hand, relay selection or *opportunistic relaying*, where only one out of the L relays needs to transmit at a given time [129], provides operational advantages without having to compromise a great deal on performance. Relay selection can be rather straightforward when the destination has knowledge of the end-to-end channel and the only noise in the channel is AWGN at the receivers [129].

Furthermore, relay selection is usually categorized into *proactive* and *reactive* relay selection based on whether the selection is done before or after the source transmits. Both selection schemes are depicted in Figure 5.2. In proactive relaying relays are selected before the source transmits and are then used for several symbols depending on the channel coherence time. Reactive relaying takes into account the ability of the relay to correctly decode the transmitted symbol and hence is usually employed in DF schemes. While conventional AF relaying is proactive we will later consider a scheme

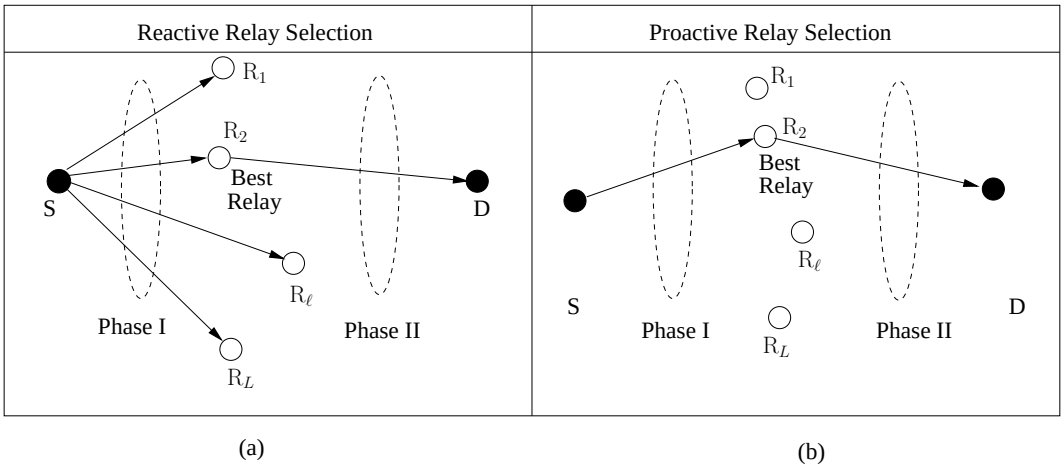

Figure 5.2 — Relay selection techniques based on time of selection: (a) Reactive selection selects relay based on the received signal at relays after source broadcasts, (b) Proactive selection selects relay prior to transmission by source based on SNRs.

that is a combination of both proactive and reactive relaying, where the need for reactive relaying arises due to the nature of interference in the channel. Naturally, reactive relaying requires greater overheads than proactive relaying but is more responsive to the real-time variations in the transmission environment.

5.3.1 Relay Selection Criterion

The conventional relay selection criterion is to maximize the end-to-end SNR of the $S-R-D$ link. From Eqn. (5.8) we have, again considering SNRs for non-interferred relays

$$\gamma^{\mathcal{G}}_{\mathrm{SR}_\ell\mathrm{D}} = \left\{ \frac{\gamma_{\mathrm{SR}_\ell}\gamma_{\mathrm{R}_\ell\mathrm{D}}}{\gamma_{\mathrm{SR}_\ell} + \gamma_{\mathrm{R}_\ell\mathrm{D}} + 1} \right\} \approx \underbrace{\left\{ \frac{\gamma_{\mathrm{SR}_\ell}\gamma_{\mathrm{R}_\ell\mathrm{D}}}{\gamma_{\mathrm{SR}_\ell} + \gamma_{\mathrm{R}_\ell\mathrm{D}}} \right\}}_{\gamma^{\mathrm{HM}}_\ell}. \tag{5.12}$$

The approximation of $\gamma^{\mathcal{G}}_{\mathrm{SR}_\ell\mathrm{D}}$ in Eqn. (5.12) as the harmonic mean (HM) of $\gamma_{\mathrm{SR}_\ell}$ and $\gamma_{\mathrm{RD}_\ell}$ allows us to use the following upper bound on $\gamma^{\mathrm{HM}}_\ell$ [129, 141, 142]

$$\gamma^{\mathrm{HM}}_\ell \leq \gamma^{\mathrm{up}}_\ell = \min(\gamma_{\mathrm{SR}_\ell}, \gamma_{\mathrm{R}_\ell\mathrm{D}}). \tag{5.13}$$

Thus a selection criterion based on maximizing the end-to-end SNR, $\gamma^{\mathcal{G}}_{\mathrm{SR}_\ell\mathrm{D}}$, translates into the following [131, 133]

$$R_{\text{best}}^{\mathcal{G}} = \underset{R_\ell \in \mathcal{R}}{\text{argmax}} \left[\min(\gamma_{\text{SR}_\ell}, \gamma_{\text{R}_\ell\text{D}}) \right]. \tag{5.14}$$

The criterion presented in (5.14) is the conventional relay selection rule formulated in a $\max - \min$ form [129, 131, 133] and has been shown to be a close approximation to maximizing the end-to-end SNR of the $S-R-D$ link. The use of the upper bound is motivated by the fact that the exact expression for $\gamma_{\text{SR}_\ell\text{D}}^{\mathcal{G}}$ is hard to analyze. In (5.14), γ_ℓ^{up} denotes the SNR for the weaker of the two links [SR, RD] for a given relay R_ℓ. Conventional selection ensures that when instantaneous SNR is used as criterion for selection, the relay with the strongest overall link is chosen. However, this selection criterion lacks robustness since the underlying assumption is that instantaneous SNRs are governed only by fading and the AWGN at the relays and thus will need modifications when employed in an interference environment.

The criterion in (5.14) will have certain implications when the end-to-end SNR is given by $\gamma_{\text{SR}_\ell\text{D}}^{\mathcal{B}}$ rather than $\gamma_{\text{SR}_\ell\text{D}}^{\mathcal{G}}$[4]. When the relay is in bad state applying the above criterion gives us

$$\begin{aligned} R_{\text{best}}^{\mathcal{B}} = \text{argmax} \left\{ \frac{\gamma_{\text{SR}_\ell}\gamma_{\text{R}_\ell\text{D}}}{\gamma_{\text{SR}_\ell} + \kappa\gamma_{\text{R}_\ell\text{D}} + 1} \right\} &= \text{argmax} \left\{ \frac{\gamma_{\text{R}_\ell\text{D}} \left(\frac{\gamma_{\text{SR}_\ell}}{\kappa}\right)}{\gamma_{\text{R}_\ell\text{D}} + \frac{\gamma_{\text{SR}_\ell}}{(\kappa)} + \frac{1}{(\kappa)}} \right\} \\ &\approx \text{argmax} \left\{ \min \left[\left(\frac{\gamma_{\text{SR}_\ell}}{\kappa} \right), \ \gamma_{\text{R}_\ell\text{D}} \right] \right\}. \end{aligned} \tag{5.15}$$

In [133], a criterion similar to (5.15) was used and it was argued that only the SR link bears relevance for the selection criterion. However, for our system the above criterion has two shortcomings. First, different from [133], the bad state occurs only with a probability $P_{\mathcal{B}}$ and hence (5.15)may not be applied at all times. Second, this would make the strength of the RD link irrelevant to the selection process and hence is inherently suboptimal. When proposing our novel algorithms we will keep this fact in mind and will try to minimize the probability of having to use (5.15) for selection.

[4]We will consider selection based on $\gamma_{\text{SR}_\ell\text{D}}^{\mathcal{G}}$ only throughout our work. The case with $\gamma_{\text{SR}_\ell\text{D}}^{\mathcal{B}}$ is considered only for the sake of discussion and greater insight into the selection problem.

We would also like to remark that continuing to use (5.14) in the interference state will in general lead to severe degradation in performance. We emphasize this point in the next subsection by considering conventional relay selection scheme in an impulsive interference environment along with a novel approach that can help mitigate such detrimental effects.

5.4 Relay Selection in Presence of Interference

In this section, we motivate the need for changes to the conventional relay selection by evaluating its performance in terms of error rate in an interference environment. We will see that selection based on (5.14) incurs heavy penalties when no efforts are made to mitigate the effect of interference at the relays. Thus definite changes are required to the $\max - \min$ criterion when the interfering signals at relay are strong enough to degrade performance at destination [133]. Since the relays do not have a priori knowledge of the interference, the system will need to adapt to the interference environment on a real-time basis. In [133], relay selection was shown to depend critically on the interference signal power to noise ratio (which we denoted as $\kappa = \sigma_{\mathcal{B}}^2/\sigma_{\mathcal{G}}^2$ earlier). However, the analysis in [133] assumes the availability of interferer information in terms of their individual powers and also the channel from the interfering source to the desired receiver. It should be noted that legacy communication systems will not already have the resources to acquire such information and hence the suggested schemes [133] pose a major disadvantage in that a complete overhaul of the receiver's estimation abilities will be required. Even if one were to put such capabilities in place, it will be highly taxing on system resources to obtain such information. Moreover, the working assumption in [133] is that all relays are similarly affected by interference on a per epoch basis which limits the usefulness of the analysis to certain specific topologies, where the relays are geographically close enough for the assumption to be true. While [135] considers the effect of interference on relay performance, the performance analysis is

based on interference at the destination only. Interference at D bears little relevance to the selection process, as performance of all relays will be affected similarly in this case. These shortcomings of the current state of the art for relay selection in interference environments motivates our current work.

5.4.1 Genie-Aided Selection

If there were a way for the destination to know which of the relays were affected by interference, then a rational selection strategy would be to avoid those relays while making a selection[5]. Having eliminated the interfered relays from consideration, we find the relay with the best end-to-end path amongst the rest of the relays. Effectively, we reduce the original set of available relays $\mathcal{R}$ to $\mathcal{R}^+$ on a symbol-by-symbol basis such that $|\mathcal{R}^+| \leq |\mathcal{R}|$. The membership of the set of unusable relays, $\mathcal{R}^- = \mathcal{R} - \mathcal{R}^+$ is governed by $P_{\mathcal{B}}$ and $\mathcal{R}^+$ and $\mathcal{R}^-$ are disjoint sets. From an implementation perspective, we expect each relay to locally perform a binary hypothesis test at each time slot to determine whether the hypothesis $\mathcal{H}_0$ (interference absent) or $\mathcal{H}_1$ (interference present) is true. For a genie-aided system the hypothesis $\mathcal{H}_\upsilon$, $\upsilon \in \{0, 1\}$ is known with zero uncertainty. In Section 5.5 we present an algorithm that elaborates the steps employing such an approach and its applicability as a solution to relay selection in presence of interference. Note that we do not make an attempt to find out the power of the interfering signal as we wish to keep the algorithm crisp and taking interference powers into account will be rather cumbersome. While the genie based approach is important conceptually, we consider in the next section a sub-optimal approach to obtaining $\mathcal{R}^+$ that is more pragmatic and requires only incremental changes at the relays.

[5]At this point, the specifics of the techniques that will allow the destination to gather such information are not important.

5.4.2 Threshold Based Relay Selection (TRS)

In this section, we propose a relay selection criterion that uses a threshold to assert a relay's membership in $\mathcal{R}^+$. In [143] SNR threshold based relay selection was proposed where a certain SNR threshold was used to select a set $\mathcal{X} \in \mathcal{R}$ of relays such that if for a relay R_ℓ, $\gamma_{\mathrm{SR}\ell} > \Lambda$ then $\mathrm{R}_\ell \in \mathcal{X}$, where Λ is the SNR threshold. The use of a threshold in [143] was to determine relays that are *reliable* in the sense that a higher SNR translates into higher probability of correct decoding. We will use a threshold for the exact opposite purpose. Here we will use a threshold as an upper bound on the instantaneous power of signal received at the relay and if it is beyond nominal levels it will be deemed unreliable as the exceptionally high received power will be attributed to the unwanted signals at the relay.

Threshold selection: It is imperative that in order to decide whether to exclude a relay from participating in the selection process we choose a threshold that does not inadvertently exclude a relay that has a good end-to-end channel. The policy that we adopt is based on received signal power at the relay. We employ a threshold Λ for the received signal power at the relay such that if $|y_{\mathrm{SR}}|^2 > \Lambda$, the signal is considered to be corrupted by interfering signals and hence should no longer be a part of $\mathcal{R}^+$. The following threshold is employed

$$\Lambda = 2(|h_{\mathrm{SR}}|^2 + \sigma_{\mathcal{G}}^2) \; . \tag{5.16}$$

The rationale behind using such a threshold being that $\sigma_{\mathcal{G}}^2$ represents the average noise power and $|h_{\mathrm{SR}}|$ the instantaneous channel gain and thus for a signal with Gaussian distribution and mean h_{SR}, Λ as given in (5.16) is a reasonable measure for identifying interfered symbols. The advantage of threshold based relay selection is in the ease of implementation as there is no need to decode the message (sent by the source) at the relays to determine if the information has been received with sufficient accuracy,

before the relay transmits it to the intended destination. It is especially suited for environments where decoding delays may exceed the maximum delay constraints of transmission or drain more power than is permitted by the relay. For example, sensor nodes might want to save power for greater longevity and hence not use the limited power to decode information not intended for itself.

We next present an algorithm that outlines the steps needed to be carried out at a system level in order to obtain $\mathcal{R}^+$ and also consider in detail, the operational aspects of the algorithm.

5.5 Next Best Relay (NBR) Selection

We introduce here a selection strategy that can dynamically compute $\mathcal{R}^+$ and use it as a basis for relay selection for a given transmitted symbol. Since the channel is quasi-static, when choosing the best relay rather than only finding out the best relay, a ranking table of all the relays can be prepared (most likely at the destination node) and the respective rank information is transmitted back to relays at the start of the transmission period. This ranking is assumed to hold good for several symbols that would typically be of the order of the coherence time $T_{\mathbb{C}}$ of the channel [129]. In the following we refer to the duration for which the ranking is valid as a *frame* and consider it to span $T_{\mathbb{C}}$ symbols. Each relay is expected to do a hypothesis test to determine the presence of interference on a symbol-by-symbol basis. The result of such a test may be stored in an indicator variable $\mathcal{I}(t)$ such that when interference is detected, $\mathcal{I}(t) = 1$ and $\mathcal{I}(t) = 0$ otherwise. When a relay is being used and it detects $\mathcal{I}(t) = 1$ for $0 < t \leq T_{\mathbb{C}}$, it transmits a beacon signal letting all the other participating relays and the destination node know that its ability to relay has been compromised and the next best relay or in other words the best relay amongst the rest of the participating relays should take over. This mechanism can be thought to be a variant of switch-and-stay combining (SSC) for diversity systems in fading channels [2]. In SSC systems when

the instantaneous SNR of the best path falls below a certain pre-defined threshold, the receiver switches to the alternate path for a dual-branch system or the next best path according to a pre-determined relative ranking of the paths for a multiple channel system. Thus when a relay that has been chosen to transmit experiences interference, it implicitly passes control to the relay with the next lower rank by broadcasting a beacon signal to let other relays know that it has been interfered. The algorithm is presented in detail below.

5.5.1 NBR-ONE Algorithm

Since we check for interference on a symbol-by-symbol basis we call this the NBR-ONE algorithm. The selection algorithm proceeds in the following manner. As mentioned above, before transmission occurs a ranking of the available relays is prepared based on the instantaneous channel SNRs ($\gamma_{\mathrm{SR}}, \gamma_{\mathrm{RD}}$) and each relay is then transmitted its own rank. The system operates based on a countdown timer with a start value of $T_{\mathbb{C}}$ and a new ranking is established based when the timer expires. The cooperative system continues to use the best relay until the best relay is determined to be hit by interfering signals. When a relay in use faces interference it sends out a beacon signal to notify other participating relays and the destination terminal of its inability to transmit. Following which control is switched from the current relay to next best relay based on the ranking. We thus establish a token based transmission system where the relay that owns the *transmit token* is used for relaying information. By default the best relay gets the token after a ranking is established and continues to hold it until either the timer for the ranking validity expires or until it is interfered. In the latter case it passes the token to the next uninterfered relay in the ranking table. A contingency may occur when all relays are interfered simultaneously. In this case we default to using the relay with rank $r = 1$ as the error rate suffers equally regardless of the relay used. This is more likely to happen when L is small as the probability that the above situation presents itself is $P_{\mathcal{B}}^{L}$. We present the above protocol in algorithmic form in

Algorithm 5.1.

When a transmitting relay sends a beacon signal to notify of its interfered state, the total duration of an epoch is extended to $2T + \delta$ where T is the duration of each time slot and δ is the duration of a beacon. Thus we add an overhead of δ every time a relay that is chosen to transmit has $\mathcal{I}(t) = 1$. While it is intuitive that such overhead will depend on $P_{\mathcal{B}}$, we show in Section 5.7 that the overall overhead for the NBR-ONE approach is independent of the number of relays L. Compared to conventional selection, there might be a disadvantage in using the NBR-ONE algorithm as proposed above in that all relays are required to have their respective antenna on at all times regardless of whether they are being used or not. Although, this in general is not very power consuming as the antenna spends a greater fraction of time in receive mode (in order to ascertain if it is interfered or not) rather than transmit mode. Moreover, selection using NBR still uses lesser resources in terms of orthogonal dimensions required (time or frequency) compared to using all relays at the same time and can thus provides all the benefits of opportunistic communication as proposed in [131]. As an aside, if the best relay is being used multiple times and needs to stem its power usage, appropriate energy thresholds may be formulated to conserve the energy levels of the best relay such that on reaching a certain lower energy threshold the best relay may not be used anymore and lower ranked relays are used.

We next provide some BER results that compare the performances of the conventional and NBR-ONE approaches wherein for the latter algorithm we use both genie-aided and TRS detection at the relays.

5.5.2 Simulation Results

We primarily aim at improving link reliability between S and D and hence evaluate BER performance of the conventional and NBR-ONE approaches in the following. We consider balanced Rayleigh faded links such that $\bar{\gamma}_{\mathrm{SR}} = \bar{\gamma}_{\mathrm{RD}} = \bar{\gamma}_{\mathrm{SD}}$. However in general,

Algorithm 5.1 Relay Selection in AF Relay Networks with NBR-ONE

Before transmission of the first symbol: At the destination (D): Create a ranking of relays using the instantaneous end-to-end SNR values. Then D sends a short packet to all R_ℓ with its rank information as follows

$$D \overset{\text{rank}(R_\ell)}{\longrightarrow} R_\ell \; \forall \; \ell \in \mathcal{R}^+$$

1: At time epoch t,
2: **for** Relay rank $r = 1 : L$ **do**
3: **if** Relay with rank r hit **then**
4: Set $I_r(t) = 1$.
5: **else**
6: $I_r(t) = 0$.
7: **end if**
8: **end for**
9: **if** $I_1(t) == 0$ **then**
10: Use R_1
11: **else if** $I_1(t) == 1$ **then**
12: R_r sends beacon signal on common channel with rank to let all relays know $R_1 \notin \mathcal{R}^+$
13: Set $r := 2$
14: **while** $r < L$ **do**
15: **if** $I_r(t) == 0$ **then**
16: relay R_r transmits.
17: break;
18: **else**
19: Relay R_r transmits beacon signal on common channel with its own rank.
20: $r := r + 1$
21: go to 15
22: **end if**
23: **end while**
24: **if** $r == L$ **then**
25: Use R_1
26: **end if**
27: **end if**

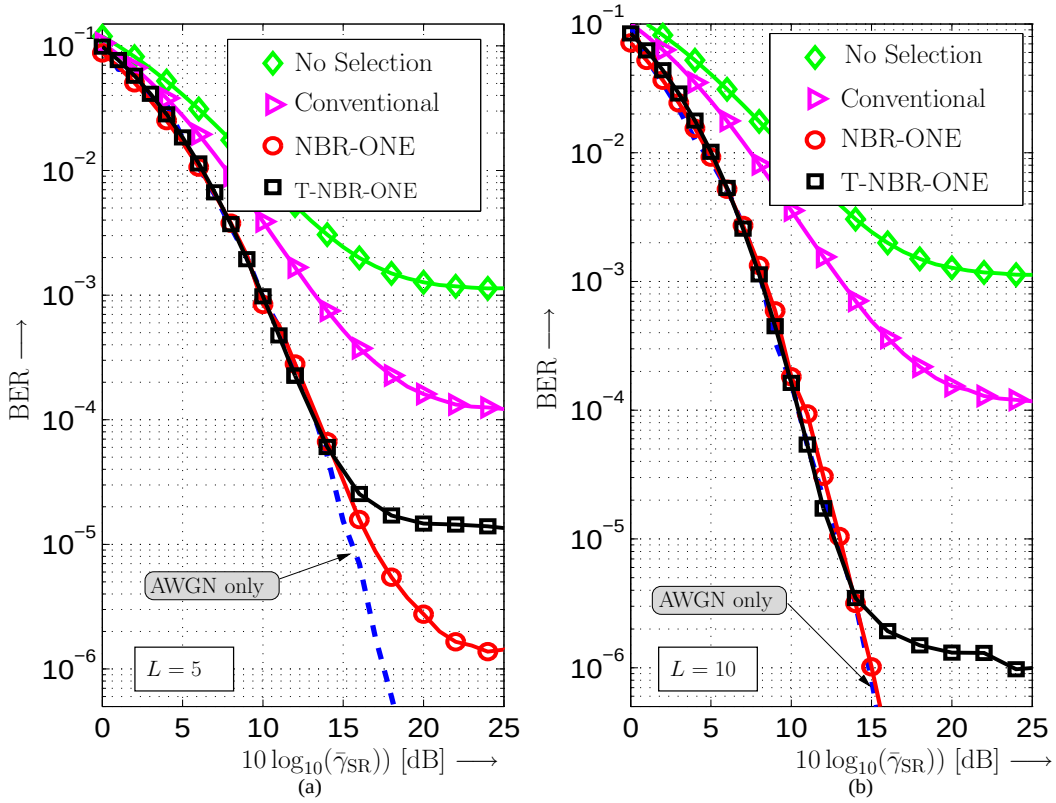

Figure 5.3 — BER for relay selection in presence of interference with $10\log_{10}\text{SIR} = 10$ dB for (a) $L = 5$ relay and (b) $L = 10$ relays. Conventional selection strategies exhibit poor performance when compared to BERs for non-interfered scenarios (AWGN only curve). A reduced selection set policy where memberships are decided based on genie-aided information or threshold greatly improves performance.

$\bar{\gamma}_{SD}$ should be expected to be lower than $\bar{\gamma}_{SR}$ and $\bar{\gamma}_{RD}$ due to pathloss factors. We will focus on this aspect in later results and consider only balanced links for this section. For all the results presented in this section we have $P_{\mathcal{B}} = 0.1$. Figure 5.3 (a) and 5.3 (b) show the performance results with fixed interference levels at the receiver with an SIR $(10\log(E_s\mathcal{E}\{|h_{SR}|^2\}/\sigma_{\mathcal{B}}^2)) = 10$ dB for $L = 5$ and $L = 10$ relays respectively. For comparison we also provide results for conventional relay selection in an AWGN only channel[6] as well, i.e., best relay selection without interference (dashed curve). When using a TRS approach in determining $\mathcal{I}_r(t)$, for the NBR-ONE algorithm, we obtain the threshold NBR-ONE (T-NBR-ONE) algorithm which is also evaluated in

[6]Throughout this chapter, an AWGN channel will imply a Rayleigh faded channel with AWGN.

the following with a threshold according to (5.16). It is evident that conventional selection is sub-optimal in presence of impulsive interference and deviates significantly from the non-interfered curves. Much of this can, however, be recovered by an NBR-ONE strategy and is arguably the best one can do in given operating conditions. While an error floor still exists for SNRs of interest with the NBR-ONE approach for $L=5$, it is lowered well below reasonably acceptable BERs for $L=10$. It is this performance that a T-NBR-ONE approach would ideally seek to achieve. However, we do see a degradation in performance for a threshold based receiver as it is uninformed with respect to instantaneous SNR. Nonetheless, in both Figures 5.3(a) and (b) we see lowering of the error floor by upto 2 orders of magnitude compared to conventional strategies. We further note that randomly selecting a relay or *non-selection* is not an option in an impulsive environment and hence one will require to put in some effort in choosing the possibly best relay in order to observe the expected performance gains.

In Figure 5.4, in line with our earlier impulsive interference models (Chapter 2), we present results for a fixed κ. While these results are presented more for illustrative purposes, we would like to mention that as in Chapter 3, a thresholding scheme will in general work better for such an interference model as the interference power is a constant multiple of the background noise and thus is more easily detectable with a threshold that changes with SNR (refer (5.16)). Also, a rather consistent performance will be seen over a range of SNRs. Nonetheless, this model may not be applicable to scenarios where the interference power is independent of background noise. For the results shown in Figure 5.4 we have $\kappa = 100$ and $L = 10$. Different from the fixed SIR case of Figures 5.3, we observe that NBR-ONE suffers a penalty compared to the AWGN channel case. This can be explained based on the fact that at high SNRs $\sigma_{\mathcal{B}}^2$ will not be very high compared to $E_S\mathcal{E}|h_{\mathrm{SR}}|^2$ and hence it is possible that although we exclude a relay due to interference on the corresponding SR link, it may otherwise be a fairly high quality link that overshadows the effect of interference. Accounting for

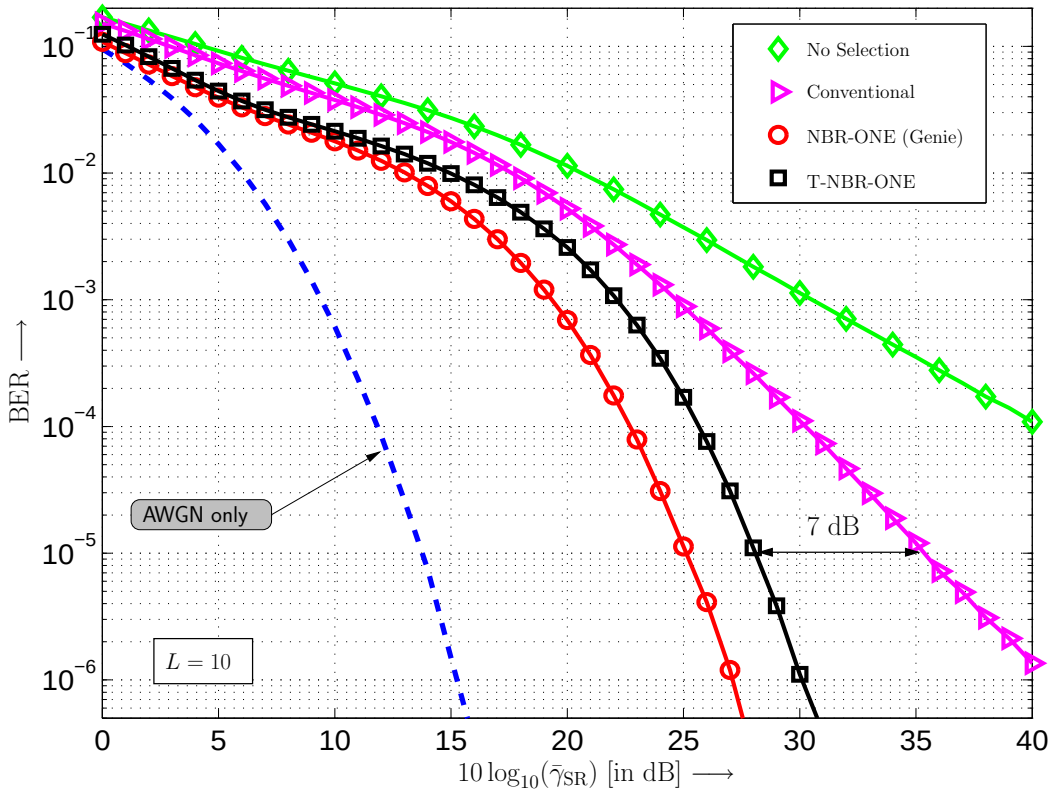

Figure 5.4 — BER vs. SNR for relay Selection in presence of interference with interfering signal power, $10\log(\text{SIR}) = 10[\log(\text{SNR}) - \log(\kappa)]$ dB with $L = 10$ relays. A simple thresholding scheme can reduce the required SNR ($10\log\bar{\gamma}$) by about 7 dB at BER $= 10^{-5}$. Simulation parameters $P_{\mathcal{B}} = 0.1$, $\kappa = 100$

this will require knowledge of individual signal and noise powers at each relay, which we do not pursue here to limit the processing at relays. It is encouraging to observe that the thresholding strategy still fares much better than conventional selection with upto 7 dB gains at a BER of 10^{-5}.

Finally, we consider the performance of the proposed scheme in heavy interference (SIR $= -20$ dB) and a degraded direct link such that $\bar{\gamma}_{SR}/\bar{\gamma}_{SD} = 10$. Figure 5.5 presents BER results with $L = [3, 5, 7]$ relays in applying the NBR-ONE approach for $\bar{\gamma}_{SR} = \bar{\gamma}_{RD}$, $P_{\mathcal{B}} = 0.1$. The system parameters are therefore chosen to represent an environment where S is very much dependent on relays for data transfer to D and the relays may also face sporadic heavy interference. Due to the strong interference (SIR $= -20$ dB), the

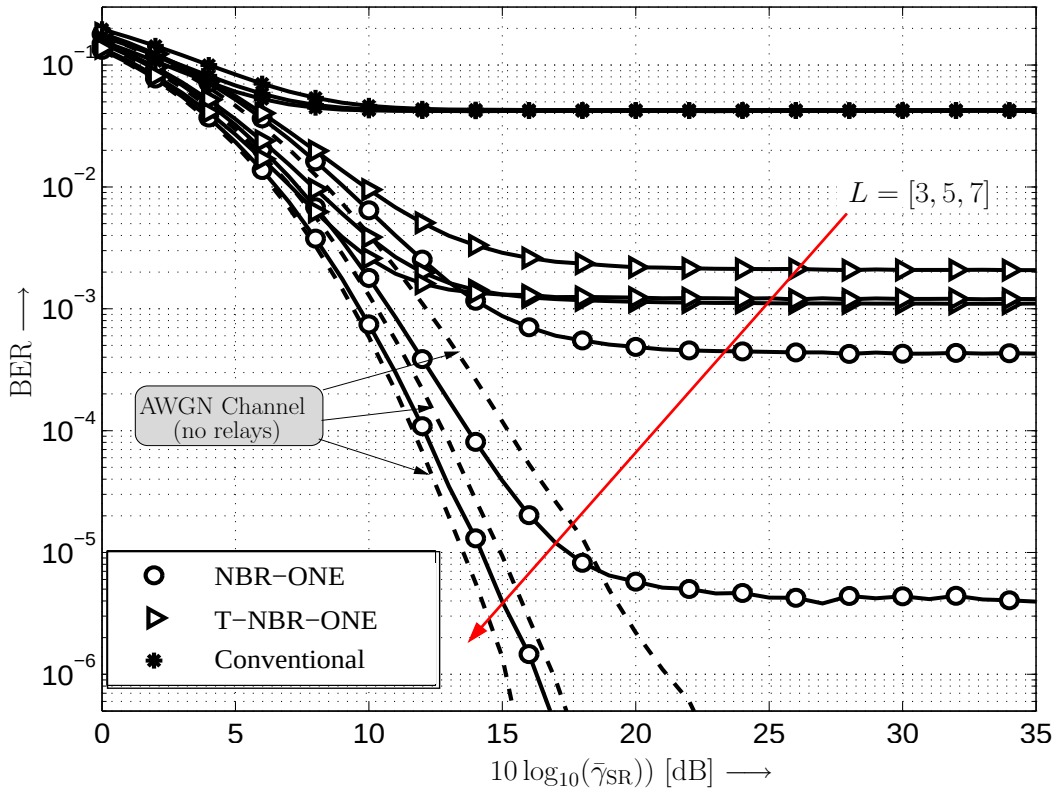

Figure 5.5 — BER vs SNR with $L = 5$ for next best relay selection strategy for i.i.d interference at relays for SIR $= -20$ dB and $P_{\mathcal{B}} = 0.1$ with $\bar{\gamma}_{SR}/\bar{\gamma}_{SD} = 10$ and $\bar{\gamma}_{SR} = \bar{\gamma}_{RD}$. Genie-aided NBR performance improvement is dependent on L and closely approaches that of AWGN channel (dashed curves) for $L = 7$ relays.

conventional selection method is seen to suffer heavily with an unacceptably high error floor regardless of the number of relays used. It is evident therefore that alternative solutions will be required in such a communication environment. NBR-ONE on the other hand can be seen to be sufficiently better than the conventional approach and is within less than 2 dB of the AWGN channel BER when $L = 7$ relays are used. Since NBR-ONE pursues an interference avoidance approach its success is dependent more on the value of $P_{\mathcal{B}}$ than $\sigma^2_{\mathcal{B}}$. Performance of T-NBR-ONE although much better than conventional selection, suffers for higher number of relays and we attribute this to the rather *simple* thresholding technique that has been employed.

We next devise methods for performance analysis of the NBR-ONE algorithm using a

moment generating function (MGF) approach to find the overall pdf of the received SNR at the relays.

5.5.3 Performance Analysis

Since the overall SNR has a non-homogeneous distribution we make certain assumptions and approximations along the way that allows us to derive a closed form solution for the relevant performance indicators such as BER and outage probability. We first consider the relays to be only in good state and accordingly when applying MRC to combine the signals from the SD and SR paths the overall SNR at the destination node can be written as (refer Eqn. (5.11))

$$\gamma_{\text{tot},\mathcal{G}}^{M^{\text{th}}} = \gamma_{\text{SD}} + \underbrace{M^{\text{th}} \max_{\ell \in \{1,2,\ldots,L\}} \gamma_{\ell}^{\text{up}}}_{T_M} \tag{5.17}$$

where $T_M = M^{\text{th}} \max_{\ell \in \{1,2,\ldots,L\}} \gamma_{\ell}^{\text{up}}$ denotes the end-to-end SNR of the M^{th} best out of L relays and $\gamma_{\ell}^{\text{up}}$ is the approximation of $\gamma_{\text{SR}_\ell\text{D}}^{\mathcal{G}}$ from Eqn. (5.14). In the following we drop the index ℓ and use γ^{up} to denote the upper bound on $\gamma_{\text{SR}_\ell\text{D}}^{\mathcal{G}}$. Since the respective links are Rayleigh faded, γ_{SR} and γ_{RD} are both exponentially distributed [2]. We use the following lemma to determine the density function for γ^{up}.

Lemma 5.5.1 *Let $\gamma_1, \ldots, \gamma_n$ be independent exponentially distributed random variables with rate parameters $\bar{\gamma}_1^{-1}, ..., \bar{\gamma}_n^{-1}$. Then $\min\{\gamma_1, \ldots, \gamma_n\}$ is also exponentially distributed, with parameter*

$$\bar{\gamma}^{-1} = \bar{\gamma}_1^{-1} \cdots + \bar{\gamma}_n^{-1} \tag{5.18}$$

This can be seen by considering the complementary cumulative distribution function

$$\begin{aligned}\Pr(\min\{\gamma_1, \ldots, \gamma_n\} > \gamma) \;&=\; \Pr(\gamma_1 > \gamma, \ldots, \gamma_n > \gamma) = \prod_{i=1}^{n} \Pr(\gamma_i > \gamma) = \prod_{i=1}^{n} \exp(-\gamma/\bar{\gamma}_i) \\ &= \exp\left(-\gamma \sum_{i=1}^{n} \bar{\gamma}_i^{-1}\right). \end{aligned} \tag{5.19}$$

Using Lemma 5.5.1 we have $f(\gamma^{\text{up}}) = \dfrac{\exp(-\gamma/\bar{\gamma}^{\text{up}})}{\bar{\gamma}^{\text{up}}}$ with $\bar{\gamma}^{\text{up}} = (1/\bar{\gamma}_{\text{SR}} + 1/\bar{\gamma}_{\text{RD}})$. Therefore,

$$T_M = M^{\text{th}} \max\{\min(\gamma_{\text{SR}}, \gamma_{\text{RD}})\} = M^{\text{th}} \max \gamma^{\text{up}}. \tag{5.20}$$

In order to determine the pdf of $\gamma_{\text{tot},\mathcal{G}}^{M^{\text{th}}}$ we first need to determine the pdf of the variable T_M which as shown above involves computing the pdf of M^{th} order statistic. We use the following theorem from the theory of order statistics [96] to determine the distribution of T_M.

Theorem 5.5.2 *If $\mathbf{X} = [X_1, \ldots, X_K]$ is a collection of K independent random variables and $\lambda(\mathbf{X})$ denotes the order statistics of $\mathbf{X}$ in a strictly non-increasing order, whereby the first element is the largest element of $\mathbf{X}$, the distribution of the M^{th} order statistic is given by [96, Chapter 7 (Example 7-2)]*

$$\phi_M(x) = K \binom{K-1}{M-1} F(x)^{K-M}[1 - F(x)]^{M-1} f(x) \tag{5.21}$$

Applying Theorem 5.5.2 to the distribution for γ^{up} and considering a total of L relays we have

$$\begin{aligned} \phi_M(\gamma^{\text{up}}) &= L \binom{L-1}{M-1} \left[1 - \exp\left(\frac{-\gamma}{\bar{\gamma}^{\text{up}}}\right)\right]^{L-M} \left[\exp\left(\frac{-\gamma}{\bar{\gamma}^{\text{up}}}\right)\right]^{M-1} \left(\frac{\exp\left(\frac{-\gamma}{\bar{\gamma}^{\text{up}}}\right)}{\bar{\gamma}^{\text{up}}}\right) \\ &= \frac{L}{\gamma^{\text{up}}} \binom{L-1}{M-1} \sum_{k=0}^{L-M} \binom{L-M}{k} (-1)^k \exp\left(\frac{-(M+k)\gamma}{\bar{\gamma}^{\text{up}}}\right) \end{aligned} \tag{5.22}$$

where $\phi_M(\gamma^{\text{up}})$ denotes the pdf of the M^{th} order statistic of γ^{up}. Computing the moment generating function (MGF) of T_M, $\mathcal{M}_{T_M}(s) = \int_0^\infty \phi_M(\gamma) \exp(-s\gamma) d\gamma$, from Eqn. (5.22) we obtain the MGF of $\gamma_{\text{tot},\mathcal{G}}^{M^{\text{th}}}$ as

$$\mathcal{M}_{\gamma_{\text{tot},\mathcal{G}}^{M^{\text{th}}}}(s) = \mathcal{M}_{\gamma_{\text{SD}}}(s)\mathcal{M}_{T_M}(s) = \left(\frac{L}{1 + s\gamma_{\text{SD}}}\right) \left\{ \binom{L-1}{M-1} \sum_{k=0}^{L-M-1} \frac{(-1)^k \binom{L-M-1}{k}}{M + k + s\gamma^{\text{up}}} \right\} \tag{5.23}$$

The pdf then follows straightforwardly as the inverse Laplace transform of $\mathcal{M}_{\gamma_{\mathrm{tot},\mathcal{G}}^{M^{\mathrm{th}}}}(s)$,

$$\begin{aligned} f_{\gamma_{\mathrm{tot},\mathcal{G}}^{M^{\mathrm{th}}}}(\gamma) = & \mathcal{L}^{-1}\left\{L\left\{\binom{L-1}{M-1}\sum_{k=0}^{L-M}(-1)^k\binom{L-M}{k}\left[\frac{(1+s\bar{\gamma}_{\mathrm{SD}})^{-1}}{(M+k+s\gamma^{\mathrm{up}})}\right]\right\}\right\} \\ = & \mathcal{L}^{-1}\left\{L\binom{L-1}{M-1}\sum_{k=0}^{L-M}(-1)^k\binom{L-M}{k}\left[\frac{\frac{\gamma_{\mathrm{SD}}}{(M+k)\bar{\gamma}_{\mathrm{SD}}-\gamma^{\mathrm{up}}}}{(1+s\bar{\gamma}_{\mathrm{SD}})}+\frac{\left(\frac{\gamma^{\mathrm{up}}}{\gamma^{\mathrm{up}}-(M+k)\bar{\gamma}_{\mathrm{SD}}}\right)}{((M+k)+s\gamma^{\mathrm{up}})}\right]\right\} \\ = & L\binom{L-1}{M-1}\sum_{k=0}^{L-M}\frac{(-1)^k}{M+k}\binom{L-M}{k}\left[\frac{\exp\left(\frac{-\gamma}{\beta}\right)-\exp\left(\frac{-\gamma}{\bar{\gamma}_{\mathrm{SD}}}\right)}{\beta-\bar{\gamma}_{\mathrm{SD}}}\right] \end{aligned} \tag{5.24}$$

where $\beta = \gamma^{\mathrm{up}}/(M+k)$.

The distribution of $\gamma_{\mathrm{tot},\mathcal{G}}^{M^{\mathrm{th}}}$ as obtained above applies only when the channel is in good state. It should be noted that when the system is forced to use a relay in an interfered state due to non-availability of any relay in good state, the MRC combining used in Section 5.2 will not reflect the true SNR of the link since the MRC weights (refer Eqn. (5.11)) only account for the channel in good state. Hence, the distribution as obtained above cannot be used to calculate the overall pdf for a relay used in bad state. Furthermore, it cannot be said with certainty that relay selection based on maximizing $\min\{\gamma_{\mathrm{SR}}, \gamma_{\mathrm{RD}}\}$ will yield the same results as the alternative criterion suggested in Section 5.3 based on $\mathrm{argmax}(\min\{\gamma_{\mathrm{SR}}/\kappa, \gamma_{\mathrm{RD}}\})$. For a given relay, $\min\{\gamma_{\mathrm{SR}}/\kappa, \gamma_{\mathrm{RD}}\}$ is very much dependent on the value of κ and in the current work we consider relays with significant interference only, whereby $\kappa \gg 1$. With balanced Rayleigh fading links, i.e., $\bar{\gamma}_{\mathrm{SR}} = \bar{\gamma}_{\mathrm{RD}}$ it is likely that $\min\{\gamma_{\mathrm{SR}}/\kappa, \gamma_{\mathrm{RD}}\}$ will yield $(\gamma_{\mathrm{SR}}/\kappa)$ for moderate to high SNRs and thus relay selection will be based on $\mathrm{argmax}(\gamma_{\mathrm{SR}}/\kappa)$ which is different from relay selection based on an end-to-end SNR criterion. The new criterion is tantamount to *partial* relay selection [133] and one would expect a bound based on the such a criterion to be rather loose. However, for an interfered link we expect $(\gamma_{\mathrm{SR}}/\kappa)$ to dominate performance parameters such as outage and BER and will use it as a lower bound while computing the same.

Outage Probability

The outage probability of the M^{th} best relay, $P_{\text{out},\mathcal{G}}^{M^{\text{th}}}(\gamma_0)$ can be readily obtained by integrating Eqn. (5.24) as follows

$$\begin{aligned} P_{\text{out},\mathcal{G}}^{M^{\text{th}}}(\gamma_0) &= F_{\gamma_{\text{tot},\mathcal{G}}^{M^{\text{th}}}}(\gamma_0) = \int_0^{\gamma_0} f_{\gamma_{\text{tot},\mathcal{G}}^{M^{\text{th}}}}(\gamma) d\gamma \\ &= L \binom{L-1}{M-1} \sum_{k=0}^{L-M} \frac{(-1)^k}{M+k} \binom{L-M}{k} \left[1 + \frac{\gamma_{\text{SD}} \exp\left(\frac{-\gamma_0}{\bar{\gamma}_{\text{SD}}}\right) - \beta \exp\left(\frac{-\gamma_0}{\beta}\right)}{\beta - \bar{\gamma}_{\text{SD}}} \right] \end{aligned} \tag{5.25}$$

The overall outage probability will be governed by the fraction of time for which each of the relays transmit. For example in a given frame, when using the NBR-ONE algorithm, the first relay will be used for $(1 - P_{\mathcal{B}})$ fraction of time in a good state and the second best relay will be used $P_{\mathcal{B}}(1 - P_{\mathcal{B}})$ fraction of time and so on. Finally, the relay with best rank transmits for $\mathrm{P}_{\mathcal{B}}^{L}$ fraction of time in the bad state. Therefore, the overall outage probability is given by

$$P_{\text{out}} = \sum_{M=1}^{L} (1 - P_{\mathcal{B}}) P_{\mathcal{B}}^{M-1} P_{\text{out},\mathcal{G}}^{M^{\text{th}}} + \mathrm{P}_{\mathcal{B}}^{L} \tilde{P}_{\text{out}}^{\text{best}}(\sigma_{\mathcal{B}}^2) \tag{5.26}$$

with $P_{\text{out},\mathcal{G}}^{M^{\text{th}}}$ as in Eqn. (5.25) and $\tilde{P}_{\text{out}}^{\text{best}}(\sigma_{\mathcal{B}}^2)$ is the outage probability of the system when the best relay amongst all interfered relays is used in a bad state. We upper bound $\tilde{P}_{\text{out}}^{\text{best}}(\sigma_{\mathcal{B}}^2)$ by 0.5 due to lack of information of its exact statistics.

Figure 5.6 plots P_{out} with varying threshold and $\bar{\gamma}_{\text{SD}} = -10$ dB, $\bar{\gamma}_{\text{SR}} = \bar{\gamma}_{\text{RD}} = 10$ dB for $L = [3, 5, 7]$ relays using both conventional selection and the NBR-ONE algorithm. P_{out} for conventional selection is based on using the best relay in good state with probability $(1 - \mathrm{P}_{\mathcal{B}})$ and in bad state with probability $\mathrm{P}_{\mathcal{B}}$. For comparison, P_{out} for an AWGN channel is also provided. At extraordinarily high γ_0 all selection schemes seem to converge as the outage probability $P_{\text{out}} \to 1$. The improvements afforded by the

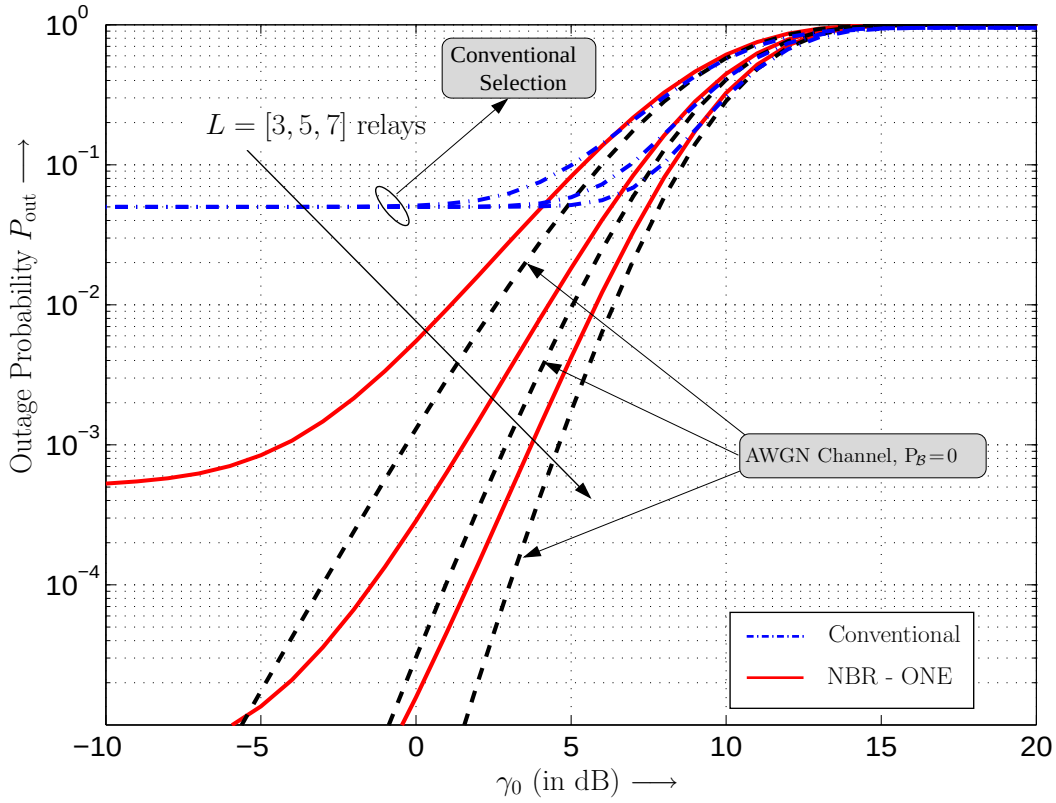

Figure 5.6 — Outage Probability using NBR-ONE algorithm in an impulsive interference environment with $P_{\mathcal{B}} = 0.1$ and SIR$=-20$ dB. An interfered relay is used with probability $\mathrm{P}_{\mathcal{B}}$ for conventional selection and with probability $\mathrm{P}_{\mathcal{B}}^{L}$ for the NBR-ONE approach.

NBR-ONE is more evident over practical values of γ_0 with a gap between the AWGN channel and interfered channel narrowing with increasing number of relays. We observe that even with 3 relays there is close to 1-2 orders of magnitude improvement in P_{out} by applying NBR. Note that the benefits indicated here are more for a best case scenario as the performance benefits offered by any practical scheme such as the T-NBR will depend on the threshold used and will be inherently suboptimal.

Average BER

The pdf derived in Eqn. (5.24) can further be used to analytically determine error rates for the NBR protocol. The BER here will be directly dependent on the rank M of the relay used. The symbol error probability conditioned on M is obtained from $\mathcal{M}_{\gamma_{\text{tot},\mathcal{G}}^{M\text{th}}}(s)$

and the alternative representation of the Q-function [2] as

$$\begin{aligned}\mathrm{P}_e(M) =& \frac{1}{\pi}\int_0^{\pi/2} \mathcal{M}_{\gamma_{\mathrm{tot},\mathcal{G}}^{M^{\mathrm{th}}}}\left(\frac{1}{\sin^2\theta}\right) d\theta \\ =& \frac{L}{2}\binom{L-1}{M-1}\sum_{k=0}^{L-M}\frac{(-1)^k}{M+k}\binom{L-M}{k}\left[1+\frac{1}{\beta-\bar{\gamma}_{\mathrm{SD}}}\left(\gamma_{\mathrm{SD}}\sqrt{\frac{\frac{\bar{\gamma}_{\mathrm{SD}}}{2}}{1+\frac{\bar{\gamma}_{\mathrm{SD}}}{2}}}+\beta\sqrt{\frac{\frac{\beta}{2}}{1+\frac{\beta}{2}}}\right)\right]\end{aligned} \tag{5.27}$$

where $\mathrm{P}_e(M)$ denotes the probability of a symbol error when the M^{th} relay is used. As in the case of P_{out} computation, the average BER also depends on $P_{\mathcal{B}}$. Incorporating the effect of $P_{\mathcal{B}}$ in Eqn. (5.27) we have

$$\mathrm{P}_e = \sum_{M=1}^{L}(1-P_{\mathcal{B}})P_{\mathcal{B}}^{M-1}P_e(M) + \underbrace{P_{\mathcal{B}}^{L}P_e^{\mathrm{best}}(\sigma_{\mathcal{B}}^2)}_{\text{error floor term}} \tag{5.28}$$

where $\mathrm{P}_e(M)$ is given by Eqn. (5.27). While the first term is rather obvious, the second term of Eqn. (5.28) is what determines the error floor of the NBR protocol. $P_e^{\mathrm{best}}(\sigma_{\mathcal{B}}^2)$ in Eqn. (5.28) is the error probability when all relays are deemed to be interfered and is bounded as follows. A rather conservative upper bound would be $P_e^{\mathrm{best}}(\sigma_{\mathcal{B}}^2) = 0.5$ assuming a 50% error rate in the interfered state. However, when considering moderate to high SNR, applying a selection policy criterion of argmax $(\gamma_{\mathrm{SR}}/\kappa)$ as explained earlier gives us a lower bound such that

$$P_{e,\gamma_{\mathrm{SR}}/\kappa}^{\mathrm{best}} < P_e^{\mathrm{best}}(\sigma_{\mathcal{B}}^2) < \frac{1}{2}; \tag{5.29}$$

where $P_{e,\gamma_{\mathrm{SR}}/\kappa}^{\mathrm{best}}$ denotes the error rate of the best relay when we replace γ_{SR} by $\gamma_{\mathrm{SR}}/\kappa$ in Eqn. (5.27). We use this term in obtaining the analytical results throughout the rest of the chapter. In order to verify the usefulness of these expressions we plot in Figure 5.7, the BER for NBR-ONE from both simulations and analytical expressions obtained above for $L = [3, 5, 7, 10]$ relays with SIR$=-20$ dB and $\bar{\gamma}_{\mathrm{SR}} = \bar{\gamma}_{\mathrm{RD}} = 10\bar{\gamma}_{\mathrm{SD}}$.

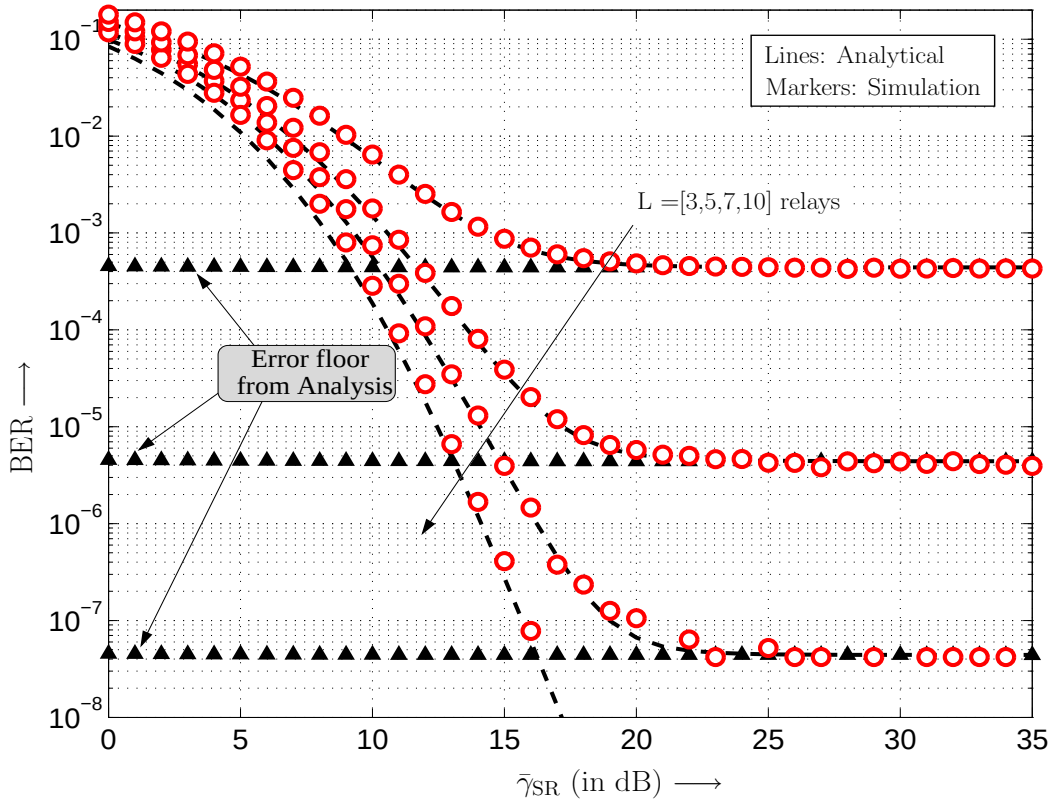

Figure 5.7 — BER vs SNR for SIR = -20 dB with $\bar{\gamma}_{SR}/\bar{\gamma}_{SD} = 10$ and $\bar{\gamma}_{SR} = \bar{\gamma}_{RD}$ when the relays check for interference every symbol but perform relay ranking only once for the entire channel coherence duration. Markers: Simulation, Lines: Analytical.

It is encouraging to see an excellent match between the analytical and simulative results for a range of relays. Interestingly, the error floor predicted from the analysis is also a perfect match implying instant availability of the performance limits of the relays system when one knows $P_{\mathcal{B}}$ and L.

5.6 NBR Selection with Improved Efficiency

As the reader may have inferred, while the approach of finding a reduced set of available relays offers rich dividends in terms of performance, the overheads associated with the process can make the strategy a little less attractive as one needs to obtain $\mathcal{R}^+$ for every symbol. In this section, we seek to devise alternative selection strategies that are more attractive in terms implementation overheads such that a search for the best relay

need not be initiated on a symbol-by-symbol basis. In doing so, we will take advantage of the memory in the interference process. The idea is to exploit the fact that for a non-i.i.d interference process less frequent updates may be required as past samples provide relevant information on the current state of the process. We next present an algorithm that uses this key fact to reduce the overheads associated with NBR-ONE selection.

5.6.1 NBR Wait-For-T (NBR-WFT) Protocol

A key parameter in deciding how often the transmit token needs to be switched from one relay to another is the average duration $\bar{\mathcal{D}}_{\mathcal{B}}$ of the interference process. Since we would like the system to switch from one relay to another as rarely as possible we use a *wait* timer, different from the one used to determine rank validity, with a stop value denoted by RESYN, and at the end of which the system needs to *resynchronize* the membership of the relays in $\mathcal{R}^+$. This resynchronization is necessitated by the fact that while the ranking of the relays based on $\gamma^{\mathcal{G}}_{\text{SRD}}$ may be valid for several hundreds of symbols (quasi-static channel), $\bar{\mathcal{D}}_{\mathcal{B}}$ may be much smaller than that. Thus $\mathcal{R}^+$ has to be updated more frequently depending on $\bar{\mathcal{D}}_{\mathcal{B}}$. NBR-ONE suggested doing this every symbol and exhibited encouraging gains but at the same time may have unacceptable overheads (see Section 5.7). When the best relay determines $\mathcal{H}_1$ to be true, it starts an up counter with a stop value RESYN and until the counter reaches the stop value, the next best relay that is not interfered is used. If we reach the last ranked relay at time $t <$ RESYN then we simply go to the top of the ranking and cycle through till we either reach a relay that is non-interfered or if none of the relays are found to be interference free, the best relay is used regardless of its state and the wait counter is set to 0. We call this the NBR Wait-For-T Full Cycle strategy. The other option would be to use the last ranked relay for the entire duration of RESYN and then revert back to the best relay. The latter method ensures that we do not go back to the best relay for at least RESYN symbols as it is expected to be in bad state for that

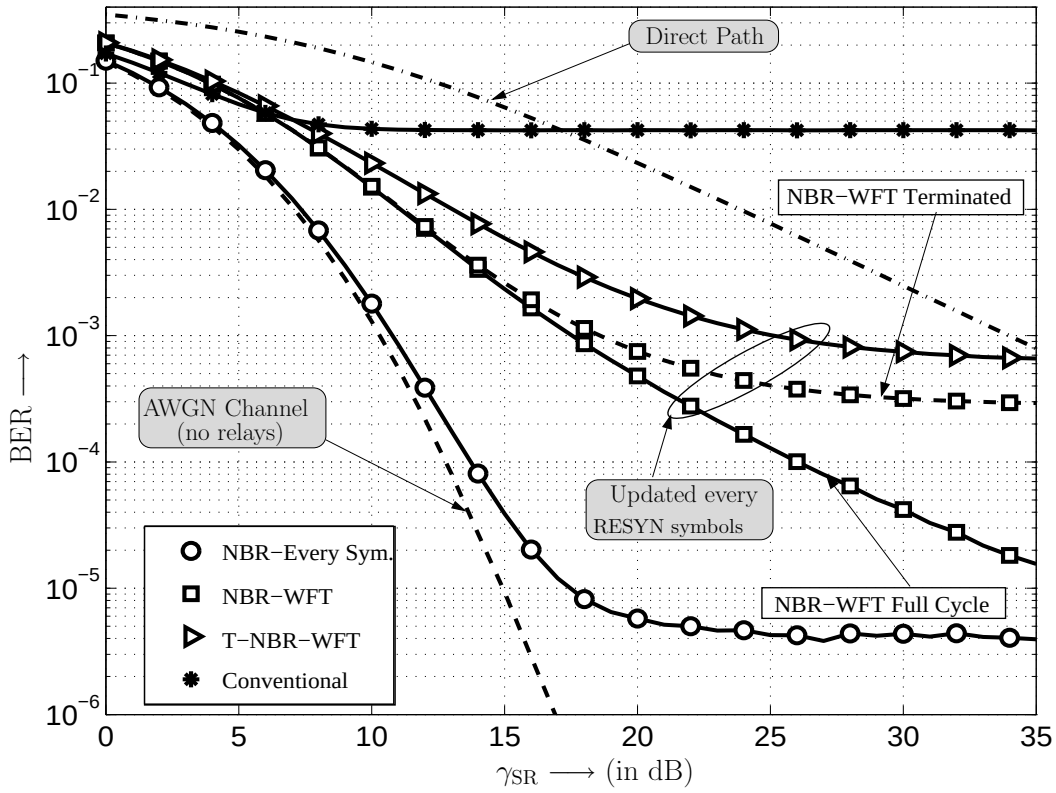

Figure 5.8 — BER vs SNR with $L = 5$ for Markovian-Gaussian interference at relays for SIR = -20 dB with $\gamma_{SR}/\gamma_{SD} = 10$ and $\gamma_{SR} = \gamma_{RD}$. Severe performance degradation can be observed for conventional relay selection while genie aided selection provides huge improvements that is conservatively approached by the Genie-NBR curve. Simulation Parameters: $\bar{\mathcal{D}}_{\mathcal{B}} = 40$ symbols, RESYN $= \bar{\mathcal{D}}_{\mathcal{B}}/2$

duration and is accordingly called the NBR-WFT Terminated strategy. NBR-WFT Terminated saves on the extra computational burden of cycling through and on an average would require less frequent transmit token handovers. NBR-WFT Full Cycle is thus a modified version of the originally proposed NBR taking into account the memory in the interference process and we present it in algorithmic form in Algorithm 5.2. The above strategies may equivalently be applied to TRS as well and the rules for selecting a relay remain unchanged. Thus we can have T-NBR-WFT Full cycle and T-NBR-WFT Terminated adaptations.

We show the capabilities of these algorithms for an exemplary case of $L = 5$ relays in Figure 5.8 with $P_{\mathcal{B}} = 0.1$, SIR $= -20$ dB and $\bar{\gamma}_{SR} = \bar{\gamma}_{RD} = 10\bar{\gamma}_{SD}$. The average

Algorithm 5.2 RELAY SELECTION IN AF NETWORKS WITH NBR-WFT

Before transmission of the first symbol: At the destination (D): Create a ranking of relays using the instantaneous end-to-end SNR values. Then D sends a short packet to all R_ℓ with its rank information

$$D \overset{\text{rank}(R_\ell)}{\longrightarrow} R_\ell \; \forall \; \ell \in \mathcal{R}^+$$

1: At time epoch t,
2: **for** Relay rank $r = 1 : L$ **do**
3: **if** Relay with rank r hit **then**
4: Set $I_r(t) = 1$.
5: **else**
6: $I_r(t) = 0$.
7: **end if**
8: **end for**
9: **if** $I_1(t) == 0$ **then**
10: Use R_1
11: **else if** $I_1(t) == 1$ **then**
12: R_1 sends beacon signal on common channel with rank to let all relays know that $R_1 \notin \mathcal{R}^+$
13: Set $r := 2$
14: Set countdown timer $t_\downarrow$ to RESYN
15: **while** $r < L$ & $t_\downarrow \leq$ RESYN **do**
16: **if** $I_r(t) == 0$ **then**
17: relay R_r transmits.
18: break;
19: **else**
20: Relay r transmits beacon signal on common channel with its own rank.
21: $r := r + 1$
22: go to 15
23: **end if**
24: **end while**
25: **if** $r == L$ **then**
26: Use R_1
27: **end if**
28: **end if**

interference duration is $\bar{\mathcal{D}}_{\mathcal{B}} = 40$ symbols and we set RESYN $= \bar{\mathcal{D}}_{\mathcal{B}}/2$. As in Chapter 2, all other Markovian parameters are obtained from $P_{\mathcal{B}}$ and $\bar{\mathcal{D}}_{\mathcal{B}}$. For comparison purposes results for an AWGN channel and the NBR-ONE algorithm are also presented. We observe that use of relays in general improves performance even in presence of strong interference compared to the direct path (note that the direct path has no interference). In particular NBR-WFT Full Cycle offers high performance gains over both direct transmission and conventional relay selection. Furthermore, NBR-WFT Terminated and T-NBR-WFT achieve performance that is orders of magnitude better than conventional selection. The NBR-WFT strategies represent a trade-off between increase in computational effort versus severe loss in performance. It is encouraging to see that the gains in performance are in fact significant enough to warrant nominal increases in complexity. However, it still remains to be discerned as to what is the fractional increase in overheads in terms of number of symbols transmitted and we provide both analytical and simulative results for the same in Section 5.7. In the next section we outline methods to analyze such a system in terms of BER and the challenges that exist in doing so.

5.6.2 Average BER Analysis

The NBR-WFT approach presents several interesting aspects brought about by the Markovianity of the interference and in the following we discuss the key aspects that need to be accounted for in the analysis. We define a *segment* of transmission as a group of transmitted symbols where the transmission is initiated by the use of the best relay and is terminated by the use of the rest of the relays for a duration $t \leq$ RESYN symbols. In the following, we denote a relay with rank r as R_r and the duration for which R_r transmits in the k^{th} segment as $T^k_{\mathcal{G},r}$. This implies that for the k^{th} segment we have $T^k_{\mathcal{G},1}$ contiguous symbols transmitted using the best relay and at the $(T^k_{\mathcal{G},1}+1)^{\text{th}}$ symbol the best relay is detected to be in bad state. Following the NBR approach, at this point we seek the relay with the next lower rank that is not interfered. For

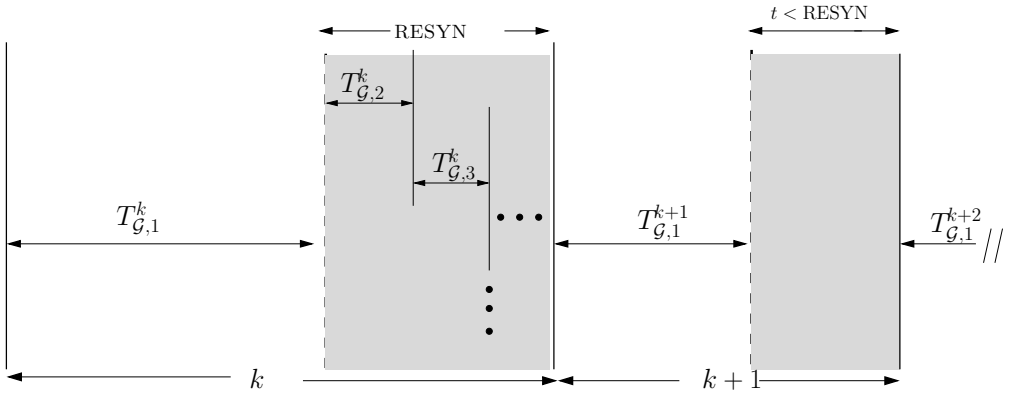

Figure 5.9 — Illustration of relay use when using the NBR-WFT approach in a Markovian Gaussian environment. RESYN is a design parameter and denotes the duration for which the best relay may not be used upon being detected as interfered. Relay with rank r transmits $T^k_{\mathcal{G},r}$ symbols per segment.

example, if R_2 is not interfered we will be using this relay for the $(T^k_{\mathcal{G},1}+1)^{\text{th}}$ symbol and all subsequent symbols for a maximum of RESYN symbols or till R_2 is detected to be in bad state. In the latter case we will have $T^k_{\mathcal{G},2} <$ RESYN. On the other hand if $R_r, r \in \{2,3,\ldots,L\}$ is detected to be in bad state as well for the $\left(\sum_{i=1}^{r-1} T^k_{\mathcal{G},i}+1\right)^{\text{th}}$ symbol then R_r is not used and hence correspondingly $T^k_{\mathcal{G},r}=0$. We illustrate the above concepts in Figure 5.9 where two consecutive segments of transmission are shown. Note that for NBR-WFT Full cycle it is possible that R_1 regains possession of the transmit token before RESYN symbols.

The average bit error rate will depend on the average time that a relay with a certain rank transmits in addition to the order statistic for that rank. For ease of notation, we define a state vector

$$\mathbf{T}^k_{\mathcal{G}} = [\, T^k_{\mathcal{G},1}, T^k_{\mathcal{G},2}, \ldots, T^k_{\mathcal{G},L} \,] \tag{5.30}$$

as the time for which each relay transmits in a good state in the k^{th} segment in decreasing order of rank. The best relay has no limits on the maximum amount of time that it can transmit for other than when it is hit by interference. Therefore there is

no upper limit on $T_{\mathcal{G},1}$[7] and we have $0 \leq T_{\mathcal{G},1} < \infty$. The same however does not hold true for $T_{\mathcal{G},r},\ r = \{2, 3, \ldots, L\}$ as we use these relays for a maximum of RESYN period assuming that they are not interfered during this period. We also define a vector $\boldsymbol{P}$ as a probability distribution over the ranks of relays such that each element of $\boldsymbol{P}$ denotes the probability that a given relay transmits in a segment. Mathematically we have,

$$\boldsymbol{P} = [\Pr(\Phi_{R_1}), \Pr(\Phi_{R_2}), \ldots, \Pr(\Phi_{R_L})], \tag{5.31}$$

where Φ_{R_r} denotes the event that R_r transmits. Clearly $\boldsymbol{P}$ is a function of $\mathcal{E}\left\{\mathbf{T}_{\mathcal{G}}^{k}\right\}$ and for a R_r we have

$$\Pr(\Phi_{R_r}) = \frac{\mathcal{E}\{T_{\mathcal{G},r}^{k}\}}{\sum_{j=1}^{L} \mathcal{E}\{T_{\mathcal{G},j}^{k}\}}. \tag{5.32}$$

Also, the length of the k^{th} segment is given by

$$T_{\mathcal{G}}^{k} = \sum_{i=1}^{L} T_{\mathcal{G},i}^{k} + T_{\mathcal{B},1}^{k} \tag{5.33}$$

which implies the duration for which the other relays transmit is $\sum_{i=2}^{L} T_{\mathcal{G},i}^{k}$. We note that individual $T_{\mathcal{G}}^{k}$s depend on $\mathrm{P}_{\mathcal{B}}$ and the transition probability matrix $\boldsymbol{T}$. In particular, the state of a relay when it acquires the transmission token in the current segment is dependent on the time elapsed between its last use and its current use according to $\boldsymbol{T}$. Once we obtain $\boldsymbol{P}$, the average BER can be obtained rather straightforwardly. However, computation of $\boldsymbol{P}$ requires the consideration of several key aspects and we illustrate them using an example system where $L = 2$ in the next section.

[7]Note that only for R_1, $T_{\mathcal{G},1}$ is not equal to the total time for which R_1 transmits as R_1 may transmit in bad state as well. However $T_{\mathcal{G},r}$ is the actual transmit time for relay $R_r,\ r \in \{2, 3 \ldots, L\}$

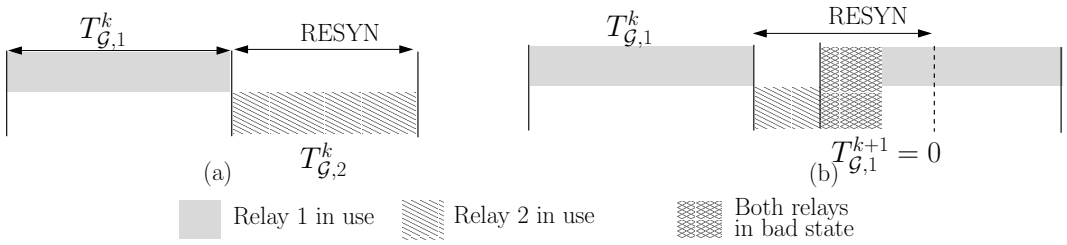

Figure 5.10 — Usage of respective relay ranks when employing an NBR approach for a 2 relay system. (a) R_2 is used for the entire duration RESYN when R_1 is interfered, i.e., R_2 is in good state for entire duration. (b) R_2 is interfered within RESYN after acquiring transmit token and hence R_1 continues to transmit in bad state.

2-relay Case

We consider a 2-relay system where there is also a direct path between the source and destination terminals as originally considered in Section 5.2. The setup is fairly simple in that when R_1 is in bad state, R_2 is used and when R_2 is found to be in bad state within RESYN symbols of use, we revert back to using R_1 regardless of its state. In order to obtain the error probabilities we are interested in computing the average values of $T_{\mathcal{G},1}$ and $T_{\mathcal{G},2}$. This requires obtaining the distribution functions of the individual $T_{\mathcal{G}}$s. The usage of the relays as explained above is depicted in Figure 5.10. While Figure 5.10(a) presents the case where R_2 is available for use, i.e., in good state for the entire duration RESYN and therefore we have $T^k_{\mathcal{G},2} = \text{RESYN}$, Figure 5.10(b) shows that when $T^k_{\mathcal{G},2} < \text{RESYN}$, R_1 is used in spite of being in bad state and therefore $T^k_{\mathcal{G},1} = 0 \; \forall \; k$, where R_1 transmits in a bad state. In the following we illustrate the scenarios where the boundary values of $T^k_{\mathcal{G},1} = 0$, $T^k_{\mathcal{G},2} = 0$ may occur and devise methods to analytically derive the probabilities $\Pr(T^k_{\mathcal{G},1})$ and $\Pr(T^k_{\mathcal{G},2})$. The probability that R_1 is in bad state after ℓ uses of R_2 in the previous (k^{th}) segment, $P_1^{k+1}(\mathcal{B}|T^k_{\mathcal{G},2} = \ell)$, is obtained from the ℓ-step transition probability of the underlying Markov chain as follows

$$P_1^{k+1}(\mathcal{B}|T^k_{\mathcal{G},2} = \ell) = \boldsymbol{T}^{\ell+1}(2,2), \qquad \text{where } \boldsymbol{T} = \begin{bmatrix} P_{\mathcal{G}\mathcal{G}} & P_{\mathcal{G}\mathcal{B}} \\ P_{\mathcal{B}\mathcal{G}} & P_{\mathcal{B}\mathcal{B}} \end{bmatrix}. \tag{5.34}$$

Therefore, denoting $P_1^{k+1}(\mathcal{B}|T_{\mathcal{G},2}^k = \ell)$ by $P_{1,\mathcal{B}|\ell}^{k+1}$, the probability distribution of $T_{\mathcal{G},1}^{k+1}$ conditioned on $T_{\mathcal{G},2}^k$ is obtained as

$$\Pr(T_{\mathcal{G},1}^{k+1}=m|T_{\mathcal{G},2}^k=\ell) = P_{1,\mathcal{B}|\ell}^{k+1}\delta[m] + (1-P_{1,\mathcal{B}|\ell}^{k+1})P_{\mathcal{GB}}(1-P_{\mathcal{BG}})^{(m-1)}u[m-1], \quad (5.35)$$

where $m = [0, 1, \ldots, \infty]$ and $u[m]$ denotes the unit step function for discrete time such $u[m] = 1$ for $m > 0$ and is $u[m] = 0$ otherwise. Following which the probability of $T_{\mathcal{G},2}^{k+1}$ may be obtained conditioned on $T_{\mathcal{G},1}^{k+1}$ and $T_{\mathcal{G},2}^k$. However, at this juncture one needs to be careful about the transitions that cause the switch from R_2 to R_1 in the $(k+1)^{\text{th}}$ segment. We provide an illustration of the various possibilities in Figure 5.11. Case I represents the simplest case where after RESYN uses of R_2, R_1 is found to be in good state and begins transmission and case II depicts the situation where $T_{\mathcal{G},2}^k <$ RESYN. Note that if the k^{th} segment for R_2 were as in case I, i.e., full use for all RESYN symbols then the probability of R_2 being in a bad state at the $(T_{\mathcal{G},1}^{(k+1)} + 1)^{\text{th}}$ symbol, $P_2^{k+1}(\mathcal{B}|T_{\mathcal{G},1}^{k+1}=m)$ is governed by the m-step transition probability, $\mathcal{G} \overset{m-\text{step}}{\longrightarrow} \mathcal{B}$, however if the k^{th} segment were to be as in case II then R_2 would make the transition $\mathcal{B} \overset{m-\text{step}}{\longrightarrow} \mathcal{B}$. Accordingly we have

$$P_2^{k+1}(\mathcal{B}|T_{\mathcal{G},1}^{k+1}=m) = \begin{cases} \boldsymbol{T}^m(2,2) & T_{\mathcal{G},2}^k < \text{RESYN} \\ \boldsymbol{T}^m(1,2) & T_{\mathcal{G},1}^k = \text{RESYN} \ . \end{cases} \quad (5.36)$$

Taking the above fact into consideration, the conditional probability for $T_{\mathcal{G},2}^{k+1}$ reads

$$\begin{aligned} \Pr(T_{\mathcal{G},2}^{k+1}=n|\ T_{\mathcal{G},1}^{k+1}=m, T_{\mathcal{G},2}^k=\ell) = {} & P_{2,\mathcal{B}|m}^{k+1}\delta[n] \ + (1-P_{2,\mathcal{B}|m}^{k+1})P_{\mathcal{GB}}(1-P_{\mathcal{BG}})^{(n-1)}\big(u[n-1] - \\ & u[n-\text{RESYN}]\big) + \ \delta[n-\text{RESYN}]\sum_{i=\text{RESYN}}^{\infty}(1-P_{2,\mathcal{B}|m}^{k+1})P_{\mathcal{GB}}(1-P_{\mathcal{GB}})^{i-1} \quad (5.37a) \\ = \ & P_{2,\mathcal{B}|m}^{k+1}\delta[n] + (1-P_{2,\mathcal{B}|m}^{k+1})P_{\mathcal{GB}}(1-P_{\mathcal{BG}})^{(n-1)}\big(u[n-1]-u[n-\text{RESYN}]\big) \\ & + \delta[n-\text{RESYN}](1-P_{2,\mathcal{B}|m}^{k+1})P_{\mathcal{GG}}^{\text{RESYN}-1}. \quad (5.37b) \end{aligned}$$

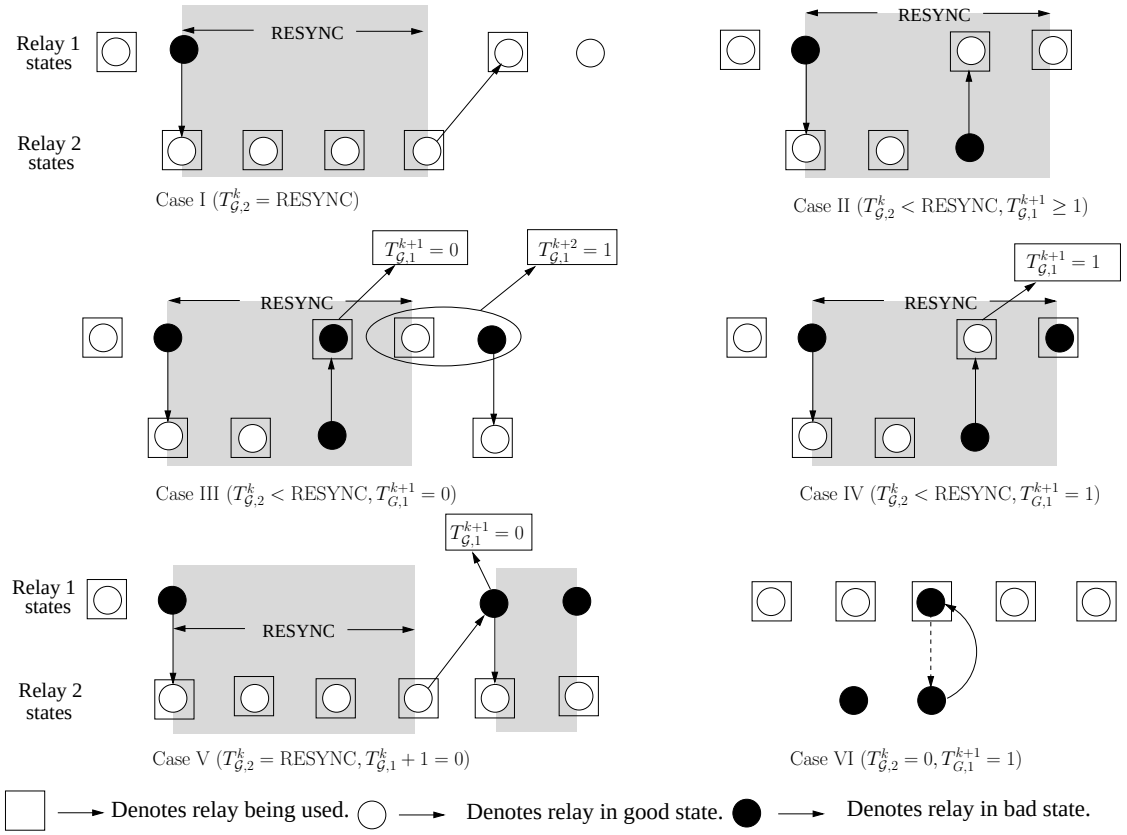

Figure 5.11 — Possible transitions for the 2-relay case in an Markovian-Gaussian interference environment where the system chooses the next best relay when the best relay is interfered. Note the distinction made with respect to the control being transferred from relay 2 to relay 1 when relay 2 does not transmit for RESYN time slots due to interference.

In obtaining Eqn. (5.37b) above we make use of the identities $\sum_{k=0}^{\infty} q^k = 1/(1-q),\ |q| < 1$, and $\sum_{k=1}^{N} q^{k-1} = (q^N - 1)/(q-1)$ [144]. Averaging $\Pr(T^{k+1}_{\mathcal{G},2} = n | T^{k+1}_{\mathcal{G},1} = m, T^k_{\mathcal{G},2} = \ell)$ over all m allows us to obtain the transition probability matrix $\mathbf{\Phi}_2$ for $T_{G,2}$ whose entries are $\Pr(T^{k+1}_{\mathcal{G},2} | T^k_{G,2})$ and the size of $\mathbf{\Phi}_2$ is $(\text{RESYN}+1) \times (\text{RESYN}+1)$. The $(n,\ell)^{\text{th}}$ element of $\mathbf{\Phi}_2$ is given by

$$\Pr(T^{k+1}_{\mathcal{G},2} = n | T^k_{G,2} = \ell) = \sum_{m=0}^{\infty} \Pr(T^{k+1}_{\mathcal{G},2} = n | T^{k+1}_{\mathcal{G},1} = m, T^k_{\mathcal{G},2} = \ell) \Pr(T^{k+1}_{\mathcal{G},1} = m | T^k_{\mathcal{G},2} = \ell). \tag{5.38}$$

We divide the infinite summation in Eqn. (5.38) in two parts, where the first part is upto some positive integer $m_{\max}$ and the second part accounts for rest of the terms upto ∞ as follows

$$\begin{aligned}\Pr(T_{\mathcal{G},2}^{k+1}=n|T_{G,2}^{k}=\ell) \;=\; & \sum_{m=0}^{m_{\max}} \Pr(T_{\mathcal{G},2}^{k+1}=n|T_{\mathcal{G},1}^{k+1}=m, T_{\mathcal{G},2}^{k}=\ell)\Pr(T_{\mathcal{G},1}^{k+1}=m|T_{\mathcal{G},2}^{k}=\ell) \\ & + \Pr(T_{\mathcal{G},2}^{k+1}=n|T_{\mathcal{G},1}^{k+1}=\infty, T_{\mathcal{G},2}^{k}) \sum_{m=m_{\max}+1}^{\infty} \Pr(T_{\mathcal{G},1}^{k+1}=m|T_{\mathcal{G},2}^{k}=\ell) \\ = \; & \sum_{m=0}^{m_{\max}} \Pr(T_{\mathcal{G},2}^{k+1}=n|T_{\mathcal{G},1}^{k+1}=m, T_{\mathcal{G},2}^{k}=\ell)\Pr(T_{\mathcal{G},1}^{k+1}=m|T_{\mathcal{G},2}^{k}=\ell) \\ & + \Pr(T_{\mathcal{G},2}^{k+1}=n|T_{\mathcal{G},1}^{k+1}=\infty, T_{\mathcal{G},2}^{k}=\ell)(1-P_{1,\mathcal{B}|\ell}^{k+1})P_{\mathcal{GG}}^{m_{\max}}. \quad (5.39a)\end{aligned}$$

Computing $\mathbf{\Phi}_2$ as above allows us to obtain the stationary distribution of $T_{\mathcal{G},2}$ through an eigen-decomposition. In particular, denoting by $\boldsymbol{\nu}_1$ the left eigenvector of $\mathbf{\Phi}_2$ corresponding to the eigenvalue of 1, we have

$$\mathcal{F}(T_{\mathcal{G},2}) = \boldsymbol{\nu}_1, \tag{5.40}$$

where $\mathcal{F}(T_{\mathcal{G},2})$ denotes the probability mass function (pmf) of $T_{\mathcal{G},2}$. Before we delve into employing Eqn. (5.40) to compute the distribution of $T_{\mathcal{G},1}$ we establish the accuracy of the above analysis by comparing it with the empirical pmf of $T_{\mathcal{G},2}$ from simulations in Figure 5.12 with $P_{\mathcal{B}} = 0.1$, $\bar{\mathcal{D}}_{\mathcal{B}} = 40$ symbols and RESYN $= \bar{\mathcal{D}}_{\mathcal{B}}/2$[8]. Note that the maximum value of $T_{\mathcal{G},2}$ is RESYN and that $T_{\mathcal{G},2}=0$ is only possible when R_1 passes the transmit token to R_2 and R_2 is also found to be interfered as well, forcing us to use R_1. In Figure 5.12, the analytical values are seen to literally overlap the simulated pmf for the 2-relay system using NBR-WFT. Two rather distinctive features of the pmf for $T_{\mathcal{G},2}$ is that the weights are heavily concentrated at the two extreme values and a uniform distribution over all other values between 0 and RESYN is observed. A high value for $\Pr(T_{\mathcal{G},2})=0$ implies that there are fairly frequent instances when the bad states of R_2

[8]The system SNR and SIR values are irrelevant for the computation of the pmf here.

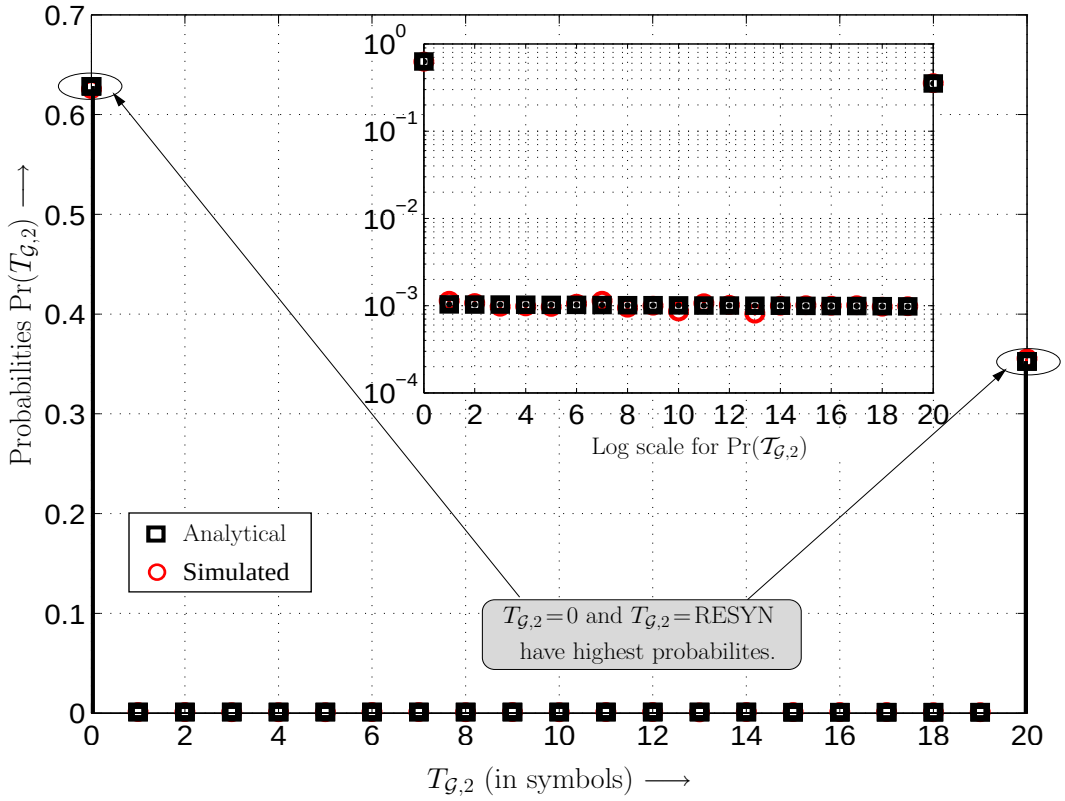

Figure 5.12 — Probability mass function for $T_{\mathcal{G},2}$ i.e. duration for which the second best relay R_2 transmits in 2-relay system. Each point in the abscissa denotes the number of contiguous bits transmitted by R_2. A logarithmic version is presented inset to show the excellent match of the analytical method to the simulated values. Simulation parameters: $P_{\mathcal{B}} = 0.1$, $\bar{\mathcal{D}}_{\mathcal{B}} = 40$ symbols, RESYN $= \bar{\mathcal{D}}_{\mathcal{B}}/2$.

and R_1 overlap. Furthermore, from the substantial weight at $\Pr(T_{\mathcal{G},2}) =$ RESYN we infer that when a burst of bad states commences at R_1, it is reasonably likely that R_2 is in good state for a duration longer than RESYN $= \bar{\mathcal{D}}_{\mathcal{B}}/2$.

Having obtained the pmf of $T_{\mathcal{G},2}$ we next consider the pmf of $T_{\mathcal{G},1}$. Fortunately, this does not require us to obtain a transition probability matrix for $T_{\mathcal{G},1}$ prior to obtaining the probability distribution as we can simply average over $\Pr(T_{\mathcal{G},1}^{k+1} = m | T_{\mathcal{G},2}^{k} = \ell)$ from Eqn. (5.35) over all $T_{\mathcal{G},2}$. However as in the case of $T_{\mathcal{G},2}$ there are certain subtle aspects in accounting for transitions from use of R_1 to use of R_2 and vice versa that require attention as they have implications in computation of the overall BER. In particular we differentiate between the cases of $T_{\mathcal{G},2} <$ RESYN and $T_{\mathcal{G},2} =$ RESYN. We ask the reader

to refer to Figure 5.11 again in order to appreciate the details better. We consider each of the above two cases separately in the following.

Computation of $T_{\mathcal{G},1}$ with $T_{\mathcal{G},2} = \text{RESYN}$

In this case R_2 would have been used for a full duration of its intended use and we will have a minimum of RESYN intermediate symbols between two successive uses of R_1. Case I and Case V from Figure 5.11 are pertinent here and we obtain $\Pr(T_{\mathcal{G},1}^{k+1} = m | T_{\mathcal{G},2}^{k} = \text{RESYN})$ from Eqn. (5.35). Note that if R_1 continues to be in bad state (see case V in Figure 5.11) it will try to pass the transmission token back to R_2 (which may or may not be in bad state). This event will be counted as $T_{\mathcal{G},1}^{k+1} = 0$. This is different for the $T_{\mathcal{G},1}^{k+1} = 0$ case we will encounter below for $T_{\mathcal{G},2} < \text{RESYN}$.

Computation of $T_{\mathcal{G},1}$ with $T_{\mathcal{G},2} < \text{RESYN}$

In this case the transmit token is invariably passed over to R_1 from R_2, regardless of its state. The reader is requested to refer to cases III and IV from Figure 5.11 for this part. In particular, case III corresponds to having $T_{\mathcal{G},1}^{k+1} = 0$ as we transition from a $\mathcal{B}$ state to a $\mathcal{B}$ state after ℓ uses of R_2, therefore we have

$$P_1^{k+1}(\mathcal{B} | T_{\mathcal{G},2} = \ell; \ell < \text{RESYN}) = P_{1,\mathcal{B}|\ell}^{'(k+1)} = \boldsymbol{T}^{\ell}(2,2), \tag{5.41}$$

which is different from Eqn. (5.34), which holds true for $T_{\mathcal{G},2} = \text{RESYN}$. Furthermore, cases III and IV also present two different situations in which we may have $T_{\mathcal{G},1} = 1$. In case III, we have R_1 in bad state when it obtains the transmit token from R_2 and may enter a good state followed by a bad state. Since we need to distinguish between usage of R_1 in good and bad states, when we use R_1 in bad state we count it as an instance of $T_{\mathcal{G},1} = 0$ and re-initialize the count for $T_{\mathcal{G},1}$ for subsequent uses of R_1. In case III, for example, although there are two contiguous uses of R_1 in a the $(k+1)^{\text{th}}$ segment, we count it as two segments yielding $T_{\mathcal{G},1}^{k+1} = 0$ and $T_{\mathcal{G},1}^{k+2} = 1$. For such instances we will have $\Pr(T_{\mathcal{G},1} = 1 | T_{\mathcal{G},2} = \ell; \ell < \text{RESYN}) = P_{1,\mathcal{B}|\ell}^{'(k+1)} P_{\mathcal{BG}} P_{\mathcal{GB}}$. Alternatively, in Case IV

R_1 is found to be in good state after acquiring the transmit token but enters into a bad state in the next symbol again rendering $T_{\mathcal{G},1}=1$, however, now with a probability $\Pr(T_{\mathcal{G},1}=1|T_{\mathcal{G},2}=\ell;\ell<\text{RESYN}) = [1-P^{'(k+1)}_{1,\mathcal{B}|\ell}]P_{\mathcal{GB}}$. In fact, we can generalize the above for cases for arbitrary values of $T_{\mathcal{G},1}>1$. The probabilities corresponding to the different transition events are summarized below.

For $T_{\mathcal{G},2}<\text{RESYN}$,

$$\Pr(T^{k+1}_{\mathcal{G},1}=m|T^{k}_{\mathcal{G},2}=\ell) = \begin{cases} \boldsymbol{T}^{\ell}(2,2); & m=0 \\ \left(P^{'(k+1)}_{1,\mathcal{B}|\ell}P_{\mathcal{BG}} + [1-P^{'(k+1)}_{\mathcal{B}|\ell}]\right)P_{\mathcal{GB}}P^{m-1}_{\mathcal{GG}}; & m\geq 1\ . \end{cases} \tag{5.42}$$

We employ the above to obtain the pmf of $T_{\mathcal{G},1}$ analytically and plot it with the empirical pmf of $T_{\mathcal{G},1}$ from simulation in Figure 5.13 with the same simulation parameters as for $T_{\mathcal{G},2}$. Theoretically we have $0\leq T_{\mathcal{G},1}<\infty$, however, for simulation purposes we will restrict it to a certain maximum value $m_{\max}$ in conformance with the approach in obtaining Eqn. (5.39a). At first glance, the pmf of $T_{\mathcal{G},1}$ seems very unreasonable as almost all weight is seen to be concentrated at $T_{\mathcal{G},1}=0$. However, this is not all that surprising when one considers that fact that higher values of $T_{\mathcal{G},1}$ correspond to those many symbols that are transmitted in good state. The fraction of symbols that are transmitted in good state is $\sum_{T_{\mathcal{G},1}=1}^{m_{\max}} T_{\mathcal{G},1}\mathbb{N}(T_{\mathcal{G},1}) + \sum_{T_{\mathcal{G},1}=1}^{\text{RESYN}} T_{\mathcal{G},2}\mathbb{N}(T_{\mathcal{G},2}) = 1-\text{P}^2_{\mathcal{B}}$, where $\mathbb{N}(T_{\mathcal{G},x}),\ x=\{1,2\}$ denotes the number of times $T_{\mathcal{G},x}$ attains a given value. From the inset figure where we zoom in to show the distribution of $T_{\mathcal{G},1}$ for values greater than 0, we see an exponential decay of terms which is in line with expectations. Note that R_1 can also transmit in bad state by assumption and therefore there will be several cases when R_1 is used and $T_{\mathcal{G},1}=0$. Overall, we see that the simulated empirical pmfs corroborate the analytically derived pmfs for R_1 and R_2. Next, we use the analytical treatise of this section in determining the average BER of a 2-relay system which was our ultimate goal.

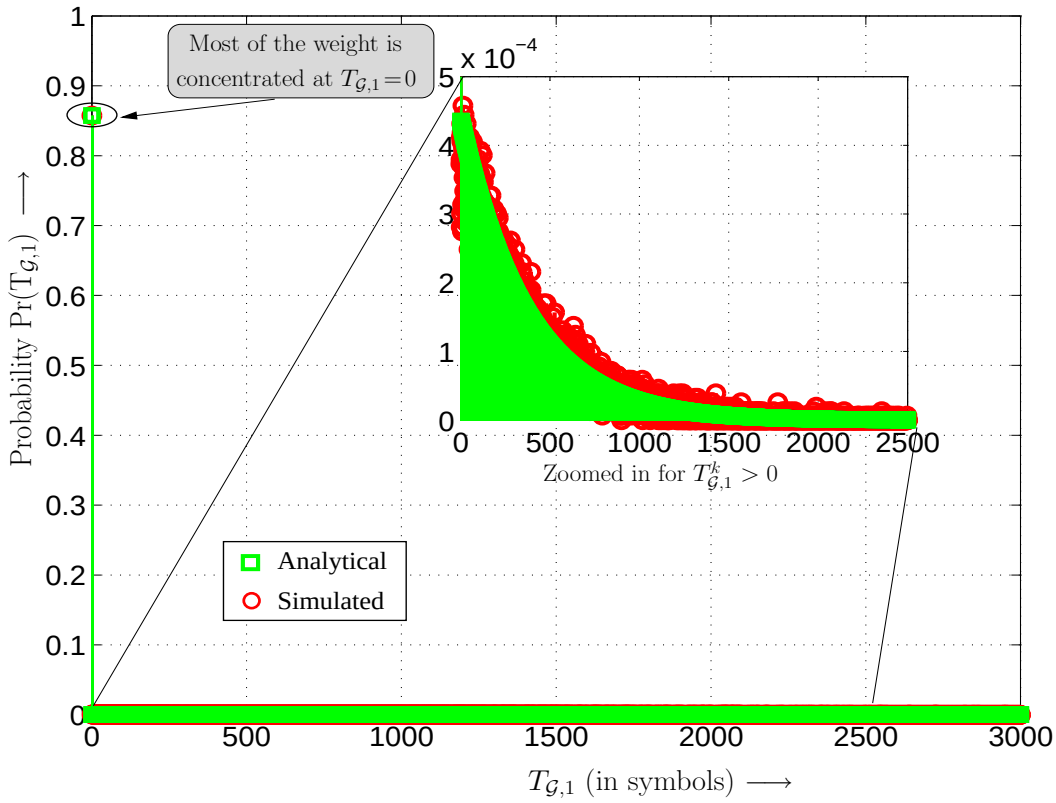

Figure 5.13 — Probability mass function for $T_{\mathcal{G},1}$ from analytical derivation in Section 5.6.2 and simulation with $P_{\mathcal{B}} = 0.1$, $\bar{\mathcal{D}}_{\mathcal{B}} = 40$ symbols, RESYN $= \bar{\mathcal{D}}_{\mathcal{B}}/2$. A good match is seen between that analytical and simulated values. Inset figure shows a zoomed in version for $T_{\mathcal{G},1} > 0$. Here the ordinate corresponds to the probability of occurrence of contiguous good states of R_1 when in use.

Average BER of 2-relay System

Using the pmfs as obtained above we can compute $\mathcal{E}\{\boldsymbol{T}^k_{\mathcal{G}}\}$ for the 2-relay system. Furthermore, this allows us to compute $\boldsymbol{P}$ (refer Eqn. (5.32)), the probabilities with which each relay transmits data in good state for a Markovian-Gaussian environment with NBR for 2 relays. Denoting the vector of error probabilities when each individual relay transmits as $\boldsymbol{E}_2 = [P_e(\mathcal{G}|1) \;\; P_e(\mathcal{G}|2)]^T$, the overall probability for transmission in bad states as P_{bad} we have the average BER as

$$\text{BER}_{2-\text{relay}} = \boldsymbol{P} \cdot \boldsymbol{E_2} + P_{\text{bad}} P_e(\mathcal{B}|1) \tag{5.43}$$

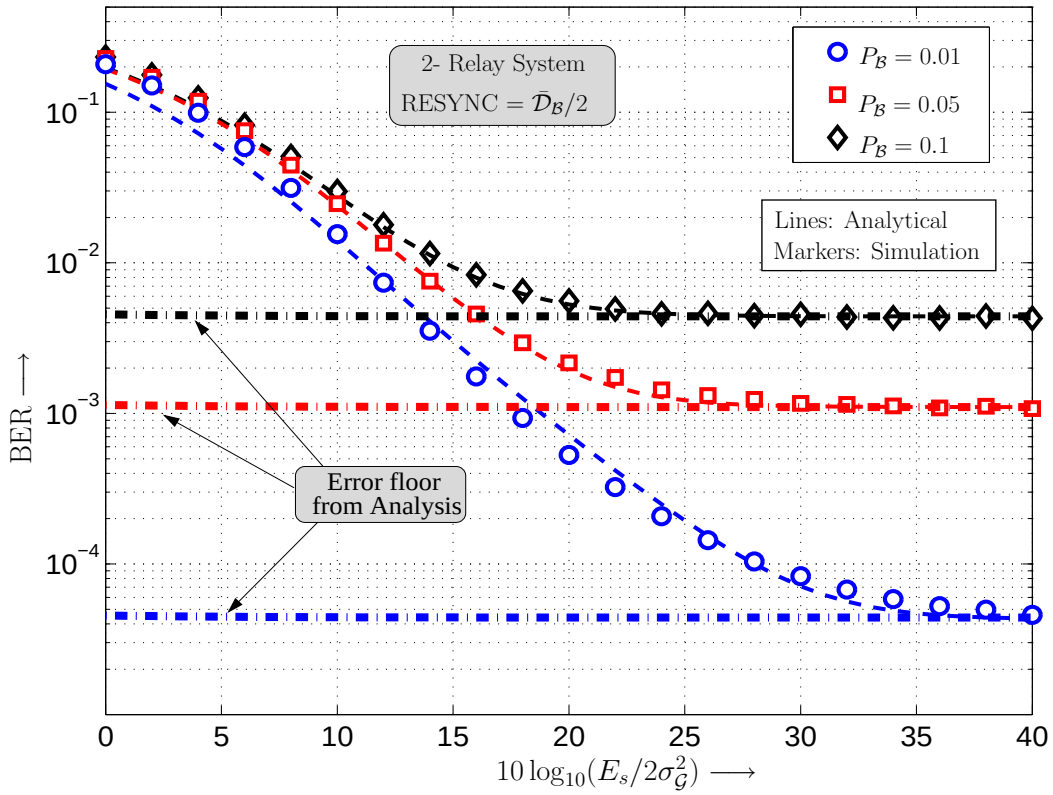

Figure 5.14 — BER vs SNR when using $L = 2$ relays with a RESYN period based transmission scheme for $P_{\mathcal{B}} = [0.01, 0.05, 0.1]$, SIR $= -20$ dB, $\bar{\mathcal{D}}_{\mathcal{B}} = 40$ symbols and RESYN $= \bar{\mathcal{D}}_{\mathcal{B}}/2$. Analytical BER based on determining fraction of time transmitted for each relay computed from the Markovianity of the interference (refer Section 5.6.2). Lines: Analytical results. Markers: Simulation.

where $P_e(\mathcal{G}|r)$ and $P_e(\mathcal{B}|1)$ are obtained from Eqn. (5.27) and Eqn. (5.29) respectively, and $P_{\text{bad}} = \mathrm{P}_{\mathcal{B}}^2$. Similar to the analysis for NBR-ONE, the second term in Eqn. (5.43) predicts the error floor of the overall system.

Using Eqn. (5.43), we plot in Figure 5.14 the error probabilities for a 2-relay system for $P_{\mathcal{B}} = [0.01, 0.05, 0.1]$ along with the curves obtained from a simulated system. Again RESYN $= \bar{\mathcal{D}}_{\mathcal{B}}/2$ is chosen and SIR $= -20$dB with $\bar{\gamma}_{\text{SR}} = \bar{\gamma}_{\text{RD}} = 10\bar{\gamma}_{\text{SD}}$. We see that results obtained from our analytical approach serves fairly well as an alternative to a system level simulation as high levels of accuracy in estimating the simulated BERs are observed over several values of $P_{\mathcal{B}}$ and SNRs.

Multiple Relay Case

In this section, we extend the analysis developed for the 2-relay case to multiple relays. The analysis for multiple relays is a little less straight-forward as one now needs to account for the amount of time that is spent in the rest of the $L-1$ relays rather than just one other relay, when the best relay is unavailable, as was considered in the previous section. We denote this duration by $T^k_{\mathcal{G},\text{rest}}$, thus $T^k_{\mathcal{G},\text{rest}} = \sum_{j=2}^{L} T^k_{\mathcal{G},j}$ and it plays a role equivalent $T^k_{\mathcal{G},2}$ in the previous section. Therefore we have $T^k_{\mathcal{G},\text{rest}} \in [0, \text{RESYN}]$. For the $r^{\text{th}}, r \in \{2,\ldots,L\}$ ranked relay we have

$$T^k_{\mathcal{G},r} \in \left[0, \min\left(\text{RESYN}, T^k_{\mathcal{G},\text{rest}} - \sum_{j=2, j\neq r}^{L} T^k_{\mathcal{G},j}\right)\right] \tag{5.44}$$

where j also denotes rank of a relay. If for relay R_r we have $T^k_{\mathcal{G},r} = 0$, then there are two possibilities. First if it were in bad state when it acquired the transmit token for a given segment and secondly the system never gets around to using that relay as higher ranked relays were available for transmission for all RESYN symbols of the segment. The latter case is unique to a system with $L > 2$ relays while the former is a familiar situation from the 2-relay analysis and is consequence of the fact that no relay other than the best one transmits in bad state. The probability $\Pr(T^{k+1}_{\mathcal{G},1} = m | T^k_{\mathcal{G},\text{rest}} = \ell_{\text{rest}})$ depends on the value of ℓ_{rest} in the same manner as it did for the 2-relay case. Note that the details of what relays were actually used during the ℓ_{rest} symbols of the k^{th} segment bear no relevance to the computation of $\Pr(T^{k+1}_{\mathcal{G},1} = m | T^k_{\mathcal{G},\text{rest}} = \ell_{\text{rest}})$. Therefore, we may still use Eqn. (5.35) for $\ell_{\text{rest}} = \text{RESYN}$ and Eqn. (5.42) for $\ell_{\text{rest}} < \text{RESYN}$.

The probability $\Pr(T^k_{\mathcal{G},\text{rest}} = \ell^k_{\text{rest}})$, however, critically depends on the number of relays. For a relay with $r \in \{2,\ldots,L\}$, we can derive $\mathcal{E}\{T_{\mathcal{G},r}\}$ by employing the Markovian property of the interference process and considering the time elapsed between two consecutive uses of R_r as illustrated in Figure 5.15. The shaded region in Figure 5.15 is

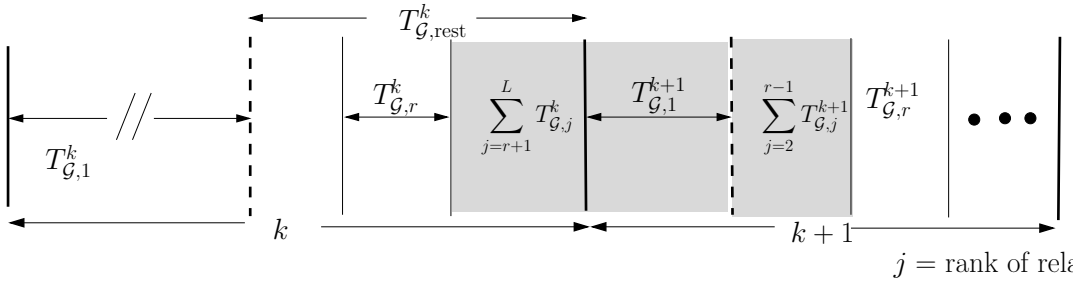

Figure 5.15 — Consecutive segments in time for L-relays using an NBR-WFT strategy is applied to a Markovian-Gaussian environment using multiple relays to depict the durations of time that need to be accounted for in evaluation of the $T^{k+1}_{\mathcal{G},r}$. The shaded region denotes the total time elapsed between use of R_r in consecutive segments.

what one needs to account for a relay R_r in order to determine the corresponding $T_{\mathcal{G},r}$. For the moment, let us assume that the r^{th} relay is used in every segment[9]. Therefore, the total time elapsed is composed of the following self-explanatory components

$$t_{\text{gap},r} = \underbrace{\sum_{j=r+1}^{L} T^k_{\mathcal{G},r}}_{t^k_{\text{after}}} + T^{k+1}_{\mathcal{G},1} + \underbrace{\sum_{j=2}^{r-1} T^{k+1}_{\mathcal{G},r}}_{t^{k+1}_{\text{before}}} \tag{5.45}$$

where $t^{k+1}_{\text{before}} = 0$ for $r = 2$ and $t^k_{\text{after}} = 0$ for $r = L$. Therefore we obtain the transition probabilities of $T_{\mathcal{G},r},\ r \in \{2, \ldots, L\}$ as follows

$$\Pr(T^{k+1}_{\mathcal{G},r} | T^k_{\mathcal{G},r}) = \begin{cases} \sum_{q=0}^{\text{RESYN}} \sum_{m=0}^{\infty} \Pr(T^{k+1}_{\mathcal{G},r} = n \mid T^{k+1}_{\mathcal{G},1} = m, t^k_{\text{after}} = q), & r = 2 \\ \sum_{p=0}^{\text{RESYN}} \sum_{m=0}^{\infty} \Pr(T^{k+1}_{\mathcal{G},r} = n \mid T^{k+1}_{\mathcal{G},1} = m, t^{k+1}_{\text{before}} = p), & r = L \\ \sum_{q=0}^{\text{RESYN}} \sum_{p=0}^{\text{RESYN}} \sum_{m=0}^{\infty} \Pr(T^{k+1}_{\mathcal{G},r} = n | T^{k+1}_{\mathcal{G},1} = m, t^{k+1}_{\text{before}} = p, t^k_{\text{after}} = q), & r \in (2, L) \end{cases} \tag{5.46}$$

A matrix $\mathbf{\Phi}_r$ with dimensions $(\text{RESYN}+1)\times(\text{RESYN}+1)$ can be constructed again on the lines of $\mathbf{\Phi}_2$ for the 2-relay case, the eigen-decomposition of which gives us the pmf of

[9]The probability of this happening is higher with a lower L and goes down exponentially with increasing number of relays and hence might be an unreasonable assumption for $L \gg 1$. However, we use it here as a first step towards evaluation of $\boldsymbol{P}$ for multiple relays.

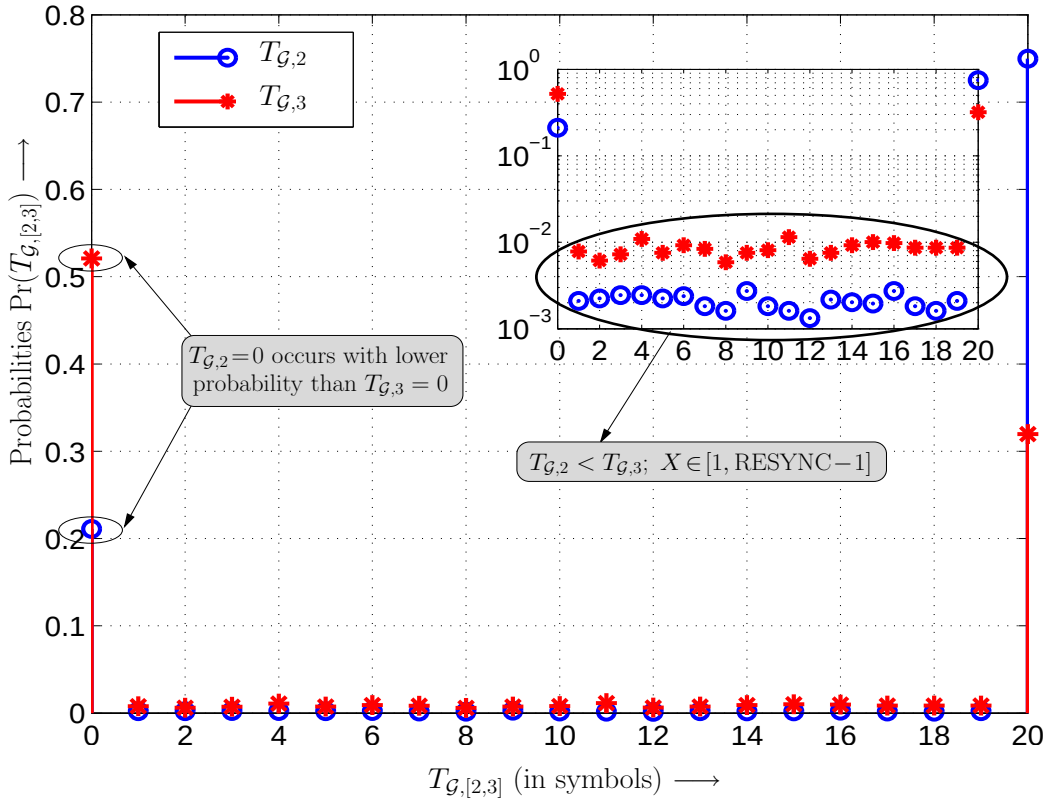

Figure 5.16 — Empirical probability mass function for $T_{\mathcal{G},2}$ and $T_{\mathcal{G},2}$ from simulation with $P_{\mathcal{B}} = 0.1$, $\bar{\mathcal{D}}_{\mathcal{B}} = 40$ symbols, $\text{RESYN} = \bar{\mathcal{D}}_{\mathcal{B}}/2$. .

$T_{\mathcal{G},r}$. However, we concede that, depending on the number of relays, computing (5.46) may turn out to be computationally intensive. Furthermore, there is a possibility that a relay may not be used in a given segment and therefore we will need to account for more than just the previous segment as has been considered so far, to compute $t_{\text{gap},r}$ accurately

Rather than using approximations in computation of $t_{\text{gap},r}$, we adopt a semi-analytical approach, where we obtain the distribution of $T_{\mathcal{G},r}$s using simulations for L parallel Markov chains. Simulation of L parallel Markov chains requires substantially less time than a system wide simulation and can provide empirical pmfs of $T_{\mathcal{G},r}$ that can be made use of in computation of average BERs. We show the results of such an approach in Figure 5.16 for $L = 3$. In particular, Figure 5.16 shows the pmf of $T_{\mathcal{G},2}$ and $T_{\mathcal{G},3}$ for a 3-relay system ($T_{\mathcal{G},1}$ has a distribution similar to that of a 2-relay case and hence

is not shown here). We see a trend similar to the 2-relay case with greater weights concentrated at the boundary values of the pmf. However, there are several notable observations in terms of the relative weights of $T_{\mathcal{G},2}$ and $T_{\mathcal{G},3}$ that are intuitively appealing. We see that $\Pr(T_{\mathcal{G},3}=0) > \Pr(T_{\mathcal{G},2}=0)$, which is reasonable since there would be several instances where $T^k_{\mathcal{G},3}=0$ owing to R_2 being in good state and thus R_3 not being used. Similarly, $T_{\mathcal{G},3}=\text{RESYN}$ only if R_2 is in bad state whenever R_1 passes the token for being in bad state itself, which occurs with lower probability than just R_1 being in bad state and is reflected in $\Pr(T_{\mathcal{G},2}=\text{RESYN}) > \Pr(T_{\mathcal{G},3}=\text{RESYN})$ in Figure 5.16. The above conditions lead to $\Pr(T_{\mathcal{G},3})$ being higher for $T_{\mathcal{G},3} \in \{1,\ldots,\text{RESYN}-1\}$ than $T_{\mathcal{G},2}$ as depicted in the inset figure (logarithmic scale) of Figure 5.16.

We use these pmfs to obtain $\boldsymbol{P}$ for the 3-relay case and the corresponding average BER is obtained by invoking Eqn. (5.43) with $\boldsymbol{E}_2$ replaced by $\boldsymbol{E}_3 = [P_e(\mathcal{G}|1)\ P_e(\mathcal{G}|2)\ P_e(\mathcal{G}|3)]^T$ and $P_{\text{bad}} = \text{P}^3_{\mathcal{B}}$. The semi-analytical results thus obtained for the average BER are plotted in Figure 5.17 for $P_{\mathcal{B}} = [0.1, 0.05]$ to ascertain is applicability to different interference scenarios. While the BER approximations are less tight in the low SNR region, the analytical curves are a fairly accurate for medium-to-high SNRs. For comparison, the corresponding curves for NBR-ONE are also shown. The NBR-WFT aims to be as close as possible to this curve and at the same time decreasing system overheads as far as possible. We next discuss the critical aspect of efficiency that led us to consider NBR-WFT approaches as an improvisation on NBR-ONE.

5.7 Efficiency Analysis

In practice, since receivers and transmitters have to expend energy in order to obtain information related to channel state, the cost of doing so should be optimized as much as possible. To this end, this section, looks into the associated costs in terms of overhead transmissions per symbol for relay selection in presence of interference. For relay selection in an impulsive noise environment one will need updates more often than one

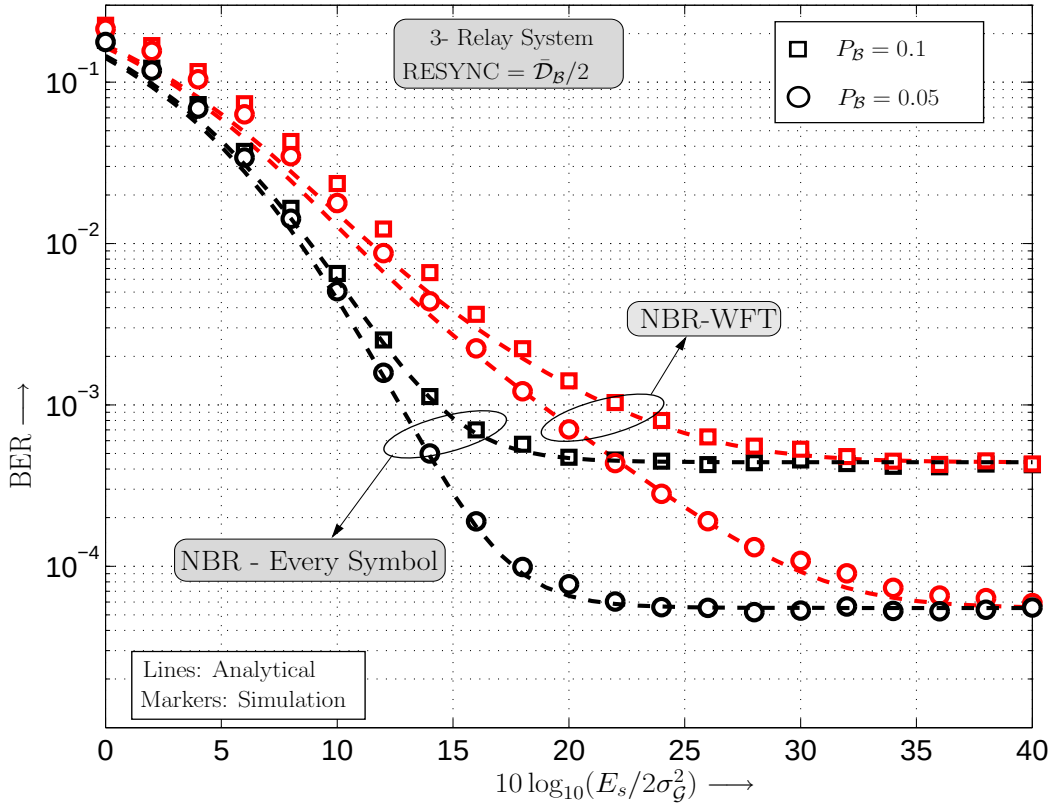

Figure 5.17 — BER vs SNR when using the NBR-Wait-for-T protocol for $L = 3$ relays with analytical results obtained from the simulated distribution of $T_{\mathcal{G}}$s. For 3 relays the distribution of the $T_{\mathcal{G}}$s obtained from independent Markovian behaviour of individual relays is seen to be sufficiently accurate for the purposes of obtaining BERs. Simulation Parameters: $\bar{\gamma}_{\text{SR}} = \bar{\gamma}_{\text{RD}}$, $\bar{\gamma}_{\text{SD}} = \bar{\gamma}_{\text{SR}}/10$, SIR $= -20$ dB, $\bar{\mathcal{D}}_{\mathcal{B}} = 40$ symbols and RESYN $= \bar{\mathcal{D}}_{\mathcal{B}}/2$. Lines: Analytical results. Markers: Simulation.

with AWGN only. We would like to remind the reader that in an interference environment certain amount of overhead is unavoidable either in the form of automatic repeat requests (ARQ) or in providing the system with requisite information regarding the current state of the relays. The NBR strategies proposed in this work need to transmit beacon signals, in addition to the overhead of a conventional selection scheme, for an interfered relay to let the system know its inability to transmit. We argue that such update signals will in itself be of much lesser duration than total time for which actual data is transmitted and make an attempt to quantify the same in the following.

We use the following definition of loss factor in order to account for the overheads

associated with the beacon signals.

Definition : *For a rank based scheme using AF relay transmission the loss factor, η is defined as the ratio of the number of beacon signals (Δ) that are sent per transmitted data symbol. Thus*

$$\eta = \frac{\Delta}{\text{PACKETSIZE}} \tag{5.47}$$

An NBR-WFT scheme for a given $\mathrm{P}_{\mathcal{B}}$ and RESYN *will be considered admissible if $\eta \ll 1$.*

In the following we characterize the efficiency of the proposed algorithms in terms of the loss factor by evaluating η for various system parameters.

5.7.1 Efficiency of NBR-ONE Algorithm

For NBR-ONE, the next best relay is used when the current relay is interfered and for R_r to be used we require $r-1$ beacon signals to be sent on a per symbol basis. The average number of beacon signals sent for an L relay system is, therefore, given by

$$\begin{aligned} \eta &= \sum_{r=2}^{L}(r-1)\mathrm{P}_{\mathcal{B}}^{(r-1)} = \mathrm{P}_{\mathcal{B}}\left[\frac{d}{d\mathrm{P}_{\mathcal{B}}}\left(\sum_{r=2}^{L}\mathrm{P}_{\mathcal{B}}^{(r-1)}\right)\right] \\ &= \left(\frac{\mathrm{P}_{\mathcal{B}}}{1-\mathrm{P}_{\mathcal{B}}^{2}}\right). \end{aligned} \tag{5.48}$$

We see from Eqn. (5.48) the loss factor for the NBR-ONE algorithm is independent of the number of relays used. Additionally the order of η is equal to that of $\mathrm{P}_{\mathcal{B}}$ which is a result that could not have been intuitively predicted as the number of beacon signals increases with an increase in rank of the transmitting relay. Using Eqn. (5.48), the respective system overheads for $\mathrm{P}_{\mathcal{B}} = [0.1, 0.05, 0.01]$ is found to be $\eta = [1.234 \times 10^{-1}, 5.54 \times 10^{-2}, 1.02 \times 10^{-2}]$ respectively. While a 10% increase in system overhead, for example, with $\mathrm{P}_{\mathcal{B}} = 0.1$ may not make NBR-ONE an attractive solution it is encouraging to note that it is constant with L and goes down proportionally with $\mathrm{P}_{\mathcal{B}}$.

5.7.2 Efficiency of NBR-WFT Algorithm

When using NBR-WFT, the number of transmit token handoffs depends on the transition probabilities and RESYN in addition to $P_{\mathcal{B}}$ and L. We note that if relays with $r > 1$ are used for the entire RESYN duration no beacon signal needs to be sent for the last used relay as the up-counter expires at this point and control is automatically restored to R_1. Thus if say K out of L relays were used for a given segment (including the best relay) then only $K-1$ beacon signals need to be transmitted if $T_{\mathcal{G},\text{rest}} = \text{RESYN}$. In all other cases, however, the system needs to account for as many beacon signals as relays in bad state during a segment of transmission. We first consider the 2-relay case as the results can be obtained exactly from expressions derived in Section 5.6.2

2 relays

For $L = 2$, the control switches back and forth between the R_1 and R_2. Two beacon signals are required when the transmit token is passed back to R_1 from R_2 if $T_{\mathcal{G},2} < \text{RESYN}$ whereas only one beacon signal is transmitted when $T_{\mathcal{G},2} = \text{RESYN}$. If $T_{\mathcal{G},1}^{k+1} = m$ and $T_{\mathcal{G},2}^{k+1} = n$ we have for every $m+n$ the following average number of beacon signals per transmitted data symbol

$$\eta_2^{\text{mem}}(n|m) = \begin{cases} \mathcal{E}_{T_{\mathcal{G},2}^k}[\Pr(T_{\mathcal{G},2}^{k+1}=n|T_{\mathcal{G},1}^{k+1}=m, T_{\mathcal{G},2}^k)] \left(\dfrac{2}{m+n+1}\right), & T_{\mathcal{G},2}^k < \text{RESYN} \\ \mathcal{E}_{T_{\mathcal{G},2}}[\Pr(T_{\mathcal{G},2}^{k+1}=n|T_{\mathcal{G},1}^{k+1}=m, T_{\mathcal{G},2}^k)] \left(\dfrac{1}{m+n}\right), & T_{\mathcal{G},2}^k = \text{RESYN} \end{cases} \tag{5.49}$$

where $\mathcal{E}_{T_{\mathcal{G},2}^k}$ denotes statistical expectation with respect to $T_{\mathcal{G},2}^k$ and $\Pr(T_{\mathcal{G},2}^{k+1}=n|T_{\mathcal{G},1}^{k+1}=m, T_{\mathcal{G},2}^k=\ell)$ is given by Eqn. (5.37b).

Multiple Relays

For multiple relays we again use the semi-analytic approach devised in Section 5.6.2 that uses L parallel Markov chains, and obtain η for different L and RESYN values in

RESYN	η = Beacon signals transmitted per symbol		
	$L = 3$	$L = 5$	$L = 7$
$\bar{\mathcal{D}}_{\mathcal{B}}/8$	2.6104×10^{-2}	2.3738×10^{-2}	2.3756×10^{-2}
$\bar{\mathcal{D}}_{\mathcal{B}}/4$	1.5454×10^{-2}	1.2641×10^{-2}	1.2681×10^{-2}
$\bar{\mathcal{D}}_{\mathcal{B}}/2$	1.0343×10^{-2}	7.3296×10^{-3}	7.3893×10^{-3}
$\bar{\mathcal{D}}_{\mathcal{B}}$	7.6926×10^{-3}	4.8518×10^{-3}	4.7397×10^{-3}
$2\bar{\mathcal{D}}_{\mathcal{B}}$	6.6186×10^{-3}	3.7198×10^{-3}	3.7213×10^{-3}
$4\bar{\mathcal{D}}_{\mathcal{B}}$	6.2912×10^{-3}	3.3104×10^{-3}	3.2822×10^{-3}

Table 5.1 — Number of extra beacon signals required per symbol NBR-WFT with varying values of RESYN over an L-relay system with $L = [3, 5, 7]$, $\mathrm{P}_{\mathcal{B}} = 0.1$ and $\bar{\mathcal{D}}_{\mathcal{B}} = 40$ symbols.

Table 5.1 with $\mathrm{P}_{\mathcal{B}} = 0.1$ and $\bar{\mathcal{D}}_{\mathcal{B}} = 40$ symbols. Somewhat predictably we see that with higher values of RESYN we have lower η. However the decrease in η can also be seen to stagnate with higher values of RESYN and also with an increase in number of relays. This leads us to conclude that a moderately high value of RESYN is preferable as we also want to be able to use the best relay as much as we can to keep performance benefits at a maximum. This point will become more clear when we discuss optimal values of RESYN from a BER perspective in the next section. It will be evident that a tradeoff is required in terms of choosing a good value for RESYN as a value that is too low attracts higher overheads but will have better performance and a very high value will imply a degradation in performance. Nonetheless, comparing these values with the corresponding efficiency results of NBR-ONE we see that there is a sharp improvement in η and thus NBR-WFT is much more favorable in terms of overheads, which was our primary motivation for devising such a scheme.

5.7.3 Optimal RESYN

The key parameter in the NBR-WFT protocol is the duration for which the other relays are allowed to transmit, i.e., the value of RESYN. We note that RESYN need

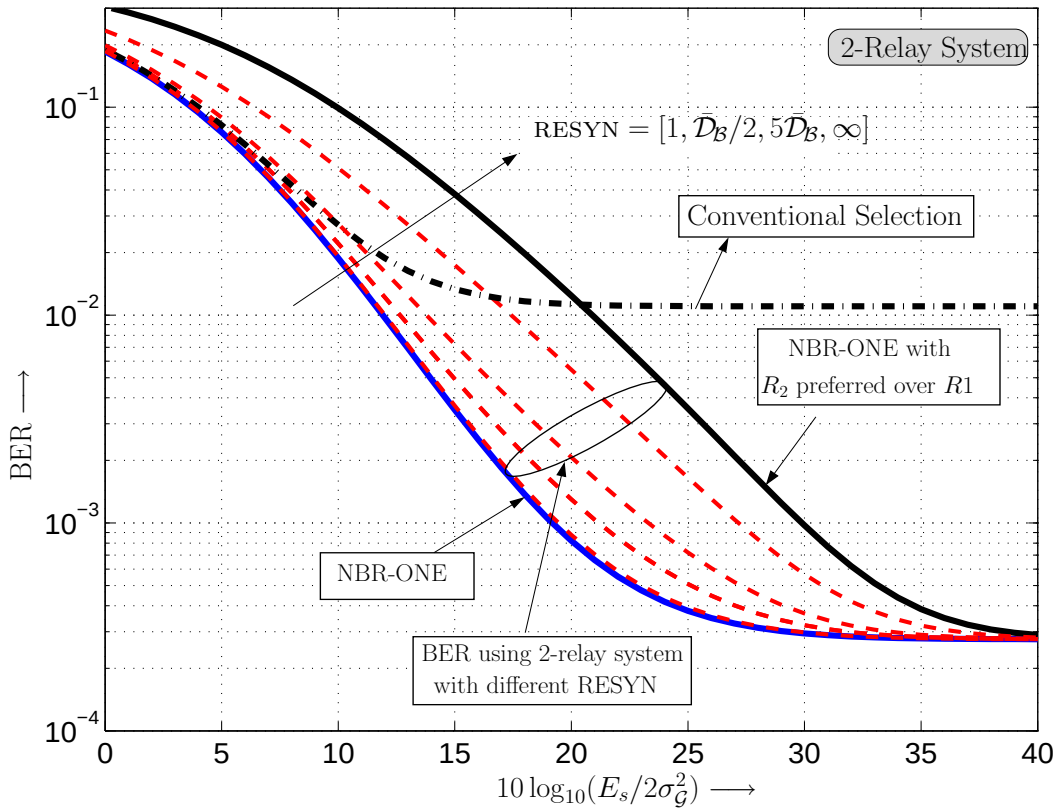

Figure 5.18 — Effect of the value of RESYN on the performance of NBR-WFT algorithm for a 2-relay system. The two extreme cases are the the use of either R_1 or R_2 only for the entire transmit duration (solid lines). Intermediate curves denote application of the NBR-WFT approach with varying values of RESYN. System Parameters: $\bar{\mathcal{D}}_{\mathcal{B}} = 40$ symbols, SIR $= -20$ dB, $\bar{\gamma}_{\mathrm{SR}} = \bar{\gamma}_{\mathrm{RD}} = 10\bar{\gamma}_{\mathrm{SD}}$ and $\mathrm{P}_{\mathcal{B}} = 0.025$.

not be arbitrarily large as the other relays are susceptible to interference as well and the system would end up switching back to the best relay before RESYN symbols for most cases if it is set too large. On the other hand setting RESYN too small will be counterproductive as it would lead to multiple switches and to keep the overheads at a minimum we would like to avoid that. For the exemplary case of a 2-relay system we present variation of BER with RESYN in Figure 5.18 where the BERs are obtained by employing the analytical methods of Section 5.6.2. We present results for NBR-ONE (solid lines) for comparison and also, for an inverse NBR-ONE approach that selects R_2 over R_1 such that R_1 transmits only when R_2 is interfered. The inverse NBR-ONE approach constitutes the other end of the performance spectrum. With values

of RESYN $= [1, \bar{\mathcal{D}}_{\mathcal{B}}/2, 5\bar{\mathcal{D}}_{\mathcal{B}}, \infty]$ we see that the performance degrades progressively with higher RESYN approaching that of inverse NBR-ONE. However, it is encouraging to note that upto $5\bar{\mathcal{D}}_{\mathcal{B}}$ the degradation is not substantial. This implies that RESYN does not have to be close to 1 and can in fact be upto several times $\bar{\mathcal{D}}_{\mathcal{B}}$ for only a graceful degradation in BERs. We acknowledge that this is again dependent on $\mathrm{P}_{\mathcal{B}}$ and L as well, however, we have found through exhaustive simulative evidence for a range of $\mathrm{P}_{\mathcal{B}}$ and $L < 10$ this holds more or less true. Thus a recommended value of RESYN would be to not exceed $5\bar{\mathcal{D}}_{\mathcal{B}}$ and the lower limit would depend on the overheads that the system can afford without loosing discernible efficiency.

Also note that when the links are of comparable quality (similar average SNR), it is more important to use a non-interfered link than to use one with the best end-to-end channel as depicted by the curve for conventional selection in Figure 5.18 (from analytical results of Section 5.5.3). This has important implications from a design perspective as it allows to prioritize objectives.

5.8 Conclusions

In this chapter, we considered the use of multiple cooperating nodes/users to enable the use of spatial diversity in wireless communication environments where the nodes are restricted to the use of only one antenna. We propose and analyze approaches of implementing cooperative diversity schemes when the cooperating relays are affected by interference phenomena that occurs intermittently and thus has certain temporal structure. We specifically consider the effect that such strong interference has on the overall bit error rate and outage probability when conventional relay selection is used in order to use only the *best* relay amongst the available relays and propose an improved approach to relay selection, the NBR approach, based on choosing the M^{th} best relay in a pool of L relays. Two flavors of the algorithm, NBR-ONE and NBR-WFT are presented that re-evaluate the interference state of relays every symbol, and after

RESYN symbols respectively. While the NBR-ONE exhibits excellent gains when the best relay, according to conventional criterion, suffers from interference it may incur higher overheads. NBR-WFT uses the memory in the interference process to reduce these overheads. The design parameter RESYN for NBR-WFT represents a trade-off in performance versus transmission efficiency. Analytical and semi-analytical approaches are developed to analyze the performance of both NBR-ONE and NBR-WFT algorithms and the results show convincing match with a system-level simulation. These analytical approaches are further employed to obtain efficiency results and its implications on the optimal value of RESYN. We show that for several cases of interest the additional overhead is only nominal and is directly proportional to the probability of interference at the relays.

CHAPTER 6

Summary of Thesis and Future Work

In this chapter we briefly recapitulate the work done in this thesis and focus on the primary learnings during the course of the work. In the latter half of the chapter we also mention some of the possible lines of extension of the work presented here that either builds on the previous chapters or can be analyzed using the same lines of thought as have been pursued in this thesis.

6.1 Summary of Results

We have considered the design of receivers for transmission environments where the noise cannot be characterized faithfully by only a Gaussian process due to its impulse-like behaviour and various heavy-tailed distributions are better suited to describe such

noise. As can be expected, traditional receivers that were designed for mitigation of Gaussian noise exhibit relatively poor performance when the noise distribution deviates from this assumption, rendering them non-robust. Additionally since interference occurs in burst on several occasions there may be inherent memory in the interfering signals. We addressed the two issues of non-Gaussianity and memory for various communication environments by proposing receivers structures that have varied levels of success in mitigating the effects of both. In particular, Chapter 2 considered robust receiver designs that are applied to a convolutionally coded system that is impaired by non-Gaussian noise that has memory. As a popular technique, a first order Markov chain models the memory in the impairments. The proposed receivers are shown to be much more successful in increasing the reliability of transmitted information than conventional detection. Subsequently a general analytical technique is developed for these receivers that incorporate the effect of non-ideal interleaving on receiver performance in terms of BER and cutoff rate. The contributions of this chapter include novel uni-parametric detectors, namely, the α-penalty function detector and the Huber penalty function detector that closely approach the performance of a hypothetical ideal detector, along with detailed insights into effects of memory on receiver performance.

We then considered a scenario where the parameters associated with a noise environment with memory is unavailable at the receiver and how such knowledge could greatly enhance the overall throughput of the system in Chapter 3. As a pertinent technology that hinges on the principles of estimation, cognitive radio is chosen to exemplify the benefits of such an approach. A solution to the estimation problem is proposed under the constraint that no pilot symbols may be used for training with respect to the noise state. The proposed algorithm is shown to be an effective way of determining the statistical parameters of the noise when the receiver has very limited information about it. We showed that the knowledge of such information is crucial to successful decoding at the receiver and that the memory in the process plays a central role in determining

the effectiveness of the algorithm. Its application to CR environments may thus help provide substantial benefits in meeting design goals.

In Chapter 4, we analyzed multiple user communication in contemporary communications technology that transmits data using pulses with large bandwidths and very low energy. Both features make the task of communicating in presence of multiple users severely challenging. We address the impulsive nature of MUI in IR-UWB systems by proposing several robust receivers that were seen to operate with greater levels of success in transmitting data than the conventional matched filter detector. The superiority of the proposed detectors is attributed to their innate capability to handle noise that has distributions with heavy tails. We further developed extensive semi-analytic expressions for theoretical analysis of the detectors for an AWGN environment. Given the elaborate frame structure of the IEEE 802.15.4a transmission frame, the analysis in itself can be seen to be fairly involved. We, however, have invoked assumptions to provide various levels of simplification to the analytic expressions and their evaluation without severely compromising on the accuracy of the analysis. A thorough discussion of the various detectors through simulative and analytic results follows and the validity of the various approximations provided earlier is examined. We also provide results for realistic IEEE 802.15.4a channels with multipath fading and show that the detectors are similarly useful in dense multipath environments.

The case of spatial diversity through cooperation is considered in Chapter 5, where we focus on cooperation by selection when the relays face strong interference intermittently. The role of interference in selection of relays is highlighted and we motivate the need for improvisations of conventional relay selection techniques to cater to an interference limited environment. We proposed relay selection techniques that have two key underpinnings: order statistics and interference avoidance. Rather than continuing to use the best relay out of a pool of relays regardless of the amount of interference at the relay, we acknowledge it and propose algorithms that allow an interfered relay to be

excused from transmission. We again take advantage of the memory in the interference to devise tradeoffs in terms of receiver performance versus complexity and provide analytical methods to understand the same. The systems designer is provided with several tools that can allow for an informed decision depending on permitted complexity limits.

6.2 Future Work

There are several communication environments that have to contend with the vagaries of the various RF impairments and as has been recognized by many researchers, noise is practical communication systems is seldom white or Gaussian. In such cases, considering the true nature of the impairments can lead to receiver designs that outperform conventional receivers designed under a Gaussian assumption. We have made an effort to address this issue for several cases in this thesis, nonetheless, there exist open problems and extensions to the work presented in this thesis that can help us understand specific communication environments better.

While we only considered convolutional codes for a coded system design, there is a lot of focus on the use of capacity achieving codes such as turbo codes and LDPC codes for future communication system. The performance gains that can be achieved using such codes would require careful attention to the specifics of iterative decoding and is thus of interest. Furthermore, most of our work, except for Chapter 4, has ignored the frequency selectivity of the channel and the applicability of the techniques to broadband communication systems, which is currently garnering a lot of attention. Incorporating such effects in the analytical techniques of this thesis can further improve its utility for system designers. In Chapter 5, we focussed on temporal correlation of the interference at individual relays. There may further be spatial correlation in the interference which will lead to a joint density function that is multivariate. Moreover, a system model with multiple sources and destinations can be envisaged transforming the problem into a multipoint to multipoint communication scenario which is more general than the

scenario we considered. Such a system model can present several challenging design issues such as scheduling of information through the relays to both avoid interference and provide adequate opportunities of transmission to each SD pair. Thus there can be several communication scenarios where a generalized solution is required and we hope that subsequent research will benefit from the contributions of our work.

Bibliography

[1] M. Zimmermann and K. Dostert, "Analysis and Modeling of Impulsive Noise in Broadband Powerline Communications," *IEEE Trans. Electromagn. Compat.*, vol. 44, no. 1, pp. 249–258, Feb. 2002.

[2] M. K. Simon and M.-S. Alouini, *Digital Communication over Fading Channels*. Wiley-IEEE Press, 2000.

[3] K. Blackard and T. R. C. Bostian, "Measurements and models of radio frequency impulsive noise for indoor wireless communications," *IEEE J. Select. Areas Commun.*, vol. 11, no. 7, pp. 991–1001, Sept. 1993.

[4] W. Henkel, T. Kessler, and H. Chung, "Coded 64-CAP ADSL in an impulse-noise environment — Modeling of impulse noise and first simulation results," *IEEE J. Select. Areas Commun.*, vol. 13, no. 9, pp. 1611–1621, Dec. 1995.

[5] T. Blankenship, D. M. Krizman, and T. S. Rappaport, "Measurements and Simulation of Radio Frequency Impulsive Noise in Hospitals and Clinics," in *Proc. of IEEE VTC*, vol. 3, May 1997, pp. 1942 – 1946.

[6] P. Cardieri and T. Rappaport, "Statitistical analysis of co-channel interference in wireless communication systems," *Wireless Communication and Mobile Computing*, vol. 1, no. 1, pp. 111 – 121, Jan-March 2001.

[7] M. Zimmermann and K. Dostert, "Analysis and modeling of impulsive noise in broad-band powerline communications," *IEEE Trans. Electromagn. Compat.*, vol. 44, no. 1, pp. 249–258, Feb. 2002.

[8] A. Nasri, R. Schober, and L. Lampe, "Analysis of Narrowband Communication Systems Impaired by MB-OFDM UWB Interference," *IEEE Trans. Wireless Commun.*, vol. 6, no. 11, pp. 4090–4100, Nov. 2007.

[9] K. Kim and G. Shevlyakov, "Why Gaussianity?" *IEEE Signal Processing Mag.*, pp. 102–113, March 2008.

[10] S. Kassam, *Signal Detection in Non-Gaussian Noise*. Berlin: Springer Verlag, 1988.

[11] D. Middleton, "Canonical and Quasicanocial Probability Models of Class-A interference," *IEEE Trans. Electromagn. Compat.*, vol. 25, pp. 76–106, May 1983.

[12] L. Berry, "Understanding Middleton's canonical formula for class-A noise," *IEEE Trans. Electromagn. Compat.*, vol. 23, pp. 337–344, Nov. 1981.

[13] D. Middleton, "Non-Gaussian Noise Models in Signal Processing for Telecommunications: New Methods and Results for Class A and Class B Noise models," *IEEE Trans. Inform. Theory*, vol. 45, no. 4, pp. 1129–1149, May 1999.

[14] K. Vastola, "Threshold Detection in Narrow-band non-Gaussian noise," *IEEE Trans. Commun.*, vol. 32, no. 2, pp. 134–139, Feb. 1984.

[15] S. Kosmopoulos, P. Mathiopoulos, and M. Gouta, "Fourier-Bessel error performance analysis and evaluation of M-ary QAM schemes in an impulsive noise environment," *IEEE Trans. Commun.*, vol. 39, no. 3, pp. 398–404, Mar. 1991.

[16] M. Ghosh, "Analysis of the Effect of Impulse Noise on Multicarrier and Single Carrier QAM Systems," *IEEE Trans. Commun.*, vol. 44, no. 2, pp. 145–147, Feb. 1996.

[17] R. Blum, R. Kozick, and B. Sadler, "An adaptive signal diversity receiver for non-Gaussian interference and noise," *IEEE Trans. Signal Processing*, vol. 47, no. 8, pp. 2100–2111, Aug. 1999.

[18] X. Wang and V. Poor, "Robust multiuser detection in non-Gaussian channels," *IEEE Trans. Signal Processing*, vol. 47, no. 2, pp. 289–305, Feb. 1999.

[19] H. V. Poor and M. Tanda, "Multiuser Detection in Flat Fading Non-Gaussian Channels," *IEEE Trans. Commun.*, vol. 50, no. 11, pp. 1769–1777, Nov. 2002.

[20] R. Pighi, M. Franceschini, G. Ferrari, and R. Raheli, "Fundamental Performance Limits for PLC Systems Impaired by Impulse Noise," in *IEEE Intl. Symp. on Power Line Commun. and Its Appl.*, Orlando, FL, Mar. 2006.

[21] M. Shao and C. Nikias, "Signal Processing with Fractional Lower Order Moments: Stable processes and Their Applications," *Proc. IEEE*, vol. 81, no. 7, pp. 986–1010, July 1993.

[22] C. Nikias and M. Shao, *Signal processing with alpha-stable distributions and applications*. New York: John Wiley & Sons, Inc., 1995.

[23] J. Ilow and D. Hatzinakos, "Analytical Alpha-Stable Noise Modeling in a Poission Field of Interferrers or Scatterers," *IEEE Trans. Signal Processing*, vol. 46, no. 6, pp. 1601–1611, June 1998.

[24] T. M. Cover and J. A. Thomas, *Elements of Information Theory*. New York: Wiley, 1991.

[25] S. Shamai and S. Verdu, "Worst Case Power Constrained Noise for Binary Input Channels," *IEEE Trans. Commun.*, vol. 38, no. 5, pp. 1494–1511, Sept. 1992.

[26] M. Mushkin and I. Bar-David, " Capacity and Coding for Gilbert-Elliot Channels ," *IEEE Trans. Inform. Theory*, vol. 35, pp. 1277 – 1290, November 1989.

[27] L. Wilhelmsson and L. Milstein, "On the Effect of Imperfect Intleaving for the Gilbert-Elliott channel," *IEEE Trans. Commun.*, vol. 47, no. 5, pp. 681–688, May 1999.

[28] J. García-Frías and J. D. Villasenor, "Turbo Decoding of Gilbert-Elliot Channels," *IEEE Trans. Commun.*, vol. 50, no. 3, pp. 357 – 363, March 2002.

[29] X. Hong, Z. Chen, C.-X. Wang, S. A. Vorobyov, and J. S. Thompson, "Cognitive Radio Networks: Interference Cancellation and Management Techniques," *IEEE Vehic. Tech. Magazine*, pp. 76–84, December 2009.

[30] X. Hong, C.-X. Wang, and J. Thompson, "Interference Modeling of Cognitive Radio Networks," in *Proc. of IEEE VTC*, May 2008, pp. 1851–1855.

[31] J. Zhang, P. Orlik, Z. Sahinoglu, A. F. Molisch, and P. Kinney, "UWB Systems for Wireless Sensor Networks," *Proc. IEEE*, vol. 97, no. 2, pp. 313–331, Feb. 2009.

[32] M. Win and R. A. Scholtz, "Impulse Radio: How it Works," *IEEE Commun. Lett.*, vol. 2, no. 2, pp. 36–38, Feb. 1998.

[33] R. A. Scholtz, "Multiple-Access with Time Hopping Impulse Modulation ," in *Proc. of IEEE MILCOM*, Boston, MA, USA, Oct. 1993, pp. 447–450.

[34] A. R. Forouzan, M. Nasiri-Kenari, and J. A. Salehi, "Performance Analysis of Time-Hopping Spread-Spectrum Multiple- Access Systems: Uncoded and Coded Schemes," *IEEE Trans. Wireless Commun.*, vol. 1, no. 4, pp. 671–681, Oct. 2002.

[35] A. Sendonaris, E. Erkip, and B. Aazhang, "User Cooperation Diversity – Part I : System Description ," *IEEE Trans. Commun.*, pp. 1927–1938, November 2003.

[36] J. N. Laneman, D. N. C. Tse, and G. W. Wornell, "Cooperative Diversity in Wireless Networks: Efficient Protocols and Outage Behavior," *IEEE Trans. Inform. Theory*, vol. 50, no. 12, pp. 2062–3080, December 2004.

[37] M. Flury and J.-Y. Le Boudec, "Interference Mitigation by Statistical Interference Modeling in an Impulse Radio UWB Receiver," in *Proc. of IEEE ICUWB*, Waltham, MA, Sept. 2006, pp. 393–398.

[38] J.-W. Moon, T. Wong, and J. Shea, "Pilot-assisted and Blind Joint Data Detection and Channel Estimation in Partial-time Jamming," *IEEE Trans. Commun.*, vol. 54, no. 11, pp. 2092–2102, Nov. 2006.

[39] S. Miyamoto, M. Katayama, and N. Morinaga, "Performance Analysis of QAM Systems under Class A Impulsive Noise Environment," *IEEE Trans. Electromagn. Compat.*, vol. 37, no. 2, pp. 260–267, May 1995.

[40] J. Häring and A. Vinck, "Performance bounds for optimum and suboptimum reception under Class-A impulsive noise," *IEEE Trans. Commun.*, vol. 50, no. 7, pp. 1130–1136, July 2002.

[41] D. Fertonani and G. Colavolpe, "Theoretical Limits and Practical Detection Schemes for Markovian-Gaussian channels," in *Proc. of IEEE ICC*, May 2008.

[42] A. W. Eckford, F. R. Kschischang, and S. Pasupathy, "Analysis of Low-density Parity-check Codes for the Gilbert-Elliott Channel," *IEEE Trans. Inform. Theory*, vol. 51, no. 11, pp. 3872 – 3889, November 2005.

[43] C. Pimentel, "Generating Series and Performance Bounds for Convolutional Codes Over Burst-Error Channels," *IEEE Trans. Veh. Technol.*, vol. 51, no. 5, pp. 1011–1017, Sept. 2002.

[44] T. Li, W. Mow, and M. Siu, "A Joint Approach to Erasure Marking and Viterbi decoding for Impulsive Noise Channels," in *4th IEEE Workshop on Signal Processing Advances in Wireless Communications (SPAWC)*, June 2003, pp. 180–184.

[45] R. Schober and L. Lampe, "Sequence detection and adaptive channel estimation for ISI channels under class-A impulsive noise," *IEEE Trans. Commun.*, vol. 52, pp. 1523–1531, Sept. 2004.

[46] P. Delaney, "Signal Detection in Multivariate Class-A interference," *IEEE Trans. Commun.*, vol. 43, no. 2/3/4, pp. 365–373, Feb./Mar./Apr. 1995.

[47] A. Viterbi and J. Omura, *Principles of Digital Communication and Coding.* New York: McGraw–Hill, 1979.

[48] D. Sargrad and J. Modestino, "Errors-and-erasures Coding to Combat Impulse Noise on digital Subscriber Loops," *IEEE Trans. Commun.*, vol. 38, no. 8, pp. 1145–1155, Aug. 1990.

[49] B. Seyfe and S. Valaee, "A New Choice of Penalty Function for Robust Multiuser detection based on M-estimation," *IEEE Trans. Commun.*, vol. 53, no. 2, pp. 224–227, Feb. 2005.

[50] M. Abramowitz and I. Stegun, *Handbook of Mathematical Functions*. New York: Dover Publications, 1972.

[51] E. Biglieri, G. Caire, G. Taricco, and J. Ventura-Traveset, "Computing Error Probabilities over Fading Channels: A Unified Approach," *Europ. Trans. Telecom.*, vol. 9, pp. 15–25, Jan./Feb. 1998.

[52] D. Rainish and J. M. Perl, "Generalized Cutoff Rate of Time and Frequency-Selective Fading Channels," *IEEE Trans. Commun.*, vol. 37, no. 5, pp. 449 – 467, May 1989.

[53] C. Schlegel and D. Costello, Jr., "Bandwidth Efficient Coding for Fading Channels: Code Construction and Performance Analysis," *IEEE J. Select. Areas Commun.*, vol. 7, no. 9, pp. 1356–1368, Dec. 1989.

[54] E. Malkamäki and H. Leib, "Coded Diversity on Block Fading Channels," *IEEE Trans. Inform. Theory*, vol. 45, no. 2, pp. 771–782, Mar. 1999.

[55] R. Gallager, *Information Theory and Reliable Communication*. New York: John Wiley & Sons, Inc., 1968.

[56] S. Boyd and L. Vandenberghe, *Convex Optimization*. Cambridge, UK: Cambridge University Press, 2005.

[57] R. McEliece and W. Stark, "Channels with Block Interference," *IEEE Trans. Inform. Theory*, vol. 30, no. 1, pp. 44 – 53, January 1984.

[58] E. Biglieri, "Coding and Modulation for a Horrible Channel," *IEEE Commun. Mag.*, vol. 41, no. 5, pp. 92 – 98, May 2003.

[59] M. Chan and R. Donaldson, "Amplitude, Width and Interarrival Distribution for Noise Impulses on Intrabuilding PLC Networks," *IEEE Trans. Electromagn. Compat.*, vol. 31, pp. 320–323, Aug. 1989.

[60] V. Degardin, M. Lienard, A. Zeddam, F. Gauthier, and P. Degauque, "Classification and Characterization of Impulsive Noise on Indoor Powerline used for Data Communications," *IEEE Trans. Consumer Electron.*, vol. 48, no. 4, pp. 913–918, Nov. 2002.

[61] M. Katayama, T. Yamazato, and H. Okada, "A Mathematical Model of Noise in Narrowband PowerLine Communication Systems," *IEEE J. Select. Areas Commun.*, pp. 1267–1276, July 2006.

[62] B. D. Fritchman, "A Binary Channel Characterization Using Partitioned Markov Chains," *IEEE Trans. Inform. Theory*, vol. 13, no. 2, pp. 221–227, April 1967.

[63] S. Tsai, "Evaluation of Burst Error Correcting Codes Using a Simple Partitioned Markov Chain Model," *IEEE Trans. Commun.*, pp. 1031–1034, Sept. 1973.

[64] C. Pimentel and I. F. Blake, "Modeling Burst Channels Using Partitioned Fritchman's Markov Models," *IEEE Trans. Veh. Technol.*, vol. 47, no. 3, pp. 885–899, August 1998.

[65] J. L. Rebelatto, R. D. Souza, and M. E. Pellenz, "On the Performance of Turbo Codes in the Presence of Typical Powerline Asynchronous Impulsive Noise," in *Proc. of IEEE Conf. on Networks*, Nov. 2005, pp. 797–801.

[66] W. Turin, *Performance Analysis and Modeling of Digital Transmission Systems*. New York: Kluwer Academic Publishers, 2004.

[67] R. Gallager, *Information Theory and Reliable Communication*. John Wiley and Sons, 1968.

[68] D. Umehara, H. Yamaguchi, and Y. Morihiro, "Turbo Decoding in Impulsive Noise Environment," in *Proc. of IEEE GLOBECOM*, Dallas, Nov./Dec. 2004, pp. 194–198.

[69] M. Zorzi, "Minimum Duration Outages in Markov Channels," in *Proc. of ICUPC*, Oct. 1997.

[70] FCC, "Spectrum Policy Task Force, Tech. Rep. ET Docket no. 02-135, Nov. 2002.

[71] A. Petrin and P. G. Steffes, "Measurement and Analysis of Urban Spectrum Usage," in *Proc. of ISART*, 2004.

[72] I. F. Akyildiz, W. Y. Lee, M. C. Vuran, and S. Mohanty, "NeXt Generation/dynamic Spectrum Access/cognitive radio wireless networks: A Survey," *Computer Networks*, vol. 50, no. 13, pp. 2127–2159, Sept. 2006.

[73] Q. Zhao and B. M. Sadler, "A survey of dynamic spectrum access," *IEEE Signal Processing Mag.*, no. 3, pp. 79–89, May 2007.

[74] X. Hong, C.-X. Wang, H.-H. Chen, and Y. Zhang, "Secondary Spectrum Access Networks," *IEEE Vehic. Tech. Magazine*, vol. 4, no. 2, pp. 36–43, June 2009.

[75] S. Haykin, "Cognitive Radio: Brain-Empowered Wireless Communication," *IEEE J. Select. Areas Commun.*, vol. 23, no. 2, pp. 201–220, Feb. 2005.

[76] R. Tandra and A. Sahai, "SNR Walls for Signal Detection," *IEEE Jour. Sel. Topics in Sig. Proc.*, vol. 2, no. 1, pp. 4–17, February 2008.

[77] E. Adamopoulou, K. Demestichas, and M. Theologou, "Enhanced Estimation of Congfiguration Capabilities of Cognitive Radio," *IEEE Commun. Mag.*, pp. 56–63, April 2008.

[78] J. Bater, H.-P. Tan, K. N. Brown, and L. Doyle, "Modeling Interference Temperature Constraints for Spectrum Access in Cognitive Radio Networks," in *Proc. of IEEE ICC*, 2007, pp. 6493–6498.

[79] N. Devroye, P. Mitran, and V. Tarokh, "Achievable Rates in Cognitive Radio Channels," *IEEE Trans. Inform. Theory*, vol. 52, no. 5, pp. 1813–1827, May 2006.

[80] A. Somekh-Baruch, S. Shamai, and S. Verdu, "Cognitive Interference Channels with State Information," in *Proc. of Inter. Symposium on Information Theory (ISIT)*, July 2008, pp. 1353–1357.

[81] D. Cabric, S. M. Mishra, and R. W. Brodersen, "Implementation Issues in Spectrum Sensing for Cognitive Radios," in *Proc. of 38th Asilomar Conf.*, 2004, pp. 772–776.

[82] D. Cabric and R. W. Brodersen, "Physical Layer Design Issues Unique to Cognitive Radio Systems," in *Proc. of PIMRC*, 2005, pp. 759–763.

[83] R. Tandra, S. M. Mishra, and A. Sahai, "What is a Spectrum Hole and What Does it Take to Recognize One," *Proc. IEEE*, vol. 97, no. 5, pp. 824–848, May 2009.

[84] P. C. Pinto and M. Z. Win, "Communication in a Poisson Field of Interferers," in *Proc. of Conference on Information Sciences and Systems (CISS)*, March 2006, pp. 432–437.

[85] G. Colavolpe, G. Ferrari, and R. Raheli, "Extrinsic Information in Iterative Decoding: A Unified View," *IEEE Trans. Commun.*, vol. 49, pp. 2088–2094, Dec. 2001.

[86] L. R. Bahl, J. Cocke, F. Jelinek, and J. Raviv, "Optimal Decoding of Linear Codes for Minimizing Symbol Error Rate," *IEEE Trans. Inform. Theory*, pp. 284–287, March 1974.

[87] D. R. Pauluzzi and N. C. Beaulieu, "A Comparison of SNR Estimation Techniques for the AWGN Channel," *IEEE Trans. Commun.*, vol. 48, pp. 1681–1691, Oct. 2000.

[88] R. Menon, R. M. Buerher, and J. H. Reed, "Outage Probability based Comparison of Underlay and Overlay Spectrum Sharing Techniques," in *Proc. of IEEE DySPAN*, Baltimore, USA, Nov. 2005, pp. 101–109.

[89] X. Yang and A. P. Petropulu, "Co-Channel Interference Modeling and Analysis in a Poisson Field of Interferers in Wireless Communications," *IEEE Trans. Signal Processing*, vol. 51, pp. 64–76, Jan. 2003.

[90] J. Bilmes, "A Gentle Tutorial on the EM Algorithm and its Application to Parameter Estimation for Gaussian Mixture and Hidden Markov Models," 1997.

[91] H. V. Poor, *An Introduction to Signal Detection and Estimation*, 2nd ed. Springer, 1994.

[92] J.-W. Moon, T. F. Wong, and J. M. Shea, "Pilot-Assisted and Blind Joint Data Detection and Channel Estimation in Partial-Time Jamming," *IEEE Trans. Commun.*, vol. 54, no. 11, pp. 2092 – 2102, Nov. 2006.

[93] A. Sahai, R. Tandra, S. Mishra, and N. Hoven, "Fundamental Design Tradeoffs in Cognitive Radio Systems," in *Proc. of TAPAS*, 2006.

[94] P. Huber, *Robust Statistics*. New York: John Wiley & Sons, Inc., 1981.

[95] E. Jondeau, S.-H. Poon, and M. Rockinger, *Financial Modeling under Non-Gaussian Distributions*. London: Springer, 2007.

[96] A. Papoulis, *Probability, Random Variables and Stochastic Processes*. New York,NY: McGraw-Hill, 1991.

[97] T. S. Rappaport, *Wireless Communications: Principles and Practice*, 2nd ed. Singapore: Pearson Education, 2002.

[98] S. ten Brink, "Convergence Behaviour of Iteratively Decoded Parallel Concatenated Codes," *IEEE Trans. Commun.*, vol. 49, pp. 1727–1737, Oct. 2001.

[99] M. Z. Win and R. A. Scholtz, "Ultra-Wide Bandwidth Time-Hopping Spread-Spectrum Impulse Radio for Wireless Multiple-Access Communications," *IEEE Trans. Commun.*, vol. 48, no. 4, pp. 679–691, Apr. 2000.

[100] G. Durisi and G. Romano, "On the Validity of Gaussian Approximation to Characterize the Multiuser Capacity of UWB TH PPM," in *Proc. of IEEE ICUWB*, Baltimore, USA, 2002, pp. 157–161.

[101] G. Durisi and S. Benedetto, "Performance Evaluation of TH-PPM UWB Systems in the Presence of Multiuser Interference," *IEEE Commun. Lett.*, vol. 7, no. 5, pp. 224–226, May 2003.

[102] M. Sabattini, E. Masry, and L. Milstein, "A Non-Gaussian Approach to the Performance Analysis of UWB TH-BPPM Systems," in *Proc. of IEEE ICUWB*, Reston,VA, USA, Nov. 2003.

[103] B. Hu and N. C. Beaulieu, "Accurate Evaluation of Multiple-Access Performance in TH-PPM and TH-BPSK UWB Systems," *IEEE Trans. Commun.*, vol. 52, no. 10, pp. 1758–1766, Oct. 2004.

[104] ——, "Accurate Performance Evaluation of Time Hopping and Direct-Sequence UWB Systems in Multi-User Interference," *IEEE Trans. Commun.*, vol. 53, no. 6, pp. 671–681, June 2005.

[105] V. Cellini and G. Donà, "A Novel Joint Channel and Multi-User Interference Statistics Estimator for UWB-IR based on Gaussian Mixture Model," in *Proc. of IEEE ICUWB*, Zurich, Switzerland, Sept. 2005, pp. 655–660.

[106] Y. Dhibi and T. Kaiser, "On the Impulsiveness of Multiuser Interferences in TH-PPM UWB Systems," *IEEE Trans. Signal Processing*, vol. 54, no. 6, pp. 2853–2857, July 2006.

[107] N. C. Beaulieu and B. Hu, "A Soft-Limiting Receiver Structure for Time-Hopping UWB in Multiple Access Interference," in *Proc. of IEEE ISSSTA*, Manaus, Brazil, Aug. 2006.

[108] ——, "An Adaptive Threshold Soft-Limiting UWB Receiver with Improved Performance in Multiuser Interference," in *Proc. of IEEE ICUWB*, Waltham, MA, USA, Sept. 2006, pp. 405–410.

[109] J. Fiorina, "A Simple IR-UWB Receiver Adapted to Multi-User Interferences," in *Proc. of IEEE GLOBECOM*, Nov.-Dec. 2006.

[110] V. Cellini, "A Robust Detection Scheme for UWB Systems in Impulsive Multi-User Interference," in *Workshop on Wireless Reconfigurable Terminals and Platforms*, Rome, Italy, Apr. 2006.

[111] T. Erseghe, V. Cellini, and G. Donà, "UWB Impulse Radio Receivers Derived From a Gaussian Mixture Interference Model," in *Proc. of IEEE ICC*, Glasgow, June 2007.

[112] T. Erseghe, "A Low-Complexity Impulse Radio Receiver Based upon Gaussian Mixtures," in *Proc. of IEEE ICC*, Glasgow, June 2007.

[113] M. Flury and J.-Y. L. Boudec, "Interference Mitigation by Statistical Interference Modeling in an Impulse Radio UWB Receiver ," in *Proc. of IEEE ICUWB*, Sept. 2006, pp. 393–398.

[114] B. Kim, J. Bae, I. Song, S. Kim, and H. Kwon, "A Comparative Analysis of Optimum and Suboptimum Rake Receivers in Impulsive UWB Environment," *IEEE Trans. Veh. Technol.*, vol. 55, pp. 1797–1804, Nov. 2006.

[115] F. D. Cassioli, M.Z.Win and A. Molisch, "Performance of low-complexity RAKE reception in a realistic UWB channel," in *Proc. of IEEE ICC*, New York City, USA, Apr.-May 2002, pp. 763–767.

[116] H. Arsalan, Z. N. Chen, and M.-G. diBenedetto, *Ultra Wideband Wireless Communication.* New Jersey, USA: Wiley-Interscience, 2006.

[117] X. Wang and H. Poor, "Robust Multiuser Detection in Non-Gaussian Channels," *IEEE Trans. Wireless Commun.*, vol. 47, no. 2, pp. 289–305, Feb. 1999.

[118] B. Seyfe and S. Valaee, "A New Choice of Penalty Function for Robust Multiuser Detection based on M-Estimation," *IEEE Trans. Commun.*, vol. 53, no. 2, pp. 224–227, Feb. 2005.

[119] J. Mitra and L. Lampe, "Robust Detectors for TH-IR UWB with Multiuser Interference," in *Proc. of IEEE ICUWB*, Singapore, Sept. 2007, pp. 745–750.

[120] G. A. Tsihrintzis and C. L. Nikias, "Performance of Optimum and Suboptimum Receivers in the Presence of Impulsive Noise Modeled as an α-Stable Process," *IEEE Trans. Commun.*, vol. 43, pp. 904–914, Apr. 1995.

[121] J. Mendel, "Tutorial on Higher-Order Statistics (Spectra) in Signal Processing and System Theory: Theoretical Results and Some Applications," *Proc. IEEE*, vol. 79, no. 3, pp. 278 – 305, Mar. 1991.

[122] W. Press, S. Teukolsky, W. Vetterling, and B. Flannery, *Numerical Recipes in C++*, 2nd ed. New York: Cambridge University Press, 2002.

[123] A. D'Amico, U. Mengali, and L. Taponecco, "Impact of MAI and Channel Estimation Errors on the Performance of Rake Receivers in UWB Communications," *IEEE Trans. Commun.*, vol. 4, no. 5, pp. 2435–2440, Sept. 2005.

[124] A. Molisch, D. Cassioli, C.-C. Chong, S. Emami, A. Fort, B. Kannan, J. Karedal, J. Kunisch, H. Schantz, K. Siwiak, and M. Win, "A Comprehensive Standardized Model for Ultrawideband Propagation Channels," *IEEE Trans. Antennas Propagat.*, vol. 54, pp. 3151 – 3166, Nov. 2006.

[125] G. J. Foschini and M. J. Gans, "On Limits on Wireless Communications in a Fading Environment when using Multiple Antennas," *Wireless Personal Communications*, vol. 6, no. 3, pp. 311–335, March 1998.

[126] "IEEE 802.16 Relay Task Group," http://wirelessman.org/relay/index.html.

[127] J. N. Laneman, G. W. Wornell, and D. N. C. Tse, "An efficient protocol for realizing cooperative diversity in wireless networks," in *Proc. of IEEE ISIT*, June 2001, p. 294.

[128] G. Scutari and S. Barbarossa, "Distributed Space-Time Coding for Regenerative Relay Networks," *IEEE Trans. Wireless Commun.*, vol. 4, pp. 2387–2399, Sept. 2005.

[129] A. Bletsas, A. Khisti, D. Reed, and A. Lipman, "A Simple Cooperative Diversity Method Based on Network Path Selection," *IEEE J. Select. Areas Commun.*, vol. 24, no. 3, pp. 659–672, March 2006.

[130] T. A. Tsiftsis, P. T. M. G. K. Karagiannidis, and S. A. Kotsopoulos, "Nonregenerative Dual-Hop Cooperative Links with Selection Diversity," *EURASIP Journal on Wireless Communications and Networking*, vol. 6, no. 2, pp. 34–42, 2006.

[131] A. Bletsas, H. Shin, and M. Z. Win, "Cooperative Communications with Outage-Optimal Opportunistic Relaying," *IEEE Trans. Wireless Commun.*, vol. 6, no. 9, pp. 3450–3460, September 2007.

[132] Y. Jing and H. Jafarkhani, "Single and multiple relay selection schemes and their diversity orders," *IEEE Trans. Wireless Commun.*, vol. 8, no. 3, pp. 1414 – 1423, March 2009.

[133] I. Krikidis, J. Thompson, S. McLaughlin, and N. Goertz, "Max-Min Relay Selection for Legacy Amplify-and-Forward Systems with Interference," *IEEE Trans. Wireless Commun.*, vol. 8, no. 6, pp. 3016–3027, June 2009.

[134] S. Al-Dharab and M. Uysal, "Cooperative Diversity over Fading Channels with Impulsive Noise," *IEEE Trans. Wireless Commun.*, pp. 4730–4739, September 2009.

[135] C. Zhong, S. Jin, and K.-K. Wong, "Outage Probability of Dual-Hop Relay Channels in the Presence of Interference," in *Proc. of IEEE VTC*, Barcelona, April 2008.

[136] Andrea Goldsmith, *Wireless Communications*. Cambridge University Press, 2005.

[137] C. S. Patel and G. L. Stuber, "Channel Estimation for Amplify and Forward Relay Based Cooperation Diversity Systems," *IEEE Trans. Wireless Commun.*, vol. 6, no. 6, pp. 2348–2356, June 2007.

[138] J. N. Laneman and G. W. Wornell, "Distributed Space-time Coded Protocols for Exploiting Diversity in Wireless Networks," *IEEE Trans. Inform. Theory*, vol. 49, no. 10, pp. 2415–2425, October 2003.

[139] S. Yiu, R. Schober, and L. Lampe, "Distributed Space-Time Block Coding," *IEEE Trans. Commun.*, vol. 54, no. 7, pp. 1195–1206, July 2006.

[140] Y. Jing and B. Hassibi, "Distributed Space-Time Coding in Wireless Relay Networks," *IEEE Trans. Wireless Commun.*, vol. 5, no. 12, pp. 3524–3536, December 2006.

[141] P. A. Anghel and M. Kaveh, " Exact Symbol Error Probability of a Cooperative Network in Rayleigh Fading Environment," *IEEE Trans. Wireless Commun.*, vol. 3, no. 5, pp. 1416–1421, Sept. 2004.

[142] S. Ikki and M. Ahmed, "Performance Analysis of Cooperative Diversity Wireless Networks over Nakagami-m fading Channel," *IEEE Commun. Lett.*, vol. 11, no. 4, pp. 334–336, April 2007.

[143] F. A. Onat, Y. Fand, H. Yanikomeroglu, and H. V. Poor, "Threshold Based Relay Selection in Cooperative Wireless Networks," in *Proc. of IEEE GLOBECOM*, Dec. 2008.

[144] I. S. Gradshteyn and I. M. Ryzhik, *Table of Integrals, Series and Products*, 7th ed. USA: Academic Press, 2007.

[145] G. Kramer, "Serially and parallel concatenated (turbo) codes," Mini Course at TU-Wien and FTW.

APPENDIX A

Closed Form BER Expression for MSMLD with i.i.d noise

The optimal pdf for memoryless case (Eqn. 2.4) can be further simplified to obtain expressions that require far less computational effort than the approach of Section 2.3. The idea is to use only one of the terms of the two-term pdf base on the value of the noise term n as follows

$$p(n) = \begin{cases} \frac{P_{\mathcal{G}}}{\sqrt{2\pi\sigma_{\mathcal{G}}^2}} \exp\left(-\frac{|n|^2}{2\sigma_{\mathcal{G}}^2}\right), & \text{if } \frac{P_{\mathcal{G}}}{\sqrt{2\pi\sigma_{\mathcal{G}}^2}} \exp\left(-\frac{|n|^2}{2\sigma_{\mathcal{G}}^2}\right) \geq \frac{P_{\mathcal{B}}}{\sqrt{2\pi\sigma_{\mathcal{B}}^2}} \exp\left(-\frac{|n|^2}{2\sigma_{\mathcal{B}}^2}\right) \\ \frac{P_{\mathcal{B}}}{\sqrt{2\pi\sigma_{\mathcal{B}}^2}} \exp\left(-\frac{|n|^2}{2\sigma_{\mathcal{B}}^2}\right), & \text{otherwise} \end{cases} \tag{A.1}$$

The corresponding threshold point can be determined evaluating the following

$$\frac{P_{\mathcal{G}}}{\sqrt{2\pi\sigma_{\mathcal{G}}^2}}\exp\left(-\frac{|n|^2}{2\sigma_{\mathcal{G}}^2}\right) \geq \frac{P_{\mathcal{B}}}{\sqrt{2\pi\sigma_{\mathcal{B}}^2}}\exp\left(-\frac{|n|^2}{2\sigma_{\mathcal{B}}^2}\right) \tag{A.2}$$

From Eqn. (A.2) the threshold value is obtained as

$$\mathcal{R} = \frac{2\sigma_{\mathcal{G}}^2}{1-\sigma_{\mathcal{G}}^2/\sigma_{\mathcal{B}}^2}\log\left(\frac{\mathrm{P}_{\mathcal{G}}/\mathrm{P}_{\mathcal{B}}}{\sigma_{\mathcal{G}}^2/\sigma_{\mathcal{B}}^2}\right). \tag{A.3}$$

Dividing the region of integration based on $\mathcal{R}$ allows us to express the pdfs for the null and alternative hypothesis as

$$p(n) = \begin{cases} p_{\mathcal{G}}(n) & |n|^2 \leq \mathcal{R}^2 \\ p_{\mathcal{B}}(n) & \text{otherwise} \end{cases} \qquad \text{and} \qquad p(n-2) = \begin{cases} p_{\mathcal{G}}(n-2) & |n-2|^2 \leq \mathcal{R}^2 \\ p_{\mathcal{B}}(n-2) & \text{otherwise} \end{cases}$$

The integrals corresponding to the regions of integration can be evaluated as

$$\mathcal{F} = \int_a^b p_{\mathcal{G}}^{1-s}(n)p_{\mathcal{B}}^{s}(n-2)dn = \frac{1}{\sqrt{2\pi}}\int_a^b \psi_{\mathcal{G}}^{1-s}\psi_{\mathcal{B}}^{s}\exp\underbrace{\left(-\frac{n^2(1-s)}{2\sigma_{\mathcal{G}}^2}-\frac{(n-2)^2 s}{2\sigma_{\mathcal{B}}^2}\right)}_{\mathcal{I}}, \tag{A.4}$$

where $\psi_{\mathcal{G}} = (P_{\mathcal{G}}/\sigma_{\mathcal{G}}^2)$, $\psi_{\mathcal{B}} = (P_{\mathcal{B}}/\sqrt{\kappa}\sigma_{\mathcal{B}}^2)$ and $\mu_{\mathcal{G}} = 2\sigma_{\mathcal{G}}^2$, $\mu_{\mathcal{B}} = 2\sigma_{\mathcal{B}}^2$. The term in the exponential, $\mathcal{I}$, can be rewritten as

$$\mathcal{I} = \frac{n^2(1-s)}{2\sigma_{\mathcal{G}}^2}+\frac{(n-2)^2 s}{2\sigma_{\mathcal{B}}^2} = \frac{\left[n-\dfrac{2s\sigma_{\mathcal{G}}^2}{(1-s)\sigma_{\mathcal{B}}^2+s\sigma_{\mathcal{G}}^2}\right]^2+\dfrac{4s\sigma_{\mathcal{G}}^2}{(1-s)\sigma_{\mathcal{B}}^2+s\sigma_{\mathcal{G}}^2}-\left[\dfrac{2s\sigma_{\mathcal{G}}^2}{(1-s)\sigma_{\mathcal{B}}^2+s\sigma_{\mathcal{G}}^2}\right]^2}{\dfrac{2\sigma_{\mathcal{G}}^2\sigma_{\mathcal{B}}^2}{(1-s)\sigma_{\mathcal{B}}^2+s\sigma_{\mathcal{G}}^2}} \tag{A.5}$$

Denoting $\Theta \triangleq \dfrac{2s\sigma_{\mathcal{G}}^2}{(1-s)\sigma_{\mathcal{B}}^2+s\sigma_{\mathcal{G}}^2}$, the integral takes the form

$$\mathcal{F} = \frac{1}{\sqrt{2\pi}}\int_a^b \psi_{\mathcal{G}}^{1-s}\psi_{\mathcal{B}}^{s}\exp\left(-\frac{s(n-\Theta)^2}{\Theta\sigma_{\mathcal{B}}^2}\right)\exp\left(\frac{s(\Theta-2)}{\sigma_{\mathcal{B}}^2}\right)dn. \tag{A.6}$$

Substituting $\nu = (n-\Theta)\sqrt{\dfrac{2s}{\sigma_{\mathcal{B}}^2\Theta}}$, we obtain

$$\begin{aligned}\mathcal{F} &= \sqrt{\frac{\Theta\sigma_{\mathcal{B}}^2}{2s}}\psi_{\mathcal{G}}^{1-s}\psi_{\mathcal{B}}^{s}\exp\left(\frac{s(\Theta-2)}{\sigma_{\mathcal{B}}^2}\right)\int_{(b-\Theta)\sqrt{\frac{2s}{\Theta\sigma_{\mathcal{B}}^2}}}^{(a-\Theta)\sqrt{\frac{2s}{\Theta\sigma_{\mathcal{B}}^2}}}\frac{1}{\sqrt{2\pi}}\exp\left(-\frac{\nu^2}{2}\right)d\nu \\ &= \sqrt{\frac{\Theta\sigma_{\mathcal{B}}^2}{2s}}\psi_{\mathcal{G}}^{1-s}\psi_{\mathcal{B}}^{s}\exp\left(\frac{s(\Theta-2)}{\sigma_{\mathcal{B}}^2}\right)\left[Q\left(\sqrt{\frac{2s(a-\Theta)^2}{\Theta\sigma_{\mathcal{B}}^2}}\right)-Q\left(\sqrt{\frac{2s(b-\Theta)^2}{\Theta\sigma_{\mathcal{B}}^2}}\right)\right]\end{aligned} \tag{A.7}$$

Applying the appropriate limits for $\mathcal{F}$, Eqn.(A.7) is accordingly evaluated.

APPENDIX B

Approximation for the $J(\cdot)$ Function

For computer implementation, the $J(\cdot)$ function introduced in Chapter 3 can be split into two intervals $0 \leqslant \sigma \leqslant \sigma_T$ and $\sigma_T < \sigma < \infty$ where $\sigma_T = 1.6363$. In order to approximate $J(\sigma)$, a polynomial in σ is used for the left interval and an exponential for the right interval. The non-linear least squares (NLLS) Marquadt-Levenberg algorithm provides the following approximation [145]

$$J(\sigma) \approx \begin{cases} a_{J,1}\sigma^3 + b_{J,1}\sigma^2 + c_{J,1}\sigma & 0 \leqslant \sigma \leqslant \sigma_T \\ 1 - \exp[a_{J,2}\sigma^3 + b_{J,2}\sigma^2 + c_{J,2}\sigma + d_{J,2} & \sigma_T < \sigma < 10 \\ 1 & \sigma \geqslant 10 \end{cases} \tag{B.1}$$

where

$$\begin{aligned} a_{J,1} &= -0.0421061, & a_{J,2} &= -0.00181491, \\ b_{J,1} &= 0.209252, & b_{J,2} &= -0.142675 \\ c_{J,1} &= -0.00640081, & c_{J,2} &= -0.0822054 \\ & & d_{J,2} &= 0.0549608 \end{aligned}$$

For the inverse $J(\cdot)$ function the curve is split into two intervals at $I_T = 0.3646$. The approximation can thus be expressed as

$$J^{-1}(I) \approx \begin{cases} a_{\sigma,1} I^2 + b_{\sigma,1} \cdot I + c_{\sigma,1}\sqrt{I}, & 0 \leqslant I \leqslant I_T \\ -a_{\sigma,2} \log[-b_{\sigma,2}(I-1)] - c_{\sigma,2} \cdot I, & I_T < I < 1 \end{cases} \tag{B.2}$$

where

$$\begin{aligned} a_{\sigma,1} &= 1.09542, & b_{\sigma,1} &= 0.214217, & c_{\sigma,1} &= 2.33727 \\ a_{\sigma,2} &= 0.706692, & b_{\sigma,2} &= 0.386013, & c_{\sigma,2} &= -1.75017 \end{aligned}$$

The function $J(\sigma)$ is a monotonically increasing (see Fig, B.1), and thus reversible, function that cannot be expressed in closed form.

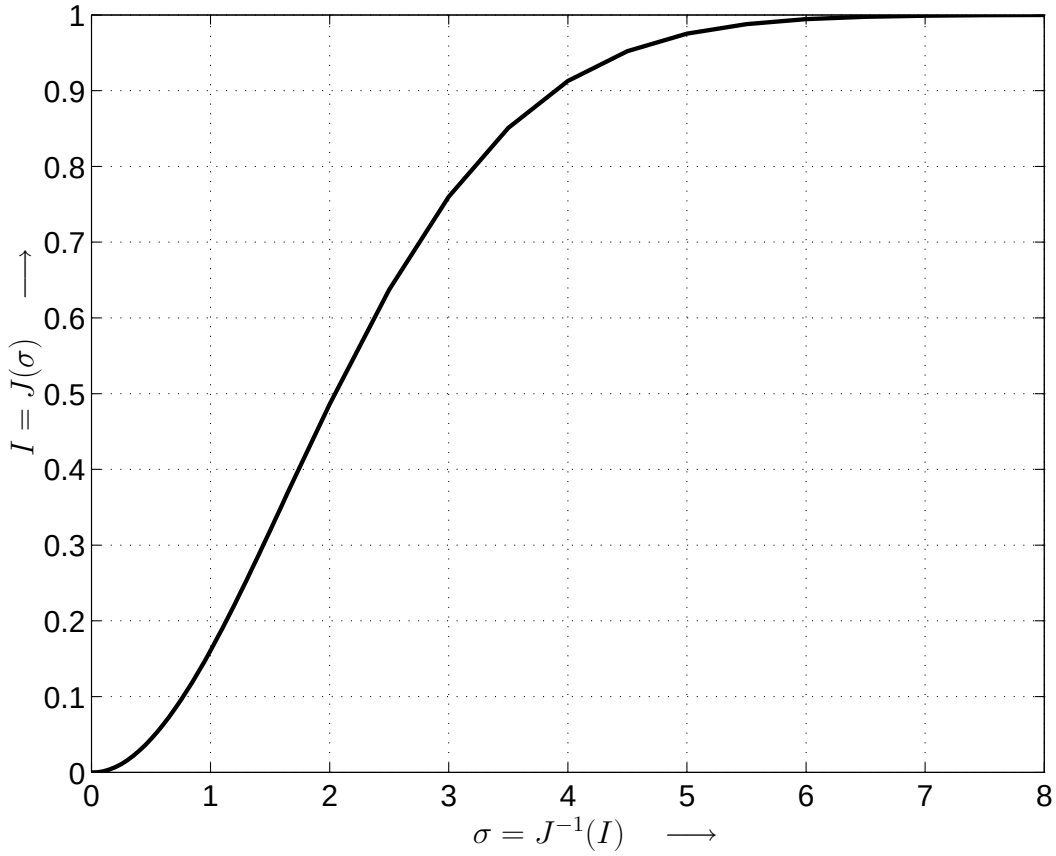

Figure B.1 — Plot of the J(σ) function

APPENDIX C

Publications Related to Thesis

The following papers have been published/submitted for publication from the work done in this thesis.

Chapter 2

- J. Mitra and L. Lampe, *Robust Decoding for channels with Impulse Noise*, in *Proc. of IEEE Global Telecommunications Conference (GlobeCom)*, San Francisco, 2006.

- J. Mitra and L. Lampe, *Coded Narrowband Transmission over Noisy Powerline Channels* , in *Proc. of IEEE International Symposium on Powerline Communications* (ISPLC), Dresden, 2009, pp. 143-148.

- J. Mitra and L. Lampe, *Convolutionally Coded Transmission over Non Markov-Gaussian Channels with Memory: Analysis and Decoding Metrics*, accepted for publication in *IEEE Transactions on Communications*, December 2009 (11 pages).

Chapter 3

- J. Mitra and L. Lampe, *Sensing and Suppression of Impulsive Interference*, in *Proc. of IEEE Cananadian Conf. on Elec. and Computer Engg.* (CCECE), **Best Student Paper**, *Invited*, pp. 219-224. St. Johns, Newfoundland, 2009.

- J. Mitra and L. Lampe, *On Joint Estimation and Decoding for Channels with Noise Memory*, *IEEE Communications Letters*, Vol. 13, No. 10, pp 730-732. October 2009.

- J. Mitra and L. Lampe, *Opportunistic Spectral Access through Suppression of Impulsive Interference*, in *IEEE Canadian Journal of Elec. & Comp. Eng. (Special Issue)*, Vol. 34, No. 3, Summer 2009, pp 105-113.

Chapter 4

- J. Mitra and L. Lampe, *Robust Detectors for TH IR-UWB Systems with Multiuser Interference*, in *Proc. of IEEE Intl. ICUWB, Singapore*, 2007, pp. 745-750.

- J. Mitra and L. Lampe, *Comparison of Detectors for Multiple-Access Interference Mitigation in TH-IR UWB*, in *Proc. of IEEE Intl. Conference on Ultra Wideband* (ICUWB), Hannover, 2008, pp. 153-156.

- J. Mitra and L. Lampe, *Design and Analysis of Robust Detectors for TH-IR UWB systems with Multiuser Interference*, *IEEE Transactions on Communications*, August 2009, Vol. 57, No. 8, pp. 2210-2214.

Chapter 5

- J. Mitra and L. Lampe, *Cooperative Strategies in Presence of Impulsive Interference*, to be submitted to *IEEE Transactions on Wireless Communications*, 2010.